MATERIAL SELECTION FOR FABRICATING AN INTERNAL GUIDANCE SCAFFOLD FOR IMPROVING CURRENT NERVE GUIDE CONDUITS

Caroline Sarah Taylor

March 2018

Thesis submitted to the University of Sheffield for the degree of Doctor of Philosophy

Department of Materials Science & Engineering, University of Sheffield, UK

Acknowledgments

First and foremost, I must thank my primary supervisor Professor John Haycock for all his support and guidance throughout my job and my PhD. Thank you for believing in me and for taking a chance on me where others didn't.

I would like to thank my second supervisor and colleague Dr Frederik Claeyssens for all his support, encouragement and enthusiasm throughout this project, especially when things didn't work.

I would also like to thank my postdoctoral colleague on the Neurimp project, Dr Adam Glen, for all his help and support throughout my PhD and for being an excellent companion on all our meetings away. Thank you for being there for me to vent my frustrations, sharing my success and for being a fantastic friend. I would also like to thank Miss Mehrie Behbehani, a wonderful colleague, fantastic scientist and a friend for life. Thank you for your help and your contributions to my work and the Neurimp (FP7) project.

To everyone at the Kroto Research institute, especially Dr Colin Sherbourne, Jonathan Field, Dr Paul Taylor, Dr Leyla Zilic, Dr Nicola Green, Dr Dharaminder Singh, Mrs Vanessa Singleton, Mark Wagner and Robert Dickinson. I had nearly 4 years at the Kroto Research Institute I will value forever. Thank you for all your support, I miss you all so much!

I would like to thank everyone on the Neurimp (FP7) project, especially everyone involved at Vornia Biomaterials Ltd, The University of Westminster, IK4-Tekiner, and Contipro for their continual guidance, support and giving me many wonderful memories from our 6 monthly meetings away.

To my wonderful family, and friends, who didn't always understand what I was talking about, but for listening and supporting me. My mum, dad, brother Matt, my now in laws and my best friends, Megan, Mims, Hayley, Kat and Regan. One last thank you to Dr Craig Macgregor-Chatwin who introduced me to the love of my life and predicted my engagement and wedding in his thesis acknowledgments. Thank you for bringing me to Sheffield.

And finally, I dedicate my thesis to my husband Luke. Because without him, I would not have applied for a job in Sheffield and I wouldn't have done what I have. Thank you for being my rock, for listening to me talk about 'swan' cells and nerve guide conduits the size of pylons. Thank you for wiping away the tears, listening to the rants, picking me up during the bad days and celebrating with during the good days.

Publications, Conferences and Awards

Journal Articles

C.J. Pateman, A.J. Harding, A. Glen, C.S. Taylor, C.R. Christmas, P.P. Robinson, S. Rimmer, F.M. Boissonade, F. Claeyssens, J.W. Haycock, Nerve guides manufactured from photocurable polymers to aid peripheral nerve repair, Biomaterials 49 (2015) 77-89. (doi.org/10.1016/j.biomaterials.2015.01.055)

Lizarraga-Valderrama, L. R., Nigmatullin, R., Taylor, C., Haycock, J. W., Claeyssens, F., Knowles, J. C. and Roy, I, Nerve tissue engineering using blends of poly(3-hydroxyalkanoates) for peripheral nerve regeneration. Eng.Life.Sci.(2015) 15: 612–621. (doi:10.1002/elsc.201400151)

Mehri Behbehani, Adam Glen, Caroline S. Taylor, Alexander Schuhmacher, Frederik Claeyssens, John W. Haycock, Pre-clinical evaluation of advanced nerve guide conduits using a novel 3D in vitro testing model International Journal of Bioprinting, v. 4, n. 1, jan. 2018. (doi:http://dx.doi.org/10.18063/ijb.v4i1.12)

Conference Presentations, Posters and Abstracts

CS Taylor, R Chen, JA Hunt, J Curran, JW Haycock (2016). The use of modified amino-silane coatings for use in peripheral nerve tissue engineering. European Cells and Materials, ECM Meeting Abstracts 2016, Collection 5; TCES (Page 79).

CS Taylor, A Glen, F Claeyssens, JW Haycock (2016). The use of Poly(3-hydroxybutyrate-co-3-hydroxyvalerate) as a material for peripheral nerve repair and nerve guide tissue engineering. European Cells and Materials, ECM Meeting Abstracts 2016, Collection 5; TCES (Page 92).

Knotková, K, Huerta-Angeles, G, Taylor, C and Haycock, J.W (2017). PCL aligned fibers useful for the formation of internal channels arrays suitable for neuron cultivation. Frontiers in polymer science 2017).

Conferences Attended

Poster presentation at University of Sheffield Engineering Symposium (USES) (2015)

Poster presentation at Biomaterials and Tissue Engineering Group 17th Annual Meeting (2015)

Oral presentation at United Kingdom Society for Biomaterials (UKSB) conference (2016)

2 x Poster presentations at Tissue and Cell Engineering Society (TCES) conference (2016)

2 x Poster presentations at Biomaterials and Tissue Engineering Group 18th Annual Meeting (2016)

Oral presentation at United Kingdom Society for Biomaterials (UKSB) conference (2017)

Oral presentation at Tissue and Cell Engineering Society (TCES) conference (2017)

Rapid fire Oral presentation and Poster presentation at European Society for Biomaterials (ESB) conference (2017)

Awards

First Prize for Poster presentation at University of Sheffield Engineering Symposium (USES) (2015)

First Prize in Second Year Poster Presentations at The University of Sheffield Material Science and Engineering PhD Poster competition.

Runner up prize for Oral presentations at United Kingdom Society for Biomaterials (UKSB) conference (2017)

Runner up prize for Tissue and Cell Engineering Society (TCES) conference (2017)

Table of Contents

Abbreviations

2D Two dimensional

3D Three dimensional

AFM Atomic Force Microscopy

BSA Bovine serum albumin

CNTF ciliary neurotrophic factor

Da Dalton

ECM Extra cellular matrix

DMEM Dulbecco's Modified Eagle's Medium

DMF Dimethylformamide

DNA Deoxyribonucleic acid

DRG Dorsal Root Ganglia

FCS Foetal calf serum

FDA Food and Drug Administration

FGF Fibroblast growth factor

FITC Fluorescein isothiocyanate

FTIR Fourier-transform infrared spectroscopy

GelMa Gelatin methacryloyl (GelMA)

GFAP Glial fibrillary acidic protein

GPa Giga Pascal

GPC Gel permeation chromatography

HFIP Hexafluoroisopropanol

HIPEs High Internal Phase Emulsions

KDa Kilo Dalton

μSL Microstereolithography

kV Kilovolts

MAP-TMS Methacryloxypropyltrimethoxysilane

MCL-PHA Medium chain Polyhydroxyalkanoate

MicroCT Micro computed tomography

mL/min Millilitre per minute

MPa Mega Pascal

MTT Methylthiazolyldiphenyl-tetrazolium bromide

NF Neurofillament

NGC Nerve Guide Conduit

NGF Nerve growth factor

NMR Nuclear magnetic resonance

PBS Phosphate buffered saline

PET Polyethylene terephthalate

PCL Polycaprolactone

PGA Polyglycolic acid

PHA Polyhydroxyalkanoates

P(3HB) Poly(3-hydroxybutyrate)

P(4HB) Poly(4-hydroxybutyrate)

PHBV Poly (3-hydroxybutyrate-co-3-hydroxyvalerate)

PLA Poly(lactic acid)

PLLA Poly(L-Lactic acid)

PLGA Poly(lactic acid-co-glycolic acid

PGA Poly(glycolic acid)

RPM Revolutions per minute

SCL-PHA Short chain Polyhydroxyalkanoate

VEGF Vascular endothelial growth factor

WCA Water contact angle

XPS X-ray photoelectron spectroscopy

Abstract

Peripheral nerve injuries affect 2.8% of all trauma patients which amounts to 8.5 million 'restricted activity days' every year. Unlike the central nervous system, nerves of the peripheral nervous system can regenerate after injury, at a rate of around 1 mm/day. Current treatments involve direct end to end suturing or using an autograft, which is the current 'gold standard' treatment to bridge large gaps (over 20mm). However, there is limited donor nerve available and limited nerve function is restored. Current nerve guide conduits (NGCs) are fabricated from both natural and synthetic materials. However, the efficiency of current nerve guide conduits is limited and conduits only treat defects up to 20mm. Research focuses primarily on improving hollow nerve guide conduits in several different ways. These include: the addition of intraluminal guidance scaffolds, coatings to modify surface chemistry or changing the conduit design by incorporating channels and pores.

The aim of this work was to investigate different blends of synthetic polymers for their potential use as an intraluminal nerve guidance scaffold. It is hypothesised that the addition of electrospun fibres to hollow nerve guide conduits will increase nerve regeneration length by providing aligned guidance for Schwann cell attachment, migration and nerve regeneration. Blends of synthetic polymers were characterised to assess surface properties, mechanical properties, biocompatibility and cytotoxicity. Electrospinning was performed to determine if polymers, and their blends, could be fabricated into aligned fibres of varying diameters. Polymers which had a higher Young's modulus, Polyhydroxybutyrate–co-Valerate (PHBV), Polycaprolactone (PCL), Polyhydroxybutyrate (P(3HB) and Polylactic Acid (PLLA) could all be fabricated into aligned fibres of varying diameters. Polymers with more elastomeric properties Polyhydroxyoctanoate (P(3HO) and Polyhydroxyoctanoate-co-hydroxydecanoate (P(3HO-co-3HD) could not be electrospun into aligned fibres. Overall, the most efficient blend ratio of the brittle polymers with the elastomeric polymers was 50:50. This ratio fabricated aligned fibres and maintained a lower Young's modulus (closer to that of native nerve).

The effect of fibre diameter on neuronal and Schwann cell adherence, viability and differentiation was investigated by culturing cells on electrospun Polyhydroxybutyrate–co-Valerate (PHBV) fibres. *In vitro* analysis concluded that 5 and 8µm diameter fibres supported neuronal cell viability and differentiation most effectively.

The effect of different material composition on neuronal and Schwann cell adherence, viability and differentiation was investigated by culturing cells onto 5 and 8 µm fibres of PHBV, PCL, P(3HB): P(3HO) (50:50) and P(3HO-co-3HD):PLLA (50:50). PCL was investigated as a control material. PHBV, P(3HB):P(3HO) (50:50) and P(3HO-co-3HD):PLLA (50:50) were investigated further due to success with regards to electrospinning, excellent

cell viability and mechanical properties compared to other investigated blends of polymers. It was hypothesised that using polyhydroxyalkanoates, and novel blends of these polymers, would improve neuronal and Schwann cell attachment and support cell proliferation and differentiation more effectively than known FDA approved biopolymers, due to their chemical composition. The novelty in this work is the use of PHA blends and the ability to electrospin them. NG108-15 neuronal cell neurite outgrowth was significantly higher when cells were cultured on the 8μm PHBV fibres compared to the other materials and fibre diameters. Schwann cell viability was significantly decreased when cultured on the 5 and 8μm P(3HO-co-3HD):PLLA (50:50) fibres, compared to the other polymer blends.

Polymer fibres were further investigated using a novel 3D *ex vivo* fibre testing model. 5mm Polyethylene glycol hollow tubes were manufactured using microstereolithography. Polymer fibres, of 5 and 8μm diameters, were threaded into tubes, and an explanted DRG body placed on the proximal end. The use of DRGs in neuronal cell culture mimics a nerve injury, as neurite extensions grow from the DRG body after removing the nerve roots. It was hypothesised that the addition of electrospun fibres to hollow nerve guide conduits would increase nerve regeneration length. Both Schwann cell migration lengths and neurite outgrowth lengths were greater on the 5μm fibres, compared to their 8μm counterparts. Schwann cell migration length was statistically greater on the 5μm PHBV fibres and P(3HO):P(3HB) (50:50) fibres. PHBV 5μm fibres supported greater neurite lengths, compared to the 8μm PCL and 8μm PHBV fibres. This study highlights the difference between using a neuronal cell line, compared to using a primary neuron (DRG) model, and using a 3D *in vitro* culture model compared to 2D *in vitro* culture. This work also reveals the potential of 5μm P(3HO):P(3HB) (50:50) and PHBV fibres, as intraluminal fibrous scaffolds to improve nerve repair and would support the use of this blend for *in vivo* investigations.

Additionally, surface modification is used to improve current nerve guide conduits, by improving biocompatibility of the surfaces of bulk biodegradable polymers with the addition of reactive chemical groups. Compared to plasma polymerisation, aminosilanisation is an alternative method to modify surfaces with amine groups as it is cost effective, scalable and cheaper. Two different chain lengths, long and short, of aminosilanes were investigated, to determine their potential use in peripheral nerve repair. It was hypothesised that the addition of aminosilanes plain glass would improve neuronal and Schwann cell adherence and neuronal cell differentiation. The novelty of this work is that aminosilanes have not been investigated for use in peripheral nerve repair and that they could be a useful addition to biopolymer NGCs. Long chain aminosilanes supported significantly longer neurite lengths from NG108-15 neuronal cells, compared to the short chain and plain glass control. Both chain lengths supported NG108-15 neuronal and Schwann cell viability. A co-culture of

primary neurons and Schwann cells was established by dissociating rat DRGs. Long chain aminosilanes supported significantly longer neurite lengths from primary neurons, compared to the short chain aminosilane, plain glass and tissue culture plastic controls. This work highlights the potential use of long chain aminosilanes for use in peripheral nerve repair, to coat conduits or intraluminal guidance scaffolds.

Besides electrospinning, pressurized gyration has recently been reported to manufacture fibrous scaffolds for tissue engineering applications. The set up established at The Department of Mechanical Engineering, University College London, was used to manufacture P(3HB) and P(3HB):P(3HO-co-3HD) (80:20) fibres. Gyrated fibres were investigated with electrospun P(3HB) fibres, to determine which manufacturing method was the most efficient in manufacturing aligned fibres, and *in vitro* and *ex vivo* analysis was performed. SEM analysis confirmed that the P(3HB) electrospun fibres were more aligned compared to both gyrated fibre types. Both gyrated and electrospun fibres supported NG108-15 neuronal cell and Primary Schwann cell proliferation and viability. However, greater neurite lengths were observed on the electrospun P(3HB) fibres compared to the gyrated PHA fibres, when culturing DRGs. Schwann cell migration length was also significantly larger on the electrospun fibres compared to the gyrated fibres. This work highlights the potential of gyration for fabricating fibrous scaffolds. However, future work will need to be performed to fabricate aligned fibre scaffolds which compare with electrospun fibres.

Overall, this thesis demonstrates that Polyhydroxyalkanoates, and blends of PHAs, can be fabricated into aligned fibre scaffolds by electrospinning. It also demonstrates that the addition of PHAs to polymer blends supports neuronal and Schwann cell attachment, proliferation and differentiation more effectively than the biopolymer alone. Although pressurized gyration is a new technique to fabricate fibre scaffolds, this thesis has shown that it does not fabricate fibres with the required alignment for nerve repair and therefore, more optimisation of the technique is required. Surface modification, using silanisation, has also been shown to be an effective technique to modify a glass surface with amine reactive groups, and therefore, can be applied to polymer surface modification.

Chapter 1: Introduction

1.1 The Nervous System

The nervous system is divided into two separate systems: the central nervous system and the peripheral nervous system (Paxinos *et al.*, 2012). The central nervous system consists of the brain, brain stem and the spinal cord, whereas the peripheral nervous system includes the nerves and supporting cells that lie outside the central nervous system (Marani *et al.*, 2012). Both the central and peripheral nervous systems consist of a complicated network of neurons, blood vessels and supporting cells (Lowe and Anderson, 2015). They work consistently together to transmit electrical signals from the outer limbs, internal glands, organs, and the brain to each other to maintain and regulate body functions such as pain, temperature control and responses to external stimuli (Marani *et al.*, 2012). Other differences between the peripheral and central nervous systems are the supporting cells, neuroglia, that are present (Lowe and Anderson, 2015). Oligodendrocytes are the supporting cells found in the central nervous system. They myelinate several adjacent central nervous system axons and maintain neurons and brain tissue (Baumann and Pham-Dinh, 2001). Schwann cells are found in the peripheral nervous system and support myelinated and non-myelinated axons (Lowe and Anderson, 2015). A single segment of an axon is myelinated by one Schwann cell, which incorporates the whole of the axon, the membrane around it and the Schwann cell itself, whereas the oligodendrocytes myelinate the axon forming layers and detach themselves (Baumann and Pham-Dinh, 2001; Lowe and Anderson, 2015).

1.2 Peripheral Nerve Regeneration Injury Types

Peripheral nerve injuries affect around 300,000 people every year in Europe alone (Belkas *et al.*, 2004a). 2.8% of all peripheral nerve injuries result from trauma and over 8.5 million 'restricted activity days' as well as 5 million bed rest days costing millions of pounds to the economy every year (Nectow *et al.*, 2012). Due to the complexity of the peripheral nervous system, treating injuries to the nerves can prove to be a big challenge. Unlike the central nervous system, the peripheral nervous system can repair itself at a rate of 1-3mm a day (Deumens *et al.*, 2010). The peripheral nervous system contains Schwann cells as its supporting cells, compared to the central nervous system, which has oligodendrocytes (Lowe and Anderson, 2015). Peripheral nerve regeneration occurs by a process called Wallerian degeneration and regeneration. When the nerve is injured, the distal stump of the axon begins to degenerate (Perry *et al.*, 1987). Schwann cell proliferation increases and macrophages infiltrate the site of injury and clear away myelin and axonal debris, along with the Schwann cells, which can take up to 3 months, depending on the distance between the

proximal and distal stumps (Deumens *et al.*, 2010). The endoneurial tubes of the distal stump collapse, due to the occurrence of phagocytosis, and become the 'Bands of Büngner' which are 'stacked processes' of the remaining Schwann cells (Pfister *et al.*, 2011). During Wallerian degeneration (which is located specifically at the distal stump), the axons, of surviving neurons, in the proximal stump start to regenerate and develop 'axonal sprouts' (Deumens *et al.*, 2010). The regenerative sprouts grow and use the 'Bands of Büngner' as guidance cues to regenerate to cross the injury site (Deumens *et al.*, 2010). During the process of Wallerian degeneration, Schwann cells initially proliferate to form the 'Bands of Büngner' before differentiating to re-myelinate the growing axons, and thus play an central role in guiding the regenerating axonal sprouts into position (Pfister *et al.*, 2011).

1.3 Peripheral Nerve Injury Types

If the axonal sprouts do not cross the injury site however, this can result in scar tissue and neuroma formation leading to neuropathic pain and loss of function of the nerve (Pfister *et al.*, 2011). This underpins the reason why surgical intervention plays a significant role in peripheral nerve injury repair. The type of treatment and surgical intervention also depends on the severity of the peripheral nerve injury. There are two ways of classifying peripheral nerve injuries. Pathological descriptions of injury by H.J. Seddon describe three types - neurapraxia, axonotmesis, and neurotmesis. This is further refined by five degrees of 'anatomical disruption and regenerative potential' by S. Sunderland (Pfister *et al.*, 2011). Here, first-degree injury (or neurapraxia) is the least severe injury and recovery arises after 12 weeks (Belkas *et al.*, 2004a). Myelin breakdown occurs after a short period, but as the axons are intact re-myelination can occur (Pfister *et al.*, 2011). In second-degree injury (axonotmesis) there is injury to the axons and so Wallerian degeneration occurs in the distal stump of the axon (Kehoe *et al.*, 2012). The basal Schwann cell lamina is still intact and therefore regenerating axons are guided into the site of injury for axon repair without surgical intervention (Pfister *et al.*, 2011). In third degree injuries, the basal Schwann cell lamina is damaged and therefore the potential for scarring arises. Wallerian degeneration and regeneration of the axon still occurs, but if the regenerating axons become impeded and are not guided across the injury site appropriately then surgical intervention will be needed to bridge the gap (Pfister *et al.*, 2011). In fourth degree injury, axonal regeneration will not occur due to the intense amount of scarring over the injury site, and therefore this must be removed surgically. With fifth degree injury (neurotmesis), the nerve must be repaired for any regeneration to occur due to the nerve being split in two. With fourth and fifth degree injuries, there is the potential for excessive scarring and therefore these severe types of injuries must be repaired by surgery (Perry *et al.*, 1987).

1.4 Current Treatments

Due to the complications of nerve regeneration, as well as the rate in which regenerative axonal sprouts grow, surgery and implantation may be needed to bridge the gap from peripheral nerve injuries (Pfister *et al.*, 2011). Surgical intervention is required for third, fourth and fifth degree injuries (W. Daly *et al.*, 2012). Very small nerve gaps, up to 10 millimetres, can be treated by end-to-end direct suturing of the two nerve ends (Deumens *et al.*, 2010). However, if the nerve is under tension when suturing is tried, other options must be considered. Autografts are the 'gold standard' for peripheral nerve repair, generally bridging larger gaps of over 20mm (J. H. Bell and Haycock, 2012). A sensory nerve, such as the sural nerve from the leg, is used to graft sensory neurons, motor neurons and mixed gaps (W. Daly *et al.*, 2012). However, they only have a 50% success rate and various limitations that affect the functionality of the nerve (Kehoe *et al.*, 2012). A major disadvantage is donor site morbidity and the need for a second surgical procedure. Other complications include an increase in recovery time for the patient, scarring and the formation of neuromas, limited amount of tissue available, as well as many structural differences of using a sensory nerve to graft a motor neuron and therefore there is a loss of function (Kehoe *et al.*, 2012). Figure 1 summarises the different repair routes that are taken to treat peripheral nerve injuries, depending on the size of the gap presented.

Various therapies are currently being used along with nerve autografting to increase the success rate of the graft, such as the addition of growth factors, electrical nerve stimulation, phototherapy and physiotherapy (Deumens *et al.*, 2010). Allografts and xenografts are also available as grafting options, although similar issues arise with using them as well as the need for immunosuppressive drugs and the risk of zoonotic infections from xenografts (Arslantunali *et al.*, 2014b). Therefore, there is a need for using alternative grafting materials for repairing peripheral nerve injuries. Nerve guide conduits are currently used to bridge gaps of up to 30 - 40mm, with reasonable results reported up to 15 - 20mm (Pateman *et al.*, 2015). The current designs are relatively simple and typically restricted to hollow tubes and cuffs. Currently there are 11 commercially available devices on the market which are either sutured in place to bridge the proximal and distal stumps or held in place with fibrin glue (J. H. Bell and Haycock, 2012). For a nerve guide conduit to be successful specific criteria in must be met. In particular, the biomaterial used must be biocompatible, non-toxic and not cause an immune response (Kehoe *et al.*, 2012). It must also be degradable and degrade at a rate which should be parallel with the rate of axonal regeneration (Nectow *et al.*, 2012). The device should also be porous, to allow exchange of nutrients into the injury site, meet sterilisation and handling specifications, and provide guidance cues to aid the regenerating axon (Kehoe *et al.*, 2012). The device should be flexible, allowing it to be sutured without it

breaking and it should exhibit similar mechanical properties to the native nerve as well as fit into place without causing any nerve tension (Nectow *et al.*, 2012).

Currently a limited range of nerve repair devices exist, manufactured from both natural and synthetic materials. Figure 2 summarises the range of devices which are currently FDA approved and commercially available (W. Daly *et al.*, 2012). Naturally derived tissue devices for nerve repair have also had recent FDA approval. Currently, AxoGen have produced a decellularised human nerve allograft (Advance® Nerve Graft) which has performed well to bridge gaps of up to 20mm (Kehoe *et al.*, 2012). Tissue is sourced from donors, and advantages of the allograft include eliminating donor site morbidity and the need for a second surgery. However, a major disadvantage is the need for immunosuppressive drugs (Kehoe *et al.*, 2012). Axogen also manufactures the Axoguard® Nerve connector, a nerve guide conduit, and the protector, a wrap, which both use porcine submucosa extracellular matrix (J. H. Bell and Haycock, 2012). Collagen is currently being used as a material in peripheral nerve repair. As one of the largest components of the extracellular matrix, it has excellent biocompatibility and is used in many devices which include: NeuraGen®, NeuroFlex™, NeuroMatrix™, NeuraWrap™ and NeuroMend™ (J. H. Bell and Haycock, 2012). The NeuraGen® tube has had great success in aiding nerve repair similar to the gold standard autografts, and has had excellent efficiency in bridging gaps up to 40mm (Kehoe *et al.*, 2012). Naturally derived materials can exhibit batch to batch variability but have excellent biocompatibility and similar mechanical properties to native tissue (Kehoe *et al.*, 2012).

There are several nerve guide conduits currently available from synthetic materials. Salumedica have produced two non-resorbable devices from their novel biomaterial Salubria, a biostable polyvinyl alcohol hydrogel, which mimics the ECM of human tissue (de Ruiter *et al.*, 2009). Salubridge™ is a protectant nerve wrap device, and the SaluTunnel™ is the nerve guide conduit. The PVA adds stability to both devices, whilst the hydrogel has comparable properties to human tissue. However, Salubria nerve guide tubes cause compression on the regenerative axonal sprouts at the suture line (Kehoe *et al.*, 2012). Polyesters are also suitable synthetic materials as nerve guide conduits as they are biodegradable and their properties can be tailored and controlled by the manufacturing method (Arslantunali *et al.*, 2014b). Due to ester linkage, polyesters degrade by hydrolysis and the rate of degradation can be controlled for use in nerve guide conduits (Tokiwa and Calabia, 2007). Neurotube® is a synthetic nerve guide conduit made from woven polyglycolic acid, developed by Synovis (William T. Daly *et al.*, 2013). It can be used to treat gaps from 8-30mm, bridging gaps up to 20mm at the same efficacy as the gold standard autograft (Kehoe *et al.*, 2012). However, it has a high degradation rate (typically six months),

degrades into acidic by products and its mechanical properties consequently decrease quickly over this timeframe, arguably before complete tissue regeneration has occurred (Kehoe *et al.*, 2012). The other polyester nerve guide conduit available currently is Neurolac™, a hollow tube made of poly(D,L-lactide-co-ε-caprolactone) (Arslantunali *et al.*, 2014b). Neurolac™ bridges gaps up to 20mm, their degradation products are less acidic over the same timeframe as those compared to the Neurotube® device, with complete degradation taking approximately 24 months (William T. Daly *et al.*, 2013). There have been many clinical studies using Neurolac™. However Poly(d-lactide-co-ε-caprolactone) is quite rigid, inflexible, and reports have shown that there has been severe reactions, blockage of the tube, complete collapse of the device and neuroma formation in patients with Neurotube™ (Kehoe *et al.*, 2012).
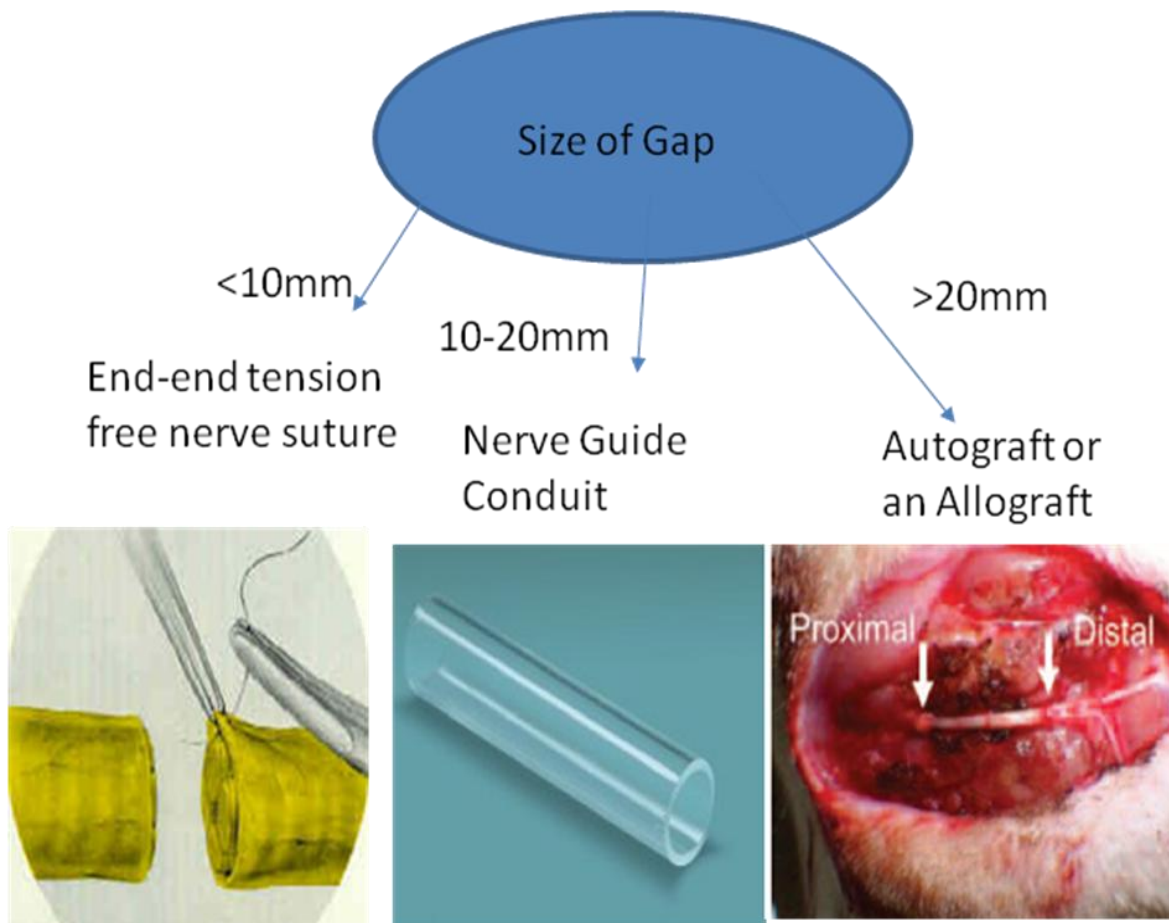
Figure 1.1. Image highlights main route of repair for nerve gaps of specific lengths (Tan *et al.*, 2012; Sabongi *et al.*, 2015; Iijima *et al.*, 2016).

Table 1.1. FDA approved devices to treat peripheral nerve injury. Adapted by Bell *et al.* (2012) (J. H. Bell and Haycock, 2012).

Commercial Name	Material	Device Type	Natural or Synthetic
NeuraGen®	Type I collagen	NGC	Natural
NeuroMatrix™	Type I collagen	NGC	Natural
Neuroflex™	Type I collagen	NGC	Natural
AxoGuard™	Porcine small intestinal submucosa	NGC	Natural
Neurotube®	Polyglycolic Acid (PLGA)	NGC	Synthetic
Neurolac®	PolyDL-lactidee-Caprolactone (PCL)	NGC	Synthetic
Nerve Protector™	Polyvinyl Alcohol (PVA)	NGC	Synthetic
SaluTunnel™	Salubria- biostable polyvinyl alcohol hydrogel	NGC	Synthetic
Salubridge™	Salubria- biostable polyvinyl alcohol hydrogel	Protectant Nerve wrap device	Synthetic
Neuromend™	Type I collagen	Wrap	Synthetic
Advance® Nerve Graft	Human Nerve	Allograft	Natural

1.5 Regeneration inside a Hollow Nerve Guide Conduit

As previously described, the peripheral nervous system can regenerate via a process called Wallerian degeneration and regeneration (Perry *et al.*, 1987; Deumens *et al.*, 2010; Pfister *et al.*, 2011). After degeneration, Schwann cells proliferate in the endoneurial tubes and form the 'Bands of Bűngner' as guidance cues for the regenerating nerve axons (Pfister *et al.*, 2011). However, nerve regeneration differs in a hollow nerve guide tube, and it is important to understand this process when designing new nerve guide conduits to improve regeneration (Kehoe *et al.*, 2012). Regeneration occurs in hollow conduits via 5 different stages: A fluid phase, matrix phase, cellular migration phase, axonal phase and a myelination phase (W. Daly *et al.*, 2012). The proximal and distal nerve stumps are sutured, or adhered in place with fibrin glue, to each end of the nerve guidance conduit. Following implantation, a protein rich plasma exudate, containing neurotrophic growth factors and ECM molecules, is released via the nerve stumps into the conduit (W. Daly *et al.*, 2012; Kehoe *et al.*, 2012). A matrix of fibrin is formed between the proximal and distal ends of the nerve conduit, and after one week, a fibrin cable is formed between both ends of the conduit (W. Daly *et al.*, 2012). The fibrin cable provides a supporting ECM scaffold, which guides the migration of Schwann cells, fibroblasts, macrophages and endothelial cells from both the

proximal and distal nerve stumps (Kehoe *et al.*, 2012). The migrating Schwann cells align themselves to the fibrin cable and proliferate, forming the Bands of Bűngner' (W. Daly *et al.*, 2012). During the axonal phase, new axonal sprouts from the proximal stump use the fibrin cable and newly formed 'Bands of Bűngner' to cross the injury site and reach the distal nerve stump (Deumens *et al.*, 2010). During the cellular and axonal phases, the fibrin cable degrades away, during a 2 week period after formation (W. Daly *et al.*, 2012). Finally, during the myelination phase, Schwann cells forming the 'Bands of Bűngner' change phenotype, from a regenerative proliferative phase, to a more 'mature myelinating phenotype' after they adhere to the regenerating axons (Deumens *et al.*, 2010). Schwann cells then re-myelinate the regenerating axons to restore function to the nerve (J. H. Bell and Haycock, 2012). Due to the formation of the fibrin cable, the rate of nerve regeneration to occur through a hollow tube increases when compared to use of an autograft (Kehoe *et al.*, 2012). This is due to the presence of the 'basal lamina endoneurial tubes' and Schwann cells in the graft, providing neurotrophic factors for the regenerating axon (Belkas *et al.*, 2004b). Current research focuses on improving conduit designs and produce a nerve guide conduit comparable to the autograft (W. Daly *et al.*, 2012).

1.6 Improving Existing Hollow Nerve Guide Conduits

There are several approaches to improving existing current hollow nerve guide conduits. One approach is to change the material of the hollow nerve guide conduit altogether. Natural materials, as the outer tube structure, can be difficult to process, have weak mechanical properties, and can cause an immune response (J. H. Bell and Haycock, 2012). However, although the synthetic materials currently used in FDA approved conduits have shorter degradation times, the degradation rates cannot be controlled, they degrade into acidic product, provoke an immune response, and material mechanical properties change rapidly after implantation (W. Daly *et al.*, 2012). Due to issues with devices currently made from both natural and synthetic materials, further research on new materials, as well as blending natural and synthetic materials together is very much needed for peripheral nerve repair.

Due to the success of nerve guide conduits made from collagen, a lot of research is being done into using natural polymers, such as glycosaminoglycans and proteins. Fibrin, fibronectin, keratin, chitosan, silk, alginate and hyaluronic acid have all been studied (Arslantunali *et al.*, 2014b). The filling of hollow synthetic conduits with proteins, such as fibronectin, fibrin and laminin, has had success in bridging gaps of up to 18mm, improving their efficiency (Belkas *et al.*, 2004a). Mosahebi *et al.* (2003) were able to bridge gaps of 10mm using an alginate/fibronectin filled conduits. Silk fibroin is of interest in repairing peripheral nerve injuries due to its flexibility and desirable mechanical properties (B. N.

Johnson and Jia, 2016). Yang *et al.* (2007) have shown that silk is biocompatible and that it can bridge gaps of 10-13mm in rat sciatic nerve. More recently, Gu *et al.* (2014) have used silk in a scaffold with chitosan to bridge 10mm gaps in rat sciatic nerve. However, manufacturing natural polymers has many issues, due to the immunological responses they provoke. Researchers are currently blending natural polymers with synthetic polyesters to overcome this. Not only would the conduit have the excellent biocompatibility of the natural polymers, and similar mechanical properties to the native nerve, but a controlled degradation rate and the various forms of manufacture that synthetic polymers attract (Arslantunali *et al.*, 2014b). Natural polymers, such as collagen, have been blended with poly(lactic acid) (PLA), poly(glycolic acid) (PGA), poly(L-Lactic acid) (PLLA) poly(lactic acid-co-glycolic acid) (PLGA), poly(ε-caprolactone) (PCL) and poly(D,L-lactide-co-ε-caprolactone) (Baumann and Pham-Dinh, 2001). Yu *et al.* (2011) showed promising results with a collagen/polycaprolactone electrospun conduit bridging 8mm gaps in rat sciatic nerves, favouring control of the rate of degradation and the conduit maintaining its mechanical properties after 4 months (Wenwen Yu *et al.*, 2011). Oh *et al.* (2008) were able to produce porous nerve guide tubes from PLGA and pluronic F127. Pores, of approximately 50nm, were formed using immersion precipitation and a 10mm rat sciatic nerve gap was bridged, more successfully compared to tubes made from neat silicon and PLGA (Oh *et al.*, 2008). This study highlights that the efficiency of synthetic nerve guide tubes can be improved by the addition of pores in the structure. Research conduits have also been supplemented with additional Schwann cells, stem cells and growth factors such as vascular endothelial growth factor (VEGF) and nerve growth factor (NGF) (Kehoe *et al.*, 2012).

Other approaches at improving peripheral nerve repair using coatings include using extra cellular matrix proteins, such as collagen and laminin as coatings on synthetic materials to aid biocompatibility. Lee *et al.* (2006) coated a PLGA tube externally and internally with collagen. The internal collagen acted as a gel and successfully bridged a 15mm gap in rat sciatic nerve compared to a 'collagen- filled vein graft' (Doug-Youn Lee *et al.*, 2006). However, more recent advances have shown that using laminin as coating for nerve guide conduits if more efficient in bridging gaps than the other extracellular matrix proteins. Armstrong *et al.* (2007) concluded this as the laminin coated P(3HB) sheets had higher Schwann cell proliferation, compared to P(3HB) sheets coated with fibrin and collagen (Armstrong *et al.*, 2007). Surfaces of nerve guide conduits have been chemically modified using plasma polymerisation to improve cellular adhesion and biocompatibility. The coating of nerve guides with natural polymers, such as collagen and laminin can cause an immune response due to how they have been derived (Perry *et al.*, 1987). Therefore, using synthetic coatings, such as allylamine and acrylic acid, to deposit chemical groups onto the polymer

surface, should avoid this issue. Buttiglione *et al.* (2007) plasma coated Polyethylene terephthalate (PET) surfaces with plasma coatings, acrylic acid and allylamine, and cultured SH-SY5Y neuroblastoma cells onto the surfaces to analyse cell responses to the surface coatings (Buttiglione *et al.*, 2007). Acrylic acid, when fed into the gas line, coats the polymer surface with carboxylic groups, whereas allylamine will cause an increase in amino groups on the surface of the polymer (J. H. Bell and Haycock, 2012). It was concluded that the addition of the amine groups to the PET surfaces caused an increase in cell proliferation and cell attachment, and that the addition of the carboxyl groups onto the surface of the PET increased the cell number but more importantly the expression of the neurofilament-200 and led to an increase in cell differentiation (Buttiglione *et al.*, 2007).

Another strategy to improve current hollow tube nerve guide conduits is by changing the design of the conduit, to incorporate channels, microgrooves and pores to guide the regenerating axon and to allow nutrient transfer (W. Daly *et al.*, 2012). The manufacturing method used determines many factors in peripheral nerve repair such as the porosity of the conduit in allowing the exchange of nutrients needed for repair, as well as the internal topography of the tube which will aid in the guidance of the regenerating axon (J. H. Bell and Haycock, 2012). Nerve conduits have been fabricated, using natural materials, by injection moulding and crosslinking methods, using gelatin, hyaluronic acid, and collagen. Blends of alginate and chitosan, and PLA with chitosan have been fabricated into conduits by mandrel coating. Other methods include freeze drying and dip-coating (Biazar and Heidari Keshel, 2013). Nerve guide conduits using synthetic materials have already been manufactured using many different techniques, such as solvent casting, injection moulding with crosslinking, injection moulding, electrospinning and 3D printing.

3D printing has become a popular technique to manufacture NGCs for research purposes. Pateman *et al.* (2015) manufactured hollow NGCs from photocurable Polyethylene Glycol, using microstereolithography, and had success when implanting conduits into a 3mm gap injury model in thy-1-YFP-H mice (Pateman *et al.*, 2015). Nerve regeneration in PEG tubes was almost comparable with the autograft control, and the study highlighted the potential of stereolithography for the production of nerve guide conduits with 'intricate guidance structures' (Pateman *et al.*, 2015). Johnson *et al.* (2015) printed 3D bifurcating nerve graft pathway from Silicone using structured light scanning (SLS) (B. N. Johnson *et al.*, 2015). Alginate, PCL, PLGA and a gelatin methacrylate hydrogel can also be printed via structured light scanning, incorporating different 'geometries, physical cues, biological supplements and gradients' (B. N. Johnson and Jia, 2016). These studies highlight the moving approach towards to a more personalised and individual approach to nerve repair and treatment. Channels can also be manufactured into nerve guide conduits, to allow space for the nerve fascicles in the regenerating nerve and provide guidance (W. Daly *et al.*, 2012; Lowe and

Anderson, 2015). Yao *et al.* (2010) manufactured collagen conduits with 1, 4 and 7 channels, and investigated mechanical and physical properties compared to the FDA approved collagen conduit NeuraGen® (Li Yao *et al.*, 2010). The collagen in this study was crosslinked with 0–60mM (1-ethyl-3-(3-dimethylaminopropyl) carbodiimide [EDC] in N-hydroxysuccinimide [NHS]) to limit the degradation and swelling which are observed when implanting NeuraGen® conduits *in vivo* (Li Yao *et al.*, 2010; Kehoe *et al.*, 2012). Crosslinked collagen conduits had significantly decreased swelling, increased degradation rate and a lower compressive strength compared to NeuraGen® conduits (Li Yao *et al.*, 2010). The study also reported no difference in rat DRG neurite outgrowth on collagen films with the EDC and NHS crosslinkers, compared to plain collagen films, suggesting that the crosslinkers did not cause any toxic effects and improved the mechanical and physical properties of collagen (Li Yao *et al.*, 2010).

The incorporation of pores into nerve guide conduits is another approach to conduit design improvement (W. Daly *et al.*, 2012). As stated, nerve guide conduits must allow the transfer of nutrients and oxygen to the injury site, 'minimise the diffusion of growth factors' outside the conduit, but must restrict the penetration of inflammatory cells (Kehoe *et al.*, 2012). Jiang *et al.* (2010) reported that the ideal pore size for nerve guide conduits should be between 5 and 30µm, as 5µm pores prevents cell proliferation, and pore sizes above 30µm allows excessive inflammatory cell penetration to the injury site (Jiang *et al.*, 2010). Pores can be incorporated into nerve guide conduits in two ways: by using a porogen, such as salt or plastic porogen, or by emulsion templating. Yang *et al* (2005) incorporated pores using salt, into PLGA nerve conduits by gas foaming (Yang Yang *et al.*, 2005b). Mechanical properties of the conduits could be controlled by the percentage of porosity for the conduits, the addition of pores enhanced nerve regeneration, by stimulating neurite outgrowth (Yang Yang *et al.*, 2005b; Arslantunali *et al.*, 2014b). Pores can also be incorporated into nerve guides by emulsion templating and additive manufacturing methods, such as microstereolithography (D. W. Johnson *et al.*, 2013). Emulsion templating involves mixing two immiscible liquids, such as water and oil, in specific volume ratios (Owen *et al.*, 2016). High Internal Phase Emulsions (HIPEs) are produced when the internal phase volume ratio (ϕ) exceeds 0.7405 (D. W. Johnson *et al.*, 2013; Owen *et al.*, 2016). By combining emulsion templated with additive manufacturing methods, scaffolds can be fabricated with specific pore size geometry, interconnectivity, as well as controlled design architecture (Jin Woo Lee *et al.*, 2011; Cooperstein *et al.*, 2015). Johnson *et al.* (2013) confirmed that high internal phase emulsions could be printed into a number of different scaffold types, and shapes, using microstereolithography, and had success printing tubes for nerve repair (D. W. Johnson *et al.*, 2013).

Another approach to improving hollow tube design, and allowing nutrient transfer, is to use electrospinning to manufacture the outer conduit (W. Daly *et al.*, 2012). Electrospinning is a very versatile technique to manufacture polymer fibres, of varying orientation and diameter (Bhardwaj and Kundu, 2010). It is a popular technique in tissue engineering to fabricate fibrous scaffolds for many different applications such as skin and nerve tissue engineering (Bye *et al.*, 2012). Details of the electrospinning process will be described further on in this chapter. Biazar *et al.* (2013) manufactured nanofibrous PHBV electrospun tubes and successfully saw the reconstruction of the nerve trunk, and nerve fibres with myelination in a 30mm gap in a rat sciatic nerve injury model (Biazar and Heidari Keshel, 2013). Mohamadi *et al* (2017) manufactured PCL/collagen/nano-bioglass conduits by electrospinning, and demonstrated significantly increased human endometrial stem cell viability on the scaffolds, compared to a tissue culture plastic control (Mohamadi *et al.*, 2017). Huang *et al.* (2015) fabricated smooth and grooved cellulose acetate butyrates electrospun fibrous conduits and implanted in a 13mm gap rat sciatic nerve injury (Huang *et al.*, 2015). Overall, the grooved nanofibre conduits significantly improved nerve regeneration compared to the smooth fibre conduits, indicating the effect surface topography has on nerve regeneration (Huang *et al.*, 2015).

Electrospun fibres can also be incorporated into the lumen of a hollow nerve guide conduit to provide intraluminal guidance for the regenerating axon (J. H. Bell and Haycock, 2012). It has been suggested that the addition of aligned electrospun fibres, to hollow nerve guides, can be used to replace, or act as an additional anchor for the fibrin cable which is formed during nerve regeneration inside a hollow tube (W. Daly *et al.*, 2012). Intraluminal guidance scaffolds provide guidance for the regenerating axon, from the distal end to the proximal stump, and mimics the extracellular matrix fibrils, to increase Schwann cell adherence and migration along the fibres (Gupta *et al.*, 2009; W. Daly *et al.*, 2012). Electrospun fibre scaffolds have been investigated in nerve tissue engineering, by looking at two different variables: fibre alignment and fibre diameter.

Chew *et al.* (2008) reported that both aligned 1µm PCL fibres promoted a more mature Schwann cell phenotype, in which cells aligned and were elongated along the fibres, compared to random 1µm PCL fibres, where cells were more randomly orientated and less elongated (Chew *et al.*, 2008). By promoting a more mature Schwann cell phenotype, nerve regeneration could be increased *in vivo* (Jessen *et al.*, 2015). Prabhakaran *et al.* (2013) reported an increase in cell proliferation on aligned fibre PHBV scaffolds, showing 'biopolar extensions' along the fibres, compared to the phenotype morphology of Schwann cells adhered on randomly orientated PHBV fibres (Prabhakaran *et al.*, 2013) . Masaeli *et al.* (2013) blended PHBV with collagen, and PHB, and observed an increase in cell proliferation on the collagen scaffolds, as well as cell extensions aligning themselves with the aligned

fibrous scaffolds, compared to the random orientated fibre scaffolds (Masaeli *et al.*, 2013). These studies highlight that Schwann cells and neuronal cells can use aligned fibres as guidance cues to aid regeneration and that fibre alignment is crucial in effective peripheral nerve regeneration (Masaeli *et al.*, 2013).

Not only does fibre alignment aid in effective peripheral nerve repair but also the fibre size of the scaffold plays a significant role. The study by Daud *et al.* (2012) compared different fibre diameters of 1, 5 and 8µm aligned fibre scaffolds, and compared the responses of rat primary Schwann cells, dorsal root ganglion and neuronal cell line NG108-15 (Daud *et al.*, 2012). It was reported that cells cultured had an increase in the number of neurites present per neuron on 5µm scaffolds, compared to the other sizes, but that longer neurites were expressed on 8µm scaffolds. There was a significant increase of live cells on both the 5 and 8µm scaffolds, compared to the 1µm fibre scaffolds (Daud *et al.*, 2012). Gnavi *et al.* (2015) reported increased Schwann cell migration and axonal growth from DRG explants on 1µm and 1.3µm gelatine fibres, compared to 0.3µm and 0.6µm gelatine scaffolds (Gnavi *et al.*, 2015b). Wang *et al.* (2010) reported significantly higher neurite outgrowth from chick DRGs cultured on aligned 1.325 and 0.759µm PLLA fibres compared to the small 0.293µm PLLA fibres (H. B. Wang *et al.*, 2009). Not only do these studies highlight the importance of using DRG nerve injury modes, but also that both fibre size and alignment play an equal role in peripheral nerve repair.

1.7 Electrospinning

Electrospinning is a very replicable and simple technique to manufacture aligned and random fibres, with varying fibre diameters, using a range of different polymer, to manufacture scaffolds for a range of different applications (Bye *et al.*, 2012). In tissue engineering applications, fibrous electrospun scaffolds act as a platform to promote cellular attachment and proliferation by mimicking the extra cellular matrix (Bhardwaj and Kundu, 2010). Both natural and synthetic polymers can be fabricated into fibres via several different parameters to optimise on the electrospinning set up. These consist of:

- Molecular weight of the polymer
- Polymer concentration and viscosity of the solution
- The choice of solvent.
- The flow rate of the polymer solution
- Distance between the needle tip and the collector
- Speed of the collector
- Voltage of the power supply (Bhardwaj and Kundu, 2010)

A liquid polymer solution is dispelled from a needle tip which is attached to a power supply.

When an electric current is applied over a liquid droplet, electrostatic forces of repulsion overcome the surface tension of the liquid droplet and becomes stretched (Bhardwaj and Kundu, 2010). This becomes known as the 'Taylor Cone' and a charged jet of polymer solution is expelled from the cone and collected on a grounded collector, either a rotating mandrel (for aligned fibres) and a static collector (for randomly orientated fibres) (Pham *et al.*, 2006). The different parameters, above, are changed depending on the size of the fibres needed to be fabricated and the orientation of the fibres. Humidity and temperature of the surrounding environment can also be a factor when electrospinning fibres. However, these cannot always be controlled (Pham *et al.*, 2006). The type of solvent used to dissolve the polymer in, is a crucial step when electrospinning a polymer of interest. The properties of the polymer solution, such as molecular weight, viscosity and polymer solution, are all parameter to optimize when electrospinning (Bhardwaj and Kundu, 2010). The molecular weight of the polymer used can influence the solution properties, such as rheology and electrical conductivity. Fibres fabricated from low molecular weight polymers form beaded fibres, therefore, higher molecular weight polymers are used more commonly (Bhardwaj and Kundu, 2010). Viscosity and polymer concentration are also crucial parameters to observe when making solutions to be spun. Using a lower polymer concentration will have low viscosity, and can fabricate fibres in the nano-range, but if the concentration of the polymer is too low, fibres will not be formed from the 'Taylor' cone, instead electrospraying. If the polymer concentration of the solution is higher, the solution will be more viscous and thicker fibre diameters can be fabricated. However, if the polymer concentration is too high, the solution will be too viscous to spin, blocking the syringe (Pham *et al.*, 2006). Due to versatility of electrospinning, a number of different polymers have been investigated in nerve tissue engineering, as use in an electrospun nerve guide conduit, or as a intraluminal guidance scaffold, to replace the fibrin cable and improve nerve regeneration (W. Daly *et al.*, 2012).

1.8 Polyhydroxyalkanoates (PHAs)

Polyhydroxyalkanoates are a family of biocompatible and biodegradable thermoplastic bio-polyesters (Arslantunali *et al.*, 2014b). Polyhydroxyalkanoates are primarily an intracellular energy and carbon source for some bacteria and are synthesized under conditions with excess carbon and a limited concentration of a growth nutrients (oxygen, nitrogen, sulphur, magnesium and phosphorus) (Sang Yup Lee *et al.*, 1999). PHAs have excellent biocompatibility and degrade quickly into non-toxic by products (Sombatmankhong *et al.*, 2006). PHAs are classified as short chain length (SCL) and medium chain length (MCL) PHAs depending on the number of carbon atoms in the monomer unit (Basnett *et al.*, 2013). Short chain PHA monomers consist of 3–5 carbon atoms whereas medium chain PHAs

consist of 6–14 carbon atoms in their monomer unit (Philip *et al.*, 2007). Due to differences in their monomer units, the physical properties of short chain and medium chain PHAs can vary (L. R. Lizarraga-Valderrama *et al.*, 2016). MCL-PHAs have long aliphatic chains in their structure, and experience low melting temperatures, low crystallinity and are very elastomeric in nature (Basnett *et al.*, 2013). Due to a lower number of carbon atoms in the monomer, SCL-PHAs have high crystallinity, higher melting temperatures, and are more brittle in nature (Valappil *et al.*, 2006). Currently, poly(3-hydroxybutyrate) (PHB) and poly(3-hydroxybutyrate-co-3-hydroxyvalerate) (PHBV), polyhydroxyoctanoate (PHO) and polyhydroxyhexanoate (PHH) have been extensively researched as materials in tissue engineering applications (Arslantunali *et al.*, 2014b). PHAs are an attractive material in peripheral nerve repair, due to their natural origin, excellent biocompatibility and biodegradability (Arslantunali *et al.*, 2014b). PHAs degrade via surface erosion and hydrolytic degradation occurs via de-esterification (Assaf *et al.*, 2017). The products of polyhydroxyalkanoate degradation, such as D,L-hydroxybutyrate, are removed by metabolic pathways in the body (Assaf *et al.*, 2017). PHAs offer a range of bioactive polyesters with a wide range of different physical and mechanical properties and can be tailored for many applications in tissue engineering (Basnett *et al.*, 2013).
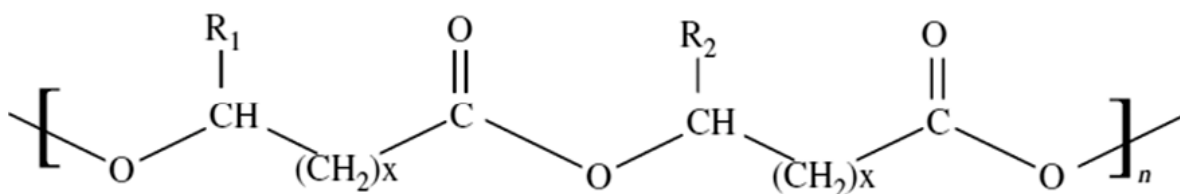
Figure 1. 2. The general structure of polyhydroxyalkanoates (PHA) (Akaraonye *et al.*, 2010; Basnett *et al.*, 2017).

1.9 Polyhydroxybutyrate P(3HB)

P(3HB) is an extensively researched material in nerve repair due to its excellent biocompatibility (Arslantunali *et al.*, 2014b). P(3HB) is a short chain polyhydroxyalkanoate and was first discovered in *Bacilus megaterium* but is now commonly produced in *Ralstonia eutropha, Alcaligenes latus* and *Bacillus cereus* using bacterial fermentation (Sang Yup Lee *et al.*, 1999). P(3HB) degrades and releases D,L-hydroxybutyrate (HB) which is a naturally occurring component in the blood and tissue (Zhao *et al.*, 2003). P(4HB) (poly(4-hydroxybutyrate) is the only PHA with FDA approval for its use as the suture material TephaFLEX® manufactured by Tepha Inc, which also produces surgical meshes (Ali and Jamil, 2016). As P(4HB) has FDA approval, the likelihood of P(3HB) getting FDA approval as a material in nerve guide tissue engineering has a high possibility. P(3HB) has been

investigated in nerve tissue engineering as a conduit material, and as an intraluminal guidance scaffold to improve regeneration. Young *et al.* (2002) bridged gaps of up to 40mm in rabbits using P(3HB) conduits but concluded that a hollow tube itself was not efficient enough to sustain optimal peripheral nerve regeneration (Young *et al.*, 2002). P(3HB) conduits have been used by Mosahebi *et al.* (2003) and were filled with an alginate/fibronectin filler to bridge gaps of 10mm in rat sciatic nerve which much more success (Mosahebi *et al.*, 2003). However, as a short chain PHA, P(3HB) is highly crystalline brittle material (Basnett *et al.*, 2013). Therefore, it is currently being blended with other polymers and medium chain polyhydroxyalkanoates, with more elastic properties, to change its mechanical properties (Philip *et al.*, 2007).
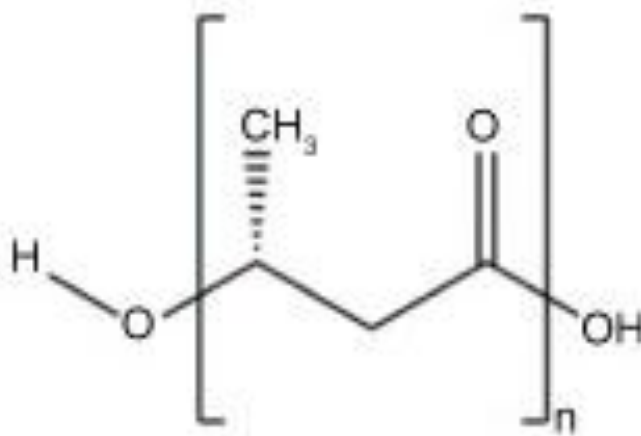
Figure 1. 3. The general structure of Polyhydroxybutyrate (P(3HB)) (Arslantunali *et al.*, 2014b).

1.10 Poly(3-hydroxybutyrate-co-3-hydroxyvalerate) (PHBV)

Poly(3-hydroxybutyrate-co-3-hydroxyvalerate) is a widely used copolymer of P(3HB) (Arslantunali *et al.*, 2014b). The incorporation of the 3-hydroxyvalerate monomer, in various ratios, into the poly(3-hydroxybutyrate) backbone causes an increase in chain flexibility and a decrease in the glass transition temperature (Zhao *et al.*, 2003). With a decrease to the melting temperature, PHBV is cheaper and quicker to produce and process, and its properties can be tailored, making it an excellent and very adaptable polymer for nerve tissue engineering and many other tissue engineering applications (Arslantunali *et al.*, 2014b). It has excellent biocompatibility and biodegradability, just like its counterparts, and is currently being investigated in many different biomedical applications, such as skin scaffolds and wound repair (Bye *et al.*, 2012). Karimi *et al.* (2014) have bridged a 30mm gap, in rat sciatic nerve, using a porous PHBV nerve guide conduit coated by oxygen plasma treatment to increase cell attachment (Karimi *et al.*, 2014). Results were compared to a PHBV tube with the addition of rat primary Schwann cells, hollow PHBV tube, autograft and control. The

tube was made by solvent casting PHBV films onto micro-patterned silicon wafers to add porosity, and after being implanted for 4 months, the sciatic trunk had regenerated and motor function was restored in all groups (Biazar and Heidari Keshel, 2013; Biazar and Keshel, 2013). There was no difference in the thickness of the reformed myelin sheath in the PHBV tube with Schwann cells and the autograft group, as well as no significant difference in motor and nociceptive recovery between the conduits and the autograft (Biazar and Keshel, 2013). This study shows the promising use of PHBV in nerve tissue engineering. Biazar *et al.* (2013) also bridged a rat sciatic nerve gap of 30mm using nanofibrous conduits made from PHBV electrospun random fibres, as well as a chitosan/PHBV electrospun fibres (Biazar and Heidari Keshel, 2013; Biazar and Keshel, 2013). The aligned fibres in the chitosan/PHBV conduits aided as guidance cues for the regenerating axon (Biazar and Keshel, 2013). PHBV is used in many regenerative medicine scaffolds, along with other synthetic polymers, and can be electrospun easily (Bye *et al.*, 2012).
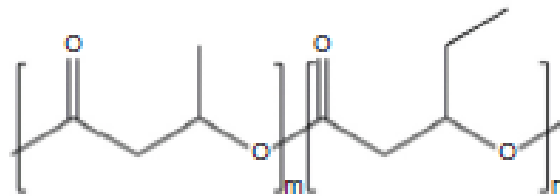
Figure 1.4. The general structure of Poly(3-hydroxybutyrate-co-3-hydroxyvalerate) (PHBV) (Arslantunali *et al.*, 2014b).

1.11 Poly(3-hydroxyoctanoate) P(3HO) and Poly(3-hydroxyoctanoate-co-3-hydroxydecanoate) P(3HO-co-3HD)

P(3HO) is a medium chain polyhydroxyalkanoate and is elastomeric in nature (Basnett *et al.*, 2013). P(3HO) is manufactured using *Pseudomonas putida, Pseudomonas oleovorans* and *Pseudomonas mendocina* using octanoate as its carbon source (Rai *et al.*, 2011). Due to its excellent elastomeric properties, P(3HO) is one the most researched medium chain PHAs (Bagdadi *et al.*, 2016). However, due to its 'low thermal stability and tensile strength' P(3HO) has yet to be investigated commercially (Basnett *et al.*, 2013). There is very little research using P(3HO) in nerve tissue engineering, but it is currently being investigated by blending it with P(3HB) to improve its biocompatibility, and improve the mechanical properties of P(3HB) (Lorena R. Lizarraga-Valderrama *et al.*, 2015). Lizarraga *et al.* (2015) have blended P(3HO) with P(3HB) in ratios of 25:75, 50:50 and 75:25 to investigate the effects of neuronal cell viability and maturation when cultured on the different PHA blends (Lorena R. Lizarraga-Valderrama *et al.*, 2015). P(3HO) has been investigated as a potential material in cardiovascular tissue engineering. Bagdadi *et al.* (2016) reported that P(3HO) supported the growth of cardiomyocytes, and the construct had similar mechanical properties to native

myocardial tissue (Bagdadi *et al.*, 2016). Basnett *et al.* (2013) has investigated P(3HO):P(3HB) blends of 80:20, 50:50 and 20:50 for their potential use in cardiovascular tissue engineering applications (Basnett *et al.*, 2013). P(3HO-co-3HD) is a co-polymer of P(3HO) and is manufactured by *Pseudomonas Mendocina* using glycerol, glucose, gluconate or 'biodiesel waste as the sole carbon source' (Basnett *et al.*, 2017). 3-hydroxydecanoate is the dominant monomer in the co-polymer and there are no studies that have investigated the use of P(3HO-co-3HD) in tissue engineering applications (Basnett *et al.*, 2017). It is a relatively novel co-polymer of P(3HO), but due to the elastomeric mechanical properties of P(3HO), is worth investigating for its potential use in peripheral nerve repair (Bagdadi *et al.*, 2016).
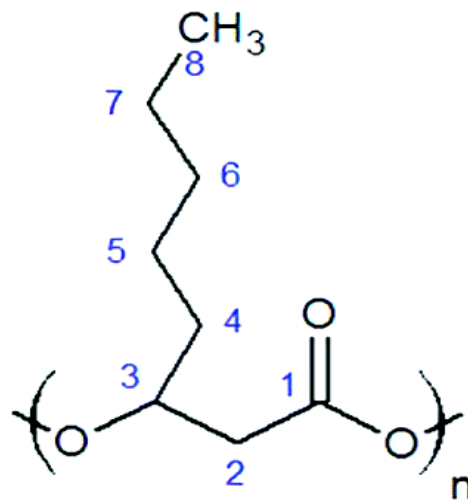
Figure 1.5. The general structure of Polyhydroxyoctanoate (P(3HO)) (Rai *et al.*, 2011).

1.12 Polycaprolactone (PCL)

Compared to natural polymers, biodegradable synthetic polymers, such as PCL, are frequently researched for applications nerve tissue engineering (Daud *et al.*, 2012). They offer mechanical stability, their properties can be tailored, and polymers can be processed via a number of different manufacturing methods. They are biocompatible and can be modified to increase cellular adhesion (Arslantunali *et al.*, 2014b). PCL is an aliphatic semi-crystalline polyester, which melts at 55-60°C and has a glass transition temperature of -54°C (Ulery *et al.*, 2011). Due to the presence of long aliphatic chains, PCL is relatively hydrophobic in nature, but experiences excellent elastomeric mechanical properties such as 'low tensile strength (~23 MPa) and a high elongation at break (470%)' (Ulery *et al.*, 2011). PCL is manufactured by polymerization of the 'cyclic monomer ε-caprolactone' (E Díaz *et al.*, 2014). PCL can degrade via enzymatic degradation, but most commonly degrades slowly via hydrolytic degradation, due to the stability of the ester bond in the polymer backbone (Ulery *et al.*, 2011). Degradation by products of PCL, succinic acid, valeric acid, and butyric acid

are non-toxic to the human body (Sanchez *et al.*, 2000; Kehoe *et al.*, 2012). Due to the long term degradation rate, PCL is an attractive material for use in long term medical devices, such as bone tissue engineering and long gap nerve injuries (Ulery *et al.*, 2011). PCL is used widely in nerve repair research and the co-polymer of PCL, Poly D,L lactide-co-carprolactone, is the material used to manufacture the FDA approved nerve conduit Neurolac® (Kehoe *et al.*, 2012). 20mm nerve gaps can be healed by Neurolac® conduits in 12 months of use, and the conduit takes up to 16 months to fully degrade (J. H. Bell and Haycock, 2012). However, reports have suggested that the Neurolac® conduits have high rigidity and are inflexible, causing neuroma formation and few myelinated fibres cross the nerve defect (Kehoe *et al.*, 2012). Therefore, several studies are investigating PCL in nerve repair by changing the degradation rate and improving mechanical properties. Assaf *et al.* (2017) recently reported the use of PCL membrane conduits with and without nano-particles of carbon and graphene (Assaf *et al.*, 2017). Conduits were implanted into a 4mm rat sciatic nerve injury model and all three conduit types supported the forming of the fibrin cable. However, the number of axons in the tube, and the area of the regenerated nerve significantly increased when using the PCL conduits with nanoparticles of carbon and graphene, compared to without and one type of nanoparticle each (Assaf *et al.*, 2017). The use of the hydrophobic PCL decreased the risk of tube encapsulation, and the addition of the carbon and graphene nanoparticles increased degradation rate and improved the chemical/mechanical properties of bulk PCL (Assaf *et al.*, 2017). Sun *et al.* fabricated PCL, sodium hydroxide treated PCL and PCL/PLA conduits. Significantly increased NG108-15 neuronal cell and primary Schwann cell adhesion was observed on the sodium hydroxide treated PCL films compared to the non-treated films (M. Sun *et al.*, 2009). *In vivo* testing showed after 2 weeks implantation, sodium hydroxide treated PCL conduits supported early nerve regeneration across the injury gap and nerve re-establishment with the distal stump (M. Sun *et al.*, 2009). This study highlights that hydrophobic PCL can be modified to experience more hydrophilic properties (M. Sun *et al.*, 2009).
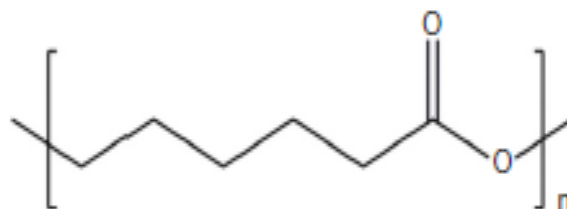
Figure 1.6. The general structure of Polycaprolactone (PCL) (Arslantunali *et al.*, 2014b).

1.13 Poly (l-lactic acid) PLLA

Another biodegradable polymer of choice for nerve repair is Poly (l-lactic acid) (PLLA) (Arslantunali *et al.*, 2014b). PLLA is an aliphatic polyester that degrades via bulk erosion by hydrolytic degradation (Ulery *et al.*, 2011). It is a highly crystalline polyester and is polymerized using lactic acid (Tokiwa and Calabia, 2007). PLLA has high mechanical properties, having a Youngs Modulus of 4.8 GPa (Ulery *et al.*, 2011). It has a melting temperature of 175°C and a glass transition temperature of 60-65°C (Ulery *et al.*, 2011). It has previously been reported that the addition of PLLA to other polymers, speeds up the degradation rate due to ester bond cleavage being a random process (Elsawy *et al.*, 2017). PLLA is hydrophobic in nature and acidic by products are released during degradation (Yoon *et al.*, 2017). PLLA is extensively research in nerve tissue engineering due to it degradation rate and biocompatibility (Arslantunali *et al.*, 2014b). It has been researched as a nerve guide conduit material, and as an intraluminal scaffold for nerve repair. The study by Evans *et al.* (1999) implanted porous PLLA conduits into a 10mm rat sciatic nerve injury (Evans *et al.*, 1999). Conduits were fabricated by solvent casting and extrusion, and pores were created by the addition of a salt porogen, which was leached before implantation (Evans *et al.*, 1999). Nerve fibre density, axon number and nerve area was comparable to that of an autograft and overall it was concluded that PLLA was a favourable scaffold material (Evans *et al.*, 1999). PLLA electrospun fibres have been fabricated by several different research groups to understand the importance of fibre alignment and fibre diameter with regards to improving nerve regeneration distances. Yang *et al.* (2005) fabricated random and aligned nano (300nm) and micro (1.5µm) electrospun PLLA fibres, and cultured Neonatal mouse cerebellum C17.2 stem cells onto scaffolds, to observe neurite outgrowth (F. Yang *et al.*, 2005a). Cells were observed to align themselves to the aligned fibres, where as they grew in a random orientation on the randomly orientated PLLA fibres. Neurite length was significantly higher from C17.2 cells cultured on the aligned PLLA microfibres compared to the other conditions (F. Yang *et al.*, 2005a). This study highlights the importance of both fibre diameter and alignment for designing and fabricating an intraluminal guidance scaffold. Although PLLA is a less favourable polyester for nerve repair, compared to PCL and PLGA, it is still highly researched due to its physical and mechanical properties (Arslantunali *et al.*, 2014b).
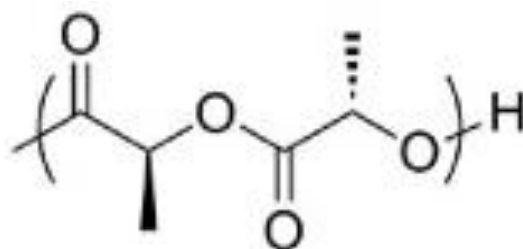
Figure 1.7. The general structure of Poly (l-lactic acid) (PLLA) (Gu and Shen, 2016).

1.14 Poly Lactic-co-Glycolic Acid (PLGA)

PLGA is another biodegradable polyester, which under investigation for use in peripheral nerve repair (Arslantunali *et al.*, 2014b). It is a co-polymer of both PLA and PGA and is formed via random copolymerization (Ulery *et al.*, 2011). Due to varying properties of both PLA and PGA, is an attractive biomaterial due to the tailoring of degradation rate, and mechanical and physical properties due to varying portions of both monomers. PGA is hydrophilic in nature, and highly crystalline, whereas PLA is more hydrophobic in nature, and semi crystalline (Gentile *et al.*, 2014). PGA has a high rate of degradation, whereas PLA is less susceptible to hydrolytic degradation due to the shielding effect from methyl side groups in its structure (Isabelle Vroman and Tighzert, 2009). PGA is currently used in the FDA approved nerve guide conduit Neurotube®, a woven mesh tube. Neurotube® has good initial mechanical properties, a quicker degradation rate than the Neurolac® tube, and has been comparable to an autograft in bridging 20mm defect gaps (Kehoe *et al.*, 2012). However, the acidic degradation products, high degradation rate and the loss of conduit stability long term remains the key issues with using the conduits. PLGA has had FDA approval for use as a suture material since 1974, a PLGA (10:90) braided suture Vicryl® (Ethicon), and most recently, Vicryl Rapide, which has a higher degradation rate (Ulery *et al.*, 2011). Due to FDA approval already, and attractive mechanical, degradation and physical properties, PLGA is currently being researched extensively for nerve tissue engineering applications. In the study by Oh *et al.* (2008) PLGA was mixed with the surfactant polyol F127, and tubes were manufactured by an immersion precipitation method. This method manufactured conduits with inner pores of 50nm and outer pores of 50µm (Oh *et al.*, 2008). Conduits were implanted into a 10mm gap defect in a rat sciatic injury model and after 24 weeks implantation, the diameter of myelinated axons and the thickness of the myelin sheath was significantly higher in PLGA-F127 tubes compared to the silicone control (Oh *et al.*, 2008). Shen *et al.* (2010) manufactured PLGA conduits by weaving cylindrical PLGA filaments. Conduits were then treated with oxygen plasma and coated with chitosan and ciliary neurotrophic factor (CNTF) to improve hydrophilicity and increase cellular attachment (Shen *et al.*, 2010). Conduits were then implanted into canine tibial defects of 25mm, for 3 months implantation. It was observed that the addition of the CNTF to PLGA/chitosan conduits increased nerve tissue percent, the average nerve fibre diameter and increased the thickness of the myelin sheath, compared to PLGA/chitosan conduits alone. The PLGA/chitosan conduits plus CNTF were comparable with the autograft control (Shen *et al.*, 2010). PLGA has also been fabricated into fibrous scaffolds to improve nerve regeneration by providing guidance for the regenerating axon. Bini *et al.* (2006) fabricated four different

PLGA scaffolds to be investigated: 'electrospun nanofibre scaffold, microbraided microfibre scaffold, aligned microfibre scaffold and PLGA polymer film'. C17.2 stem cells were seeded onto the different scaffolds and attached and adhered on all of them. C17.2 cells adhered in a random manner on the PLGA nanofibre scaffold and aligned onto the fibres in the case of the microbraided and aligned microfibre PLGA scaffolds (Bini *et al.*, 2004). Cellular adhesion was lower on the PLGA films, compared to the random nanofibre scaffolds due the porosity of the films, and the rougher topography of the fibres (Bini *et al.*, 2006). Overall, PLGA is an attractive material for nerve tissue engineering.
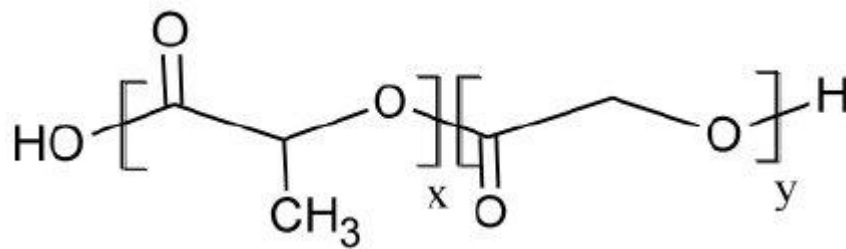
Figure 1. 8. The general structure of Poly Lactic-co-Glycolic Acid (PLGA) (Shabir *et al.*, 2011).

1.15 Aims and objectives

The main aim of this study was to develop and fabricate an aligned fibre intraluminal guidance scaffold, from a novel blend of Polyhydroxyalkanoates and FDA approved biodegradable polymers, to be used in conjunction with a nerve guide conduit. Polymer blends would be characterised for chemical, mechanical and physical properties before assessing fabricating of aligned fibres. Scaffolds would then be tested *in vitro,* using immortal cell lines and primary cells, before assessing fibres with an organotypic *ex vivo* DRG explant 3D culture model to determine which fibre material combination and diameter is assessed *in vivo*. It is hypothesised that the addition of electrospun aligned fibres to a hollow nerve guide conduit will increase nerve regeneration distance compared to a hollow tube. It is also hypothesised that using a blend of polymers, including polyhydroxyalkanoates, will support neuronal and Schwann cell adhesion and differentiation more effectively than using the FDA approved biodegradable polymers PCL, PLLA and PLGA. From the literature, it is hypothesised that fibre diameters of between 4-9µm will support neuronal cell differentiation more efficiently than fibre diameters which are smaller and larger. Other aims of this work was assessing the potential use of aminosilanes for use in peripheral nerve repair, and whether pressurized gyration could be used to manufacture aligned fibre scaffolds rather than using electrospinning. It is hypothesised that the addition

of aminosilanes to glass coverslips will improve neuronal and Schwann cell adhesion, and this technology could be applied to polymer NGCs.

The objectives of this study are:

- Characterise chosen polymers and choose most appropriate blends depending on mechanical, chemical and physical properties.
- Perform electrospinning of chosen polymers and novel polymer blends. Note electrospinning condition, reproducibility, fibre alignment and fibre diameter fabricated.
- Determine most efficient fibre diameter for nerve regeneration by performing in vitro analysis using NG108-15 neuronal cells and Schwann cells.
- Perform in vitro analysis of polymer blends with two different fibre diameters, using NG108-15 neuronal and Schwann cells in mono and co-culture, to assess which material blend should be taken forward to *ex vivo* organotypic culture.
- Determine which fibre diameter, and material blend, is the most effective in supporting DRG neurite outgrowth and Schwann cell migration by using a 3D organotypic *ex vivo* DRG culture system. Material blend that supports the furthest Schwann cell migration length and DRG neurite outgrowth length will be further investigated using *in vivo* testing externally.
- Investigate the potential use of aminosilanes in peripheral nerve repair applications. Characterise aminosilanes using WCA, AFM and XPS, and assess aminosilanes using *in vitro* analysis.
- Conduct analysis on PHA fibres manufactured by pressurised gyration, and whether this method could replace electrospinning to fabricate aligned polymer fibres.

Chapter 2: Materials for Peripheral Nerve Repair: Characterisation and Evaluation

2.1 Introduction

There are currently four FDA approved synthetic polymer nerve guide conduits (NGCs) available to treat nerve injuries: SaluTunnel™ and Nerve Protector™ (polyvinyl alcohol (PVA), Neurotube® (polyglycolic acid (PGA) and Neurolac® (polycaprolactone (PCL) (W. Daly *et al.*, 2012). Although NGCs manufactured from natural polymers, such as type 1 collagen (NeuraGen®) offer excellent biocompatibility, they lack the structural stability that synthetic polymers offer due to increased degradability, and unwanted immune responses due to batch variability (Kehoe *et al.*, 2012). Therefore, the use of synthetic polymers avoids these issues, due to the ability to tailor degradation rates, mechanical and physical properties, and ease of manufacturing conduits (Nectow *et al.*, 2012). Biocompatibility, and surface topography, of synthetic polymers can be also be modified to improve cellular adhesion via surface modification techniques such as plasma polymerisation (J. H. Bell and Haycock, 2012).

Material choice is critical when designing and manufacturing a successful nerve guide conduit. The conduit must be biocompatible, allow cellular adhesion, be biodegradable and not illicit an immune response (Arslantunali *et al.*, 2014a). The material must allow the exchange of nutrients in and waste products out of the conduit, be flexible and mimic the native nerve tissue, whilst maintaining its mechanical structure *in vivo* (Nectow *et al.*, 2012). Current research in nerve tissue engineering focuses on blending synthetic polymers with natural biopolymers to fabricate conduits with improved cellular adhesion, mechanical and physical properties (Arslantunali *et al.*, 2014b). However, natural biopolymers are expensive and difficult to manufacture into conduits using current techniques, such as injection moulding and casting. Therefore, using biocompatible synthetic polymers, such as polyhydroxyalkanoates (PHAs) can eliminate these concerns. Polyhydroxyalkanoates are synthetic storage polymers produced by a variety of bacterial species (Philip *et al.*, 2007). After production, PHAs are purified and bacterial endotoxin is removed. Due to their natural origin, PHAs are favourable in many tissue engineering applications such as skin, nerve and cardiac tissue engineering (Basnett *et al.*, 2013). PHAs have excellent biocompatibility, are biodegradable and P(4HB) has FDA approval for use as a suture material (Sombatmankhong *et al.*, 2006). PHAs can be tailored, to achieve the required mechanical and degradation properties for required applications and are cheaper to produce compared to natural biopolymers such as collagen (Arslantunali *et al.*, 2014b). Due to these properties,

PHAs are attractive materials to blend with other synthetic materials, and other PHAs for various tissue engineering applications.

When considering polymers for use in a blend for peripheral nerve repair, primary considerations of the materials involved are their mechanical properties, surface chemistry and topography (Nectow *et al.*, 2012). The ideal blend of materials should match, or be as close to, the mechanical properties of the native nerve, such as modulus and tensile strength, whilst maintaining structural integrity (W. Daly *et al.*, 2012). If the conduit/scaffold is brittle and stiff, the device will fail by causing compression to the regenerating nerve, limiting tissue inflammation, as seen in some cases for Neurolac® (Kehoe *et al.*, 2012). In the body, nerves are exposed to a number of different mechanical forces constantly, such as shear and compressive stresses (Topp and Boyd, 2006). Therefore, tensile testing was performed on all the polymers and polymer blends to confirm the Young's modulus, tensile strength and elongation at break. As well as mechanical properties, other physical properties of materials, for use in nerve tissue engineering should also be considered, such as the degradation prolife of the polymers, suturability, and the physical fit of the nerve in the conduit with regards to swelling after surgery (Nectow *et al.*, 2012).

The static sessile drop method was performed on all polymers and blends, to measure the water contact angle and determine surface wettability. Surfaces are deemed hydrophilic when the contact angle of the water droplet on a surface is less than 90° and indicates wettability, where as a high contact angle of above 90° indicates a hydrophobic nature (Basnett *et al.*, 2013). Cellular adhesion is increased on rougher surfaces compared to smooth surfaces, due to surface topography and hydrophilic nature (Lorena R. Lizarraga-Valderrama *et al.*, 2015). Fan *et al.* (2002) confirmed that significantly higher numbers of neuronal cells adhered to rough silicon surfaces compared to smooth silicon surfaces (Fan *et al.*, 2002). However, if a polymer exhibits a hydrophilic nature, this can indicate a quicker degradation rate due to increased hydrolytic degradation (E Díaz *et al.*, 2014).

Cell viability and cytotoxicity tests are also performed in material evaluation, to determine if any polymers cause neuronal cell toxicity. The choice of cell type for initial biocompatibility testing is the NG108-15 neuronal cell line, which is a mouse neuroblastoma and rat glioma hybrid cell line (Tsai *et al.*, 2005). Although NG108-15 neuronal cells do not mimic the regeneration rate of a regenerating axon *in vivo*, they are a well characterised cell line and have been used extensively in *in vitro* neuronal research (Armstrong *et al.*, 2007). Neurites outgrow from the cell bodies when serum is removed from cell medium, causing the cells to mature and differentiate (Daud *et al.*, 2012). Neurite lengths can be measured to determine

the effect the material type has on the differentiating neuronal cell line. Cell viability in this chapter was determined by performing the live/dead cell viability and an MTT assay.

In this chapter, a range of blends of synthetic biopolymers were characterised and evaluated for their potential as an intraluminal aligned scaffold for use in nerve repair.

Mechanical properties of known synthetic polymers, used or currently being investigated for their use in peripheral nerve repair, were recorded in to the table below. Mechanical properties of P(3HB), P(3HO), P(3HO-co-3HD) and PHBV were provided by Professor Ipsita Roy (The University of Westminster, U.K.) and properties of PLGA, PLLA and PCL were provided by Vornia Biomaterials Ltd (as part of the Neurimp FP7 project) (Basnett *et al.*, 2013).

Table 2.1. A table to show the mechanical properties of polymers to be investigated as blends in this chapter. Molecular weight was recorded.

Material	σ, MPa	$\varepsilon_{failure}$, %	E, MPa	Molecular Weight (kDa)	Supplier	Reference
P(3HB)	25.7 ± 0.5	3.8 ± 0.6	1700 ± 300	452	The University of Westminster	(Lorena R. Lizarraga-Valderrama *et al.*, 2015)
PLLA	11.3 ± 1.6	2.0 ± 0.4	990 ± 120	300	Vornia Biomaterials Ltd	(Bergström and Hayman, 2016)
PCL	9.65 ± 0.71	33 ± 6	170 ± 14	70-90	Vornia Biomaterials Ltd	(Eshraghi and Das, 2010)
P(3HO-co-3HD)	10.4 ± 1.0	440 ± 10	8.7 ± 1.1	350	The University of Westminster	(Basnett *et al.*, 2017)
P(3HO)	8.6 ± 3.8	1200 ± 200	0.8 ± 0.1	677	The University of Westminster	(Lorena R. Lizarraga-Valderrama *et al.*, 2015)
PLGA	1.8 ± 0.1	140 ± 20	30.5 ± 5.6	120	Vornia Biomaterials Ltd	(Leung *et al.*, 2008)
PHBV	26.9 ±	4.1 ±	1373 ±	410	Goodfellow Ltd	(Sombatmankhong *et al.*, 2006)
Rat Sciatic Nerve	1.4-2.7	50-80	0.57-0.58	n/a	n/a	(Borschel *et al.*, 2003)

From the mechanical data table (Table 2.1) six synthetic polymer blends were fabricated and then characterised to determine their physical and biological properties, and whether the blends could be used to improve nerve regeneration in a nerve guide conduit. From the table above, the Young's modulus of P(3HO) and P(3HO-co-3HD) are closest to the Young's modulus of native peripheral nerve. PCL has the closest percentage strain to the native nerve, whereas PLGA has the closest tensile strength 1.8 ± 0.1MPa, compared to 1.4-2.7MPa. Higher amounts of the elastomeric polymers, P(3HO) and P(3HO-co-3HD) were used in most of the blends in a ratio of 95:5 with a more brittle polymer (PCL, P(3HB) and PLLA). The use of PLGA in the blends was disregarded due to the excessive cost of the solvent used (more detail of this in chapter 3). Four of the six blends contained P(3HB) in varying amounts due to the excellent biological properties reported in literature (Lorena R. Lizarraga-Valderrama *et al.*, 2015). Overall, the final blends to be investigated were:

- P(3HO): P(3HB) (75:25)
- P(3HO): P(3HB) (50:50)
- P(3HO): P(3HB) (25:75)
- P(3HO-co-3HD): PLLA (95:5)
- P(3HO-co-3HD):PCL (95:5)
- P(3HO-co-3HD): P(3HB) (95:5)

The aims of this chapter is to characterise the mechanical and physical properties of FDA approved biodegradable polymers PCL, PLGA and PLLA, and polyhydroalkanoates P(3HB), P(3HO) and P(3HO-co-3HD), as well as the six investigated blends above. It is hypothesised that blends containing PHAs will support NG108-15 neuronal cell viability and support more metabolic active cells, than those blends not containing PHAs. It is also hypothesised that blends more elastomeric polymers, such as P(3HO), with more brittle polymers, such as P(3HB), will improve mechanical properties of the brittle polymers for soft tissue engineering applications.

2.2 Methods

2.2.1 Preparation of polymer films by spin coating

10 wt% solutions of the polymers, and their respective blends, were dissolved in a relevant solvent at room temperature overnight (1g of polymer in 9g of solvent). From the literature and previously published work, the polyhydroxyalkanoates and blends containing PHAs, were dissolved in chloroform, where as PLLA and PCL were dissolved in dichloromethane,

and PLGA was dissolved in Hexafluoroisopropanol (HFIP). Once the polymer/blend was dissolved, a 100μL of the solution was pipetted, using a syringe, onto a 13mm glass coverslip. The solution was spun at 100xg for 30 seconds under a vacuum of 25.5°C. Samples were left to dry overnight in a fume cupboard and were sterilised with 70% ethanol for 1 hour, and then washed with sterile PBS overnight before any cell culture.

2.2.2 Water contact angle measurement

Contact angles of the polymer films were measured using a Drop Shape Analysis DSA 100 System (Krűss Scientific). Briefly, flat polymer film samples were placed onto the platform and a 10μL droplet of water was introduced onto the film. A camera was then used to take an image of the water droplet, and the water contact angle measured. Three droplets of water were measured per film, in the middle and to both sides of each sample. Three samples were tested per material to produce an average value.

2.2.3 Mechanical testing of material blends

Mechanical testing of spin coated films, of the different polymer blend, was performed at three different establishments: The University of Westminster (U.K.), IK4-Tekniker (Eibar, Spain) and Vornia Biomaterials Ltd (Ireland). P(3HO):P(3HB) (25:75), (50:50) and (75:25) testing was performed at The University of Westminster using a Perkin Elmer Dynamic Mechanical Analyser 7 (Norwalk, USA) and by the methodology published by Lizarraga *et al.* (Lorena R. Lizarraga-Valderrama *et al.*, 2015). Polymer films were mechanically tested in a dry environment and the Young's modulus, ultimate tensile strength, and elongation at break was calculated from the data provided.

2.2.4 NG108-15 neuronal cell culture

NG108-15 neuronal cell culture was performed as per the methods in Daud *et al.* (2012). NG108-15 neuronal cells, supplied from the European Collection of Cell Cultures (ECACC), were used between passages 11-20 for experiments. NG108 cells were grown in Dulbecco's Modified Eagle Medium (DMEM) containing 10% foetal calf serum, 1% penicillin / streptomycin, 1% glutamine and 0.5% amphotericin B at 37°C in a humidified atmosphere with 5% CO_2. 40,000 cells were seeded onto polymer films in a 24 well plate in 2mL of Dulbecco's Modified Eagles Medium (DMEM) containing 10% foetal calf serum, 1% penicillin/streptomycin, 1% glutamine and 0.5% amphotericin B, incubated at 37°C in a humidified atmosphere with 5% CO_2 for 7 days. After 48 hours, culture medium was

replaced with serum free Dulbecco's Modified Eagles Medium (DMEM) containing 1% glutamine, 1% penicillin/streptomycin and 0.5% amphotericin B to induce neuronal cell differentiation. Samples were incubated at 37˚C in a humidified atmosphere with 5% CO_2 and the culture medium replaced every 2-3 days (Daud *et al.*, 2012).

2.2.5 Cell viability using an MTT assay

40,000 NG108-15 neuronal cells were seeded onto the different polymers and polymer, and left in culture for 7 days. Cell viability was determined for each polymer/blend at 4 different time points (24 hours, days 3, 5 and 7) using an MTT (3,4,5-dimethylthiazol-2,5-diphenyl tetrazolium bromide) assay. Briefly, old culture medium was removed from the wells and the samples were washed in sterile PBS for 5 minutes. 1mL of MTT solution (0.5mg/mL in PBS) was then added to each sample and incubated for 60 minutes at 37°C. The solution was then aspirated using a pipette and 600μL of acidified isopropanol was added to each sample. Samples were incubated at room temperature for 15 minutes to allow for the colour change from the MTT reduction (due to 3D nature of the polymer films). The mixture was aspirated again, and three aliquots of 200μL of acidified isopropanol was placed into a 96 well plate. Optical density was read using a BIO-TEK ELx 800 microplate reader set at wavelengths of 540nm and referenced at 630nm.

2.2.6 Live/Dead analysis of NG108-15 neuronal cell line on PHA blends

Live/dead analysis was performed as per the methods in Daud *et al*. Live/dead analysis was conducted to determine cell viability and number of live cells versus dead cells. Briefly, old medium was removed from samples and fresh serum-free DMEM, containing 0.001% Syto-9 (Invitrogen) and 0.0015% propidium iodide (Invitrogen), was introduced to cells (Daud *et al.*, 2012). Samples were incubated at 37˚C and 5% CO_2 for 30 minutes. After a wash in PBS, cells were imaged using an upright Zeiss LSM 510 confocal microscope. An argon ion laser was used to visualise live cells stained with Syto-9 (λex = 494 nm / λem = 515 nm) and a helium-neon laser for dead cells stained with propidium iodide (λex = 536 nm / λem = 617 nm). Three fields of view were imaged per sample and results calculated by cell numbers (live versus dead cells) and by live / dead cells as percentages per polymer sample type. Cells were counted using the ITCN Cell counter plugin on Image J NIH software (Usaj *et al.*, 2010; Schneider *et al.*, 2012).

2.2.7 Statistical Analysis

GraphPad Instat (GraphPad Software, USA) was used to perform statistical tests on data collected. One way analysis of variance ($p < 0.05$) was conducted to analyse the differences between the data, with a Tukey's multiple comparisons test to compare statistical differences between samples. Data was reported as mean ± SD, $p<0.05$. Each experiment was performed three independent times with each sample repeated three times as $n=3$.

2.3 Results

2.3.1 Water contact angles of polymers and PHA blends

Polymer surfaces were assessed to determine surface wettability, and hydrophobic / hydrophilic characteristics, by measuring the water contact angle. Figure 2.1A shows the water contact angles recorded for the polymers, before specific polymer blends were decided. Overall, PCL, P(3HB) and PHBV had a significantly lower water contact angle, compared to the other polymers, indicating a more hydrophilic nature and high wettability. PLLA, PLGA, P(3HO), P(3HO-co-3HD) and P(3HO-co-3HD-co-3HDD) all recorded water contact angles below 90° indicating that all the polymers were hydrophilic. Water contact angles of PCL, PHBV and P(3HB) were 72 ± 2.12°, 67.22 ± 2.73° and 74 ± 1.05°, compared to the other polymers, PLLA, PLGA, P(3HO), and P(3HO-co-3HD), which were 87.93 ± 5.19°, 86.27 ± 6.36°, 80.44 ± 3.57° and 83.4 ± 3.57° respectively.

When comparing the six polymer blends, P(3HO):P(3HB) (75:25) and P(3HO-co-3HD):PLLA (95:5) had contact angles of above 90° (91.11 ± 3.69° and 94.44 ± 3.57°) indicating low wettability and a hydrophobic nature, due to the long aliphatic chains present in P(3HO) and P(3HO-co-3HD), as well as a higher number of carbon atoms in their structure (Rai *et al.*, 2011; Lorena R. Lizarraga-Valderrama *et al.*, 2015). Contact angles of the PHA blends containing higher amounts of P(3HB) had lower water contact angles compared to the other blends, due to the four carbon atoms in the P(3HB) polymer, compared to the eight carbons in the P(3HO) (Rai *et al.*, 2011; Basnett *et al.*, 2013). Although four of the six blends were hydrophilic, and had higher surface wettability, no significant difference was detected between all six blends. Overall, P(3HO):P(3HB) (25:75) had the lowest water contact angle and therefore the most hydrophilic.
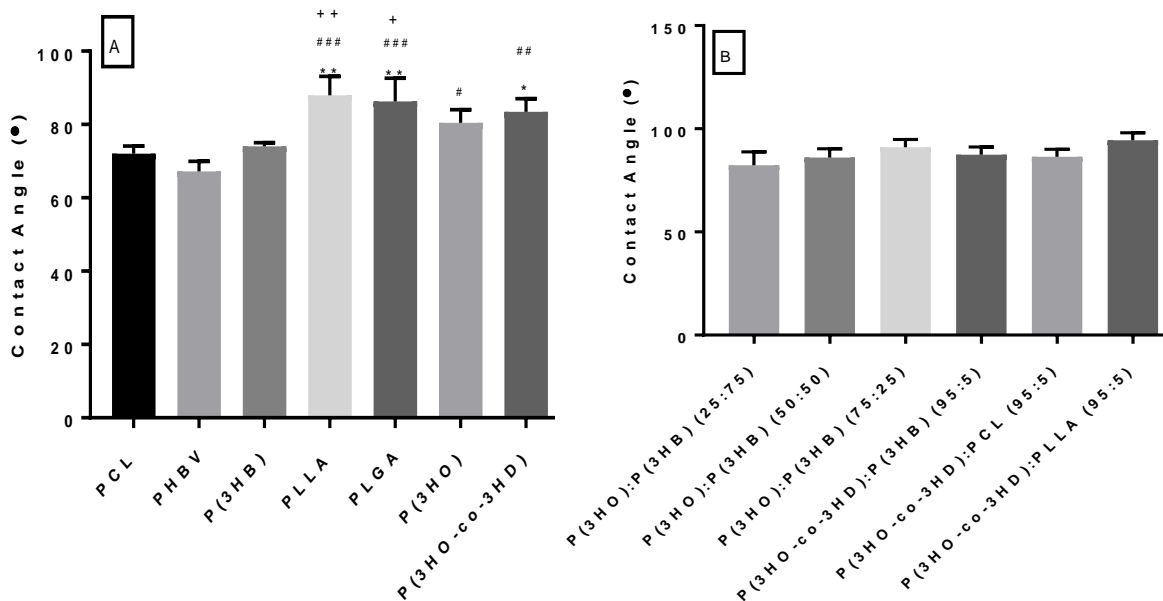
Figure 2.1. Graphs to show water contact angles of A) polymers and B) polymer blends. PCL, PHBV and P(3HB) had a significantly lower water contact that the other polymers. A one way anova withTukey's multiple comparisons tests was used to analyse data (mean ± SD, n= 3 independently fabricated samples, *p < 0.05 and **p < 0.01 compared to PCL, #p < 0.05, ##p < 0.01 and ###p < 0.001 compared to PHBV and +p < 0.05 and ++p < 0.01 compared to P(3HB). No significant differences were detected between the polymer blends.

2.3.2 Mechanical characterisation of PHA blends

From mechanical data confirmed in table 2.1, the investigated blends were spin coated to produce a polymer blend that would be closest to the mechanical properties of native peripheral nerve. Blends containing high amounts of P(3HO) and P(3HO-co-3HD) were chosen due the low Young's modulus and elastomeric properties (Rai *et al.*, 2011). Blends were also chosen to contain different amounts of P(3HB) due to its excellent biological properties (Chen and Wu, 2005). Mechanical testing of P(3HO):P(3HB) (25:75), (50:50) and (75:25) was performed at The University of Westminster. Mechanical testing of P(3HO-co-3HD) blends was performed at Vornia Biomaterials Ltd, part of the Neurimp project, and provided to me. Figure 4 shows that blends containing high amounts of P(3HO) and P(3HO-co-3HD) had a low Young's modulus, with the modulus of P(3HO): P(3HB) (75:25), the tensile strength and percentage strain, being closest to that of native rat sciatic nerve of 0.57-0.58 MPa, 1.4-2.7 MPa, and 50-80% strain (Borschel *et al.*, 2003). Blends containing higher amounts of P(3HB) had a higher Young's modulus due to the brittle nature of the short chain PHA and the high degree of crystallinity (Philip *et al.*, 2007). This data suggests that P(3HO):P(3HB) (75:25) would be the most suitable blend for nerve regeneration based solely on its mechanical properties

Table 2.2. A table to show the mechanical properties of the 6 PHA blends, being investigated for use in nerve tissue engineering. Data was provided from The University of Westminster and Vornia Biomaterials Ltd. Published data from (Lorena R. Lizarraga-Valderrama *et al.*, 2015).

Material	σ, MPa	$\varepsilon_{failure}$, %	E, MPa	Reference
P(3HO): P(3HB) (75:25)	0.71 ± 0.08	73.82 ± 18.08	1.25 ± 0.18	Published data provided from Neurimp project
P(3HO): P(3HB) (50:50)	2.2 ± 0.91	94 ± 4.50	21.83 ± 1.0	Published data provided from Neurimp project
P(3HO): P(3HB) (25:75)	17.8 ± 0.82	41 ± 2.10	143.4 ± 2.06	Published data provided from Neurimp project
P(3HO-co-3HD): PLLA (95:5)	7.75 ± 0.35	320 ± 3.05	4.85 ± 0.70	Unpublished data provided from Neurimp project
P(3HO-co-3HD) :PCL (95:5)	6.35 ± 0.25	335 ± 1.23	3.13 ± 1.23	Unpublished data provided from Neurimp project
P(3HO-co-3HD): P(3HB) (95:5)	10.0 ± 0.91	350 ± 4.05	9.9 ± 1.4	Data provided from Neurimp project

2.3.3 Cell viability of NG108-15 neuronal cells on PHA blends using MTT assay

To initially assess cell viability, an MTT assay was performed at culture times of 24, 72, 120 and 168 hours on all the individual polymers, and the six investigated polymer blends. No significant differences were detected at a given time point between polymers, indicating similarly metabolically active cells. At 72 hours and 168 hours, cell viability was significantly higher on TCP control, compared to the polymer samples. Of note, cell viability increased on all polymer samples over time, suggesting all polymers supported cell attachment and proliferation.

With regards to the investigated polymer blends, no significant difference was detected between samples at 24 hours and 168 hours in culture. However, at 72 hours and 120 hours, cell viability was significantly higher on P(3HO):P(3HB) blends, compared to the P(3HO-co-3HD) blends with P(3HB), PCL and PLLA. This indicated that higher amounts of viable, metabolically active cells attached to these materials. However, after 168 hours in culture, no significant difference was detected between the six polymer blends, although

viability was higher on the P(3HO):P(3HB) blend. Cell viability and cell metabolic activity increased on all six blends over time, indicating that all polymer blends supported viable cell attachment and proliferation in culture. Overall, the P(3HO):P(3HB) blends were the most effective at supporting cellular adhesion and proliferation.
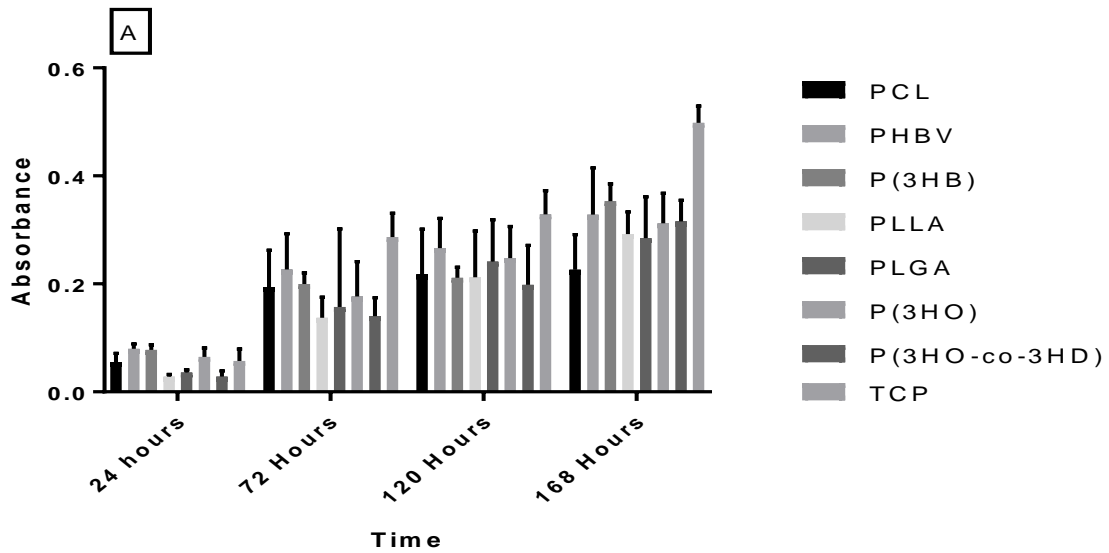
B)

Time (Hours)	Comparison Test	Significant?	Summary	Adjusted P Value
72	PLLA vs. TCP	Yes	*	0.0341
72	P(3HO-co-3HD) vs. TCP	Yes	*	0.0412
168	PCL vs. TCP	Yes	****	<0.0001
168	PHBV vs. TCP	Yes	**	0.0094
168	P(3HB) vs. TCP	Yes	*	0.045
168	PLLA vs. TCP	Yes	***	0.0007
168	PLGA vs. TCP	Yes	***	0.0004
168	P(3HO) vs. TCP	Yes	**	0.0032
168	P(3HO-co-3HD) vs. TCP	Yes	**	0.004

C
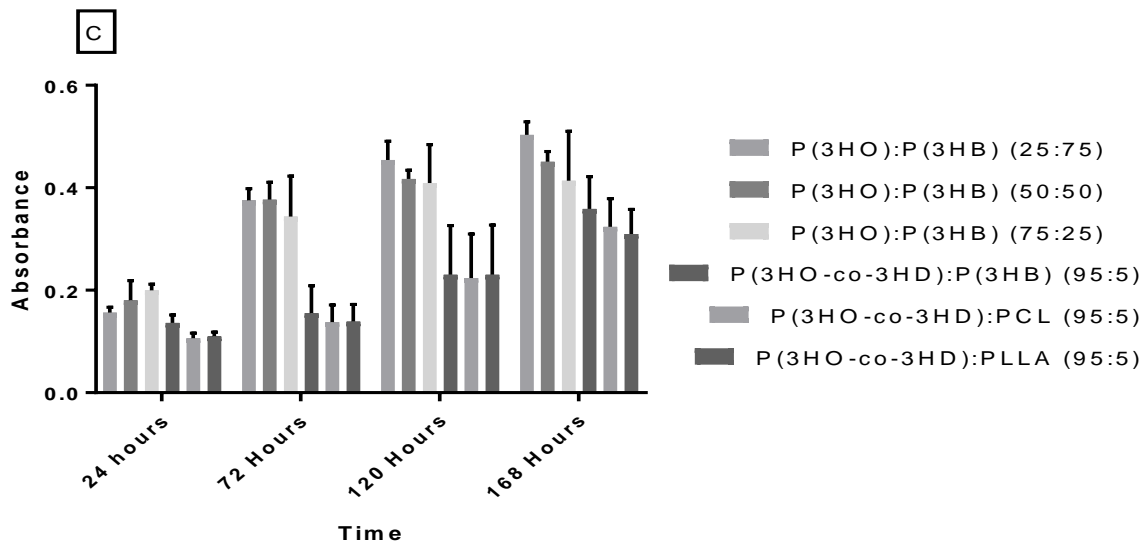
D)

Time (Hours)	Comparison Test	Significant?	Summary	Adjusted P Value
72	P(3HO):P(3HB) (25:75) vs. P(3HO-co-3HD):P(3HB) (95:5)	Yes	****	<0.0001
72	P(3HO):P(3HB) (25:75) vs. P(3HO-co-3HD):PCL (95:5)	Yes	****	<0.0001
72	P(3HO):P(3HB) (25:75) vs. P(3HO-co-3HD):PLLA (95:5)	Yes	****	<0.0001
72	P(3HO):P(3HB) (50:50) vs. P(3HO-co-3HD):P(3HB) (95:5)	Yes	****	<0.0001
72	P(3HO):P(3HB) (50:50) vs. P(3HO-co-3HD):PCL (95:5)	Yes	****	<0.0001
72	P(3HO):P(3HB) (50:50) vs. P(3HO-co-3HD):PLLA (95:5)	Yes	****	<0.0001
72	P(3HO):P(3HB) (75:25) vs. P(3HO-co-3HD):P(3HB) (95:5)	Yes	***	0.0009
72	P(3HO):P(3HB) (75:25) vs. P(3HO-co-3HD):PCL (95:5)	Yes	***	0.0003
72	P(3HO):P(3HB) (75:25) vs. P(3HO-co-3HD):PLLA (95:5)	Yes	***	0.0003
120	P(3HO):P(3HB) (25:75) vs. P(3HO-co-3HD):P(3HB) (95:5)	Yes	****	<0.0001
120	P(3HO):P(3HB) (25:75) vs. P(3HO-co-3HD):PCL (95:5)	Yes	****	<0.0001
120	P(3HO):P(3HB) (25:75) vs. P(3HO-co-3HD):PLLA (95:5)	Yes	****	<0.0001
120	P(3HO):P(3HB) (50:50) vs. P(3HO-co-3HD):P(3HB) (95:5)	Yes	**	0.001
120	P(3HO):P(3HB) (50:50) vs. P(3HO-co-3HD):PCL (95:5)	Yes	***	0.0007
120	P(3HO):P(3HB) (50:50) vs. P(3HO-co-3HD):PLLA (95:5)	Yes	**	0.0011
120	P(3HO):P(3HB) (75:25) vs. P(3HO-co-3HD):P(3HB) (95:5)	Yes	**	0.0019
120	P(3HO):P(3HB) (75:25) vs. P(3HO-co-3HD):PCL (95:5)	Yes	**	0.0012
120	P(3HO):P(3HB) (75:25) vs. P(3HO-co-	Yes	**	0.0019

	3HD):PLLA (95:5)			
168	P(3HO):P(3HB) (25:75) vs. P(3HO-co-3HD):P(3HB) (95:5)	Yes	*	0.019
168	P(3HO):P(3HB) (25:75) vs. P(3HO-co-3HD):PCL (95:5)	Yes	**	0.0018
168	P(3HO):P(3HB) (25:75) vs. P(3HO-co-3HD):PLLA (95:5)	Yes	***	0.0007
168	P(3HO):P(3HB) (50:50) vs. P(3HO-co-3HD):PLLA (95:5)	Yes	*	0.0242

Figure 2.2. A) NG108-15 neuronal cell viability (MTT absorbance) when grown on individual polymer substrates. Cell viability was determined at 24, 72, 120 and 168 hours. B) Statistics shown for A) in table. .A two way anova with Tukey's multiple comparisons tests was used to analyse data (mean ± SD, n= 3 independently fabricated samples, *p < 0.05, **p < 0.01, ***p < 0.001 and ****p < 0.0001.) C) NG108-15 neuronal cell viability (MTT absorbance) when grown on polymer blends. Cell viability was determined at 24, 72, 120 and 168 hours. D) Table to show the statistics from figure 2.2C. . A two way anova withTukey's multiple comparisons tests was used to analyse data (mean ± SD, n= 3 independently fabricated samples, *p < 0.05, **p < 0.01, ***p < 0.001 and ****p < 0.000. 1)

2.3.4 Live/Dead analysis of NG108-15 neuronal cell line on polymer films

Cells were labelled with 0.001% Syto-9 (Invitrogen) and 0.0015% propidium iodide (Invitrogen) to visualise cell location, live and dead cells on each surface. Figure 2.3 shows confocal micrograph taken of NG108-15 neuronal cells cultured on the polymer films. The highest number of live cells was seen on PCL, PHBV, P(3HB) and P(3HO) (figure 2.3A, B, C and F), respectively. Lower numbers of cells were visualised on PLLA, PLGA and P(3HO-co-3HD) films. Confocal images were then quantified to determine the number of live and dead samples per field of view, as well as cell viability.
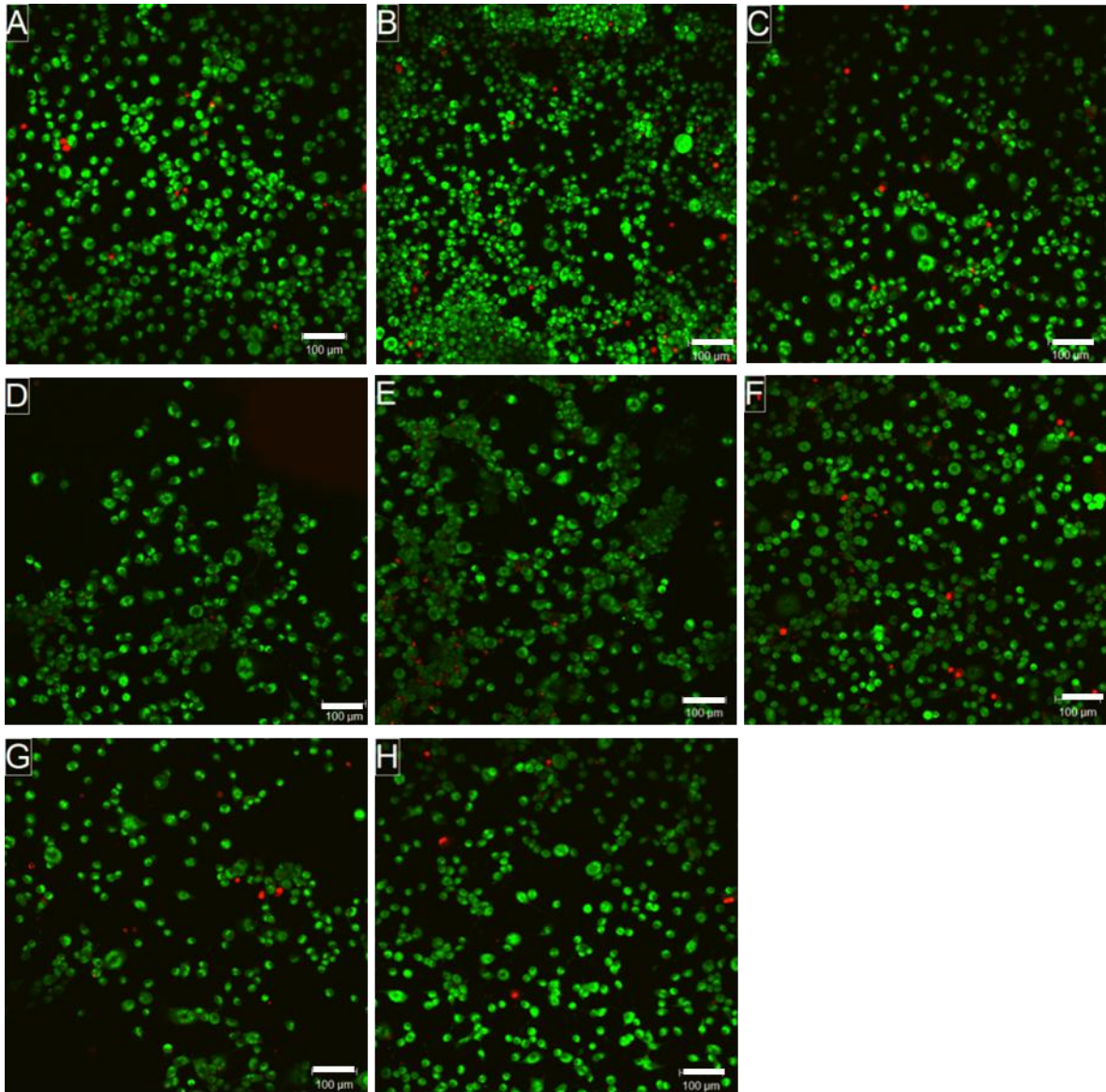
Figure 2.3. Confocal micrographs of A) PCL, B) PHBV, C) P(3HB), D) PLLA, E) PLGA, F) P(3HO), G) P(3HO-co-3HD) films and H) TCP control. Cells were labelled with Syto-9 (green stain for live cells) and propidium iodide (red stain for dead cells). Scale bar = 100µm.

Figure 2.5. A) Live/dead analysis of NG108-15 neuronal cells cultured on polymer films expressed as the average total number of live versus dead cells. A one way anova with Tukey's multiple comparisons tests was used to analyse data (mean ± SD, n=3 independent experiments, **p < 0.01, ***p < 0.001 and ****p < 0.0001 compared to PHBV, +p < 0.05 compared to P(3HB) and #p < 0.05 compared to TCP). B) Percentage cell viability was calculated (mean ± SD n=3 independent experiments, no significant differences were seen).

Micrographs from figure 2.3 were quantified and confirmed that the highest number of live cells was on PHBV and P(3HB), followed by PCL (660.67 ± 128.65 cells, 509.67 ± 124.59 cells and 501.89 ± 118.09 cells). The number of live cells on PHBV and P(3HB) films was significantly higher than those cultured on PLLA, PLGA and P(3HO-co-3HD) films, suggesting that presence of P(3HB) in both polymers correlated with an increase in NG108-15 neuronal cell adhesion and proliferation. The largest number of dead cells was seen on the PHBV films (45.96 ± 14.36 cells), most likely due to the highest total number of cells. No significant differences were detected indicating that all the polymer films supported NG108-15 neuronal cell attachment and proliferation. Overall, PHBV and P(3HB) were effective at supporting higher levels of cell adhesion.

2.3.5 Live/Dead analysis of NG108-15 neuronal cell line on investigated polymer blends

Confocal micrographs were taken of each sample, to determine cell viability. Higher numbers of live cells could be seen on P(3HO):P(3HB) (25:75), (50:50) and (75:25) (figures 2.4.A, B and C respectively). Lower numbers of live cells were visualised on P(3HO-co-3HD) blends. Higher numbers of dead cells were visualised on the P(3HO):P(3HB) (25:75) and the P(3HO-co-3HD):P(3HB) (95:5) blends. Confocal images quantified to determine the number of live and dead samples per field of view, as well as cell viability.
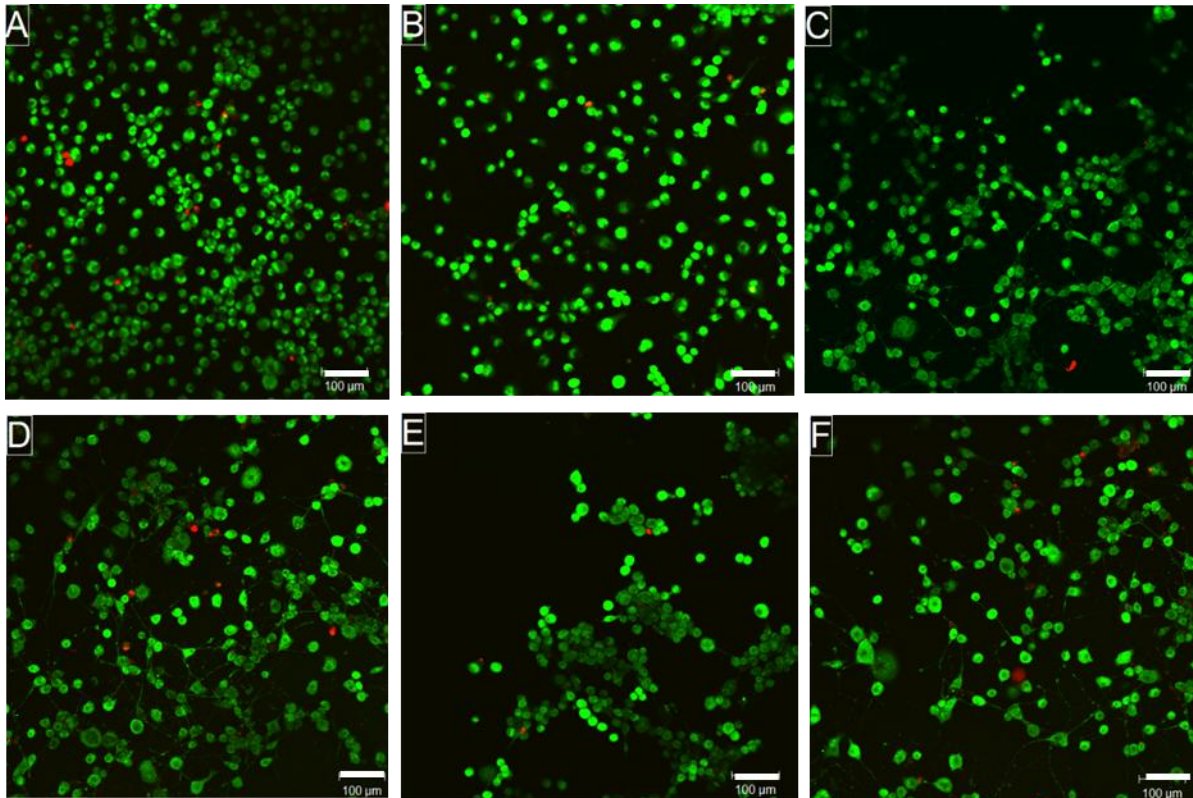
Figure 2.4. Confocal micrographs of NG108-15 neuronal cells cultured on A) P(3HO):P(3HB) (25:75), B) P(3HO):P(3HB) (50:50), C) P(3HO):P(3HB) (75:25), D) P(3HO-co-3HD):P(3HB) (95:5), E) P(3HO-co-3HD):PLLA (95:5) and F) P(3HO-co-3HD):PCL (95:5) films. Cells were labelled with Syto-9 / propidium iodide. Scale bar = 100μm.

The highest numbers of live cells were observed on P(3HO):P(3HB) (25:75) and (50:50) films, 456 ± 50.67 cells and 423.03 ± 57.69 cells respectively. The highest number of dead cells were observed on the P(3HO):P(3HB) (75:25) and P(3HO-co-3HD):PLLA films, (23.14 ± 9.29 cells and 22.33 ± 11.71 cells). Blends containing considerable amounts of P(3HB) had higher numbers of live cells, indicating increased cellular adhesion and proliferation. Out of the blends containing considerable amounts of P(3HO-co-3HD) (figure 8D-F), P(3HO-co-3HD):P(3HB) (95:5) supported higher amounts of NG108-15 neuronal cell adhesion and proliferation. The number of live cells cultured on P(3HO):P(3HB) (25:75) was significantly higher than the number of live cells cultured on the P(3HO-co-3HD):PLLA (95:5) blend, but no other statistical differences were detected between the other polymer blends. Live cell number did increase as the amount of P(3HB) increased in the blends. Figure 2.5 illustrates that all blends supported cell viability above 90%, indicating that all were biocompatible.
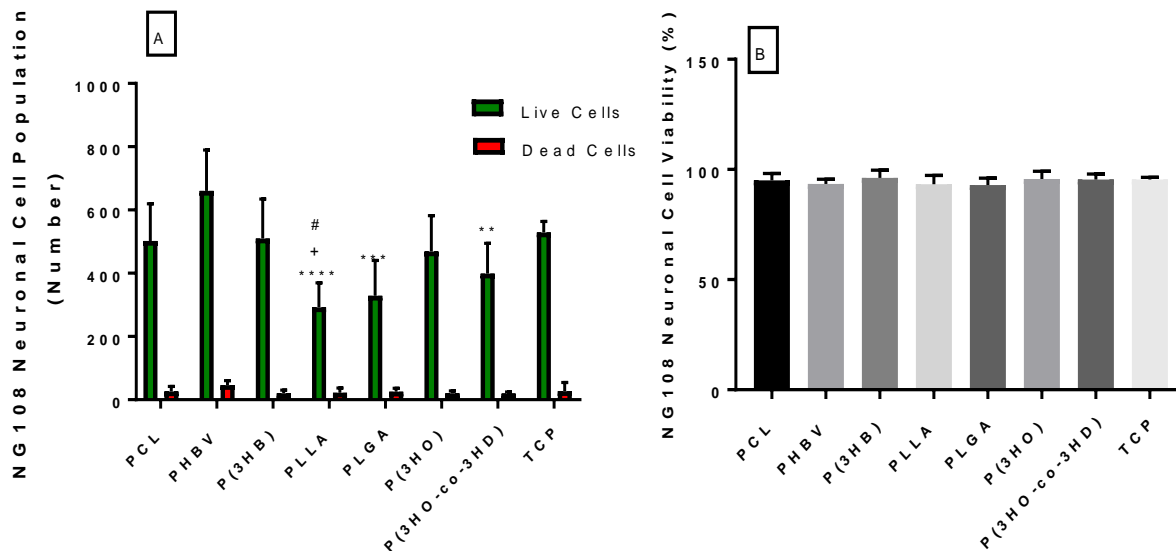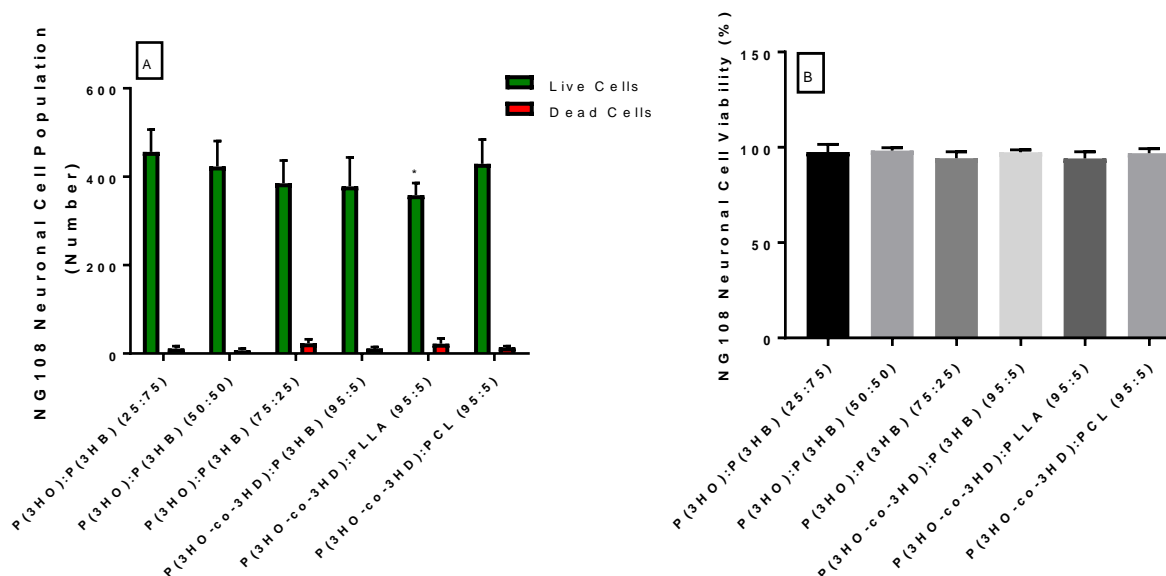
Figure 2.5. A) Live/dead analysis of NG108-15 neuronal cells cultured on a range of polymer films expressed as A) the average total number of live versus dead cells and B) percentage cell viability. A one way anova withTukey's multiple comparisons tests was used to analyse data (mean ± SD, n=3 independent experiments, *p < 0.05 compared to P(3HO):P(3HB) (25:75).

2.4 Discussion

The aims of this chapter was to form blends of biodegradable polymers currently being investigated in peripheral nerve research, and characterise polymer blends to determine, if any, had potential for use as an intraluminal aligned fibre guidance scaffold to improve nerve regeneration length. Mechanical properties, surface characteristics and cytotoxicity of seven different polymers were analysed. Mechanical properties shown in table 2.1 were provided by polymer suppliers, and from this data, six different polymer blends were characterised for their potential as a scaffold substrate. Polymer films were produced by spin coating a 10wt% of each in chloroform, DCM or HFIP, according to the literature. Water contact analysis confirmed that all the polymers were hydrophilic, with contact water angles below 90°. Water contact angles of PCL, P(3HB) and PHBV were significantly lower than the other polymers investigated. P(3HO) and P(3HO-co-3HD) are well known hydrophobic polymers due to the presence of long aliphatic chains in their structure, compared to PHBV and P(3HB) (Lorena R. Lizarraga-Valderrama *et al.*, 2015). PLLA and PLGA are linear aliphatic polyesters, which also display hydrophobic surface characteristics (Xiao L *et al.*, 2012). When blending PHAs together, and with PLLA and PCL, the water contact angle increased. The high contact angle for P(3HO) was in agreement with that reported in the literature (Basnett *et al*; 2013), which gives a high water contact angle that decreased with the addition of hydrophilic P(3HB). Overall, the increase of the amount of P(3HB) blended with P(3HO) decreased the water contact angle, which was also observed by (Lorena R. Lizarraga-Valderrama *et al.*, 2015).

It was hypothesised that blending softer elastomeric polymers with more brittle polymers would improve the mechanical properties of the more brittle polymer. Mechanical properties of the polymers were provided by the manufacturers and six blends of polymers investigated for potential as intraluminal fibrous scaffolds. P(3HO) and P(3HO-co-3HD) had the lowest Young's moduli, close to that of native rat sciatic nerve (at 0.5MPa). Therefore, these elastomeric polymers were incorporated into polymers blends. It has previously been reported that P(3HB) has excellent biocompatibility and is a commonly researched material for nerve repair (Arslantunali *et al.*, 2014b). Therefore, varying amounts of P(3HB) were incorporated into blends with P(3HO). Both PLLA and PCL are used in nerve guide conduits, and have FDA approval (Kehoe *et al.*, 2012). However, due to both polymers having a high Young's modulus, 0.05wt% of the polymers were incorporated into the blends. Although PLGA had a lower Young's modulus than PCL, PLLA, PHBV or P(3HB), and a tensile strength close to rat sciatic nerve, it was disregarded from the blends. This was due to the excessive cost of the HFIP solvent used to dissolve the polymer, as well as the lower Young's modulus of P(3HO) and P(3HO-co-3HD). Mechanical properties of P(3HO):P(3HB) blends have previously been reported by Lizarraga *et al.* (2015). Young's modulus of the blends increased as the amount of P(3HB) increased (from 25:75 to 75:25) due to the brittleness of P(3HB) and the elastomeric nature of P(3HO) (Lorena R. Lizarraga-Valderrama *et al.*, 2015). Mechanical properties of P(3HO-co-3HD) blends with P(3HB), PLLA and PCL were investigated and provided by The University of Westminster, as part of the Neurimp (FP7) project. P(3HO-co-3HD):PCL (95:5) had the lowest Young's modulus compared to P(3HO-co-3HD):PLLA (95:5) and P(3HO-co-3HD):P(3HB) (95:5), which corresponds to the data in table 2.1, in which PCL had the lowest Young's modulus compared to PLLA and P(3HB). This was also supported by the literature as P(3HB) and PLLA are well known brittle polymers, compared to PCL (Misra *et al.*, 2006; Bergström and Hayman, 2016). Overall, this data would suggest that the P(3HO-co-3HD) blends would be an effective material of choice for the fibre scaffold, due to having favourable mechanical properties.

An MTT assay and live/dead assay was performed to determine NG108-15 neuronal cell viability and metabolic activity when cultured on the different polymer blends. Each polymer investigated has a different chemical structure, and the material composition, such as charge, determines which proteins, in the cell culture medium, are initially adsorbed (Schmidt *et al.*, 2009). However, over time, proteins that have a lower affinity to the polymer surface can replace proteins that have a higher affinity to the surface, and this competitive protein exchange is known as the Vroman effect (L. E. O. Vroman, 1987). Cells adhere to the proteins absorbed on the polymer surface via cell-adhesion molecules, and so which

proteins and the amount of protein absorbed on the polymer surface plays a crucial role in initial cell adhesion events, proliferation and cell survival (Curran *et al.*, 2006). It was hypothesised that all polymer blends containing PHAs would support NG108-15 neuronal cell viability and metabolic activity more efficiently compared to those blends that did not contain PHAs. All polymer films supported viable NG108-15 neuronal cell growth after seven days in culture, and cell viability increased when grown on each polymer over 7 days in culture. Overall, cell viability was significantly higher on the tissue culture plastic control, compared to the polymer films. There was an increase in cell viability on the P(3HO):P(3HB) blends, compared to the P(3HO-co-3HD) blends, indicating an increase in viable cell attachment and proliferation after 24 hours. However, at days 3 and 7, cell viability was higher on the P(3HO):P(3HB) blends, compared to the P(3HO-co-3HD) blends, indicating that the P(3HO):P(3HB) blends supported increased neuronal cell metabolism and proliferation after 3 days in culture.

Cell viability of NG108-15 neuronal cells cultured on polymers and polymer blends was also assessed by a live/dead assay, which uses Syto-9 and propidium iodide to bind and label live and dead cells respectively. Syto-9 exhibits enhanced fluorescence when it binds to nuclei acids of cells with intact cell membranes, whereas propidium iodide binds to DNA but cannot pass across the plasma membrane of intact cells (Stiefel *et al.*, 2015; Crowley *et al.*, 2016). However, when both dyes are used in the assay, propidium iodide can be co-visualised in dead cells (Stiefel *et al.*, 2015). With regards to the polymers, there was a significantly higher number of live cells on PHBV and P(3HB) films compared to P(3HO-co-3HD), PLLA and PLGA films. It has previously been reported that P(3HB) and its co-polymer PHBV have excellent biocompatibility (Scandola *et al.*, 1997). This is due to the presence of 3-hydroxy butyric acid monomers, found in both polymers, being a product of cell metabolism and found naturally in the blood in low concentrations (Verlinden *et al.*, 2007). The increase in live cell numbers on the PHBV and P(3HB) could also be explained by an increase in protein adsorption, indicating that these polymer films have a rougher surface topography that the other polymers indicated. It is well known that surface topography and roughness improves and increases protein adsorption, due to a large surface area, and therefore cellular adhesion (Anselme *et al.*, 2010). This has been confirmed by Misra *et al.* (2010) in which the addition of Bioglass particles to P(3HB) films increase surface roughness and increased total protein adsorption (Misra *et al.*, 2010). Figure 2.1A confirmed that PCL, P(3HB) and PHBV were hydrophilic compared to the other polymers. Interesting, it has been reported that hydrophilic surfaces 'adsorb a lower quantity of proteins' compared to hydrophobic surfaces, and that the proteins adsorbed do not go under any conformational changes, which occurs on hydrophobic surfaces (Anselme *et al.*, 2010). However, the study

by Basnett *et al.*(2013) reported that increasing surface roughness, and hydrophilicity, increased protein adsorption on blends of P(3HB) and P(3HO) (Basnett *et al.*, 2013).

With regards to the polymer blends, the number of live cells was significantly higher on the P(3HO):P(3HB) (25:75) blend than the P(3HO-co-3HD):PLLA (95:5) blend. No other significant differences were detected between samples. Interestingly, live NG108-15 neuronal cell number decreased as the concentration of P(3HB) in the blend decreased. This observation was also reported by Basnett *et al.* (2013) and Lizarraga *et al.* (2015). Basnett *et al.* (2013) reported that human microvascular endothelial (HMEC-1) cell viability was higher on P(3HO):P(3HB) 20:80 blends compared to 50:50 and 80:20 blends (Basnett *et al.*, 2013). Lizarraga *et al.* (2015) reported a significant increase of live NG108-15 neuronal cell attachment on the P(3HO):P(3HB) 25:75 and 50:50 blends compared to the 75:25 blend. Both studies also report the decrease in water contact angle as the amount of P(3HB) increases, due to the presence of long aliphatic chains in P(3HO) causing its hydrophobic nature. However, water contact angles was similar for all of the investigated blends, and live NG108-15 neuronal cells attached to the all the investigated blends was similar. Basnett *et al.* (2013) also reported the addition of P(3HB) to P(3HO) increased surface roughness, and increased protein adsorption which could explain the significant difference in live cell adherence between the P(3HO):P(3HB) (25:27) and P(3HO-co-3HD):PLLA (95:5) blend (Basnett *et al.*, 2013). PLLA and P(3HO) are reported to be smooth materials (Hai Li *et al.*, 2012). Further work, characterising the surface topography of the blends, and protein absorption studies would clarify this. Overall, cytotoxicity analysis of the investigated blends would suggest that the P(3HO):P(3HB) blends, of all the polymers investigated, would be the most effective at supporting NG108-15 neuronal cell attachment and proliferation and would be considered more biocompatible.

Future work for this chapter would include using techniques, such as SEM and AFM to characterise surface roughness, to explain the increase live adhered cells on P(3HB) and PHBV films. Protein absorption studies would also be performed to understand the mechanisms of initial cellular adhesion on the polymer films in more detail.

In summary, this chapter investigated the mechanical and surface properties of six potential new blends of PHAs for their use as potential intraluminal nerve scaffolds. Overall, P(3HO-co-3HD) blends had the closest mechanical properties to native nerve, having a similar Youngs modulus and tensile strength. However, work in this chapter reports that the P(3HO):P(3HB) blends supported neuronal cell attachment and proliferation more effectively, and that these blends should be considered as lead materials. Therefore, these six blends were taken forward (in chapter 3), to assess whether they could be electrospun

into aligned micro-fibre scaffolds, considering physical properties such as fibre diameter (assessed in chapter 4), before *in vitro* and *ex vivo* analysis thereafter.

Chapter 3: Fabrication of Electrospun Fibres from Material Blends

3.1 Introduction

Electrospinning is becoming a commonplace, scalable and versatile technique used in many different areas of tissue engineering (Bye *et al.*, 2012). The technique is used to fabricate micrometer and nanometer sized aligned and random fibres, for use in many different applications (Bhardwaj and Kundu, 2010). It is commonly used to fabricate 3D tissue engineered scaffolds, a temporary scaffold to mimic the extra cellular matrix and promote cell attachment whilst the tissue repairs and regenerates (Pham *et al.*, 2006). When an electric charge is applied over a polymer droplet, the droplet stretches, to form a 'Taylor Cone' (Y. S. Lee and Arinzeh, 2011). A charged jet of polymer solution is then expelled from the 'Taylor Cone' forming a fibre (Bhardwaj and Kundu, 2010). Many different polymers can be fabricated into fibres by electrospinning, and there are many different variables associated with electrospinning to fabricate polymer fibres of different size and orientation (Pham *et al.*, 2006). These include:

• 	Polymer concentration and molecular weight

• 	The flow rate of the polymer solution

• 	Distance between the needle tip and the collector

• 	Speed of the collector

• 	Voltage of the power supply

Polymer fibres are collected on an electrically conducting surface such as tin foil which is attached to either a rotating metal drum, to form aligned fibres, or onto a static collector, usually to fabricate random fibres (Y. S. Lee and Arinzeh, 2011). Random and aligned fibres, varying in diameter, are used for specific applications in tissue engineering due to differences in cell responses from fibre alignment and orientation, as well as fibre diameter (Sill and von Recum, 2008). Randomly orientated nanofibre scaffolds, with varying diameter, are commonly used in areas of soft tissue engineering, such as skin tissue engineering (James *et al.*, 2011). Nanofibre meshes are ideal for applications like wound healing, due to having a large surface area, high porosity and varying pore size. These features on the scaffold allow for nutrient permeability, as well as preventing any fluid buildup, preventing infection and rejection of the scaffold (X. Wang *et al.*, 2013). A wide range of biomaterials have been fabricated into meshes for skin tissue engineering applications, but the most commonly used synthetic materials used are PLLA, PLGA and PCL (Sheila MacNeil, 2008).

These materials are used in many different areas of skin tissue engineering, such as wound repair, oral and buccal tissue engineering, and pelvic floor scaffolds (S. MacNeil *et al.*, 2011; Roman *et al.*, 2016). Research in skin tissue engineering primarily focuses on improving angiogenesis, as well as fabricated drug releasing scaffolds (Hearnden *et al.*, 2012; Gigliobianco *et al.*, 2015).

Aligned fibre scaffolds of varying diameter, are commonly used in areas of tissue engineering where the ECM of the regenerating tissue is highly complex, structured and orientated (Sill and von Recum, 2008). By mimicking the precise architecture of the ECM, aligned fibre scaffolds can be used in many different applications of tissue engineering, from cardiovascular tissue engineering to nerve tissue engineering (X. Wang *et al.*, 2013).

Aligned fibre scaffolds can be used in cardiovascular tissue engineering, as the fibres can mimic ECM collagen fibres found in the ventricular myocardium (Engelmayr *et al.*, 2008). Yu *et al.* (2014) fabricated functionalized PLGA fibre scaffolds with N-acetyl- GRGDSPGYG (RGD), and N-acetyl-GYIGSRGYG (YIGSR) peptides, as well as laminin, to improve bioactivity of PLGA fibres for cardiomyocyte culture, for use in engineered cardiac constructs (J. Yu *et al.*, 2014). Both random and aligned fibres were fabricated for the study, in which cardiomyocytes cultured on the aligned fibres, extended along the direction of the fibre, and contracted along the direction of the fibres. Positive staining of F-actin and α-actin was more intense on aligned fibres, compared to random fibres, suggesting an increase in focal adhesions formed from cardiomyocytes cultured on aligned fibres (J. Yu *et al.*, 2014). Kai *et al.* (2011) came to the same conclusions culturing cardiomyocytes on both random and aligned fibres made with PCL and PCL/Gelatin (50:50) in which cardiomyocytes orientated themselves to the aligned fibres, and there was increased expression of F-actin and α-actin (Prabhakaran *et al.*, 2012). Cell alignment to aligned fibres can also be seen when culturing smooth muscle cells and skeletal muscle cells. Gia *et al.* (2014) observed orientated morphology of smooth muscle cells cultured on aligned electrospun polyurethane fibres and polyurethane/collagen aligned fibres, compared to their random counterparts (Jia *et al.*, 2014). Higher expression of smooth muscle actin α and myosin heavy chain proteins was observed on the aligned fibres, compared to the random fibres. Similarly, skeletal muscle cells, C2C12 murine myoblasts, were able to attach, align and then elongate on aligned PLGA fibres in the study by (Aviss *et al.*, 2010). Myotube formation, on random and aligned PLGA fibres, was also confirmed by the expression of fast myosin heavy chain sarcomeric protein, in which higher expression was observed on the aligned fibres, as well as myotubes aligning to the fibres, confirming myoblast differentiation (Aviss *et al.*, 2010). Overall, electrospun aligned fibres provide the correct topography for morphogenesis to occur in skeletal muscle cells, by mimicking the 'anisotropic structural organisation' of the ECM and

myofibrils (Qazi *et al.*, 2015). Similarly with smooth muscle tissue, alignment of the cells is crucial for 'controlling the constriction of blood vessels' (Jia *et al.*, 2014). Therefore, attachment and alignment of smooth muscle cells to aligned fibre scaffolds will promote vascular tissue repair and regeneration (Jia *et al.*, 2014).

Contact guidance exhibited by cells cultured on aligned fibres is of particular advantage with regards to nerve tissue engineering (X. Wang *et al.*, 2013). This is due to the effect that the scaffold material, and fibre alignment, can have on both Schwann cell attachment and elongation, as well as on neuronal cell attachment, differentiation and neurite outgrowth length (Y. S. Lee and Arinzeh, 2011). Schwann cell attachment and alignment is crucial for peripheral nerve repair, as Schwann cells provide guidance to the regenerating axon and as well as myelinate the regenerating nerve (Deumens *et al.*, 2010). Aligned fibre scaffolds are used, in nerve tissue engineering, to mimic the 'Bands of Büngner', the ECM formed by Schwann cells and endoneurial tubes of the distal stump during Wallerian degeneration, to provide guidance cues to the regenerating axon (Pfister *et al.*, 2011). The study by Chew *et al.* (2008) confirmed that electrospun aligned and random fibre scaffolds provided contact guidance for human Schwann cells, in which Schwann cells aligned and elongated along aligned fibres, whereas on random fibres, cells were more randomly orientated, and less elongated (Chew *et al.*, 2008). As well as changes in cell morphology, aligned fibres also promote a more mature Schwann cell phenotype, compared to random fibres, in which PO expression was significantly increased (Chew *et al.*, 2008). Gupta *et al.* (2009) also reported the alignment and elongation of Schwann cells attached to aligned fibres, compared to randomly orientated fibres, in which Schwann cells were clustered, orientating in different directions (Gupta *et al.*, 2009). By promoting a mature Schwann cell phenotype, nerve regeneration *in vivo* could be increased by incorporating electrospun fibres into a nerve guide conduit (Jessen *et al.*, 2015).

As well as influencing Schwann cell alignment and attachment, the orientation of fibre scaffolds, for use in nerve tissue engineering, also influences neuronal cells. Corey *et al.* (2007) cultured SH-EP and SH-SY5Y human neuroblastoma cell lines as well as primary rat dorsal root ganglia explants, onto PLLA aligned and random nanofibre scaffolds (Corey *et al.*, 2007). SH-EP and SH-SY5Y neuroblastoma cells were observed to attach and orientate to the aligned fibres, in which actin fibres were observed aligned to the PLLA fibres. Neurite outgrowth of Dorsal root ganglia explants was 20% longer on the aligned nanofibre scaffolds, compared to the random orientated fibre scaffolds. Schwann cell migration from dorsal root ganglion explants was also observed, in which Schwann cells were seen to attach and elongate along the direction of the fibres (Corey *et al.*, 2007). Prabhakaran *et al.*

(2013) also reported the alignment of PC12 cells to aligned PHBV/collagen fibres, compared to random PHBV/collagen fibres, in which NF200 expression was also higher on aligned fibre scaffolds (Prabhakaran *et al.*, 2013). Most recently, the same effect was observed by Hu *et al.* (2017) in which β III tubulin expression of differentiated adipose-derived mesenchymal stem cells cultured on aligned PHBV nanofibres was significantly higher than those cells cultured on randomly orientated PHBV fibres (F. Hu *et al.*, 2017).

Several studies report that Schwann cells, primary neuronal cells, and human neuroblastoma cell lines attach, proliferate and differentiate more efficiently on aligned fibre scaffolds, than randomly orientated fibre scaffold in vitro. Kim *et al.* (2008) reported that neurite outgrowth and Schwann cell migration, from dorsal root ganglion explants, was increased on aligned poly(acrylonitrile-co-methylacrylate) fibres, compared to randomly orientated fibres (Kim *et al.*, 2008). Both randomly and aligned poly(acrylonitrile-co-methylacrylate) fibres were then placed into polysulfone nerve guide conduits, and implanted for 16 weeks, before undergoing behavioral tests, electrophysiology testing and immunohistochemical analysis at the end of the experiment. Overall, aligned poly(acrylonitrile-co-methylacrylate) fibres incorporated in the NGC promoted the successful regeneration of axons 'across a 17 mm nerve gap, reinnervating muscles, and reforming new neuromuscular junctions' compared to the random fibres which did not promote any regeneration (Kim *et al.*, 2008). This study confirms that fibre alignment is a crucial factor for designing an electrospun internal scaffold for use in a nerve guide conduit. The alignment of the fibres is crucial for Schwann cell attachment and maturation, but also to provide guidance for the regenerating axon and Schwann cells (Daud *et al.*, 2012).
In this chapter, solutions of individual materials, as well as blends of materials, were electrospun, to investigate whether the material blend could be electrospun, to investigate if fibres were aligned, and what diameters could be fabricated. To begin with, individual polymers were electrospun to determine the correct conditions to fabricate aligned fibres with specific diameters. The polymers used in this chapter included PLGA, PLLA, PCL and a range of polyhydroxyalkanoates. Diameters from 1-10μm were fabricated for each material.

The objectives of this chapter, is to electrospin the polymers and investigated blends characterized in chapter 2. It is hypothesized that the more brittle polymers, such as PCL, PLLA etc can be electrospun, as seen in the literature, but that the more elastomeric polymers, such as P(3HO) will need to be blended with a more brittle polymer to allow for successful electrospinning. To determine fibre diameter, scanning electron microscopy was used to take micrographs of fibres, and measure individual fibre diameter. Micrographs were also used to determine the angular variance of fibres, to confirm whether fibres were aligned.

Successful fabricated aligned fibres were taken forward to work described in chapter 5 for *in vitro* analysis. The most efficient fibre diameter for promoting neuronal cell differentiation and neurite outgrowth is described in chapter 4.

3.2 Materials and Methods

3.2.1 Fabrication of electrospun fibres

To fabricate fibres from blends of materials, electrospinning of polymers was first performed to understand the parameters required for the process. PCL, P(3HB), P(3HO), PLLA, PLGA, P(3HO-co-3HD) and PHBV) were all dissolved into different solvents, at different concentrations, to determine the most efficient solvent and polymer concentration required for electrospinning. Electrospinning of solutions was performed using a high-power voltage supply (Genvolt UK), a single syringe pump (WPI-Europe) and a rotating cylindrical collector attached to a motor (diameter of 6cm-IKA Works). A 1mL plastic syringe (Terumo) was attached to the syringe pump and a 20G needle attached to the end of the syringe. The needle was connected to the high voltage power supply (figure 1). During the first attempt of a solvent/polymer wt% solution, the voltage was from 10kV up to 18kV to determine the correct voltage which would fabricate an aligned polymer jet, parallel to the collector (figure 2). Voltages used were between 8-18kV, and once the correct voltage was established, three different parameters were changed to fabricate fibres. These were:

- Speed of the collector (33.5, 75.5, and 134 xg)

- Distance of the needle from the collector (10, 15 and 20cm)

- Flow rate of polymer released from the needle (1, 2, 3 and 4 mL / hr)

All electrospinning was performed using a 20G needle. Humidity and temperature could not be modified/kept constant during electrospinning but were recorded on the day of spinning. All fibre conditions were collected onto a sheet of aluminium foil on the cylindrical collector and analysed initially by light microscopy to determine alignment. If alignment was not seen by light microscopy, the condition was noted down as not working and analysis was not continued further. Fibre conditions that appeared aligned were cut into sections for analysis by scanning electron microscopy to determine fibre diameter and alignment. The entire process was then repeated for co-polymers and different polymer blends, to find the conditions required to fabricate aligned fibres with varying diameters for potential in vitro analysis. Figure 1 below shows a picture of the set up used to fabricate PHBV electrospun fibres.
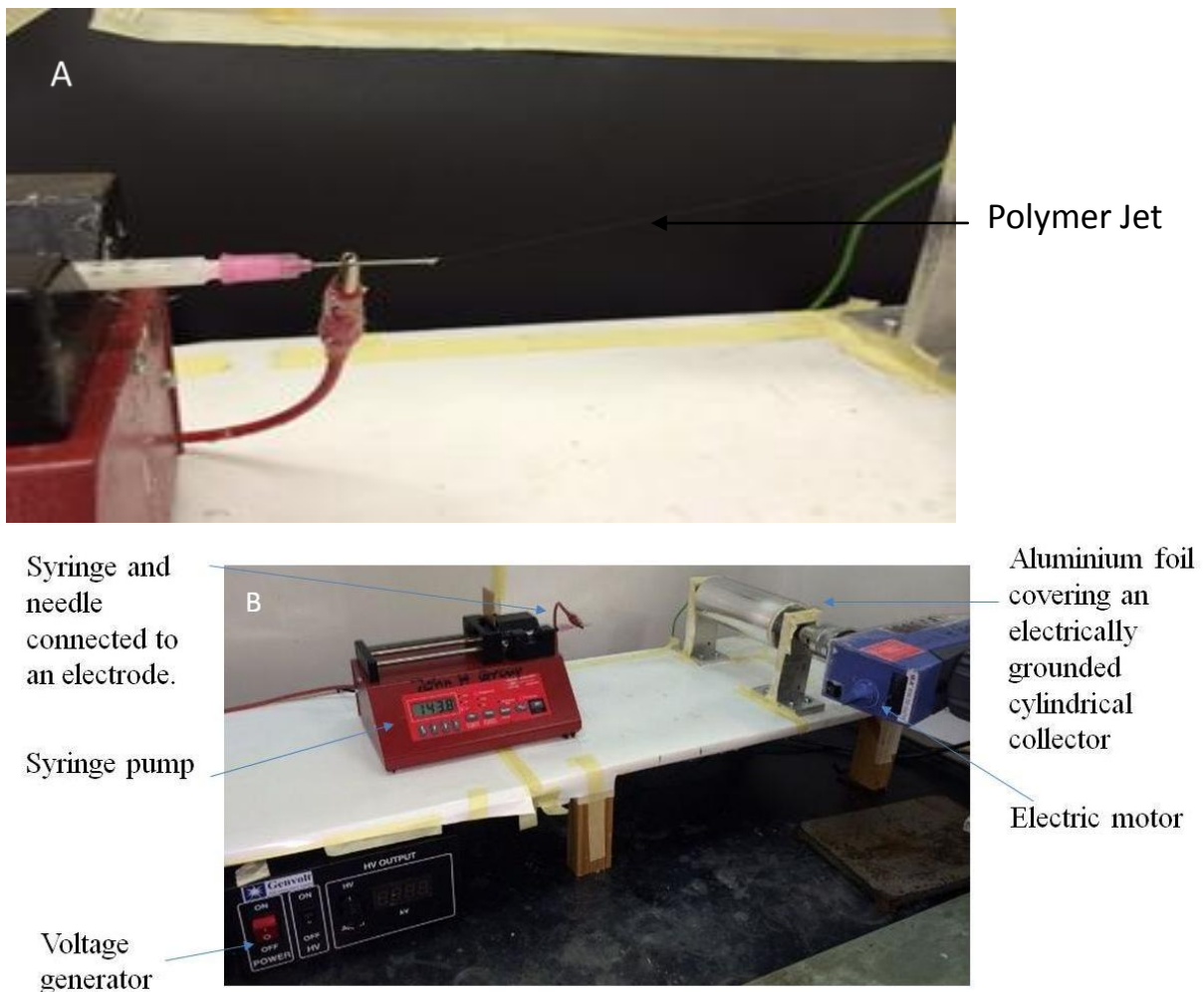
Figure 3.1A) Image to show the 'Taylor' cone, and the polymer jet formed by the addition of an electric current over a polymer drop. B) Electrospinning set up to fabricate electrospun fibres.

3.2.2 Characterisation of electrospun fibres

To determine fibre diameter and alignment, three independently electrospun batches of the same electrospinning conditions were analyzed using scanning electron microscopy. Fibres were cut to size and stuck to specimen holders, and were sputter coated with a 20nm thick gold coat. A FEI Sirion field emission gun scanning electron microscope was used to take images of the fibres. Images were analyzed by using National Institutes of Health (NIH) Image J software (Schneider *et al.*, 2012). From each independently spun batch of fibres, diameters were taken from 50 fibres, and the fibre alignment was determined by measuring the angle of each fibre against a reference fibre (at 180˚). Fibre alignment was conducted using image NIH software Image J (Schneider *et al.*, 2012).

2.2.3 Statistical analysis

GraphPad Instat (GraphPad Software, USA) was used to perform statistical tests on data collected. One way analysis of variance ($p < 0.05$) was conducted to analyse the differences between the data, with a Tukey's multiple comparisons test to compare statistical differences between samples. Data was reported as mean ± SD, $p<0.05$. Each experiment was performed three independent times with each sample repeated three times as n=3.

3.3 Results

3.3.1 Polycaprolactone (PCL)

Daud *et al.* (2012) initially established conditions at the University of Sheffield when they fabricated electrospun PCL fibres of 3 different diameters of 1, 5 and 8µm using DCM as a solvent (Daud *et al.*, 2012). Polycaprolactone is an established and well characterised material in our group and conditions were a good starting point to electrospin other materials thereafter. The table below was taken from the publication by Daud *et al.* (2012) to reproduce PCL electrospun fibres.

Table 3.1. Modified from Daud *et al* (2012).

Parameters	Small (1µm)	Intermediate (5µm)	Large (8µm)
Solvent	CF and DCM (1:1)	DCM	DCM
Concentration (wt%)	10	10	20
Flow Rate (mL/hr)	0.3	4	6
Voltage (kV)	14	15	18
Needle to collector distance (cm)	20	20	20
Needle size	27	20	20
Collector Speed (xg)	134	134	134
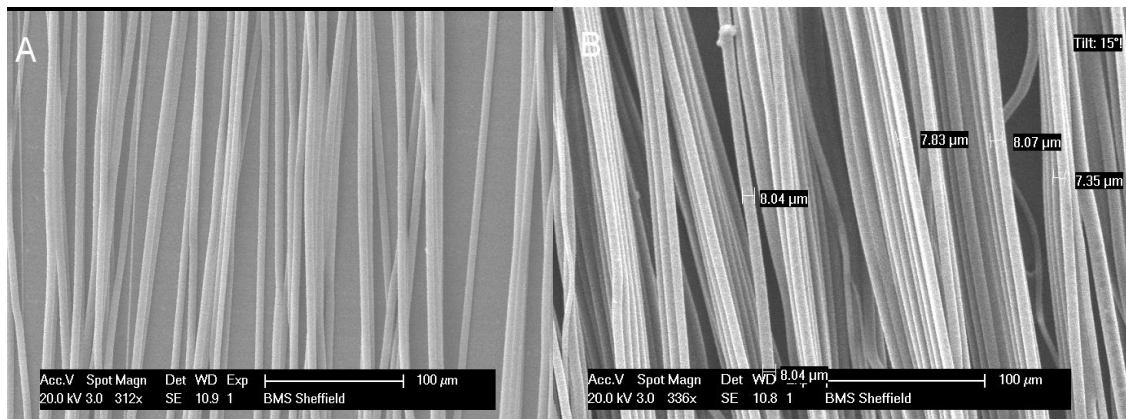
Figure 3.3. A) 5µm PCL electrospun scaffold and a B) 8µm electrospun PCL scaffold.

Figure 3.3 shows scanning electron micrographs of 5 and 8µm PCL fibres fabricated using the conditions produced by (Daud *et al.*, 2012). Fibres appeared aligned and of the correct diameter. The micrographs were quantified, to check alignment and fibre diameter. Figure 5A confirms that all three different conditions fabricate 1, 5 and 8µm fibres which are statistically different to each other. Figure 5B also confirms that all conditions fabricate aligned fibres, with more than two thirds of each fibres measured in the 0-2˚ category, and little or no fibres in the 6-8, 8-10 or 10-12 degrees categories. PCL fibres could be easily removed from the tin foil collector, and when removed were threadlike. This data confirms that the conditions published can be easily reproduced, fabricating aligned fibres of known diameters

Figure 3.4. A) Graph to show the average fibre diameter of the complete set of data of different fibre diameters. An average of 30 fibres was assessed for each fibre size a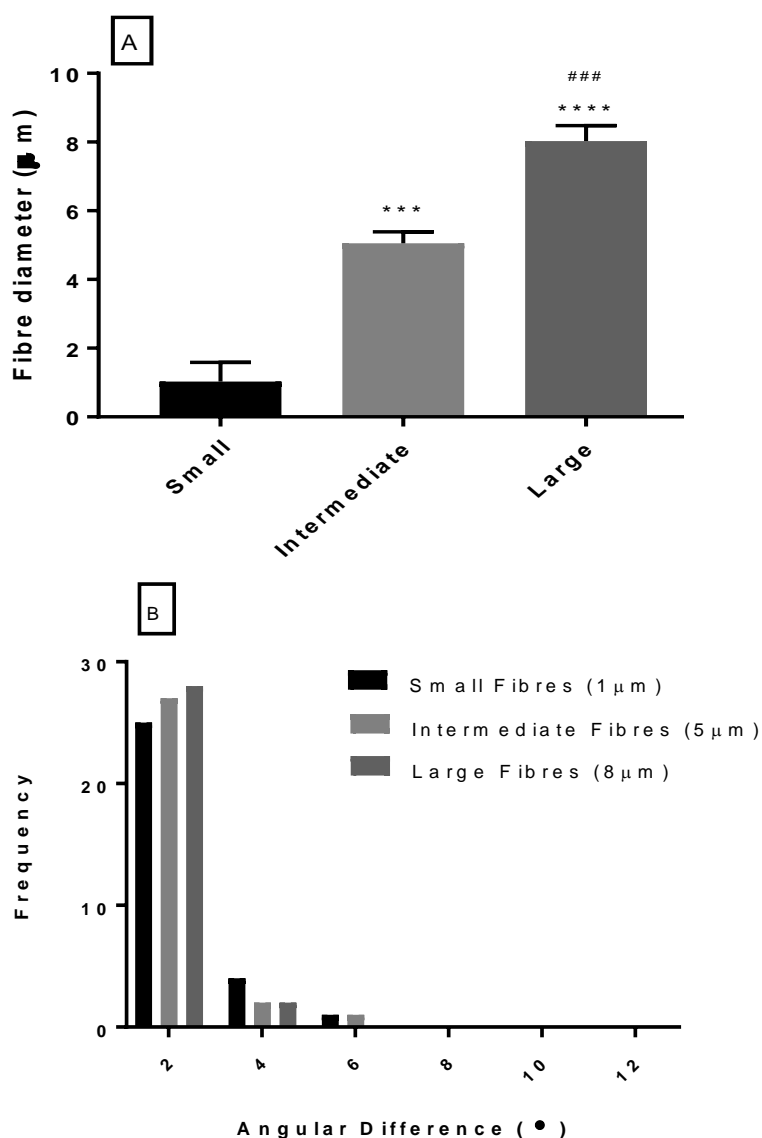nd mean of the diameter is presented. A one way anova with Tukey's multiple comparisons tests was used to analyse data (Mean ± SD, n= 3 independently fabricated samples ***p < 0.01 compared to 1μm fibres, ****p < 0.0001 compared to 1μm fibres, ###p < 0.01 compared to 5μm fibres). B) Histogram to determine alignment of PCL fibres fabricated using the conditions in Daud *et al.* (2012). 30 fibres were measured per independently electrospun batch of fibres. (n=3)

3.3.2 Poly(3-hydroxybutyrate) P(3HB)

P(3HB), of Mw 452kDa, was manufactured by Rinat Nigmatullin, in the Applied Biotechnology Research Group at The University of Westminster and sent (Valappil *et al.*, 2007a). 7 and 10 wt% solutions of P(3HB) were dissolved in chloroform. Both concentrations of polymer were electrospun at 4mL/hr, 20cm from the collector at a speed of 134 xg. Little success was found with the 7wt% solution, but fibres were formed from the 10wt%. Different parameters, such as working distance, flow rate and speed of the collector, were modified to fabricate different fibre diameter. Solutions of 8, 10 and 12wt% were produced and voltages between 8-20kV applied to produced a polymer jet. Flow rates of 1,2,3 and 4ml/hr were

investigated, and collector speeds of 33.5, 75.5, and 134 xg. The distance between the needle tip and the collector was changed from 10,cm, 15cm and 20cm. The results of the changing of the parameters are presented below.

Table 3.2. Table of successful electrospinning conditions for P(3HB). 20G needles were used for all conditions and spun for 2 minutes (Mean ± SD, n= 3 independently fabricated samples)

Condition Number	Polymer Solution (%)	Voltage (kV)	Distance (cm)	flow rate (mL/h)	Speed (xg)	Size of fibres (µm)
1	12	12	12	1	148	2.3 ± 0.3
2	8	15	12	1	134	2.5 ± 0.7
3	12	18	20	4	134	3.5 ± 0.7
4	12	15	20	3	134	3.6 ± 0.6
5	12	22.5	20	2	134	4.2 ± 0.5
6	12	15	20	1	134	4.3 ± 0.9
7	8	15	12	1	148	4.5 ±0.8
8	12	12	20	4	134	4.6 ± 1.5
9	12	12	12	4	248	4.8 ± 2.0
10	12	15	10	3	134	6.8 ± 0.7
11	12	15	20	4	134	7.9 ± 1.5

A range of fibre diameters, from 2.3 – 7.9µm could be fabricated from P(3HB). Polymer solutions of 12 wt% concentration were spun with the most success and voltages of 12-22.5 kV produced a polymer jet from the Taylor cone. For quantitative analysis of electrospun fibres, samples were analysed using a FEI Sirion field emission gun scanning electron microscope. Three independent batches of each diameter of material fibre size were used and 100 different fibre diameters, in total, were taken for each condition to determine the average fibre diameter. To determine the variation between data, the diameters plotted into a graph and presented below.
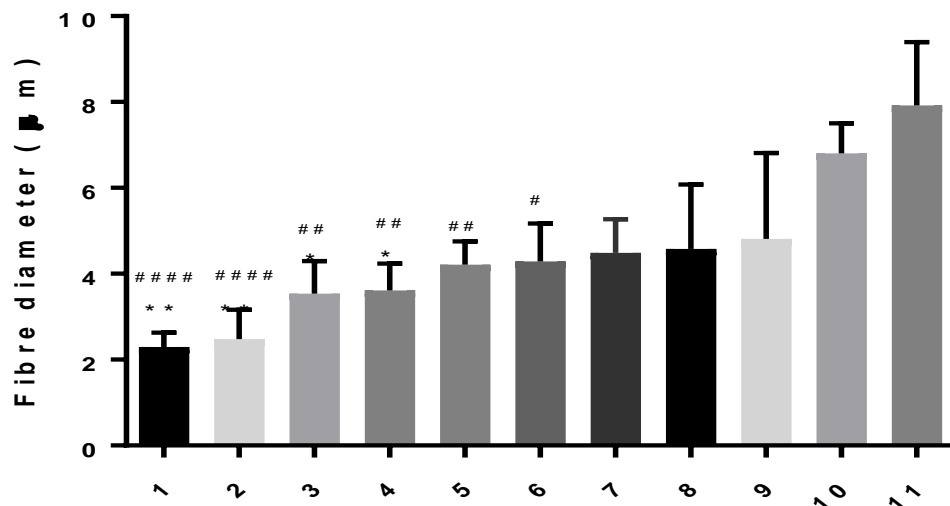
Figure 3.5. A graph to show the different fibre diameters fabricated from different conditions of P(3HB). A one way anova with Tukey's multiple comparisons tests was used to analyse data (Mean ± SD, n= 3 independently fabricated samples *p < 0.05, **p < 0.01 compared to condition 10, #p< 0.05, ##p< 0.01, ####p < 0.0001 compared to condition 11).

Overall, figure 3.5 shows that the diameters of fibres fabricated in conditions 1-6 are statistically smaller than the diameters of fibres fabricated from electrospinning conditions 10 and 11. No statistical differences were detected between fibre diameters fabricated from electrospinning conditions 1-9. The largest average fibre diameter was 7.9 ± 1.5µm, fabricated by figure 11, followed by 6.8 ± 0.7µm fabricated by figure 10. The smallest fibre diameter fabricated was 2.3 ± 0.3µm. Figure 8 shows that fibres fabricated appeared much aligned and fibres could be removed from the tin foil easily, with a threadlike consistency.
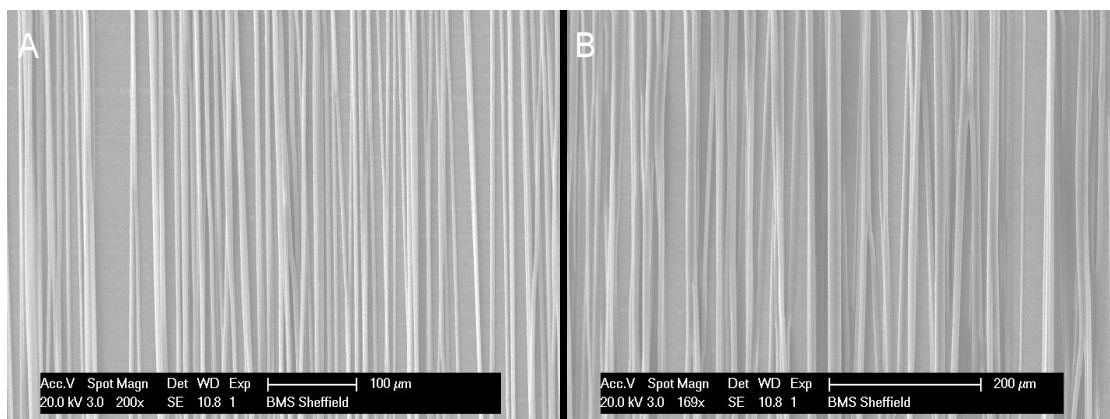
Figure 3.6. Scanning electron micrographs of A) 4.21µm and B) 6.86µm P(3HB) electrospun scaffolds.

Fibre alignment was determined, using Image J by using a reference fibre (at 180˚) and measuring fibres against the reference fibre (Schneider *et al.*, 2012). 30 fibres per sample per batch were measured and the angular variance in the different conditions determined. Data was split into groups of 2˚ (0-2˚, 2-4˚, 4-6˚etc).
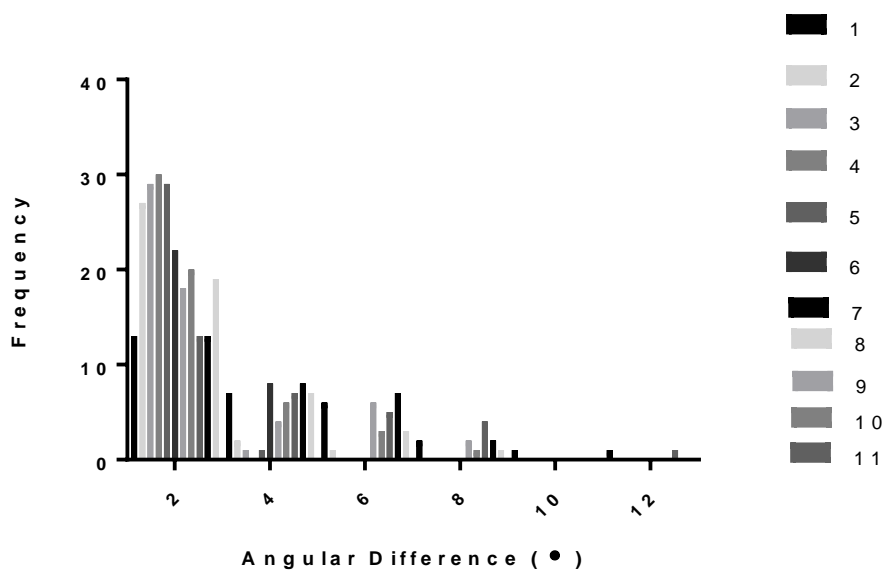
Figure 3.7. Graph to show illustrate the angular difference between samples linked to the table of electrospinning conditions. For all conditions, at least two thirds of the fibres were located in the 0-2˚category confirming parallel alignment.

Electrospinning P(3HB) produced 11 successful electrospinning conditions and fibre diameters from 2.3- 7.9 µm fibres, and that these fibres were aligned (figure 9). Angular variance illustrated the fabrication of parallel aligned fibres. Around 20 out of 30 fibres, for fibres fabricated from conditions 2, 3, 4, 5, 6 and 10, measured 0-2˚ from the centrally aligned reference fibre. Fibres fabricated by electrospinning conditions 1, 7 and 11, appeared the least aligned as less than 50% of all fibres measured 0-2˚ from the central reference fibre. Overall it was concluded that electrospinning P(3HB) could fabricate some aligned fibres with different diameters. The chosen solvent for P(3HB) was chloroform and that 10-12wt% solutions fabricated larger diameters.

3.3.3 Poly(3-hydroxyoctanoate) P(3HO)

P(3HO), 677kDa in molecular weight, was manufactured by Rinat Nigmatullin, in the Applied Biotechnology Research Group at The University of Westminster (Rai *et al.*, 2011), P(3HO) was dissolved in chloroform. Solutions of 8, 10 and 12wt% were produced and voltages between 8-20kV applied to produced a polymer jet. Flow rates of 1,2,3 and 4ml/hr were investigated, and collector speeds of 33.5, 75.5, and 134 xg. The distance between the needle tip and the collector was changed from 10cm, 15cm and 20cm. Figure 3.8, shows that electrospun fibres could be fabricated from P(3HO). However, fibres could not be removed from the foil. This was due to the fibres merging together due to the solvent not evaporating fully before reaching the collector.
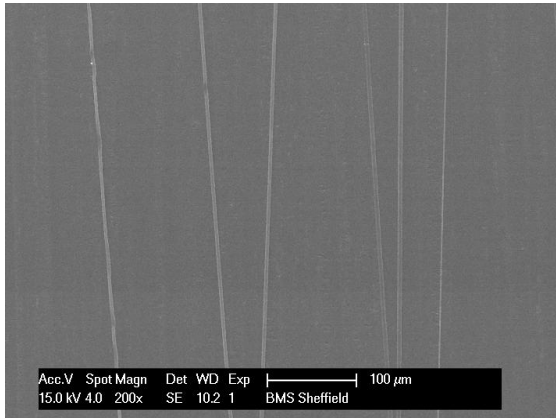
Figure 3.8. SEM micrograph of spun P(3HO) fibres, average diameter 4.55µm.

3.3.4 PolyLactic-Glycolic Acid (PLGA)

PLGA, from Vornia Biomaterials Ltd, Ireland, with a molecular weight of 42kDa, was electrospun on the set up. The recommended solvent selected to spin PLGA was hexafluoroisopropanol (HFIP). Conditions from the study by Aviss *et al.* (2010) were used to electrospin PLGA in HFIP. A 20wt% solution was made up in HFIP and voltages between 8-20kV applied to produced a polymer jet. Flow rates of 1,2,3 and 4ml/hr were investigated, and collector speeds of 33.5, 75.5, and 134 xg. The distance between the needle tip and the collector was changed from 10,cm, 15cm and 20cm. Figure 3.9 shows the result of fibres fabricated from a condition with a flow rate of 1mL/hr, speed collector of 1500rpm, with a working distance of 15cm (Aviss *et al.*, 2010). This condition fabricated a randomly orientated fibre scaffold. The average fibre diameter of this scaffold was 3.2µm, and if the fibre diameter was to be increased, a higher flow rate and polymer concentration was needed. However, the 20wt% solution was very viscous and difficult to electrospin. The polymer concentration was dropped to 16wt% and electrospun at 5mL/hr, a 15cm working distance, 75.5 xg collector speed and a voltage of 15kV was applied. This fabricated electrospun fibres of 2.7µm which were much more aligned (figure 3.9B).
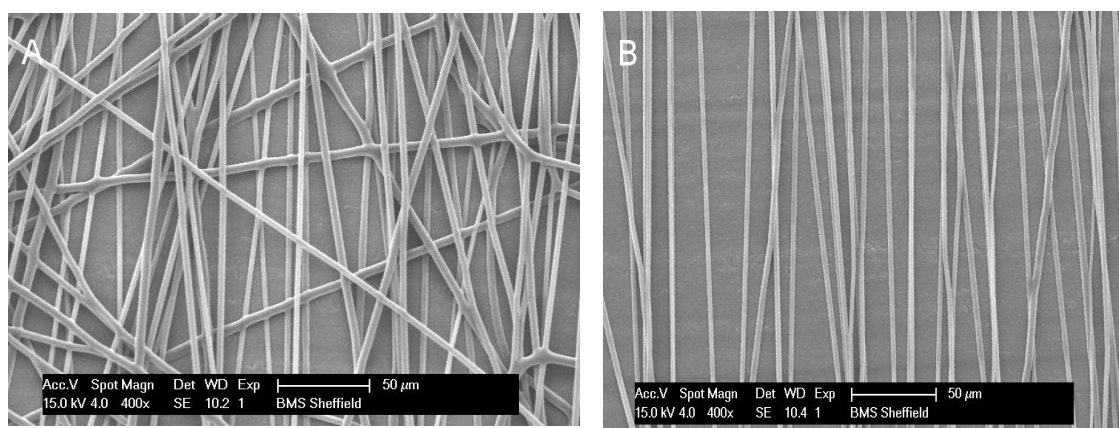
Figure 3.9. Scanning electron microscopy micrographs of A) 20 wt% PGA Scaffold (average fibre diameter= 3.2µm) and B) 16 wt% Scaffold. (Average fibre diameter= 2.7µm)

The working distance of 15cm was kept constant, and the flow rate kept at 5mL/hr. The collector speed was decreased to 1000rpm to produce thicker fibres. This is illustrated in fibres fabricated by condition 7 (table 3.3) which were 4.5µm in diameter. However, similar to the 20wt% solution, the 16wt% solution was observed by eye to be viscous. Decreasing the concentration of the polymer did not permit fabrication of aligned fibres with higher diameters.

Table 3.3. Summary of electrospinning conditions used to fabricate aligned PLGA microfibres.

Condition Number	Polymer Solution (%)	Voltage (kV)	Distance (cm)	Flow rate (mL/h)	Speed (xg)	Size of fibres (µm)
1	16	20	15	5	33.5	1.5 ± 0.3
2	16	20	15	5	134	1.6 ± 0.4
3	16	15	15	5	134	1.9 ± 0.5
4	16	20	15	5	75.5	2.5 ± 0.7
5	16	15	15	5	75.5	2.7 ± 0.4
6	16	15	15	5	33.5	3.1 ± 0.6
7	16	20	15	5	33.5	4.3 ± 0.3
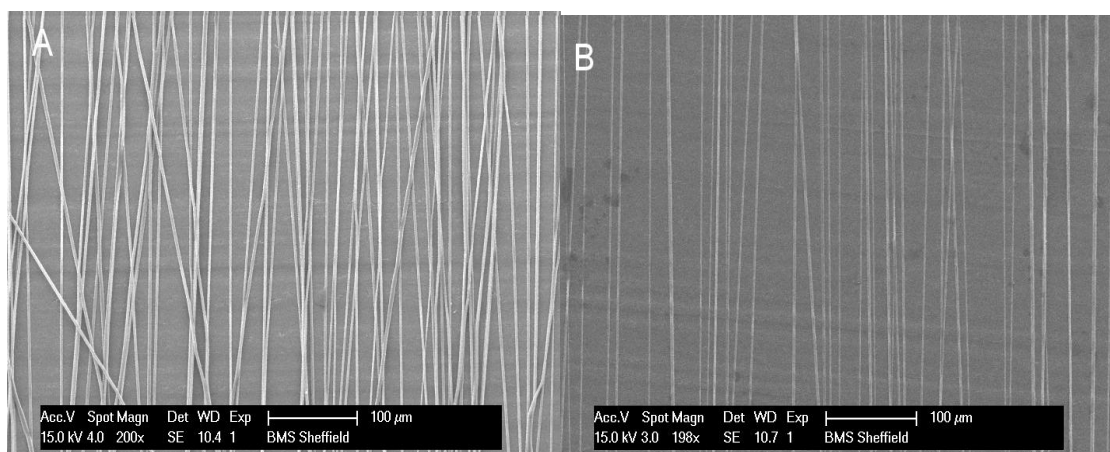
Figure 3.10. Scanning electron micrographs of A) 2.7µm PGA electrospun scaffold fibres and B) 1.92µm PGA electrospun scaffold fibres.

3.3.5 Poly(3-hydroxyoctanoate-co-3-hydroxydecanoate) (P(3HO-co-3HD)

P(3HO-co-3HD), with a Mw of 350 KDa, was manufactured by Rinat Nigmatullin, in the Applied Biotechnology Research Group at The University of Westminster. P(3HO-co-3HD) was dissolved in chloroform overnight at room temperature on a magnetic stirrer platform. Solutions of 8, 10 and 12wt% were produced and voltages between 8-20kV applied to produced a polymer jet. Flow rates of 1,2,3 and 4ml/hr were investigated, and collector speeds of 33.5, 75.5, and 134 xg. The distance between the needle tip and the collector was changed from 10,cm, 15cm and 20cm.

A table of two electrospinning conditions where individual fibres were fabricated of P(3HO-co-3HD) that didn't fuse together or bead (table 3.4).

Table 3.4. Two successful conditions of P(3HO-co-3HD) fibres (Mean ± SD, n= 3 independently fabricated samples).

Parameters	1	2
Polymer Concentration (wt%)	10	10
Voltage (kV)	18	19
Flow Rate (mL/hr)	2	3
Collector speed (xg)	134	134
Working distance (cm) from needle to collector	15	15
Fibre Diameter (µm)	3.6 ± 0.6	4.5 ± 0.4

Scanning electron micrographs were taken of the fibres electrospun from the conditions in table 3.4. Very little fibres collected onto the foil collector during electrospinning. Aligned

fibres were fabricated using the electrospinning parameters in condition two, compared to condition one. However, when the electrospinning time was increased to fabricate aligned fibre mats, fibres merged with each other and alignment was lost. This was because of the short working distances used to collect the fibres, and that fibres had not dried in time.
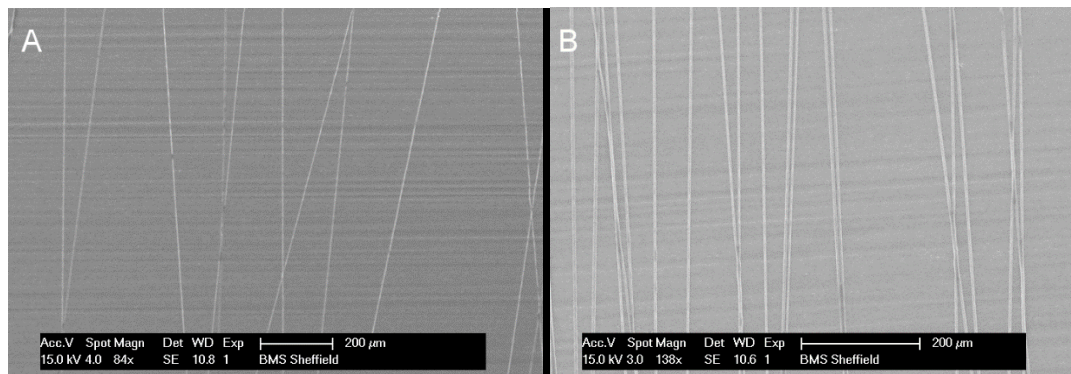
Figure 3.11. Scanning electron microscopy micrographs of P(3HO-co-3HD) electrospun scaffolds with average diameters. Scaffold A) was fabricated by condition 1 and scaffold B) was fabricated by condition 2.

3.3.6 Polyhydroxybutyrate-co-Valerate (PHBV)

PHBV, with a molecular weight of 600,000 g/mol, was purchased from Goodfellow Ltd, UK. Initially, 10wt% solutions of PHBV were spun using the conditions described by Daud *et al.* (2012). 7.8μm fibres were produced and characterised using scanning electron microscopy, but it was confirmed they were not as aligned, and some fibres could be seen fused together (figure 3.12A). A 14wt% solution of PHBV in chloroform was spun at 4mL/hr, 12kV, 33.5 xg speed with a working distance of 20cm (Sombatmankhong *et al.*, 2006). However, due to the higher molecular weight of the PHBV used, these conditions resulted in fibres with a beaded like morphology (figure 18B). Due to many different parameters associated with electrospinning, conditions were kept constant throughout batches, changing one parameter at a time. PHBV fibres were fabricated using voltages between 10-15kV, and changing the speed of the collector, distance from the collector and flow rate of the polymer ejected. Flow rates of 1,2,3 and 4ml/hr were investigated, and collector speeds of 33.5, 75.5, and 134 xg. The distance between the needle tip and the collector was changed from 10,cm, 15cm and 20cm.

Figure 3.12. (A) SEM image analysis of 10% PHBV solution electrospun at 15kv, 20cm working distance, 4mL/h flow rate and collector speed of 2000rpm. 7.8μm f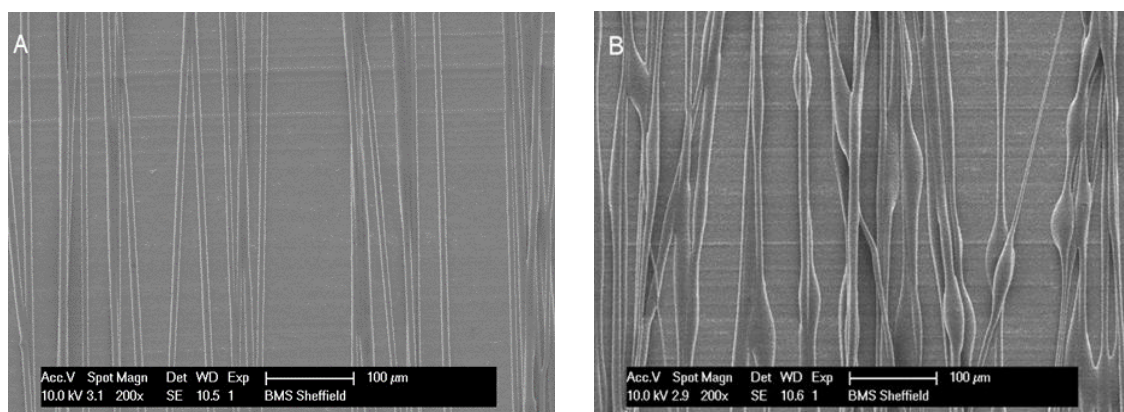ibres were produced but slightly fused. (B) SEM image analysis of electrospun fibres replicating conditions from Sombatmankhong et al (2006) in which beaded fused fibres were formed.

When increasing the polymer concentration, an increase in fibre diameter was observed. To compensate a more viscous solution, the voltage needed to be increased to form a parallel jet, to fabricate aligned fibres. By increasing the polymer concentration, this increased the likeliness of fabricating beaded and fused fibres, especially at low collector speeds, in which increasing the voltage also avoided this. Fibre diameter could be increased by reducing the speed of the collector, increasing the flow rate, as well as decreasing the working distance between the syringe and the collector. At 12kV, the 14wt% PHBV solution produced an aligned jet which produced aligned fibres. A range of electrospinning conditions were explored and SEM image analysis was used to determine the most successful conditions, with regards to fibre alignment and diameter. Successful conditions fabricated aligned fibres with varying diameters (Table 3.5).

Table 3.5. 10 conditions were chosen for producing aligned PHBV fibres of different diameters. (Mean ± SD, n= 3 independently fabricated samples

Condition Number	Polymer Solution (%)	Voltage (kV)	Distance (cm)	flow rate (mL/h)	Speed (xg)	Size of fibres (μm)
1	10	13	20	1	134	1.9 ± 0.5
2	14	12	20	3	134	3.8 ±0.6
3	14	10	20	1	33.5	4.1 ± 0.6
4	14	15	20	4	134	5.1 ± 0.9
5	14	12	20	4	134	6.0 ± 0.6
6	14	10	20	4	134	6.2 ± 0.7
7	12	15	20	4	134	7.5 ± 0.9
8	10	10	20	4	134	8.1 ± 0.4
9	15	12	20	4	134	9.3 ± 1.1
10	15	12	20	4	33.5	10.2 ± 0.5

SEM micrographs of all fibres samples were taken for the 10 conditions detailed above, to determine fibre diameter and alignment (angular) differences. To determine the fibre diameter fibres were measured using the ruler tool in Image J to determine statistical differences between diameters (Schneider *et al.*, 2012).
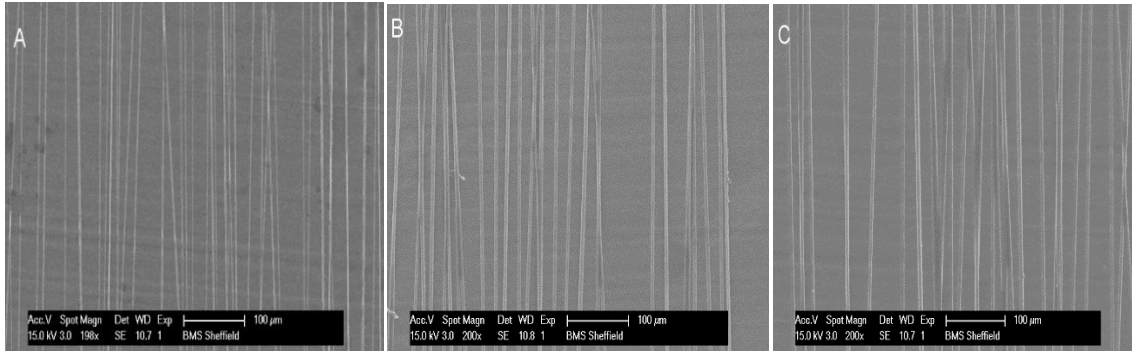
Figure 3.13. Scanning electron micrographs of (A) 1.9µm PHBV fibres, B) 4.2µm PHBV fibres, and C) 6.0µm PHBV fibres.
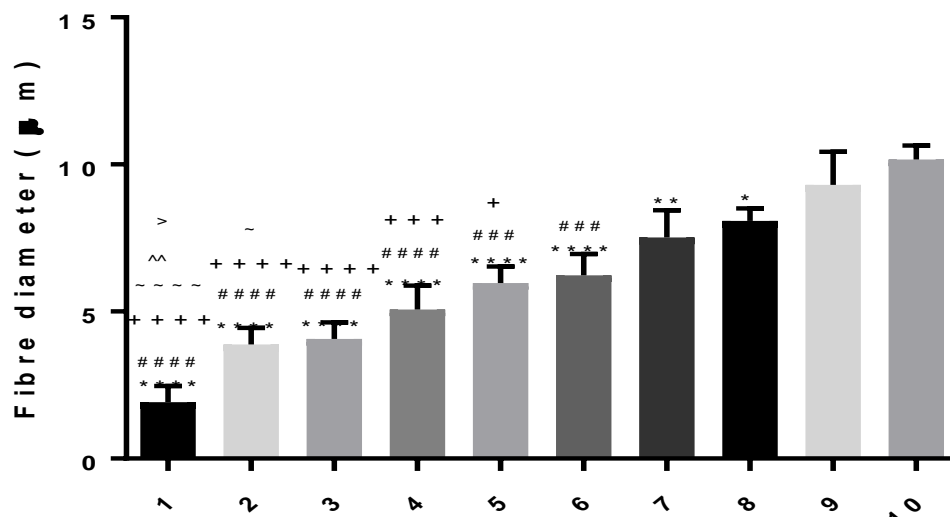
Figure 3.14. Graph to show the average fibre diameter of 10 electrospinning conditions that fabricate aligned fibres. An average of 30 fibres was assessed for each fibre size and mean of the diameter is presented. A one way anova with Tukey's multiple comparisons tests was used to analyse data (Mean ± SD, n= 3 independently fabricated samples *p < 0.05, **p < 0.01, ***p < 0.001, ****p < 0.0001 compared to condition 10, ###p < 0.001, ####p < 0.0001 compared to condition 9, +p < 0.05, +p < 0.01, +++p < 0.001, ++++p < 0.0001 compared to condition 8, ~p < 0.05, ~~~~p < 0.0001 compared to condition 5, ^^p < 0.01 compared to condition 4, >p < 0.05 compared to condition 3).

Electrospinning conditions 1-8 fabricated fibres that had statistically smaller fibre diameters, compared to the diameter of fibres fabricated in condition 10, which at measured 10.27 ± 0.5µm. Diameters of fibres fabricated in conditions 1-6 were significantly smaller than the diameter of fibres fabricated in condition 9, 9.3 ± 1.1µm. The smallest diameter of fibres fabricated were 1.9 ± 0.5µm, condition 1.

To confirm if fibres fabricated were aligned, the angular variance for each condition was calculated. A central reference fibre, measuring 180˚ on image J, was used to calculate the

angular variance of the fibres in degrees (Schneider *et al.*, 2012). Each fibre was placed into an angular degree category of 0-2, 2-4, 4-6, 6-8 and 8-12˚. 30 fibres, per condition, were measured, and results illustrated in figure 21B. Over two thirds, of all fibres per condition, measured 0-2˚from the central reference fibre, indicating that all PHBV fibres were aligned. Aligned PHBV fibres could be produced from all 10 electrospinning conditions and were reproducible.
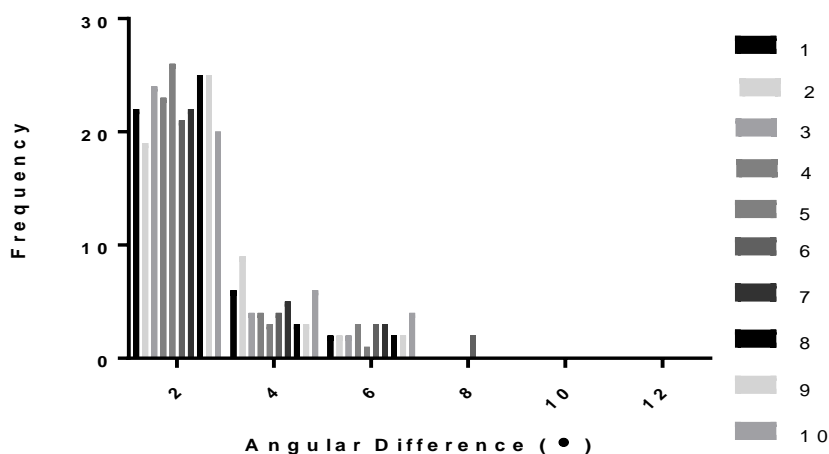
Figure 3.15. Histogram to illustrate alignment of PHBV fibres fabricated. A central aligned fibre, at 180˚, was used as a reference point to measure the angular variance of adjacent fibres. Per independently electrospun batch of fibres, 30 fibres were measured. (n=3)

3.3.7 Polyhydroxybutyrate:Polyhydroxyoctanoate P(3HO):P(3HB) (25:75)

Previous biocompatibility studies in chapter 2, and from solvent casted film analysis by Lizarraga *et al.* (2015) revealed that longer neurites expressed from NG108-15 neuronal cells were observed when cultured on the P(3HO):P(3HB) (25:75) blend compared to blends of 50:50 and 75:25 (Lorena R. Lizarraga-Valderrama *et al.*, 2015). Blends were then produced to manufacture fibres by electrospinning. Three different polymer concentrations, 8wt%, 10wt% and 12wt%, were investigated and electrospun by dissolving the different polymer concentrations in chloroform. Flow rates of 1,2,3 and 4ml/hr were investigated, and collector speeds of 33.5, 75.5, and 134 xg. The distance between the needle tip and the collector was changed from 10,cm, 15cm and 20cm. Scanning electron micrographs were taken of fibres to determine the fibre diameter and alignment. The most successful electrospinning conditions are presented below.

Table 3.6. Electrospinning fabrication conditions of P(3HO):P(3HB) (25:75) fibres with different average fibre diameters (mean ± SD, n = 3 independently fabricated samples).

Number	Solution (%)	Voltage (kV)	Distance (cm)	Flow rate (mL/h)	Speed (xg)	Size of fibres (µm)
1	8	8.5	10	1	134	1.8 ± 0.4
2	8	8.5	15	2	134	2.3 ± 0.5
3	10	10	20	1	134	3.2 ± 0.2
4	10	10	15	2	134	4.1 ± 0.3
5	12	10.5	20	4	134	5.0 ± 0.4
6	10	8.9	15	4	134	6.1 ± 0.7
7	12	10.5	20	4	75.7	7.1 ± 1.2
8	10	8	10	4	33.5	8.3 ± 1.2
9	10	15	10	3	75.5	9.0 ± 1.2
10	12	10.5	10	4	134	10.6 ± 1.2

Fibre diameters from 1.8 - 10.6µm were produced using the P(3HO):P(3HB) (25:75) blend. Polymer solutions of 8, 10 and 12 wt% concentration were spun with the most success and voltages of 8.5-10.5 kV produced aligned polymer jets to formed from the Taylor cone (Bhardwaj and Kundu, 2010). To determine fibre diameter, and to detect differences between diameters fabricated, samples were analysed by scanning electron microscopy. Three independent batches of each diameter of material fibre size were used and 100 different fibre diameters, in total, were taken for each condition to determine the average fibre diameter. To determine the variation between data, the diameters were plotted into a graph and presented below.
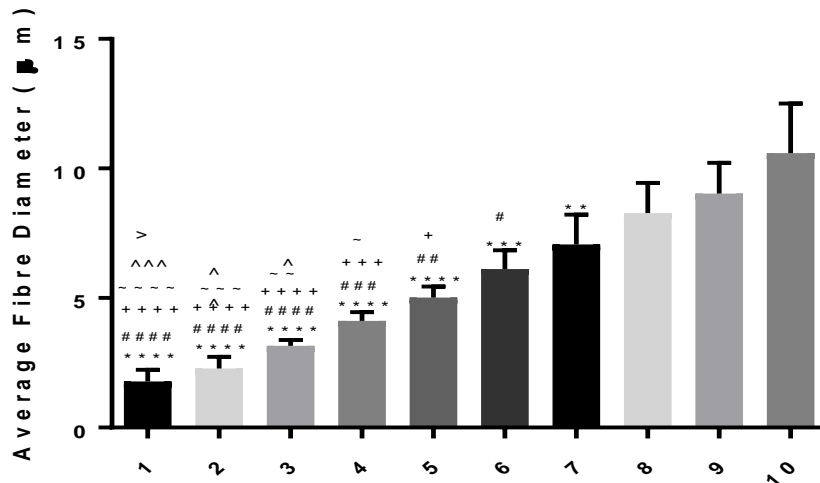
Figure 3.16. 10 different fibre diameters produced using 10 different electrospinning conditions of P(3HO):P(3HB) 25:75. A one way anova with Tukey's multiple comparisons tests was used to analyse data (Mean ± SD, n= 3 independently fabricated samples, **p < 0.01, ***p < 0.001, ****p < 0.0001 compared to condition 10, #p < 0.05, ##p < 0.01, ###p < 0.001, ####p < 0.0001 compared to condition 9, +p < 0.05, ++p < 0.01, +++p < 0.001, ++++p < 0.0001 compared to condition 8, ~p < 0.05, ~~p < 0.01, ~~~p < 0.001, ~~~~p < 0.0001 compared to condition 7, ^p < 0.05, ^^p < 0.01, ^^^p < 0.001, ^^^^p < 0.0001 compared to condition 6, >p < 0.05 compared to condition 5).

Significant differences were detected between the fibre diameters, in which condition number 10 produced fibre diameters which were significantly larger, (10.6 ± 1.9µm) compared to fibre diameters produced from conditions 1-7. The smallest average diameter measured (1.8 ± 0.4µm condition 1), was significantly smaller than the average diameters measured for conditions 5-10. Overall, the average fibre diameter ranged from 1.8µm - 10.6µm. Of note, there was large variance of fibre diameters of fibres fabricated from conditions 7-10. This could be due to a few reasons such as fibre fusion, higher viscosity of solution required to fabricate thicker fibres, or changes in humidity and temperature

Four scanning electron micrographs of conditions 3, 6, 8 and 10, were measured at 3.2µm, 6.1µm, 8.2µm and 10.6µm. Overall, fibre diameter increased, from figure 3.17 A-D. To determine fibre alignment, the angular variance between fibres per diameter was determined.
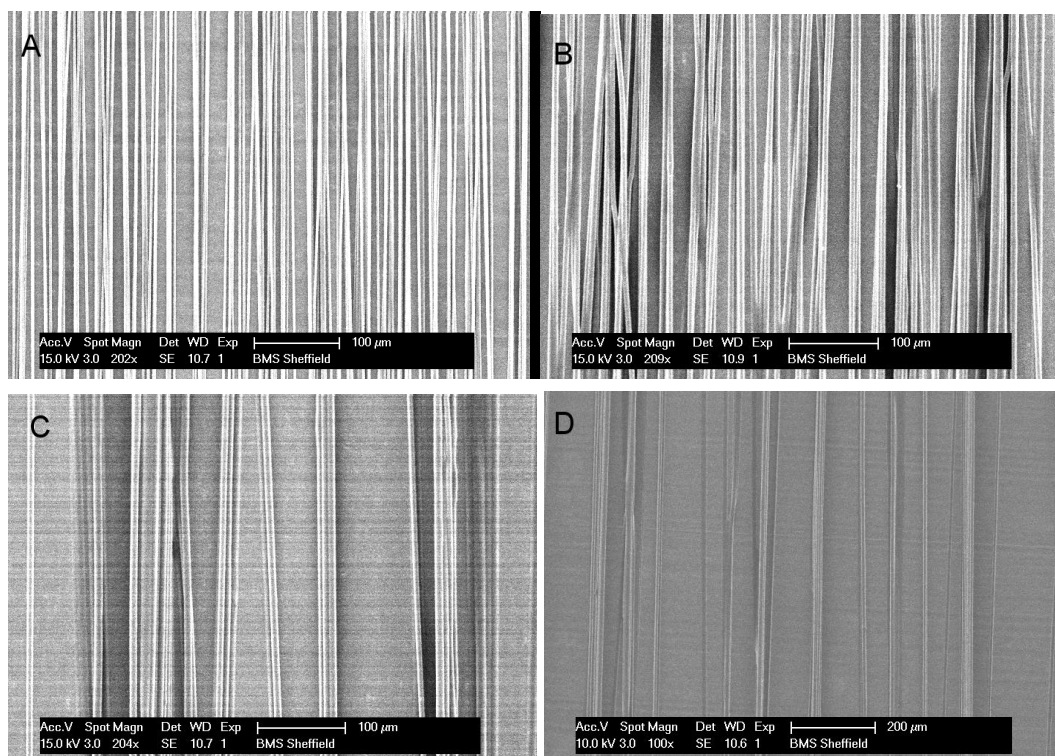
Figure 3.17. SEM micrographs of P(3HO):P(3HB) (25:75) fibres scaffolds with average diameters of A) 3.2μm B) 6.1μm C) 8.2μm and D) 10.6μm
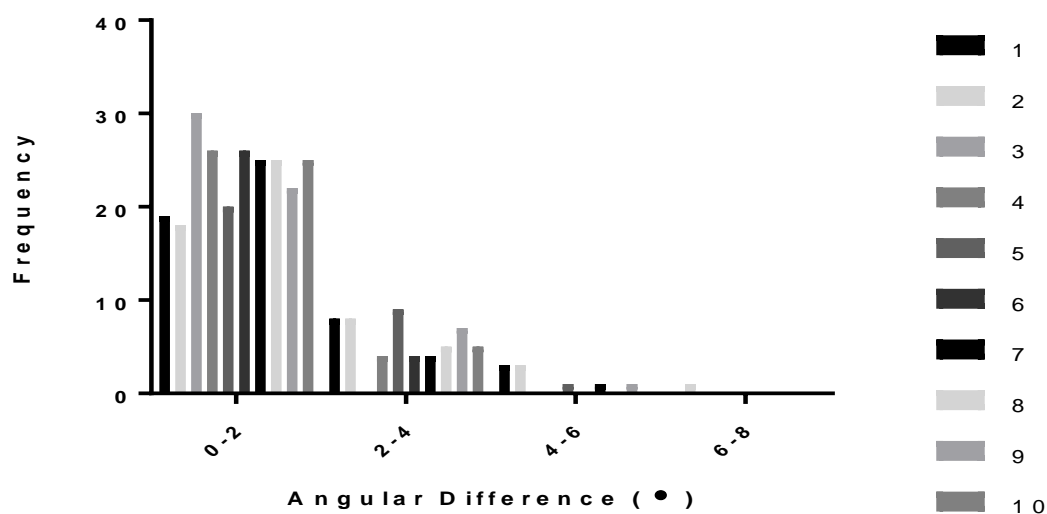
Figure 23. Graph to show the angular difference between samples linked to the table of electrospinning conditions. For all conditions, except no.1 and 2, at least two thirds of the fibres were recorded in the 0-2˚category confirming parallel alignment.

Fibre alignment studies illustrated that all conditions, except conditions 1 and 2, fabricated aligned fibres. A minimum of 20, out of 30 fibres measured between 0-2° from the central reference fibre. 19 out of 30 fibres measured between 0-2° from the central reference fibre when manufactured from conditions 1 and 2. Fibres fabricated from conditions 1 and 2 measured between 2-4° from the central reference fibre which indicated good alignment. P(3HO):P(3HB) (25:75) can be electrospun to fabricate aligned fibres with varying diameters. Fibres could also be removed from the tin foil collector with ease and could be

manipulated by hand without losing alignment. Fibres produced from electrospinning conditions 3, 4 and 5 resulted in the most aligned fibres, with little variance between fibre diameters. Fibres produced from electrospinning conditions 7, 8, 9 and 10, although aligned, had a higher variance in fibre diameter.

3.3.8 Polyhydroxybutyrate:Polyhydroxyoctanoate P(3HO):P(3HB) (50:50)

P(3HO) and P(3HB) were then formed into a blend of ratio 50:50. 0.5g of each polymer was weighed out before adding 9g of chloroform and mixing the solution overnight on a magnetic stirrer plate. No difficulties were experienced when electrospinning either P(3HO):P(3HB) (25:75) or P(3HO):P(3HB) (50:50). Electrospun fibres were fabricated from three different polymer concentrations, 8wt%, 10wt% and 12wt%. Flow rates of 1,2,3 and 4ml/hr were tried, and collector speeds of 33.5, 75.5, and 134 xg. The distance between the needle tip and the collector was changed from 10,cm, 15cm and 20cm. The most successful conditions are presented below.

Table 3.7 Conditions used to fabricate 50:50 P(3HO):P(3HB) electrospun fibres (mean ± SD, n= 3 independently fabricated samples).

Number	Solution (%)	Voltage (kV)	Distance (cm)	Flow rate (mL/h)	Speed (xg)	Size of fibres (µm)
1	8	11.5	15	3	75.5	2.0 ± 0.6
2	8	11.6	10	1	134	2.7 ± 0.3
3	10	10	10	2	134	3.6 ± 0.5
4	10	10.5	15	1	134	4.3 ± 0.3
5	10	12.5	15	3	134	5.0 ± 0.4
6	8	9.5	20	2	33.5	6.1 ± 1.9
7	10	10	10	2	33.5	7.3 ± 0.9
8	10	12.5	10	3	134	7.9 ± 0.5
9	10	12.5	10	3	33.5	9.1 ± 1.5

In order to determine fibre diameter for each condition, fibres spun onto foil were cut into sections and analysed by scanning electron microscopy. Fibre diameters of electrospun P(3HO):P(3HB) (50:50) ranged from 2.0µm - 9.1µm.
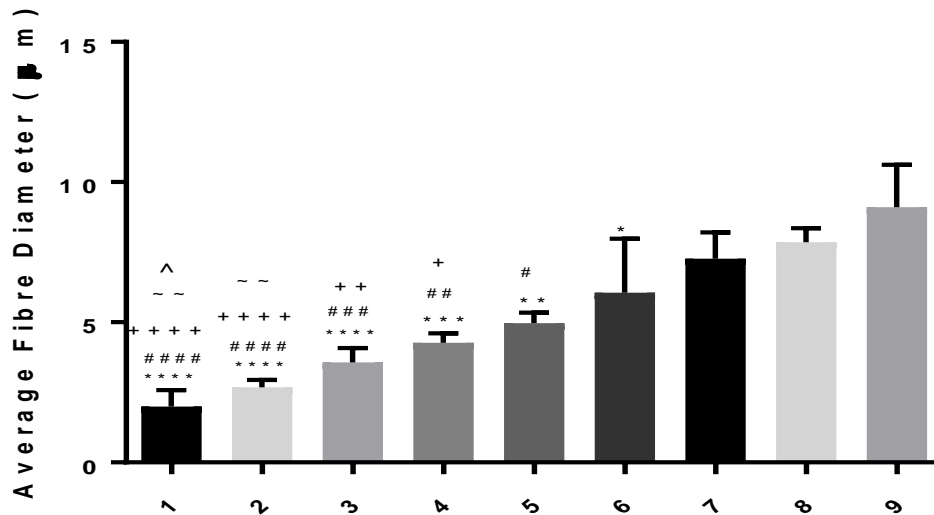
Figure 3.18. Graph of the different fibre diameters fabricated from different conditions of P(3HO):P(3HB) (50:50). A one way anova with Tukey's multiple comparisons tests was used to analyse data (Mean ± SD, n= 3 independently fabricated samples, *p < 0.05, **p < 0.01, ***p < 0.001, ****p < 0.0001 compared to condition 9, #p < 0.05, ##p < 0.01, ###p < 0.001, ####p < 0.0001 compared to condition 8, +p < 0.05, ++p < 0.01, +++p < 0.001, ++++p < 0.0001 compared to condition 7, ~~p < 0.01 compared to condition 6, ^p < 0.05 compared to condition 5).

Larger fibre diameters, fabricated by electrospinning conditions 5-9, are significantly larger than those fabricated in conditions 1-4 (figure 3.18). The largest diameter of fibres produced were 9.1 ± 1.5µm (condition 9) followed by 8.3 ± 2.0µm, produced by condition 8. Variance between fibres diameters produced from conditions 8 and 9, are much larger compared to diameters fabricated by conditions 1-5. This could be due to increased viscosity, and increased flow rate causing a blockage in the needle. This can be seen in figure 3.20 (condition 9), identifying fibres which are much larger than others and fibres merging together due to incomplete solvent evaporation. This is also seen in figure 3.20C (condition 7). Notwithstanding, the majority of fibres shown in both micrographs are aligned. Figure 3.20A and B shows SEM micrographs of conditions 1 and 5. Fibres in figure 3.20A are much smaller than the other micrographs.
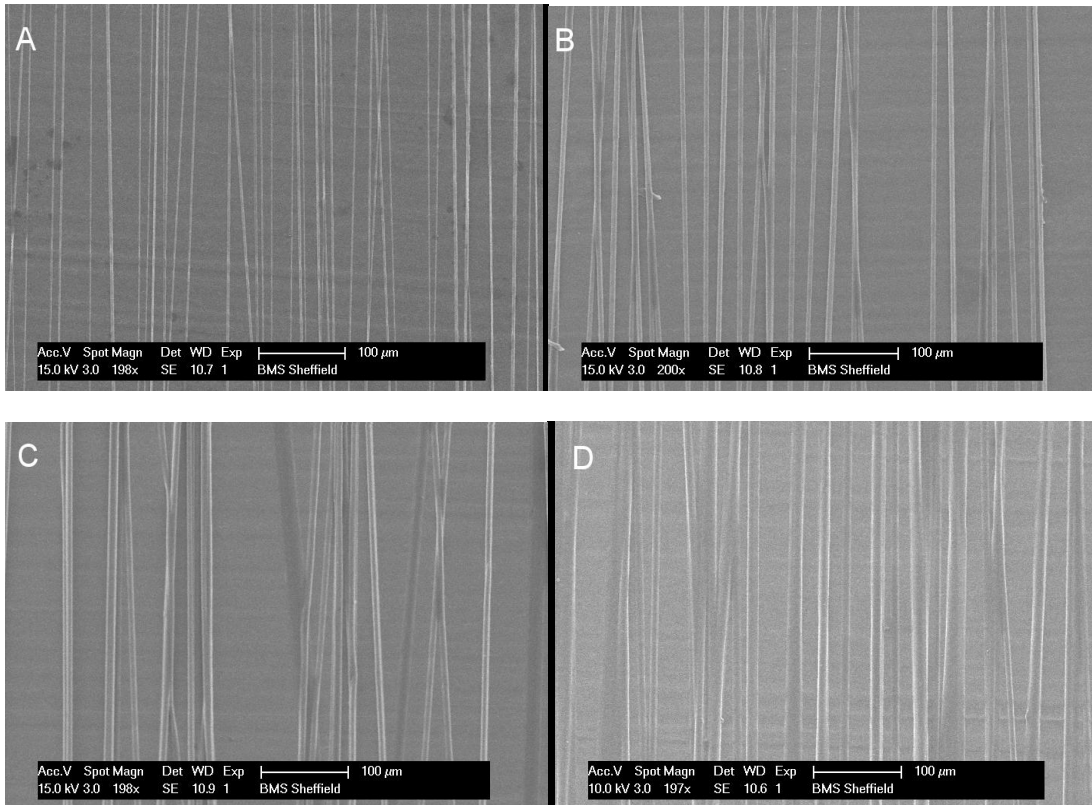
Figure 3.19. SEM micrographs of P(3HO):P(3HB) (50:50) electrospun fibres with average diameters of A) 2.0µm fibres, B)5.0µm fibres, C) 7.3µm fibres and D) 9.1µm fibres.

In order to determine fibre alignment, a centrally aligned fibre was located, and the angular variance of the surrounding fibres was measured to determine alignment of the fibre fabricated.
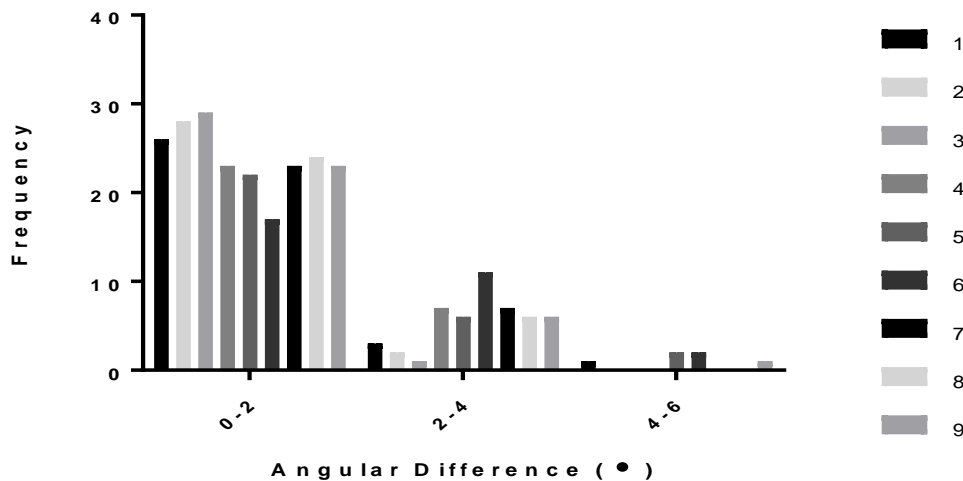
Figure 3.20. Graph to show the angular difference between samples linked to the table of electrospinning conditions. For all conditions, except no.6, at least two thirds of the fibres were located in the 0-2˚category confirming parallel alignment.

Angular variance (measured in degrees) of P(3HO):P(3HB) (50:50) fibres is illustrated in figure 27. Alignment studies confirmed that all conditions, apart from condition no. 6, resulted in parallel aligned fibres. Condition 6 resulted in 17/30 fibres of 0-2°, with the rest of the fibres aligning at 2-4° and 4-6°. To note, no fibres were measured above 6° compared to the centrally aligned reference fibre, indicating the ability to fabricate nearly parallel aligned fibres of P(3HO):P(3HB) (50:50). Fibres could also be removed from the foil collector with ease and could be manipulated by hand without losing alignment. Conditions 1-5, and 7-8, resulted in fibres with very little variance in diameter. All conditions except 9, fabricated fibres which were aligned, with very few stray fibres. Therefore, fibres produced from conditions 1-5, and 7-8 would be potential diameters for use as an intraluminal guidance scaffold or a nerve guide conduit. This depends on which diameters are the most efficient for neuronal cell differentiation, and Schwann cell/neuronal cell viability, conducted in chapter 4. Although not as biocompatible as P(3HO):P(3HB) (25:75), the higher concentration of P(3HO) in this blend would indicate that the mechanical properties of the 50:50 blend would be closer to that of native nerve tissue compared to the P(3HO):P(3HB) (25:75) blend.

### 3.3.9 Polyhydroxybutyrate:Polyhydroxyoctanoate P(3HO):P(3HB) (75:25)

A blend of P(3HO):P(3HB) (75:25) was produced, to fabricate electrospun fibres. Three polymer solutions of 8, 10 and 12wt% solutions were fabricated to attempt electrospinning. Flow rates of 1,2,3 and 4ml/hr were investigated, and collector speeds of 33.5, 75.5, and 134 xg. The distance between the needle tip and the collector was changed from 10,cm, 15cm and 20cm. Only 8 and 10wt% polymer solutions fabricated fibres. Higher voltages (15-18kV) were needed for working distances below 10cm. At 15cm, lower voltages (8-10kV) produced fibres. There were also some problems to visualise fibres by SEM as the gold coating was observed to absorb into the fibres. However, some successful conditions were produced to fabricate P(3HO):P(3HB) (75:25) fibres and these are reported below.

Table 3.7. Electrospinning conditions and fibre diameters of P(3HO):P(3HB) (75:25). (Mean ± SD, n = 3 independently fabricated samples)

Condition Number	Solution (%)	Voltage (kV)	Distance (cm)	Flow rate (mL/h)	Speed (xg)	Size of fibres (um)
1	10	7.6	15	2	134	3.7 ± 1.0
2	10	8.5	15	2.5	134	5.6 ± 0.9
3	10	14.9	10	4	75.5	5.7 ± 1.0
4	10	15.6	15	4	75.5	6.0 ± 0.7
5	10	16	10	1	134	6.0 ± 1.2
6	10	15	20	3	33.5	6.4 ± 0.4
7	10	15	15	2	134	6.5 ± 0.5
8	10	9	20	2	134	6.6 ± 1.3
9	8	16.6	10	3	33.5	6.7 ± 1.8

Scanning electron micrographs were taken of these fibres to determine diameter, variation and alignment. Fibre diameters were fabricated across a smaller range compared to other PHA blends, from 3.7 - 6.7µm (table 3.7). There was no significant difference found between samples, identifying considerable variance between fibre diameters measured per condition. This is most likely due to the high concentration of P(3HO) causing the fibres to fuse and stick together, resulting in varying fibre diameters.
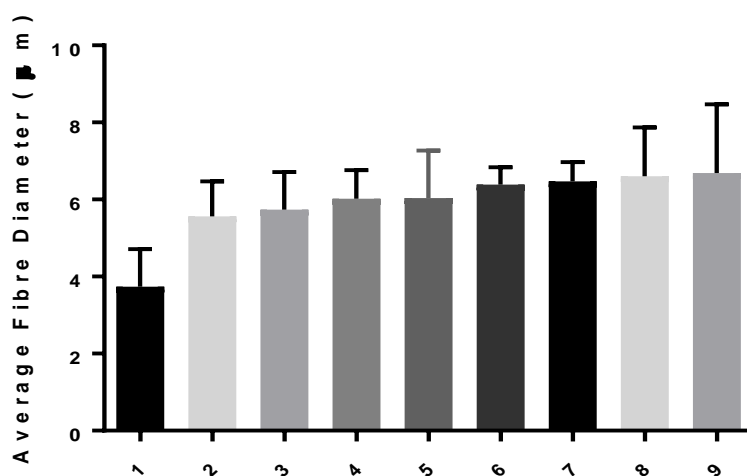
Figure 3.21. Graph showing different fibre diameters fabricated from different conditions of P(3HO):P(3HB) (75:25). A one way anova with Tukey's multiple comparisons tests was used to analyse data (Mean ± SD, n = 3 independently fabricated samples. No statistical differences detected between samples).

Scanning electron micrographs of four P(3HO):P(3HB) (75:25) electrospinning conditions are seen below in figure 30. As seen in figure 30A and B, individual fibres could be formed, with little crossover of fibres. However, figure 30C and D illustrates issues identified with gold coating for visualisation of samples by SEM, as well as the presence of dust particles which stuck to the fibres. This would indicate difficulties sterilising these fibres, as well as removing them from the foil collector. To confirm fibre alignment, angular variance between fibres was measured and the results presented in figure 31.
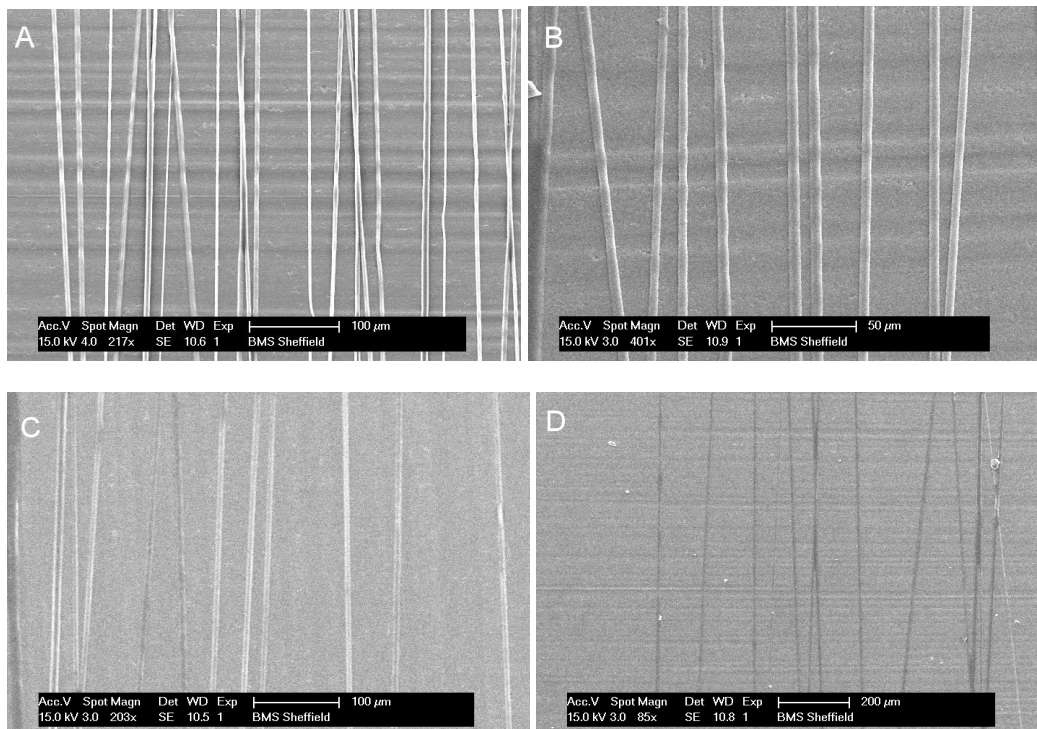
Figure 3.22. Scanning electron micrographs of P(3HO):P(3HB) (75:25) electrospun fibres with average diameters of A) 3.7µm fibres, B) 5.6µm fibres, C) 6.4µm fibres and D) 6.6µm fibres
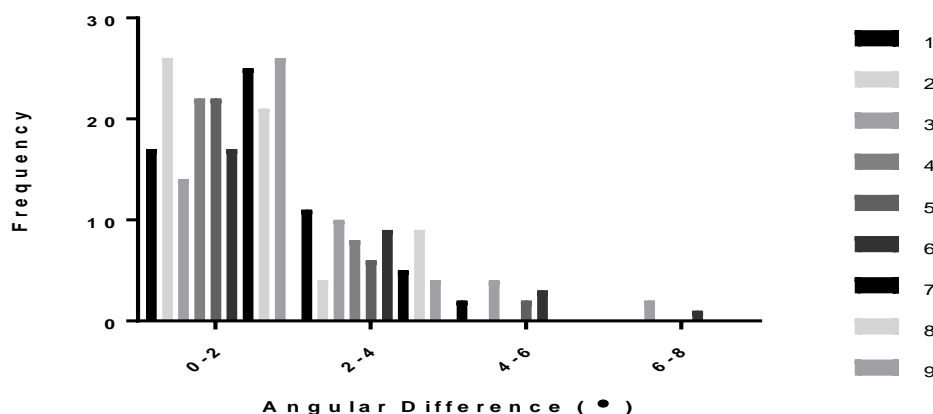
Figure 3.23. Graph to show the angular difference between samples linked to the table of electrospinning conditions. For all conditions, except no.1,3 and 6, at least two thirds of the fibres were located in the 0-2˚ category confirming parallel alignment.

All electrospinning conditions, apart from 1, 3 and 6, were found to fabricate parallel aligned fibres. More than 20, of the 30 measured fibres, measured 0-2˚ from the reference central fibre. Although some difficulties arose with electrospinning P(3HO):P(3HB) (75:25) fibres, parallel aligned fibres with different diameters could be fabricated. However, once removed from the foil collector, fibres were difficult to handle, and stuck together, losing any alignment produced. When electrospinning much thicker mats by electrospinning for a longer time period, fibres fused together, and the diameter was lost

3.3.10 P(3HO-co-3HD):P(3HB) (95:5)

Blends of 95wt% P(3HO-co-3HD) and 5wt% of the synthetic polymers were fabricated, and electrospinning of these blends was performed. P(3HO-co-3HD) and P(3HB) were dissolved in chloroform at a ratio of 95:5. Voltages of 6-15kV were investigated before changing any other parameters. A low voltage of 7-9kV was the most successful to produce a polymer jet. This could be due to a strong electric charge of the polymers, requiring a lower voltage for electrospinning. Flow rates of 1,2,3 and 4ml/hr were investigated, and collector speeds of33.5, 75.5, and 134 xg. The distance between the needle tip and the collector was changed from 10,cm, 15cm and 20cm. The table below presents the successful conditions that fabricated electrospun fibres of P(3HO-co-3HD):P(3HB) (95:5).

Table 3.8. Electrospinning conditions and diameters of fibres of 95:5 P(3HO-co-3HD):P(3HB) (mean ± SD, n=3 independently run experiments).

| Condition Number	Solution (%)	Voltage (kV)	Distance (cm)	Flow rate (mL/h)	Speed (xg)	Size of fibres (µm)
1	10	8	10	1	134	2.7 ± 0.3
2	10	8	10	1	134	3.6 ± 0.5
3	10	8	15	3	33.5	4.0. ± 1.
4	10	8	10	3	75.5	4.9 ± 0.6
5	10	8.4	15	3.2	134	6.3 ± 0.9
6	10	7	15	3.4	134	7.3 ± 1.4
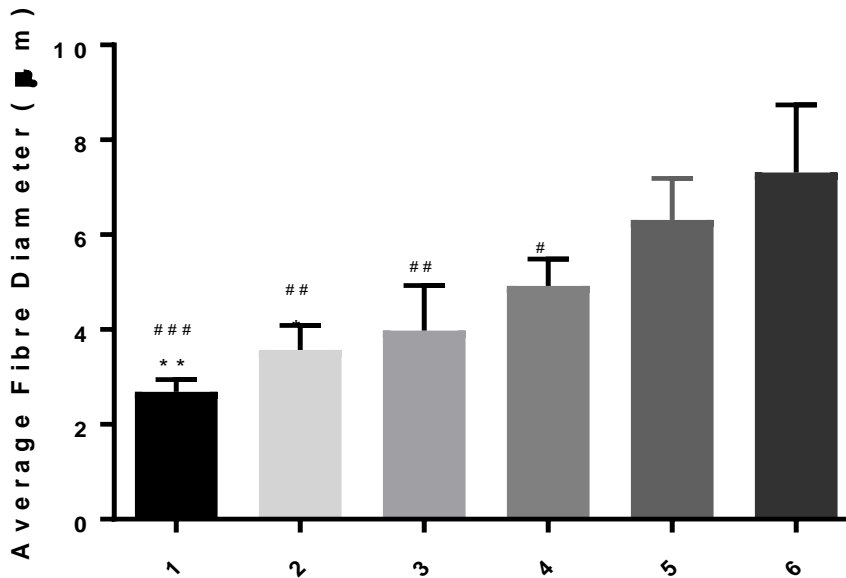
Figure 3.24. Graph of different fibre diameters fabricated by a range conditions of P(3HO-co-3HD):P(3HB) (95:5). A one way anova with Tukey's multiple comparisons tests was used to analyse data (Mean ± SD, n=3 independently run experiments, samples *p < 0.05, **p < 0.01 compared to condition 5, #p < 0.05, ##p < 0.01 compared to condition 6).

A range of different fibre diameters, from 2.7 - 7.3µm, were fabricated using this blend. In order to determine statistical variance fibre diameters were plotted below (figure 3.24). Conditions 1 - 4 resulted in fibres of 2.7 ± 0.3µm, 3.6 ± 0.5µm, 4.0 ± 1.0µm and 4.9 ± 0.6µm which were significantly different to condition 6. Fibres with an average diameter of 7.3 ± 1.4µm were manufactured. However, there was a larger variance between fibre diameters produced from electrospinning condition 6, compared to variance of smaller fibre diameters fabricated by electrospinning conditions 1-4. This indicates that as the average fibre diameter increases, the variance in diameters is much larger, due to merging of fibres together. This is most likely due to the high amount of the P(3HO-co-3HD) in this blend. Micrographs are presented below to show individual fibres. There was some fibre beading and fusion arising from conditions when using a working distance >20cm. When this was reduced to 15cm, individual fibres were formed. Larger diameters fabricated produced more aligned fibres.
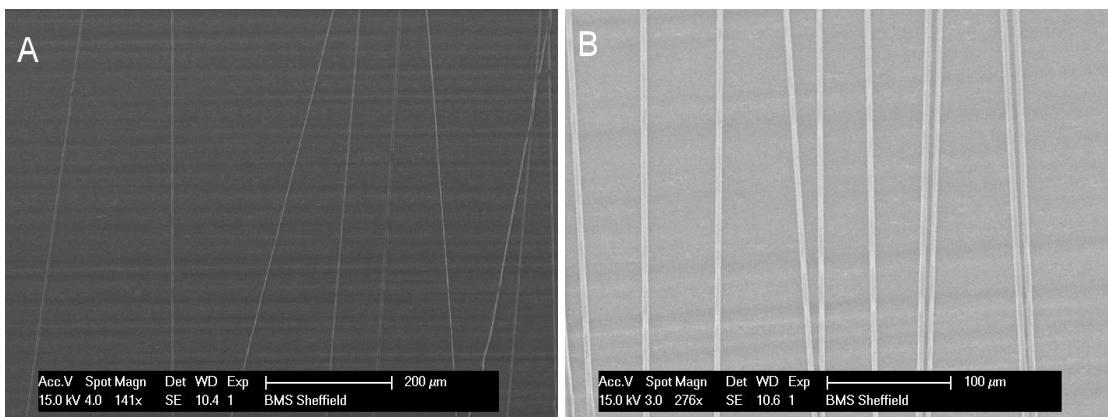
Figure 3.25. Scanning electron micrographs of P(3HO-co-3HD):P(3HB) (95:5) electrospun fibres with average diameters of A) 3.98µm and B) 4.92µm.
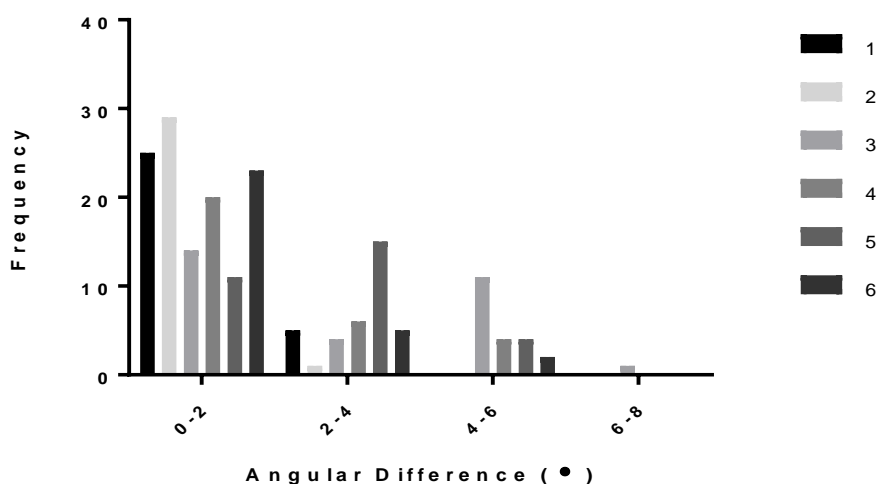
Figure 3.26: Graph showing the relationship between angular variance and electrospinning condition. For all conditions, except 3 and 5, at least two thirds of fibres showed alignment between 0-2˚.

Fibre alignment was determined by measuring the angular variation between fibres, as a basis to explore whether this blend might be an intraluminal scaffold candidate. Figure 3.26 illustrates that four of the six conditions resulted in parallel aligned fibres, with more than 20-30 fibres measuring 0-2˚ from the centrally aligned reference fibre. No fibres measured above 8° degrees from the reference fibre. However, when fabricating fibre mats, with increased fibre density, fibres fused together, and alignment was lost, due to incomplete solvent evaporation. After vacuum drying, and soaking fibres in PBS, fibres could not be removed from the foil collector.

3.3.11 P(3HO-co-3HD):PLLA blends

P(3HO-co-3HD) and PLLA (Mw 100kDa, Vornia Biomaterials Ltd, Ireland) were dissolved at a ratio of 95:5 in chloroform. Solutions of 8, 10 and 12wt% were produced and voltages between 8-20kV applied to produced a polymer jet. Flow rates of 1,2,3 and 4ml/hr were investigated, and collector speeds of 33.5, 75.5 and 134 xg. The distance between the needle tip and the collector was changed from 10,cm, 15cm and 20cm.
Issues arose electrospinning P(3HO-co-3HD) and PLLA in chloroform (as seen in figure 3.27A), and so two solvent combinations were investigated, chloroform: DCM mix (1:1) and chloroform: DCM mix (9:1). Electrospun fibres were fabricated with some alignment as seen below in figure 2.37B and C.
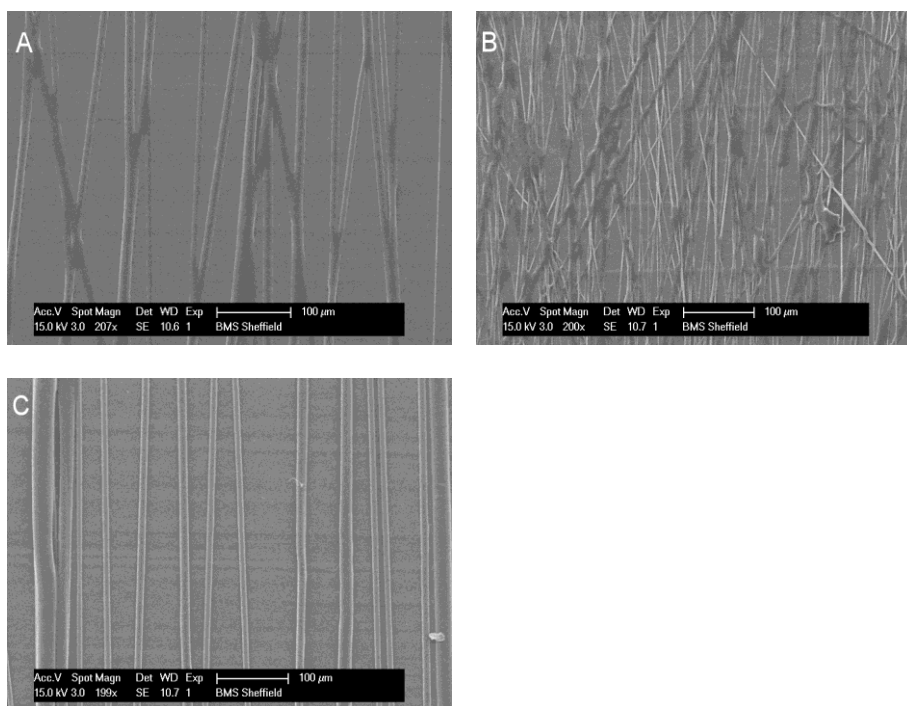
Figure 3.27. SEM images of 10wt% P(3HO-co-3HD):PLLA (95:5) electrospun fibres dissolved in A) chloroform, B) chloroform:DCM (1:1) and C) chloroform:DCM (9:1) (average diameter 8.97μm)

Although adding DCM to chloroform at a ratio of 1:1 improved the quality of the fibres, aligned fibres fabricated could not be removed from the foil collector and were wet due to the high concentration of the P(3HO-co-3HD) and incomplete solvent evaporation.

Due to the ability to fabricate P(3HO):P(3HB) (25:75) and (50:50) fibres, P(3HO-co-3HD) was blended with higher amounts of PLLA. Although it was predicted that P(3HO-co-3HD):PLLA (75:25) would experience similar problems to the P(3HO):P(3HB) (75:25), it was still attempted. Initially, 10wt% solutions of all three blends, dissolved in DCM, were produced and electrospun at a rate of 4mL/hr, collector speed of 134g and a working distance of 20cm. The best voltage for all three blends was 15kV. Figure 3.28 shows scanning electron micrographs of the three blends at this condition.
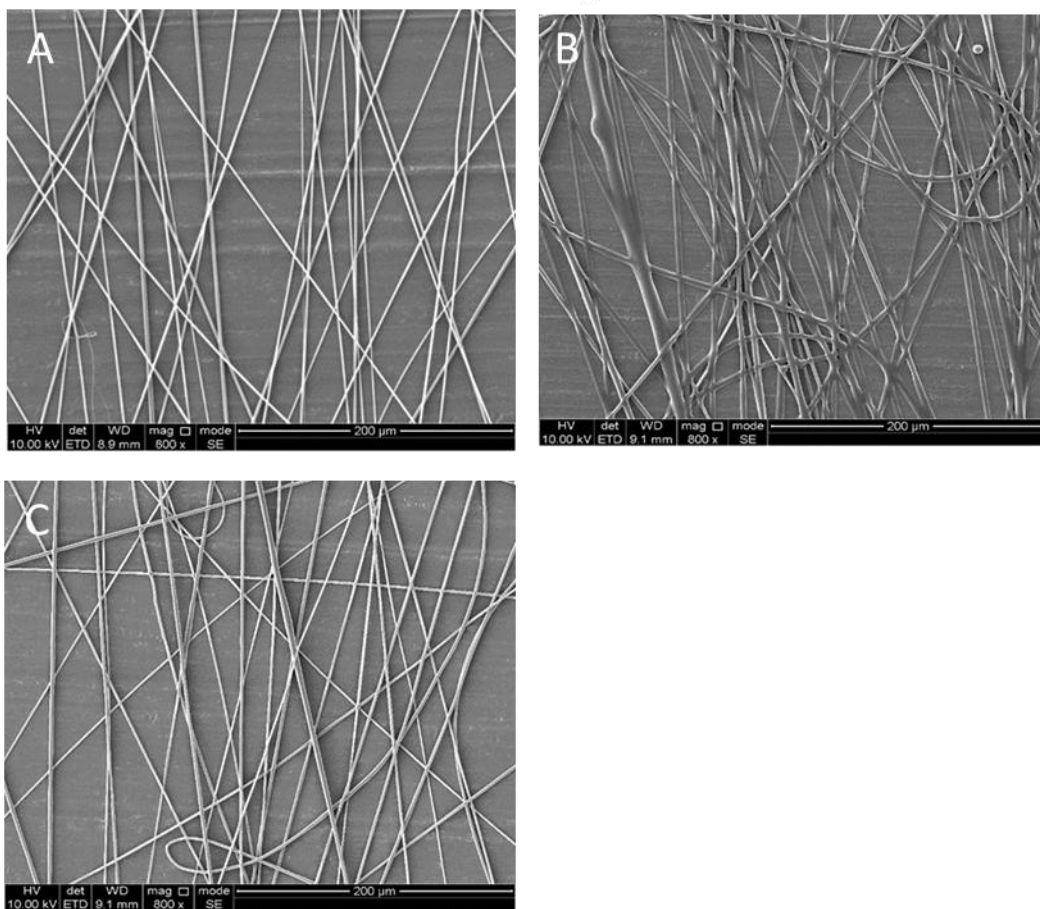
Figure 3.28. SEM micrographs of 10wt% A) P(3HO-co-3HD):PLLA (75:25) fibres, B) P(3HO-co-3HD):PLLA (50:50) fibres and C) P(3HO-co-3HD):PLLA (25:75) fibres.

As predicted, the P(3HO-co-3HD): PLLA (75:25) resulted in thick and fused fibres and was difficult to remove from the foil. The 50:50 and 75:25 blends produced even, individual fibres, and could be removed the foil. However, the 10wt% solution produced randomly orientated fibres, and a quick analysis of fibre diameter confirmed sizes of 2.7 ± 0.5µm and 1.9 ± 0.3µm. The flow rate used to fabricate these fibres was 4mL/hr. Any increase above this rate resulted in the syringe becoming blocked due to the viscosity of the solution. Therefore, the polymer wt% was increased to 12wt% and 15wt%. Scanning electron micrographs of these conditions are shown below.
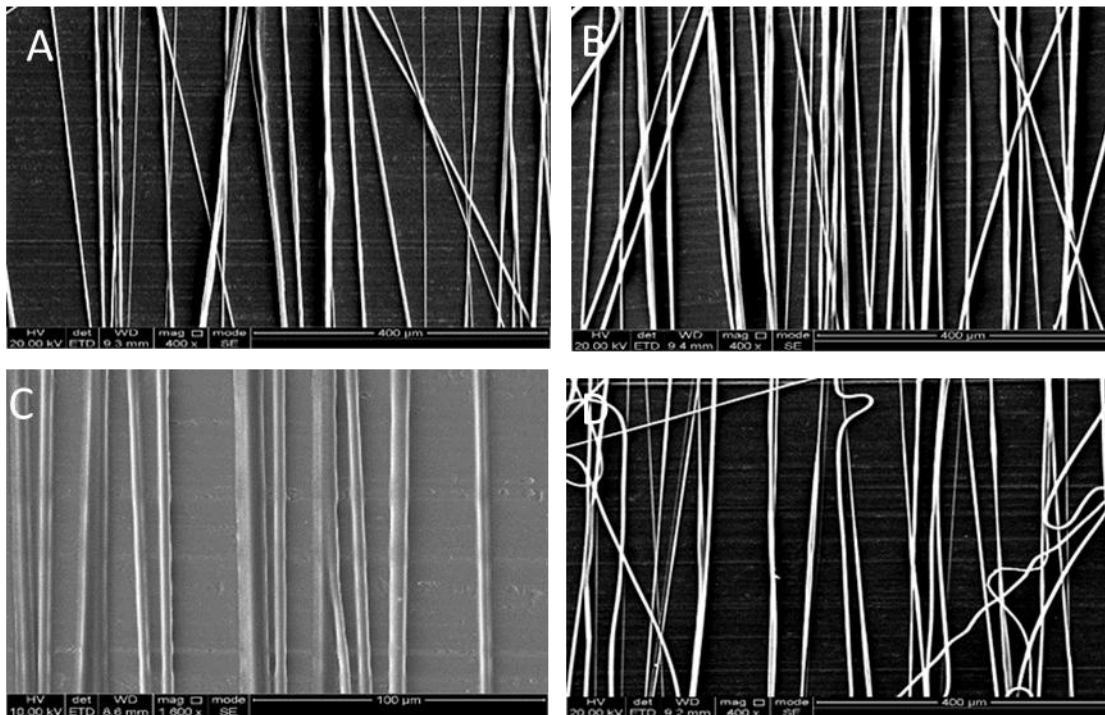
Figure 3.29. SEM micrographs of A) 12wt% P(3HO-co-3HD):PLLA (50:50) fibres, B) 15wt% P(3HO-co-3HD):PLLA (50:50) fibres, C) 12wt% P(3HO-co-3HD):PLLA (75:25) fibres and D) 12wt% P(3HO-co-3HD):PLLA (25:75) fibres.

By increasing the polymer concentration, more aligned fibres of P(3HO-co-3HD):PLLA were fabricated. Overall it was confirmed that the P(3HO-co-3HD):PLLA (50:50) blend would be investigated further to fabricate aligned fibres of known diameters. A quick analysis of the samples, as illustrated in figure 3.29A, confirmed the average diameter of fibres was 4.97 ± 0.74μm, and the average diameter of fibres fabricated in figure 38C was 8.89 ± 0.45μm.

12 and 15wt% solutions of P(3HO-co-3HD):PLLA (50:50) were fabricated and voltages between 8-20kV applied to produced a polymer jet. Flow rates of 1,2,3 and 4ml/hr were investigated, and collector speeds of 33.5, 75.5 and 134xg. The distance between the needle tip and the collector was changed from 10,cm, 15cm and 20cm.

Table 3.8 shows a summary of conditions for the fabrication of visually aligned fibres of varying diameter. To confirm fibre diameter, and the statistical differences between fibre diameters fabricated, fibres were measured using the ruler tool on NIH software image J (Schneider *et al.*, 2012). Over 100 diameters were measured for 3 different batches of fibres fabricated and fibre diameters can be observed in figure table 3.8, along with the condition that fabricated it.

Table 3.8. Electrospinning conditions and fibre diameters of P(3HO-co-3HD):PLLA (50:50) fibres. (mean ± SD, n=3 independently run experiments).

Condition Number	Solution (%)	Voltage (kV)	Distance (cm)	Flow rate (mL/h)	Speed (xg)	Size of fibres (µm)
1	12	8	20	2	134	3.5 ± 0.5
2	12	8	20	4	134	5.0 ± 0.7
3	12	8	15	4	134	7.8 ± 0.5
4	15	15	20	4	134	8.9 ± 0.5
5	12	8	10	4	134	10.1 ± 1.7
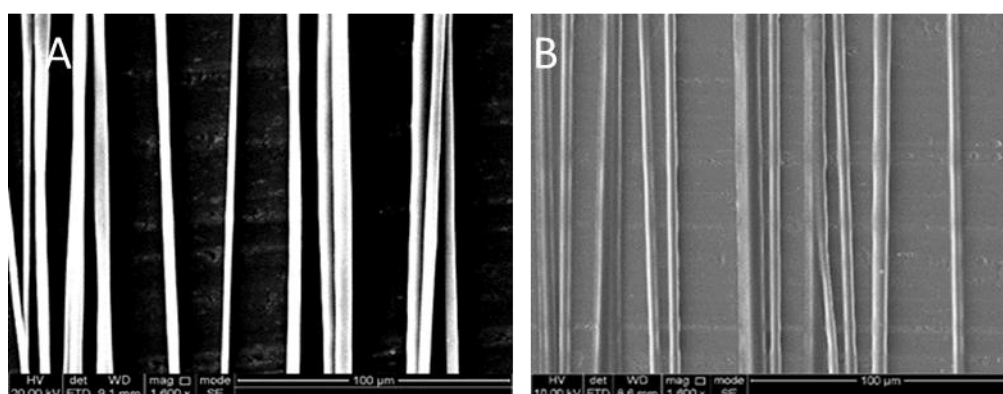
Figure 3.30. SEM micrographs of A) 4.97 ± 0.74µm (condition 2) and B) 7.81 ± 0.47µm (condition 3) P(3HO-co-3HD):PLLA (50:50) electrospun fibres.

No significant differences were detected between fibres fabricated from conditions 1 and 2, suggesting an overlap of fibre diameters measured (figure 3.31). However, fibres formed from both conditions 1 and 2 had significantly smaller diameters compared to fibre diameters fabricated from conditions 3, 4 and 5. The largest average fibre diameter fabricated was 10.1 ± 1.7µm (condition 5) followed by 8.9 ± 0.5µm (condition 4). Conditions 1 and 2 produced fibres with an average diameter of 3.5 ± 0.5µm and 4.97 ± 0.7µm. Similarly, to the other PHA blends, the fibres fabricated from condition 5 had large variance, compared to the other conditions, indicating that there are limitations when electrospinning larger diameters of fibres.
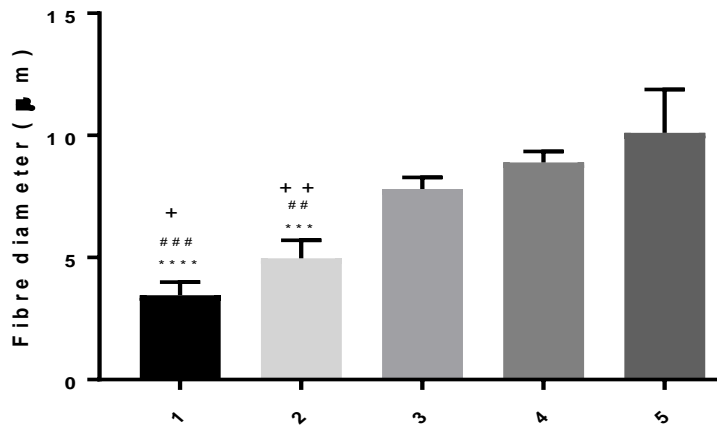
Figure 3.31. Different fibre diameters fabricated according to a range of conditions for P(3HO-co-3HD):P(LLA) (50:50). A one way anova with Tukey's multiple comparisons tests was used to analyse data (mean ± SD, n=3 independently run experiments, samples ***p < 0.001, ****p < 0.0001 compared to condition 5, ##p < 0.01, ###p < 0.001 compared to condition 4, +p < 0.05, ++p < 0.01 compared to condition 3).

To determine if P(3HO-co-3HD):PLLA (50:50) fibres fabricated in figure 3.32 were aligned, the angular variance was measured. Electrospinning conditions 2, 3 and 4 resulted in fibres that were aligned (figure 42) due to the majority of fibres measuring 0-2° from the centrally aligned, and very little fibres measuring 2-4° from the central fibre. Fibres fabricated using electrospinning conditions 1 and 5 were less aligned, but over 20 fibres measured 0-2° from the central reference fibre. With regards to condition 5, some fibres measured 6-8° from the reference fibre indicating stray fibres. However, no fibres were measured above 8-10° or 10-12° from the central reference fibre.
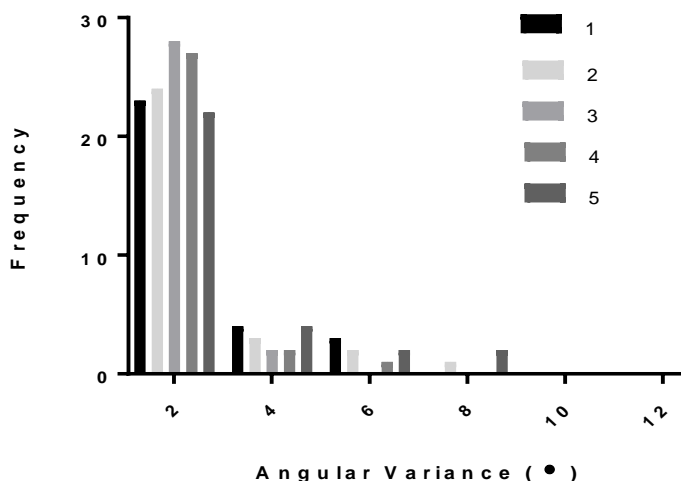
Figure 3.32. Graph to show the angular difference (degrees) between samples by electrospinning condition. Conditions 2 and 3 produced the highly aligned fibres, compared to the other processing conditions. For all conditions, at least two thirds of the fibres were in the 0-2°category, confirming near parallel alignment.

Five different diameters were fabricated for P(3HO-co-3HD):PLLA (50:50). Fibres fabricated using conditions 1, 2, 3 and 4, were concluded be the most appropriate as an internal fibre

scaffold for use in nerve repair, due to minor difference in variation between fibre diameters and parallel alignment of fibres.

3.4 Discussion

Overall, the majority of materials that were electrospun fabricated aligned fibres. The electrospinning of blends of short and medium chains together, along with other biodegradable polymers is novel, and has not been reported before. Four different parameters were investigated throughout this chapter, to fabricate electrospun fibres. These were: Polymer concentration, flow rate of the polymer, the distance between the needle and the collector, and the speed of the collector. Voltage was initially investigated when electrospinning a new material and blend, to determine which voltages would produce a polymer jet. In an ideal set up, temperature and humidity would be controlled throughout the electrospinning process. Therefore, batches of fibres were manufactured on the same day and the temperature monitored throughout. For each investigated parameter, there were 3-4 variables. To begin electrospinning a new blend of materials or material, parameters were also kept the same using a 10wt% solution of the polymer, a flow rate of 4mL/hr, distance of 20cm and collector speed of 134xg. It was observed that increasing the flow rate and polymer concentration, and decreased the distance between the needle and collector, would fabricate thicker fibres. Viscosity was not measured, and so further work would include recording the viscosity of each solution before electrospinning, to ensure reproducibility.

The reported brittle polymers, P(3HB), PHBV, PCL, PLLA and PLGA, manufactured fibres with the best alignment, and very little variances in fibre diameter per electrospinning condition (Ulery *et al.*, 2011). Material characterisation was performed in chapter 2 in which P(3HO) and P(3HO-co-3HD) were materials of particular interest due to their lower Young's moduli of 0.8 ± 0.1MPa and 8.7 ± 1.1MPa (Lorena R. Lizarraga-Valderrama *et al.*, 2015; Basnett *et al.*, 2017). As previously discussed, the ideal nerve guide conduit should be manufactured using materials which mimic native nerve tissue, matching the physical and the mechanical properties (Nectow *et al.*, 2012). Borschel *et al.* (2002) noted that the Young's moduli of native rat sciatic nerve was 0.58 ± 0.15 MPa, before using a decellularization process (Borschel *et al.*, 2003). Therefore, the medium chain polyhydroxyalkanoates, P(3HO) and P(3HO-co-3HD) were of particular interest to begin electrospinning, due to their chemical novelty and appropriate mechanical properties for nerve (Bagdadi *et al.*, 2016). Overall, the medium chain polyhydroxyalkanoates were difficult to electrospin, due to their elastomeric properties. Although individual aligned fibres could be fabricated, there were difficulties removing fibres from the foil collector. Once

removed, fibres stuck together, losing any alignment. It was also noted, from chapter 2, that the biocompatibility of medium chain polyhydroxyalkanoates was not as good as the short chain polyhydroxyalkanoates, P(3HB) and its co-polymer PHBV.

Therefore, blends of short and medium chain PHAs, as well as blending medium chain PHAs with FDA approved polyesters, were investigated to take advantage of medium chain PHAs appropriate mechanical properties, as well as the advantageous biocompatibility of P(3HB), PCL, and PLLA (Nectow et al., 2012). Although mechanical testing did show that PLGA had the lowest tensile strength of all the synthetic polymers, it was the closest to native sciatic nerve (1.8 ± 0.1 MPa), however the material was not taken forward to blend with medium chain PHAs due to the cost of using HFIP as a carrier solvent (Kehoe et al., 2011). Blends of P(3HO):P(3HB) have previously been investigated by Basnett et al. (2013) and Lizarraga et al. (2015). Basnett et al. (2013) investigated P(3HO), and blends of 80:20, 50:50, 20:80 P(3HO) with P(3HB) for their potential in cardiovascular tissue engineering due to the elastomeric properties of P(3HO). All blends with P(3HB) were more biocompatible than P(3HO), but also observed was that degradation time of the films with higher concentrations of P(3HB) was shorted (Basnett et al., 2013). This data suggested that a blends of P(3HO) and P(3HB) would approximate the mechanical properties required for peripheral nerve repair, have biocompatibility as a scaffold, as well as an ability to tailor the degradation rate of the fibres inside an NGC. It can also be manufactured as a scaffold for a variety of gap lengths. The data published by Lizarraga et al. (2015) suggested that the P(3HO):P(3HB) (25:75) blend was the most biocompatible, as well as most efficient for supporting NG108-15 neuronal cell differentiation (Lorena R. Lizarraga-Valderrama et al., 2015). This blend could be electrospun into many different diameters of fibre with excellent alignment. However, out of all three PHA blends, this material was the stiffest, with a higher Young's modulus. P(3HO):P(3HB) (75:25) was the most elastomeric blend out of the three. However, when fibres were fabricated, they were very sticky and fused together. Fibres could not be removed from the foils either, and lost alignment. P(3HO):P(3HB) (50:50) could also be electrospun well, with a variety of fibres fabricated, with excellent alignment. P(3HO):P(3HB) (50:50) was also biocompatible, but as seen in the study, as well as in chapter 2, the mechanical properties of this blend were closer to that of native nerve, when compared to the P(3HO):P(3HB) (25:75) blend (Lorena R. Lizarraga-Valderrama et al., 2015).

Blends of P(3HO-co-3HD) and synthetic polymers (at a 95:5) ratio were also investigated. However, due to the high concentration of P(3HO-co-3HD) in the blend, these materials could not be electrospun efficiently. Overall, the most efficient blend of a medium chain PHA with a synthetic blend was at 50:50 ratio. Any higher concentration of medium chain PHA,

and sticky fibres were fabricated, in which correct fibre diameter could not be defined due to fusion, thick mats could not be fabricated, fibres could not be removed from the collector foil and once removed, fibres lost any alignment fabricated by electrospinning.

Table 3.9 summarises polymers that could be electrospun, the range of fibres fabricated, any comments / observations associated with the electrospinning process, as well as considerations for taking the material forwards for in vitro analysis.

Table 3.9. Summary table of all the different blends of materials used to fabricate electrospun fibres and the range of different diameters produced. Decisions given as to why blends forward to in vitro testing, and how fibres handled after fabrication.

Material/Blend	Aligned electrospun fibres fabricated?	Range of fibre diameters fabricated (µm)	Comments	Taken forward for in vitro testing	Reason
PCL	Yes	1.02-8.07	Ease of production, easily removed from foil	Yes	Control material, easily fabricated, known effect on neuronal and Schwann cells
P(3HB)	Yes	2.3-8.07	Ease of production, easily removed from foil	No	Fibres easily fabricated, material very biocompatible but too brittle. Blended with softer materials to fabricate fibres.
P(3HO) and P(3HO-co-3HD)	No	N/A	Difficult to remove from foil, sticky fibres.	No	Very soft, elastomeric materials, correct mechanical properties for native nerve, but could not be processed via electrospinning. Sticky fibres fabricated.
PGA	Yes	1.55-4.32	Ease of production, easily removed from foil	No	Already FDA approved material for NGCs, expensive due to cost of HFIP as solvent. Also, material is not novel.
PHBV	Yes	1.92-10.17	Ease of production, easily removed from foil	Yes	Ease of fabrication, excellent biocompatibility, and extensive range of fibre diameters to choose from for in vitro testing. Although slow degrading, changing HV content can tailor mechanical properties and degradation.
P(3HO):P(3HB) (25:75)	Yes	1.77-10.59	Ease of production, easily removed from foil	No	Ease of fabrication, excellent biocompatibility, and extensive range of fibre diameters to choose from. Due to low amount of P(3HO), mechanical properties stiffer than other blends using P(3HO).

P(3HO):P(3HB) (50:50)	Yes	1.99-9.11	Ease of production, easily removed from foil	Yes	Ease of fabrication, excellent biocompatibility, and wide range of fibre diameters to choose from for in vitro testing. Softer blend than 25:75 but could be electrospun unlike 75:25. Compromise of mechanical properties, biocompatibility and processability.
P(3HO):P(3HB) (75:25)	Yes	3.73-6.61	Difficult to remove from foil, sticky fibres.	No	Small range of diameters fabricated, sticky material, and fibres could not be removed from the foil. Correct mechanical properties but could not handle fibres well. Not as biocompatible as other blends.
P(3HO-co-3HD):P(3HB) (95:5)	Yes	2.68-6.46	Difficult to remove from foil, sticky fibres.	No	Very soft, elastomeric material, correct mechanical properties for native nerve, but could not be processed via electrospinning. Sticky fibres fabricated.
P(3HO-co-3HD):PLLA (95:5)	Yes	8.97	Difficult to remove from foil, sticky fibres.	No	Very soft, elastomeric material, correct mechanical properties for native nerve, but could not be processed via electrospinning. Sticky fibres fabricated.
P(3HO-co-3HD):PLLA (75:25)	No	N/A	Difficult to remove from foil, sticky fibres.	No	Stiffer than the 95:5 blend but still very soft material, could not remove fibres from foil due to stickiness.
P(3HO-co-3HD):PLLA (50:50)	Yes	2.61-7.81	Ease of production, easily removed from foil	Yes	Ease of fabrication, good range of fibre diameters to choose from for in vitro testing. Softer blend than 25:75 but could be electrospun unlike 75:25. Compromise of mechanical properties, biocompatibility and processability. Good biocompatibility from P(3HO-co-3HD) and correct degradation properties using PLLA.
P(3HO-co-3HD):PLLA (25:75)	Yes	1.94-5.77	Ease of production, easily removed from foil	No	Ease of fabrication of fibres and easily removed from foil. However, large amount of PLLA would increase degradation rate of fibres, as well as make blend stiffer.

Overall, two different blends of PHAs should be taken forward for in vitro analysis. The two blends were P(3HO):P(3HB) (50:50) and P(3HO):PLLA (50:50). Both blends could be electrospun efficiently and fabricated statistically different fibre diameters with a high degree of alignment. Samples could be removed from the tin foil collector with ease and be handled well. Both blends offer a compromise on biocompatibility, as well as mechanical properties. PCL and PHBV were also taken forward to *in vitro* testing. PCL was used as a control material, as the response of NG108-15 neuronal cells and primary Schwann cells grown on PCL fibres with different diameters has been documented (Daud *et al.*, 2012). PHBV was also taken forward for *in vitro* analysis as NG108-15 neuronal cells showed the highest degree of attachment (chapter 2). Fibre diameter selection and in vitro analysis is presented in chapter 4. PHBV fibre diameters of 2, 4, 6, 8 and 10µm were fabricated to determine which fibre diameter was the most effective at supporting neuronal and Schwann cell attachment, proliferation, and neuronal cell differentiation. From this, further in vitro analysis was performed using the different material types, to establish which blend of PHA would be the most suitable to be fabricated into fibres, and inserted into hollow NGC tubes, to provide guidance for the regenerating axon and improve nerve regeneration efficiency.

Chapter 4: How important is Fibre Diameter in Peripheral Nerve Repair?

4.1 Introduction

As discussed in chapter 3, fibre alignment, both *in vitro* and *in vivo*, is an important parameter for successful nerve and axon regeneration, muscle reinnervation and neuromuscular junction formation (Kim *et al.*, 2008). Fibre alignment is also important in providing contact guidance for primary Schwann cells to adhere, align, mature and elongate (Gupta *et al.*, 2009). It has also been reported that aligned fibres promote a more mature Schwann cell phenotype, which would benefit peripheral nerve repair when inserted into a nerve guide conduit (Chew *et al.*, 2008). By mimicking the ECM and 'Bands of Büngner', aligned fibre scaffolds can be used in combination with a nerve guide conduit, to improve the efficiency of nerve regeneration, promoting Schwann cell attachment to the fibres, and providing aligned guidance cues for the regenerating axon (Kim *et al.*, 2008).

However, as well as fibre alignment, fibre diameter is also a factor to consider when designing an aligned intraluminal fibrous scaffold to aid nerve repair. Aligned nanofibre scaffolds have been well documented for use in peripheral nerve repair, using many different synthetic and natural materials but most recently, it has been suggested that using aligned fibres in the micrometre range would be more beneficial for the regenerating axon (Y. S. Lee and Arinzeh, 2011). Gnavi *et al.* (2015) cultured RT4-D6P2T Schwann cell line as well as primary Schwann cells on randomly orientated gelatine scaffolds with diameters of 0.3, 0.6 1 and 1.3μm (Gnavi *et al.*, 2015a). Overall, 1 and 1.3μm fibres promoted Schwann cell migration and axonal growth from DRG explants, but smaller nanofibres, promoted higher Schwann cell adhesion and proliferation (Gnavi *et al.*, 2015a). When culturing neuronal neonatal mouse cerebellum C17.2 stem cells onto random and aligned PLLA fibres, Yang *et al.* (2005) reported that less 'cells differentiated into the neuronal lineage' on random fibres, compared to aligned fibres (F. Yang *et al.*, 2005a). However, when observing two different fibre diameters of aligned fibres, 300nm and 1.5μm, neonatal stem cell differentiation rate was quicker on 0.3μm compared to the 1.5μm, inducing longer neurite outgrowth (F. Yang *et al.*, 2005a; Schaub *et al.*, 2016). This study initially suggested that nanofibre scaffolds promoted increased neuronal cell differentiation and neurite outgrowth compared to aligned micrometer fibre scaffolds (Schaub *et al.*, 2016). However, Wang *et al.* (2010) fabricated aligned PLLA electrospun scaffolds of 1.325μm, 0.759μm and 0.293μm in diameter and concluded that chick DRG neurite outgrowth length was significantly higher on the 1.325 and

0.759μm fibres, compared to the small 0.293μm fibres (H. B. Wang *et al.*, 2010). Neurite outgrowth from chick DRGs cultured on the 0.293μm fibres was less guided than DRG neurite outgrowth on 1.325 and 0.759μm fibres (H. B. Wang *et al.*, 2010). Schwann cell migration, from chick DRG explants, was also significantly higher than on 1.325μm fibres compared to the other two diameters (H. B. Wang *et al.*, 2010). This study showed that larger fibre diameters were more effective in promoting neurite outgrowth using an *ex vivo* DRG model, as well as confirming that smaller fibre diameters are not as efficient in directing the outgrowth of neurites from primary neurons (Schaub *et al.*, 2016).

Yao *et al.* (2009) investigated 4 different diameters of aligned fibres for use as electrospun fibre conduits for nerve repair, also comparing these diameters to a random fibre scaffold (L. Yao *et al.*, 2009). 0.8, 3.7, 5.9 and 8.8μm PCL fibre films were fabricated, and PC12 cells were cultured onto scaffolds (W. Daly *et al.*, 2012). Overall, PC12 neuronal cell neurite outgrowth was significantly higher on the 3.7 and 5.9μm fibres, compared to the random fibres. However, no significant differences were detected between these fibre diameters (L. Yao *et al.*, 2009). Daud *et al.* (2012) investigated using 1, 5 and 8μm PCL fibres for potential use in peripheral nerve repair. When culturing NG108-15 neuronal cells on fibres, maximum neurite outgrowth on the 8μm fibres was significantly higher than on any of the other diameters and flat controls, and numbers of live NG108-15 neuronal cells was significantly higher on the 5 and 8μm PCL fibres compared to cells cultured on the 1μm fibres (Daud *et al.*, 2012). However, when observing Schwann cell growth and elongation, primary Schwann cell length were significantly higher on the 1μm fibres, compared to the other diameters, but no significant differences were detected in Schwann cell viability (Daud *et al.*, 2012). Wen *et al.* (2006) cultured explanted rat DRGs on polypropylene fibre filaments with diameters of 5, 30, 100, 200 and 500μm, in which neurite length and Schwann cell migration was significantly higher on the 5 and 30μm fibres, compared to any of the other diameters (Wen and Tresco, 2006).

Both the study by Daud *et al.* (2012) and Wang *et al.* (2010) suggests that using fibres in micrometre range is more effective for neurite outgrowth and Schwann cell migration and maturation when using a DRG *ex vivo* model (H. B. Wang *et al.*, 2010; Daud *et al.*, 2012). The study by Wen *et al.* (2006) suggest that diameters above 30μm are not as effective for promoting neurite outgrowth and Schwann cell migration (Wen and Tresco, 2006). Overall, the literature suggests that different neuronal cell lines, neuronal stem cells, and primary neurons, differentiate more efficiently on different fibre diameters, but that the most effective diameters in promoting the longest average neurite outgrowth length are between 0.75μm and 5μm (Schaub *et al.*, 2016).

Therefore, this chapter focussed on investigating whether different fibre diameters influenced NG108-15 neuronal cell differentiation and neurite outgrowth, and Schwann cell proliferation and maturation. It is hypothesised, from the literature, that higher fibre diameters will support NG108-15 neuronal cell adherence and differentiation more effectively than smaller fibre diameters. NG108-15 neuronal cells were chosen as per the reasons in chapter 2. NG108-15 neuronal cells are a well characterised neuronal cell line used extensively in *in vitro* research (Armstrong *et al.,* 2007). From the results of aligned electrospun fibres fabricated in chapter 3, 5 different diameters of PHBV fibres were chosen to investigate the effect of different fibre diameters on neuronal and Schwann cells. This was due to the wide range of fibres that could be reliably fabricated, excellent alignment created using electrospinning, as well as ease of reproducibility. It was hypothesised that larger fibre diameters would support longer NG108-15 neuronal cell neurite outgrowth, and that smaller fibre diameters would support increased Schwann cell adherence.

4.2 Methods and Materials

4.2.1   Fabrication of electrospun PHBV fibres

Five different diameters of PHBV fibres were chosen for *in vitro* testing, to determine the effect of fibre diameter on neuronal and Schwann cells. These diameters were 1.92, 4.07µm, 5.97, 8.08µm and 10.17µm taken from conditions 1,3,5,8 and 10 in chapter 3 to assess the effect that small micrometer increments had on cell viability and NG108-15 neuronal cell differentiation. PHBV electrospun fibres were manufactured by the conditions in the table below. To assess reproducibility of the fibres produced in chapter 3, new batches of PHBV fibres were characterised by scanning electron microscopy to assess fibre diameter and alignment.

Table 4.1. Five successful conditions were chosen for producing aligned PHBV fibres of different diameters (see chapter 3 for previous work).

Condition Number	Polymer Solution (%)	Voltage (kV)	Distance (cm)	Flow rate (mL/h)	Speed (xg)	Size of fibres (µm)
1	10	13	20	1	134	1.92 ± 0.55
3	14	10	20	1	33.5	4.07 ± 0.56
5	14	12	20	4	134	5.97 ± 0.56
8	10	10	20	4	134	8.08 ± 0.43
10	15	12	20	4	33.5	10.17 ± 0.47

4.2.2 Fabrication of spin coated PHBV films

PHBV (Goodfellow Ltd, UK) of average Mw 600,000 g/mol, was dissolved in chloroform to produce a 10wt% solution. Solutions were stirred for overnight, at room temperature, on a stirrer plate at 1000rpm. Before spin coating, glass coverslips were treated with a 1:1 solution of sulfuric acid (H_2SO_4) and hydrogen peroxide (H_2O_2) (Fisher Scientific) to clean the glass slides, and then treated with 10wt% solution of 3-(trimethoxysilyl)-propyl methacrylate in toluene (MAPTMS) (see previous chapter for detailed method). 100µL of PHBV solution was added to the glass coverslip, and spin coated to produce a PHBV film attached to the glass coverslips. The solution was accelerated at 100xg for 30 seconds under a vacuum of 25.5C. Samples were left to dry overnight in a fume cupboard before cell culture work.

4.2.3 Characterisation of polymer flat films and electrospun PHBV fibres

To determine fibre diameter and alignment, three independently electrospun batches of the same electrospinning conditions were analysed by scanning electron microscopy. Fibres were cut to size and mounted on specimen holders, and sputter coated with a 20nm thick gold coat. An FEI Sirion field emission gun scanning electron microscope was used to take images of the fibres. Images were analysed using National Institutes of Health (NIH) Image J software (Schneider *et al.*, 2012). From each independently spun batch of fibres, diameters were taken from 50 fibres, and the fibre alignment was determined by measuring the angle of each fibre against a reference fibre (at 180˚). Fibre alignment was conducted using image J software (Schneider *et al.*, 2012). Surface coverage of the fibres was analysed by determining the fibre density (number of fibres per µm). Fibres, per 100µm, were counted manually for each batch of electrospun fibres and fibres per µm determined.

4.2.4 Preparation of aligned PHBV electrospun fibres and polymer thin films for neuronal cell culture

Aligned PHBV electrospun fibres of 1.92, 4.07, 5.97, 8.08 and 10.17 µm diameter were cut into 25mm x 25mm squares, to fit into 6 well plates. Fibres were removed from the tin foil and adhered to tissue culture well plates with a 10wt% solution of PHBV in chloroform at the top and bottom of the well plate. PHBV spin coated films, on glass coverslips, were glued down into the middle of a 6 well plate. Fibres, glued down to the well plate at each end, were held into position by large medical grade 316L stainless steel cell culture rings (inner diameter = 26mm, outer diameter = 35mm) and then a smaller stainless steel cell culture ring, (inner diameter = 13 mm, outer diameter = 20 mm) was placed into the middle of the sample, to decrease fibre surface area (see figure 4.1). Samples were sterilised using 70% ethanol for 3 hours, followed by a wash in PBS. Samples were immersed in PBS and left in

PBS overnight to ensure all contaminants had been removed. Before cell seeding, samples were washed again in PBS for 5 minutes (Daud *et al.*, 2012).
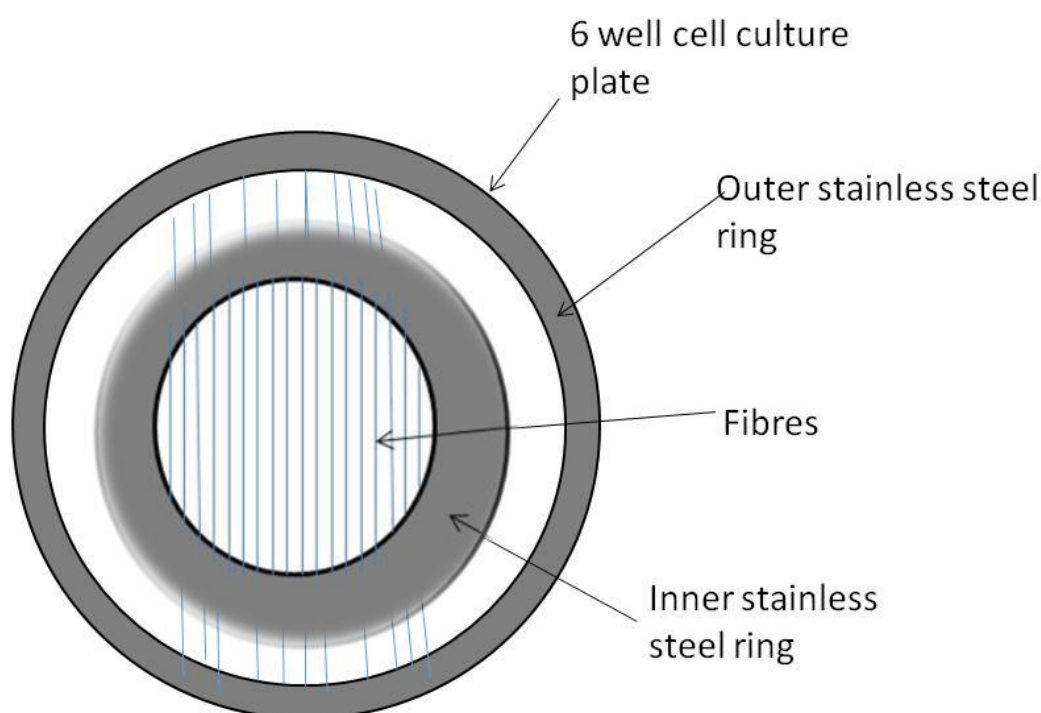
Figure 4.1. Diagram to illustrate the experimental set up for the fibre/cell interaction studies

4.2.5 NG108-15 neuronal cell culture

NG108-15 neuronal cells, supplied from the European Collection of Cell Cultures (ECACC), were used between passages 11-20 for experiments. Please see chapter 2, *Methods* section 2.1.4 for more details.

4.1.6 Immunolabelling of NG108-15 neuronal cells for βIII tubulin

Immunolabelling was performed as per the methods in Daud *et al.* (2012). Fibre samples and polymer flat films, containing NG108-15 neuronal cells, were washed with PBS, three times for 5 minutes, before being fixed with 3.7% paraformaldehyde for 20 minutes. After washing with PBS, cells were permeabilized with 0.1% Triton X-100 for 45 minutes, washed in PBS, and binding sites blocked with 3% bovine serum albumin (BSA) for 30 minutes. After a final wash, cells were incubated, for 48 hours, with a mouse anti-β III-tubulin antibody (neuronal cell marker for NG108-15 neuronal cells and neurites) (1:250) (Promega, UK) diluted in 1% BSA at 4ºC. After a wash in PBS, cells were incubated at room temperature, for 90 minutes, with Texas Red-conjugated anti-mouse IgG antibody (1:200 dilution in 1% BSA from Vector Labs, USA). Samples were washed in PBS and then incubated at room temperature with 4′,6-diamidino-2-phenylindole dihydrochloride (DAPI) (Sigma Aldrich) (300

nM) for 30 minutes, to stain the cell nuclei. DAPI was removed and samples immersed in PBS for imaging with an upright Zeiss LSM 510 confocal microscope, using a helium-neon laser (543 nm) for Texas Red excitation (λex = 589nm / λem = 615 nm). A Ti:sapphire laser (800 nm) was used to image DAPI (λex= 358 nm / λem = 461 nm) for visualising cell nuclei. Images were taken of the cells on the fibres. A starting point and end point was set on the confocal microscope to image the top of the fibres and the bottom of the scaffold to ensure that cells on the tissue culture plastic control were not images. As fibres were auto-fluorescent, cells attached to the fibres could be imaged, and were raised as not to image any cells on the tissue culture plastic. Z-slices were taken every 1-2μm and images were analysed in 2D converted images and 3D Z stacks (Daud *et al.*, 2012).

4.2.7 Isolation of rat primary Schwann cells

Rat primary Schwann cells were isolated using the method described by Kaewkhaw *et al*. Briefly, adult male Wistar rats (10-12 weeks old) were sacrificed, in accordance to the Animals Scientific Procedures Act (1986), and the sciatic nerves extracted, and placed into serum free DMEM. The epineurium was removed from the nerves, and the nerve fascicles dissociated mechanically, and then enzymatically dissociated by adding the nerves to 0.15% collagenase, for 90-120 minutes at 37°C. After centrifugation, primary Schwann cells were seeded into 35mm petri dishes and left for 7 days in Schwann cell growth medium (DMEM plus D-Valine, with 10% FCS, 1% penicillin/streptomycin, 0.5% amphotericin B, 1% glutamine, 1% N_2 supplement (Gibco BRL, UK), 20 mg/mL bovine pituitary extract, and 5mM of forskolin (Sigma Aldrich). Fibroblasts do not express the enzyme D-amino acid oxidase which metabolises D-Valine into L-Valine amino acid which is essential for growth and proliferation (Kaewkhaw *et al.*, 2012). Therefore the presence of the D-Valine in the cell culture medium inhibits fibroblast growth and proliferation. Media was replaced every 3 to 4 days until petri dishes were 90% confluent. Schwann cells were cultured up to passage 1 and used up to passage 7 for experiments. 60,000 rat primary Schwann cells per sample (13mm^2 area) were seeded onto polymer films and fibres for 6 days, and media was replaced every 2 days using Schwann cell growth media (Kaewkhaw *et al.*, 2012).

4.2.8 Co-culture of NG108-15 neuronal cells and rat primary Schwann cells on PHBV fibre diameters

Following the method published by Daud *et al.* (2012), 50,000 Schwann cells (per 13mm^2) were seeded onto PHBV fibres and cultured in Schwann cell growth medium for 7 days. Medium was removed on day 8, and 7000 NG108-15 neuronal cells were seeded onto each PHBV fibre sample, and co-culture medium (DMEM:F12, medium containing 1% glutamine, 1% penicillin/streptomycin, and 1% N_2 supplement) was added to the samples. Co-cultures

were grown for 6 days and the medium was replaced with fresh medium every 2-3 days. Samples were then labelled and imaged to determine cell viability and NG108-15 neuronal cell differentiation (Daud *et al.*, 2012).

4.2.9 Immunolabelling of rat primary Schwann cells for S100β

Immunolabelling of primary Schwann cells was performed as per the methods in Daud *et al.* (2012). Samples were washed one with PBS, before being fixed with 3.7% paraformaldehyde and permeabilized with 0.1% Triton X-100. Unreactive binding sites were blocked with 7.5% BSA for 60 minutes at room temperature and washed with PBS. Cells were incubated overnight, at 4˚C, with a rabbit-anti S100β antibody (Schwann cell Marker) (1:100) (Dako, Denmark) diluted in 1% BSA. After washing with PBS, cells were immunolabelled with a FITC-conjugated secondary anti-rabbit IgG antibody (1:100) (Vector Labs, USA) diluted in 1% BSA for 120 minutes at room temperature. Samples were washed with PBS, cell nuclei labelled with DAPI, and immersed in PBS for imaging. Schwann cells cultured on fibres were imaged using an upright Zeiss LSM 510 confocal microscope using an argon ion laser (488 nm) for FITC excitation (λex= 495 nm / λem = 521 nm) and a Ti:sapphire laser (716 nm) for DAPI (λex= 358 nm / λem = 461 nm). A starting point and end point was set on the confocal microscope to image the top of the fibres and the bottom of the scaffold to ensure that cells on the tissue culture plastic control were not images. Z-slices were taken every 1-2µm and images were analysed in 2D converted images and 3D Z stacks (Daud *et al.*, 2012).

4.2.10 Live/Dead analysis of NG108 neuronal cell line and primary Schwann cells

Live/dead analysis was conducted to determine cell viability and number of live cells versus dead cells. See chapter 2, 2.1.6 *Methods* section for details.

4.2.11 Neurite outgrowth assessment

Four different parameters were analysed for neurite outgrowth: 1) percentage of cells expressing neurites; 2) average number of neurites per polymer sample; 3) average neurite length per polymer sample / fibre diameter and 4) maximum neurite length per polymer sample / fibre diameter. Images were analysed using Image J (NIH) and neurites were traced using the Neuron J plugin tracer software from the cell body to the neurite tip (Popko *et al.*, 2009; Schneider *et al.*, 2012). 90 neurites (10 on average from each field of view image for each sample) were measured to determine maximum and average neurite length for each polymer type. Average number of neurites per neuron was counted using ITCN cell counter software on Image J (Usaj *et al.*, 2010; Schneider *et al.*, 2012). The percentage of

neurite bearing cells was determined by counting total number of cells showing neurites stained positively with β III tubulin, divided by the total number of cells stained positive with the nuclei stain DAPI. Three fields of view (841µm x 841µm) from each sample were measured from 3 independent experimental runs (n=3).
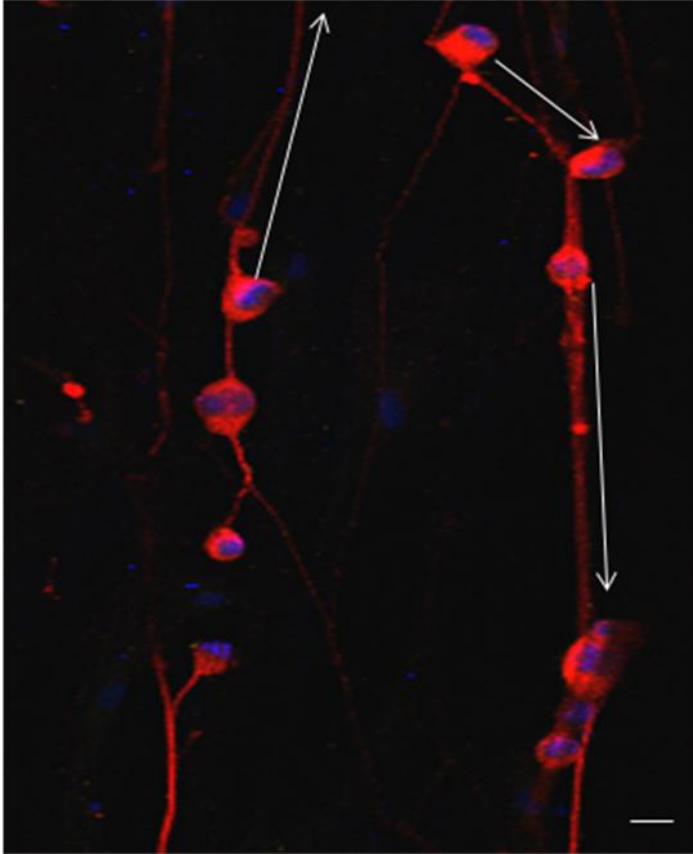
Figure 4.2. Confocal images to illustrate how neurites are measured from the neuron body to the tip of the neurite. The ruler tool on image J can be used to measure straight neurites, whereas the plugin neuron J can trace more difficult neurites to measure (scale bar= 5µm) (Popko *et al.*, 2009).

4.2.12 Assessment of primary Schwann cell morphology and Schwann cell migration length

To determine the effect of fibre diameter on Schwann cell morphology, the average Schwann cell length was calculated as a marker. Using the ruler tool on NIH Image J, the cell length was measured from tip to tip of the cell (Schneider *et al.*, 2012). For each condition, 100 primary Schwann cells were measured, and the average Schwann cell length determined for each sample ± SD (Daud *et al.*, 2012).

4.2.13 Statistical Analysis

GraphPad Instat (GraphPad Software, USA) was used to perform statistical tests on data collected. One-way analysis of variance ($p < 0.05$) was conducted to analyse the differences between the data, incorporating Tukey's multiple comparisons test if $p < 0.05$. Data was

reported as mean ± SD, p<0.05. Each experiment was performed three independent times with each sample repeated three times as n=3.

4.3 Results

4.3.1 Production of aligned PHBV fibres with different fibre diameters fabricated by electrospinning

PHBV fibres were produced using the conditions from table 4.1. Conditions were selected to assess the effect that 2µm increments had on neuronal and Schwann cell viability and differentiation. Scanning electron micrographs were taken for all conditions to determine fibre diameter and angular variance. Figure 4.3 shows SEM micrographs taken aligned fibres with diameters of 1.92, 4.07, 5.97, 8.08, and 10.17 µm fibres. Visually, differences were observed in the size of fibres between each sample, with a minor variation in fibre size of 10µm fibres (figure 4.3E). Spin coating was used to fabricate a PHBV flat film for a material control, which can be seen in figure 4.3F. Small pores could be seen in the PHBV film and further material analysis of PHBV, and spin coating conditions, can be found in chapter 2. To determine fibre diameter of fibres electrospun for each condition, samples were quantified by SEM, and measured using the ruler tool in Image J.
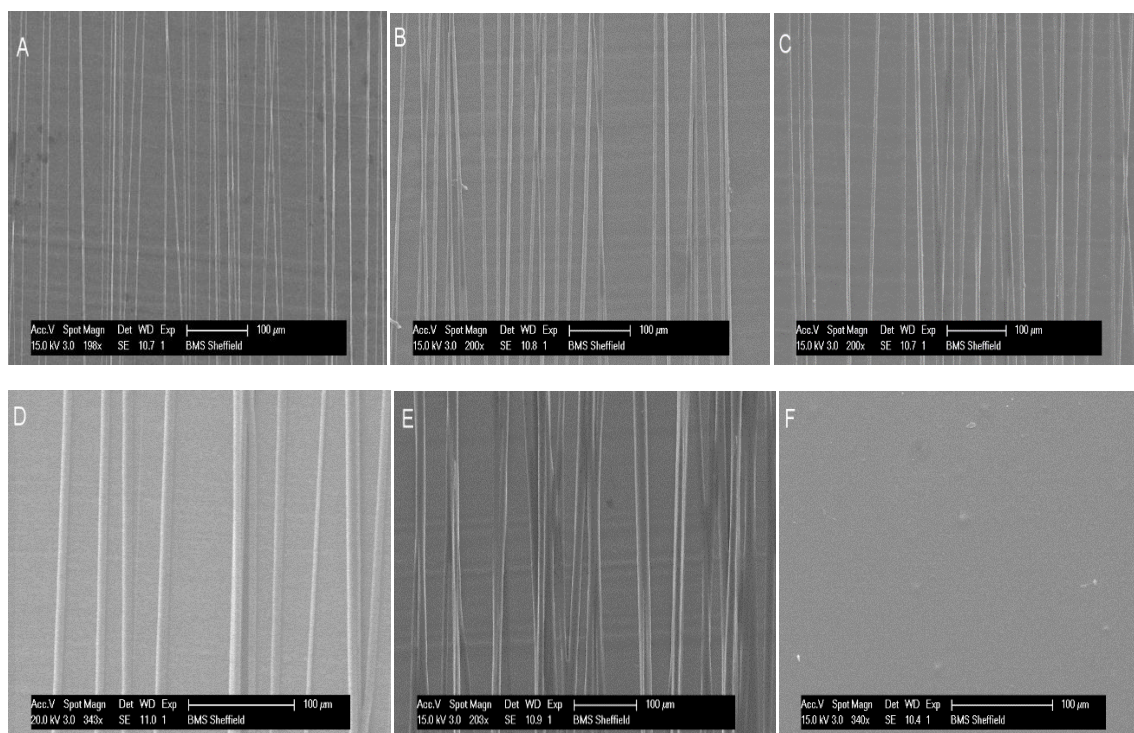
Figure 4.3. Scanning electron micrographs of (A) 1.92µm PHBV fibres, B) 4.07µm PHBV fibres, C) 5.97µm PHBV fibres, D) 8.08µm PHBV fibres, E) 10.17µm PHBV fibres and F) PHBV spin coated film. Fibre diameter and angular variance was determined by image analysis of SEM images.
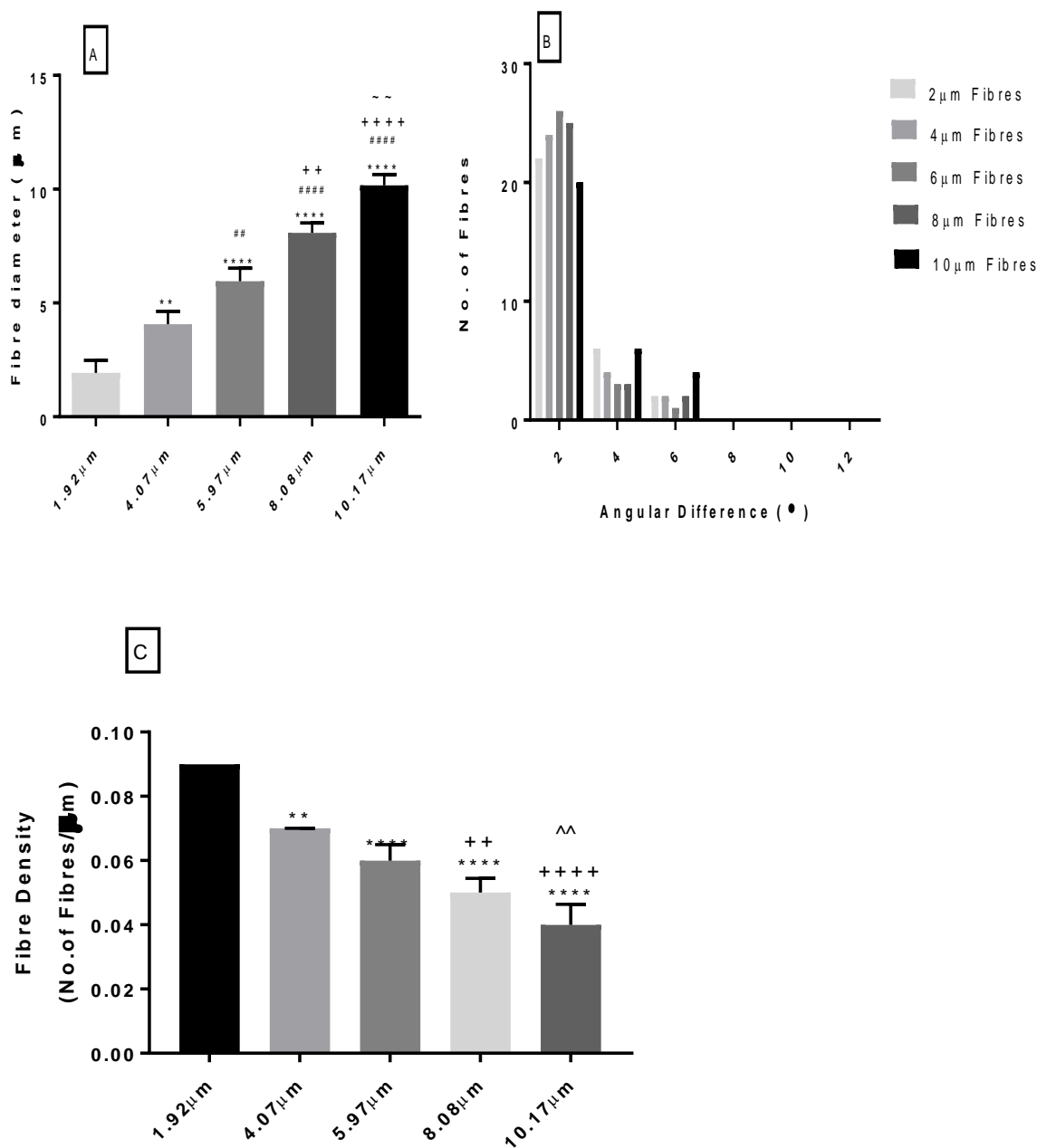
Figure 4.4. A) Graph to show the average fibre diameter of the complete set of data of different fibre diameters (Figure 4.) An average of 30 fibres was assessed for each fibre size and mean of the diameter is presented. A one way anova with Tukey's multiple comparisons tests was used to analyse data (Mean ± SD, n= 3 independently fabricated samples **p < 0.01 compared to 1.92µm fibres, ****p < 0.0001 compared to 1.92µm fibres, ##p < 0.01 compared to 4.07µm fibres, ####p < 0.0001 compared to 4.07µm fibres, ++p < 0.01 compared to 5.97µm fibres, ++++p < 0.0001 compared to 5.97µm fibres, ~~p < 0.01 compared to 8.08µm fibres). B) Combines the angular variance between PHBV fibres of 1.92µm fibres, with the other diameters. Expressed as a histogram, a central aligned fibre, at 180˚, was used as a reference point to measure the angular variance of adjacent fibres. C) Surface coverage of the fibres as fibre density, number of fibres per µm. A one way anova with Tukey's multiple comparisons tests was used to analyse data (**p < 0.01, ****p < 0.0001 compared to 1.92µm fibres, ++p < 0.01 and ++++p < 0.0001 compared to 4.07µm fibres, and ^^p < 0.01 compared to 5.97µm, Per independently electrospun batch of fibres, 30 fibres were measured. (n=3)

Figure 4.4A shows that all PHBV diameters manufactured from the 5 investigated

electrospinning conditions produced individual fibres with very little variance in diameter. It

107

also shows that the fibres created under their different conditions had significantly different diameters. To confirm if fibres were aligned, the angular variance for each fibre sample was calculated. A central reference fibre, measuring 180˚ on image J, was used to measure the alignment and angular variance of the fibre orientation. Each fibre was placed into an angular category of 0-2, 2-4, 4-6, 6-8 and 8-12˚. 30 fibres, per condition, were measured, and results shown as a histogram in figure 4.4B. Over two thirds, of all fibres per condition, were found in the 0-2˚category. The least aligned fibres were the 10.17µm fibres. As the angular variance increased, fewer and fewer fibres were found. Overall, there were higher numbers of fibres that ran parallel to each other and there was only a low number stray fibres detected. This confirms that all 5 conditions fabricated aligned PHBV fibres that could be reproduced accurately for alignment, as well as fibre diameter. Surface coverage of the fibres was determined by calculating the fibre density. The number of fibres per µm was determined and was 0.09 ± 0.000076, 0.07 ± 0.000055, 0.06 ± 0.0000765, 0.05 ± 0.000046, and 0.04 ± 0.000012 for the1.92, 4.07, 5.97, 8.08 and 10.17µm respectfully. Fibre density corresponded with the SEM micrographs in figure 4.3 in which the 1.92µm fibres take up the majority of the SEM image, and there are larger gaps between fibres in the 10.17µm fibres.

4.3.2 NG108-15 neuronal cell differentiation studies and fibre diameter

Serum was removed from the growth medium after 48 hours, to promote NG108-15 neuronal cell differentiation and outgrowth of neurites. Neuronal cells were fixed and labelled for βIII tubulin, a neuronal cell marker to detect neurites, and for DAPI, to label the cell nucleus, which aided confocal micrograph interpretation. To determine if there was a relationship between fibre diameter and NG108-15 neuronal cell differentiation and neurite outgrowth, the following markers were determined: i) the number of cells bearing neurites (as a percentage); ii) the average number of neurites (present per neuron); iii) the average length of neurites (in μm). From these parameters, the most effective fibre diameter at promoting NG108-15 neuronal cell maturation and outgrowth of neurites, could be determined. Figure 4.5 shows confocal micrographs of NG108-15 neuronal cells labelled on the different fibre diameters and controls.

Visually, it was seen that a high number of N108-15 neuronal cells expressed neurites, when cultured on all the different fibre sizes. It was also observed that the neurites, present from the neuronal cells grown on the fibre samples, aligned themselves along the direction of the fibres, and grew in an aligned orientation (see arrows). This indicates that all the PHBV fibres not only support NG108-15 neuronal cell attachment and proliferation, but also differentiation and neurite outgrowth, providing a directional guidance support for the

growing neurites. Neurites extending from NG108-15 neuronal cells cultured on the PHBV films and tissue culture plastic controls, grew out in a random orientation. Out of all the fibre samples, the longest neurites were observed on 8.08µm fibres, and overall, the longest neurites could be seen on sample control and 8.08µm fibres. Confocal micrographs were quantified to determine the percentage of neurite bearing cells, per condition, the average number of neurites extending per neuron, per condition, and the average neurite length, per condition. The results are presented in figure 4.6A-C.
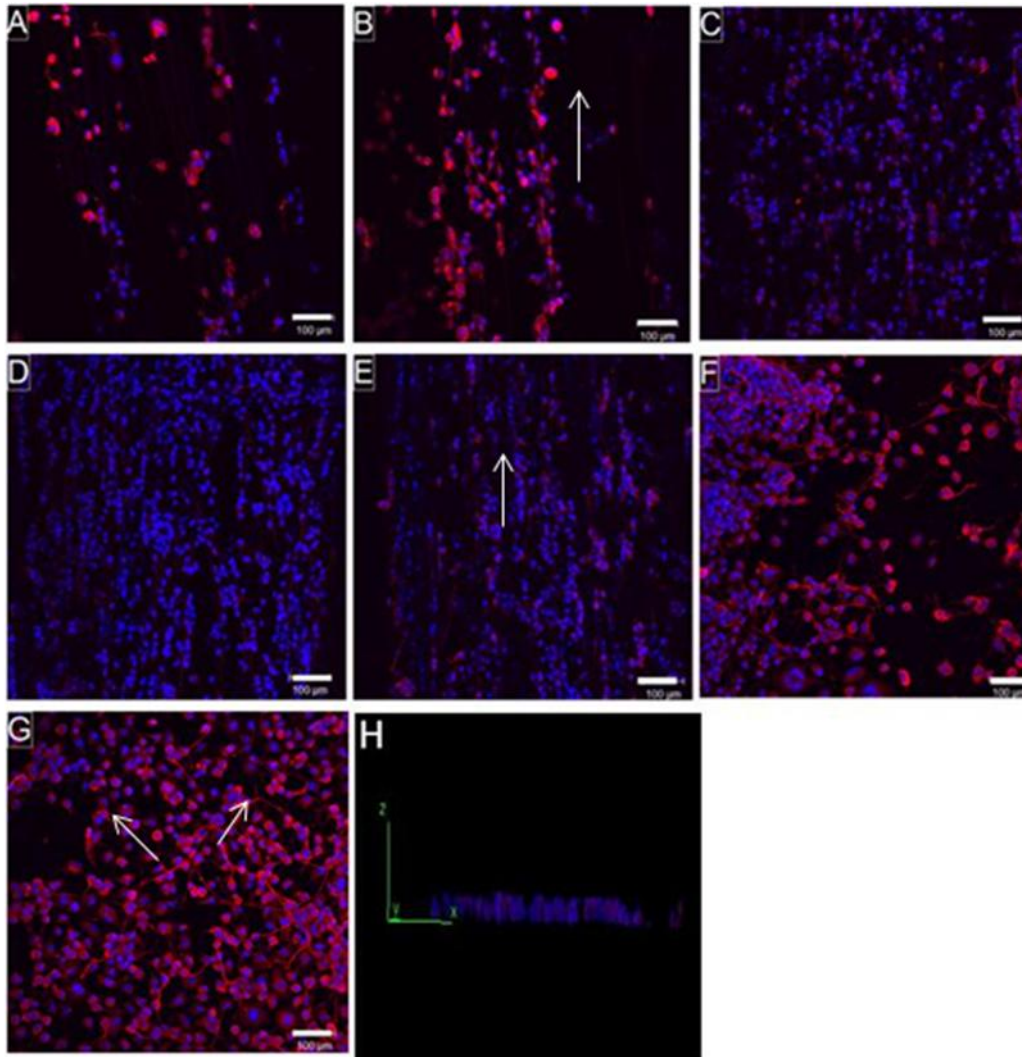
Figure 4.5. Confocal microscopy images of NG108-15 neuronal cells immunolabelled against β III tubulin (red) and cell nuclei (blue). Cells were stained after 6 days in culture on (A) 1.92µm PHBV fibres, B) 4.07µm PHBV fibres, C) 5.97µm PHBV fibres, D) 8.08µm PHBV fibres, E) 10.17µm, F) PHBV spin coated flat films, G) Tissue culture plastic control and H) 3D composite image of neuronal cells on fibres. Neurites expressed from NG108-15 neuronal cells aligned themselves with aligned fibres, whereas on the PHBV flat films and tissue culture plastic control, they grew in a randomly orientated direction. From confocal images, average neurite length, maximum neurite length, percentage of neurite bearing cells and average number of neurite per neuron was determined. The arrows indicate the direction of neurite outgrowth. Scale bar = 100µm.

Figure 4.6A shows that the highest percentage of cells bearing neurites were found on the PHBV and tissue culture plastic control (58.27 ± 3.79% and 62.75 ± 5.79% respectively). However, there was a significantly higher percentage of NG108-15 neuronal cells bearing neurites on 5.97µm fibres (45.87 ± 8.11%) compared to cells grown on 1.92µm fibres (21.75

± 5.79%). The percentage of neuronal cells showing neurites cultured on 4.07, 8.08 and 10.17µm fibres was 33.69 ± 8.11%, 43.43 ± 1.50% and 41.30 ± 5.02% respectively (figure 4.6A). This could indicate that 1.92µm fibres promote NG108-15 neuronal cell differentiation the least, compared to the other fibre diameters.
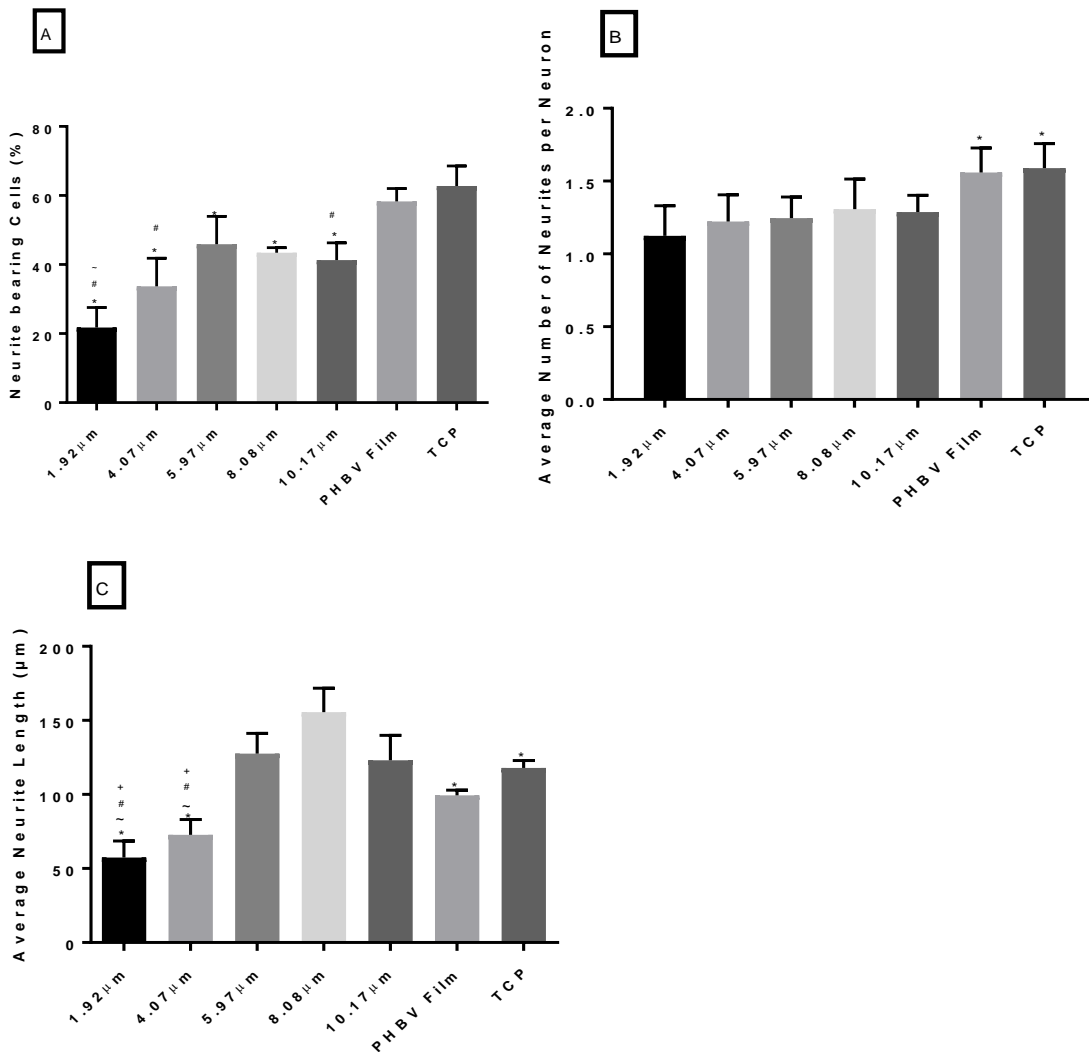
Figure 4.6. Analysis of NG108-15 neuronal cell differentiation on different PHBV fibre diameters, PHBV spin coated flat films and tissue culture plastic control. A) Neurite bearing NG108-15 neuronal cells after 6 days in culture, expressed as a percentage. Mean ± SD, n=3 *p<0.05 against TCP, # p<0.05 against PHBV films and ~p<0.05 against 5.97µm fibres). All cells and neurite bearing cells were counted for each field of view (841µm X 841µm) to calculate the percentage of cells expressing neurites. B) The average number of neurites expressed per neuron. (Mean ± SD, n=3 *p<0.05 against 1.92µm fibres). For each field of view (841µm X 841µm), up to 30 cells, and all neurites expressing by those cells, were manually counted on image J to calculate the average number of neurites expressed per neuron. C) The average neurite length measured per diameter and controls. 100 neurites per diameter/sample were measured, using Image J, to determine the average neurite length. (Mean ± SD, n=3 independent experiments *p<0.05 against 8.08µm fibres, # p<0.05 against 5.97µm fibres, +p<0.05 against 10.17µm fibres, ~p<0.05 against TCP).

Figure 4.6B reports that the PHBV and tissue culture plastic controls had a significantly higher average number of neurites per neuron (1.55 ± 0.16 and 1.58 ± 0.17) compared to the fibrous scaffolds. Out of the different fibre diameter variables, cells expressing the highest average number of neurite per neuron were detected on the 8.08µm fibres (1.31 ± 0.21) followed by cells grown on the 10.17µm fibres (1.29 ± 0.11). The average number of

neurites found on the 1.92, 4.07 and 5.97µm fibres were 1.12 ± 0.21, 1.22 ± 0.18, and 1.24 ± 0.15 respectively. Cells grown on the 8.08µm fibres had a higher number of neurites, and the least number of neurites were found on cells grown on the 1.92µm fibres. However, no significant differences were found between the fibre diameter samples, which suggest that no fibre diameter was more efficient in promoting NG108-15 neuronal cell neurite outgrowth than the other.

The average neurite length of neurites extending from NG108-15 neuronal cells grown on the samples is shown in figure 4.6C. Neurites from NG108-15 neuronal cells grown on 8.08, 5.97, and 10.17µm fibres had a significantly higher average neurite length, (155.57 ± 16.24µm, 127.54± 13.66µm and 10µm123.08 ± 16.84µm) compared to the neurite lengths of cells cultured on 1.92 and 4.07µm fibres (57.35 ±11.15µm, 72.73 ± 10.38µm respectively). Neurites grown on 8.08µm fibres had a significantly higher average length, compared to the PHBV films and the tissue culture plastic, which were 99.47 ± 3.39µm, 117.93 ± 4.98µm respectively. Neurites growing from neuronal cells cultured on 8.08µm fibres were the longest, followed by neurites grown from neuronal cells cultured on the 5.97µm fibres and 10.17µm fibres. This indicates that fibre diameter does have an effect of NG108-15 neuronal cell neurite outgrowth length. Compared to the controls, neurites extended from neuronal cells cultured on 8.08µm fibres grew further, longer, and aligned themselves to the fibres, whereas lengths of neurites cultured on flat films, grew out on a random orientation and were significantly shorter. With regards to the fibre samples, the average length of neurites from neuronal cells cultured on the 5.97, 8.08 and 10.17µm fibres was significantly higher than those cultured on the 1.92 and 4.07µm. The size of fibres are larger than the diameter of the neuronal cell bodies, indicating NG108-15 neuronal cells differentiate more efficiently on fibres larger than their size.

4.3.3 Cell viability and biocompatibility assays of NG108-15 neuronal cells and fibre diameter
After culture, neuronal cells were stained with Syto-9 and propidium iodide to assess cell viability different fibre diameters. Figure 4.7 shows that all fibre diameters, the PHBV flat film and the tissue plastic control supported attachment and proliferation of NG108-15 neuronal cells. Neuronal cells attached and aligned on the fibre diameters, whereby they adhered and orientated randomly on the flat PHBV film and tissue culture plastic control. 8.08 and 10.17µm fibres appeared to support the highest number of NG108-15 neuronal cell adherence, compared to the other fibre diameters. Confocal micrographs were quantified to determine attached live and dead cell numbers, and to confirm the cell viability of each scaffold/sample as a percentage of live versus dead cells.
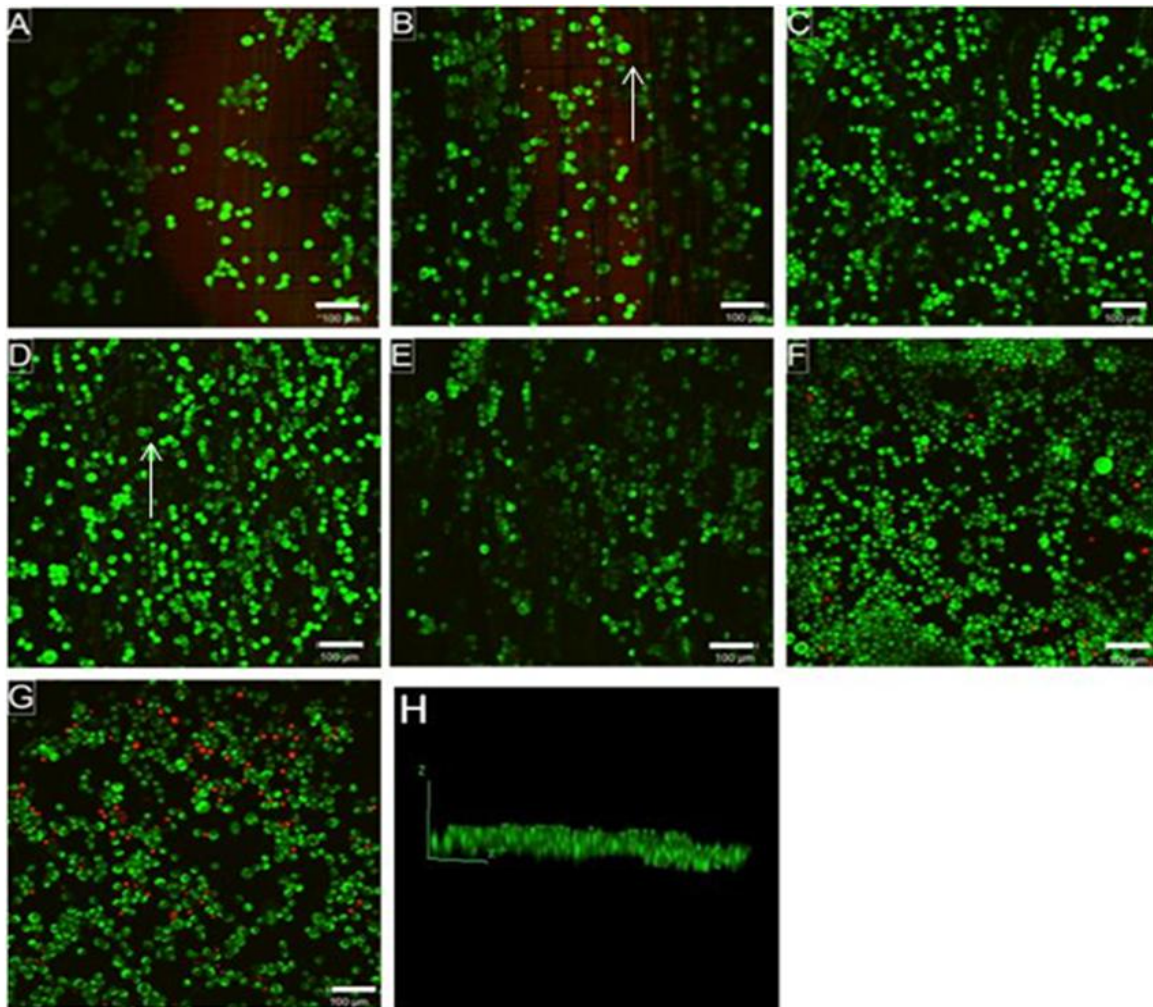
Figure 4.7. Confocal micrographs of NG108-15 neuronal cells cultured on (A) 1.92µm PHBV fibres, B) 4.07µm PHBV fibres, C) 5.97µm PHBV fibres, D) 8.08µm PHBV fibres, E) 10.17µm, F) PHBV spin coated flat films, G) Tissue culture plastic control and H) 3D composite image of neuronal cells on fibres. Live/dead assay was conducted to assess cell viability. Green cells represent live cells, and red cells represent dead cells. Scale bar = 100µm.

Figure 4.8A shows that the highest number of live cells, per field of view, is supported on the PHBV flat films (660.66 ± 228.65) compared to the other samples. With regards to the individual fibre diameters, 8.08µm fibres supported the growth of the highest number of live cells (564.55 ± 215.69) compared to 1.92, 4.07, 5.97 and 10.17µm fibres. (263.22 ± 117.92, 427.33 ± 198.31, 340.55 ± 121.18 and 399.22 ± 205.69 respectively). 1.92µm fibres had the lowest number of live cells compared to all the other fibres. The highest number of dead cells was found on tissue culture plastic (67.62 ± 20.84) but out of the fibre samples, 1.92µm fibres had the highest number of dead cells (23.44 ± 7.21) compared to the 4.07, 5.97, 8.08 and 10.17µm fibres. (13.33 ± 11.97, 13.34 ± 3.87, 14.67 ± 3.31, and 11.56 ± 4.45). Of note, higher numbers of live cells were adhered to fibres with the lowest fibre density, as seen in figure 4.4.

Out of all the fibre diameters 8.08μm fibres had the highest amount of NG108-15 neuronal cell growth and 1.92μm fibres promoted the least in regards of (attachment and growth.) However, statistical analysis confirmed that there was no difference between live cell numbers and dead cell numbers dependant on fibre diameter. Cell viability, as a percentage, is shown in Figure 4.8B in which all the samples had cell viabilities of 90% or above. 1.92μm fibres had the lowest cell viability (91.49 ± 2.15%) but that cells grown on the 4.07μm fibres had the highest cell viability (97.03 ± 1.75%). 5.97, 8.08 and 10.17μm fibres had cell viabilities of 96.20 ± 0.20%, 96.94 ± 1.63% and 96.1 ± 3.10% respectfully. No significant differences were detected between cell viability percentages between all samples and overall it can be concluded that the PHBV fibres, and films were biocompatible, and did not cause any toxic effects to NG108-15 neuronal cells. PHBV fibres support the attachment and proliferation of NG108-15 neuronal cells, as well as promote differentiation.
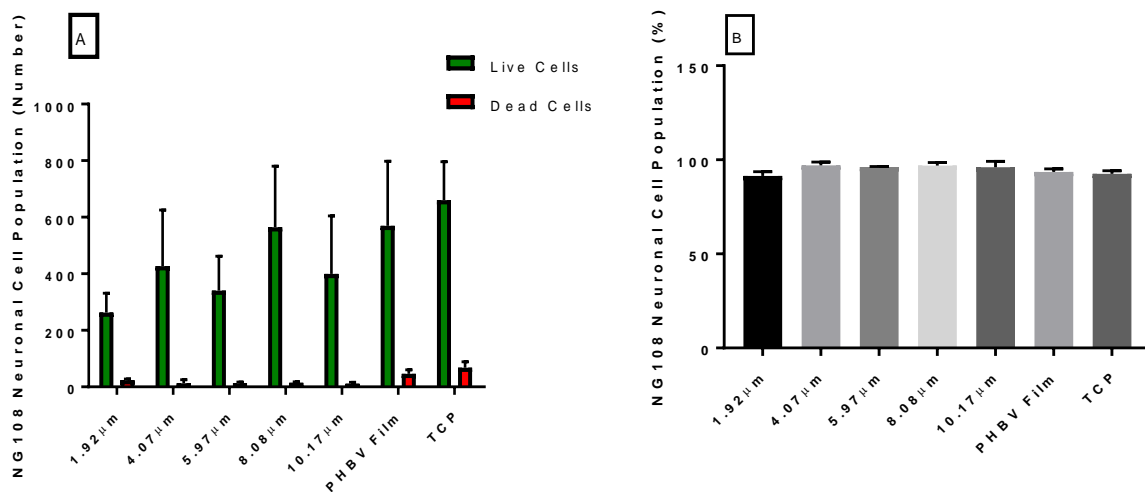
Figure 4.8. Live/dead analysis of NG108-15 neuronal cells cultured on different fibre diameters, PHBV flat film and tissue culture plastic control. A) Number of live cells against dead cells per sample and B) live/dead analysis expressed as a percentage. A one way anova with Tukey's multiple comparisons tests was used to analyse data (Mean ± SD, n=3 independent experiments P< 0.05). No significant difference were detected between samples.

4.3.4 Primary Schwann cell culture on aligned PHBV fibres with different diameters

Schwann cells were labelled for S100β, a primary Schwann cell marker, to visualise Schwann cell morphology on fibre scaffolds, and confirm phenotype. Figure 4.9 shows confocal micrographs taken of primary Schwann cells cultured on fibres and flat films. Schwann cells aligned themselves in fibres in a parallel orientation. It also appeared as if their morphology had changed, when comparing with Schwann cells cultured on the tissue culture plastic control. Schwann cells on PHBV films elongated compared to the tissue plastic control. This indicated that Schwann cell morphology had been maintained on PHBV. With regards to the fibre samples, all Schwann cells stained positively for S100β, confirming a maintained phenotype. Visually, more Schwann cells attached to fibres with smaller

diameters, and migrated along fibres. In contrast, on the larger diameters, fewer cells seemed to adhere. Interestingly, figure 4.9E shows Schwann cells adhered to the sides of fibres, whereas on 1.92µm fibres (figure 4.9A) Schwann cells adhered to the middle of fibres.

The average length of Schwann cells, cultured on the PHBV fibres and films, was calculated as a marker of morphology, to determine Schwann cell phenotype. Overall, no statistical differences were detected between the average Schwann cell lengths calculated on the PHBV fibres. However, an overall trend was observed between fibre diameter and average Schwann cell length. The longest average Schwann cell length was calculated on the 1.92µm fibres, followed by the tissue culture plastic as seen in figure 4.9 (95.26 ± 15.74µm and 88.42 ± 14.01µm respectively). This indicated that a smaller diameter promoted a more mature Schwann cell phenotype, and therefore a longer average Schwann cell length. Thus, fibre diameters of 4.07, 5.97, 8.08, and 10.17µm had cell lengths of 85.59 ± 13.09µm, 82.60 ± 11.98µm, 79.86 ± 10.49µm and 67.25 ± 10.88µm respectively. Although a trend could be seen, with regards to fibre diameter, the relationship between Schwann cell morphology and fibre diameter could not be confirmed.
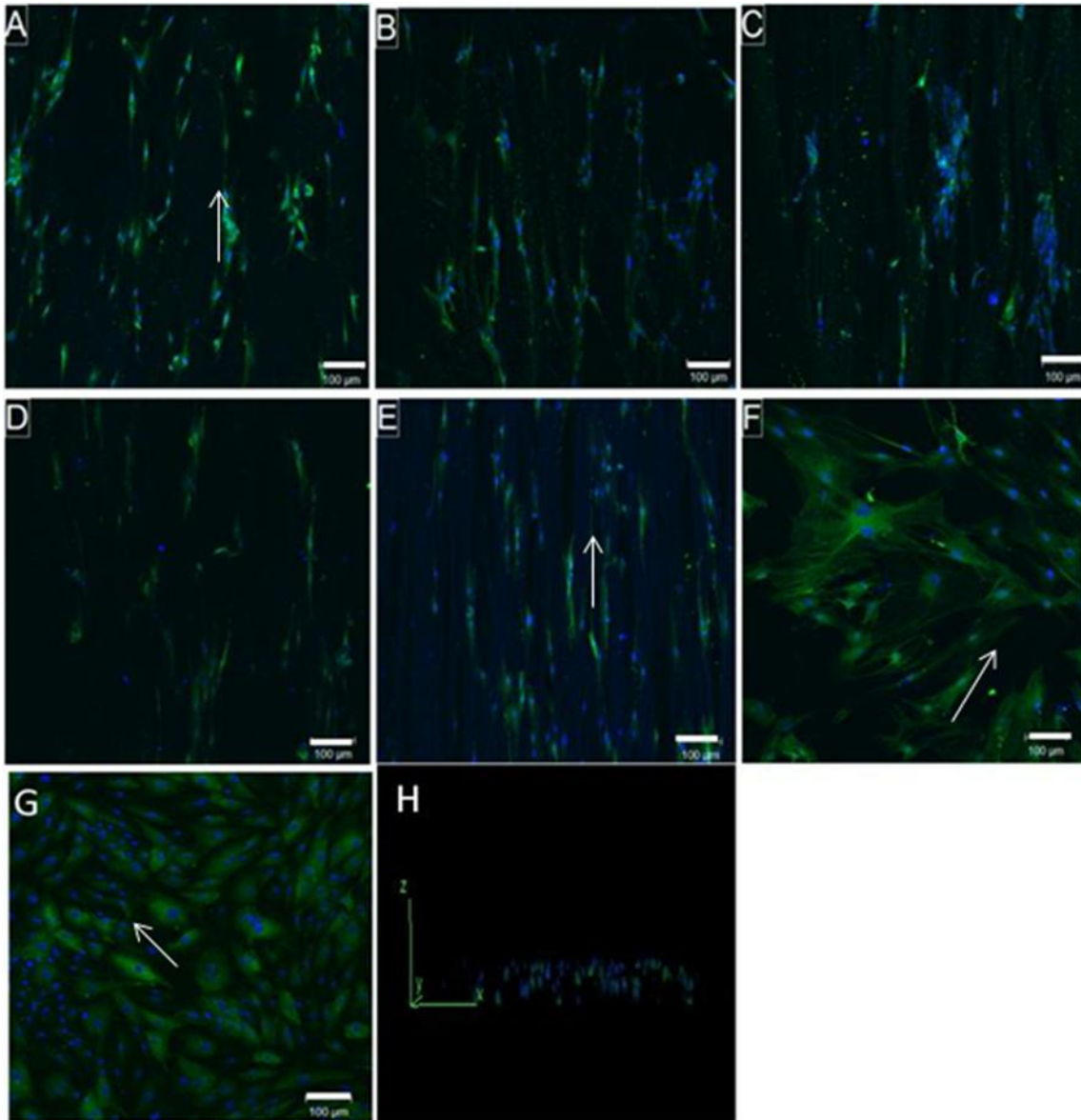
Figure 4.9. Confocal micrographs of rat primary Schwann cells immunolabelled against S100β (green) and cell nuclei (blue). Cells were stained after 6 days in culture on (A) 1.92μm PHBV fibres, B) 4.07μm PHBV fibres, C) 5.97μm PHBV fibres, D) 8.08μm PHBV fibres, E) 10.17μm, F) PHBV spin coated flat films, G) Tissue culture plastic control and H) 3D composite image of Schwann cells on fibres. Schwann cells aligned themselves with the fibres, and elongate, whereas on the PHBV flat films and tissue culture plastic control, they grew in a randomly orientated direction (see arrows). From confocal images, the average Schwann cell length was measured, to determine a maintained phenotype. Scale bar= 100μm.
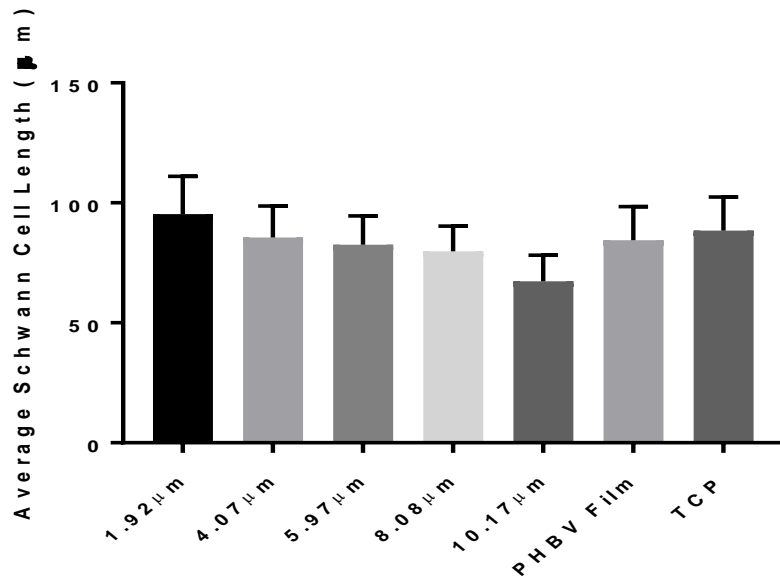
Figure 4.10. Schwann cell morphology was examined by calculating the average cell length. 100 Schwann cells, per condition, were measured from tip to tip, to determine the average Schwann cell length. A one way anova with Tukey's multiple comparisons tests was used to analyse data (mean ± SD, n=3 independent experiments). All Schwann cells retained phenotypical Schwann cell morphology and no significant differences were detected between samples.

4.3.5 Primary Schwann cell viability on aligned PHBV fibres with different diameters

Primary Schwann cell viability on the PHBV fibres, with varying diameters, was calculated to investigate the relationship between fibre diameter and cell viability. Schwann cells were labelled with Syto-9 and propidium iodide and confocal micrographs were taken. Figure 4.11 shows primary Schwann cells cultured on electrospun PHBV fibres, with different diameters, PHBV films and tissue culture plastic control. The highest number of adhered Schwann cells was observed on 1.92μm fibres, followed by the tissue culture plastic control. Very few dead cells were observed on any of the fibre samples, indicating that all the PHBV fibre scaffolds supported Schwann cell attachment and proliferation.
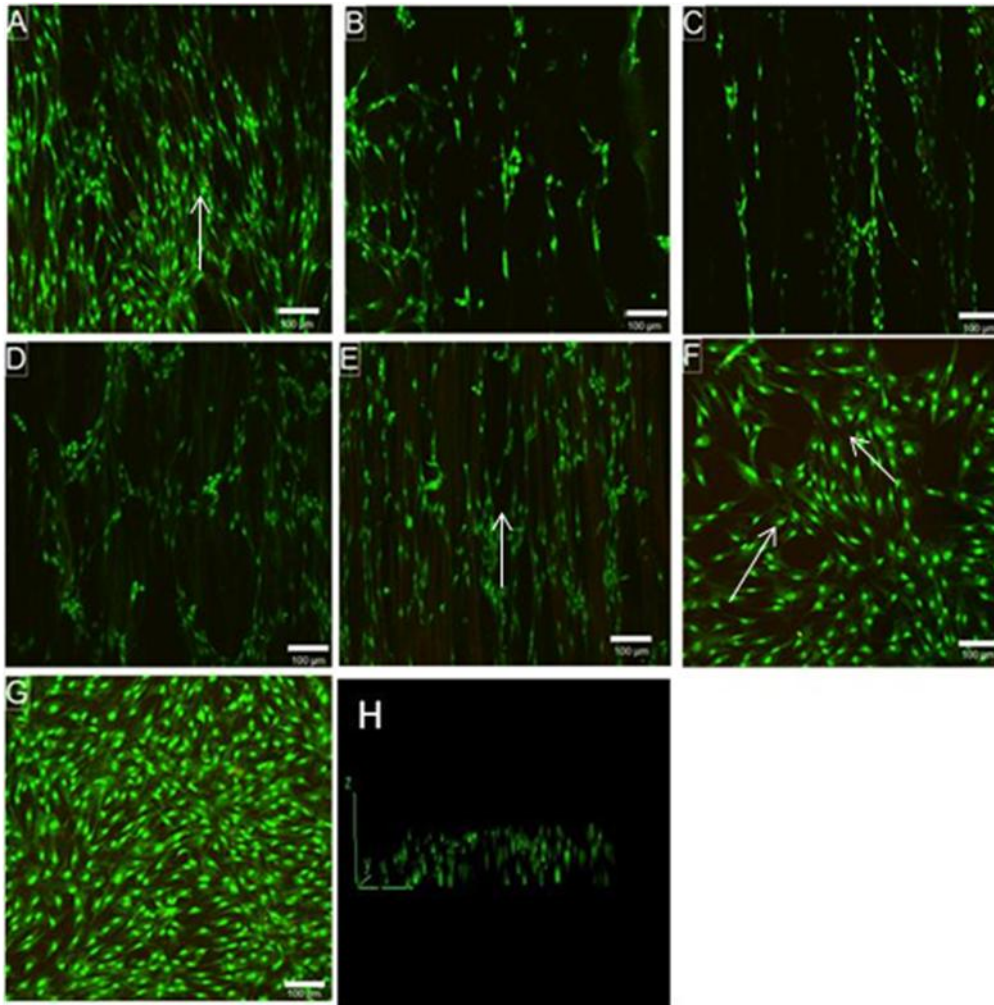
Figure 4.11. Confocal micrographs of primary rat Schwann cells cultured on (A) 1.92µm PHBV fibres, B) 4.07µm PHBV fibres, C) 5.97µm PHBV fibres, D) 8.08µm PHBV fibres, E) 10.17µm, F) PHBV spin coated flat films, G) Tissue culture plastic control and H) 3D composite image of Schwann cells on fibres. Live/dead assay to assess cell viability. Green cells represent live cells, and red cells represent dead cells. Scale bar = 100µm.

Primary Schwann cells were quantified to determine the average number of live and dead cells per field of view (841µm x 841µm) and calculate percentage cell viability per condition. Figure 4.12A shows significantly higher numbers of attached live Schwann cells on 1.92µm fibres and tissue culture plastic control, compared to the other fibres diameters and PHBV film. Figure 4.4C confirmed that the 1.92µm fibres had the highest fibre density, compared to the other diameters, and so fibre density increased Schwann cell attachment. As fibre diameter increased, the number of live adhered primary Schwann cells also decreased. The numbers of attached live Schwann cells on the 4.07, 5.97, 8.08, and 10.17µm fibres were all quite similar, suggesting that after 1.92µm, increasing the fibre diameters by 2µm increments did not influence primary Schwann cell attachment and proliferation.
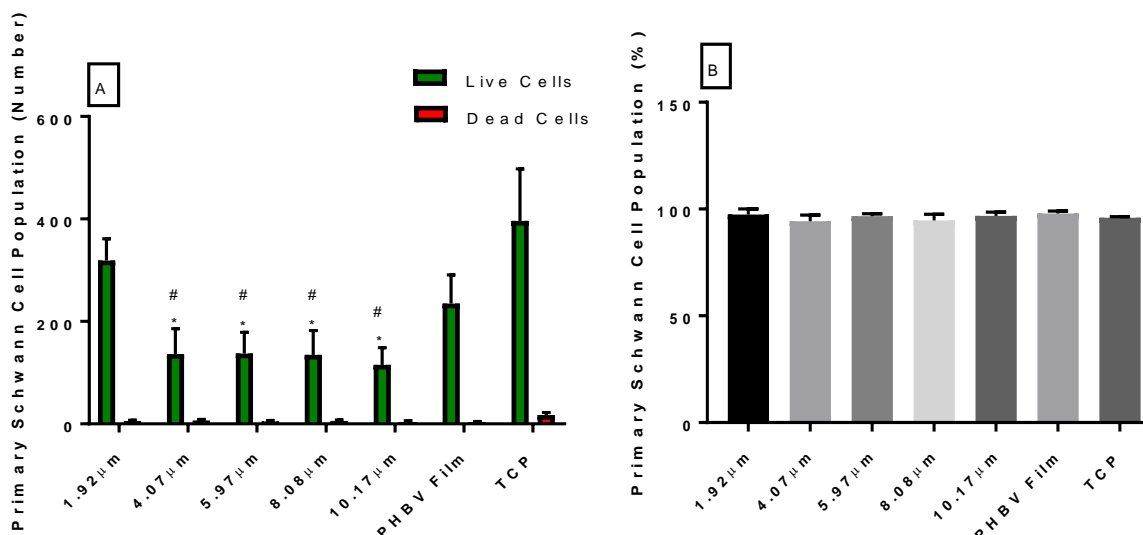
Figure 4.12. Live/dead analysis on rat primary Schwann cells cultured onto PHBV fibres, films and tissue culture plastic control. A) Cell numbers of live cells versus dead cells are expressed as numbers, per field of view. A one way anova with Tukey's multiple comparisons tests was used to analyse data (Mean ± SD, n=3 independent experiments *$p < 0.05$ in comparison with 1.92μm fibres, #$p < 0.05$ in comparison to TCP). B) Cell numbers of live versus dead cells expressed as a percentage of cell viability. All samples have a live cell viability of above 95% and no significant differences were detected between samples.

All fibrous scaffold and control samples had a cell viability of above 95%. This indicated that all samples supported Schwann cell attachment and proliferation, with no adverse effects observed.

4.3.6 Differentiation studies of co-cultures of NG108-15 neuronal cells and primary Schwann cell on different PHBV fibre diameters

The addition of Schwann cells to neuronal cell cultures has been reported to increase neuronal cell neurite outgrowth (Armstrong *et al.*, 2007). Daud *et al.* (2012) also reported this, co-culturing NG108-15 neuronal cells and rat primary Schwann cells on aligned PCL microfibres of 1, 5 and 8μm (Daud *et al.*, 2012). Comparing these results, the effect of 2μm fibre diameter increments on co-cultures of neuronal and Schwann cells was determined, as well as the difference in materials, as previously reported in chapter 2. PHBV films promoted increased NG108-15 neuronal cell differentiation, growth and proliferation compared to PCL films. Figure 4.13 shows confocal micrographs of co-cultures of neuronal cells and Schwann cells on the different diameters PHBV fibres, films and tissue culture plastic.
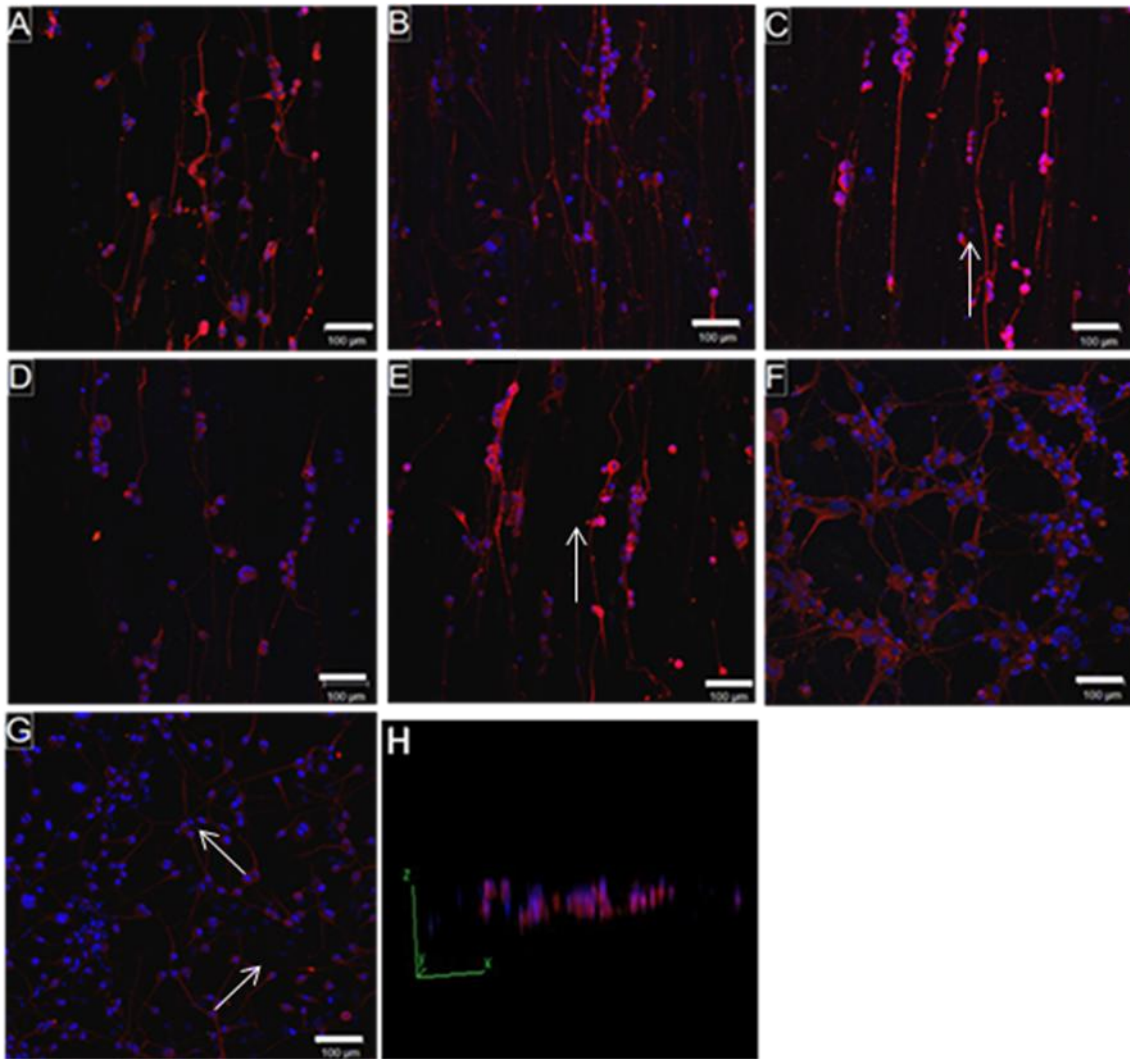
Figure 4.13. Confocal micrographs of co-cultures of NG108-15 neuronal cells co-cultured with rat primary Schwann cells, immunolabelled against β III tubulin (red), S100β (green) and cell nuclei (blue). Cells were stained after 6 days in culture on (A) 1.92µm PHBV fibres, B) 4.07µm PHBV fibres, C) 5.97µm PHBV fibres, D) 8.08µm PHBV fibres, E) 10.17µm, F) PHBV spin coated flat films, G) tissue culture plastic control and H) 3D composite image of neuronal and Schwann cells on fibres. Neurites expressed from NG108-15 neuronal cells aligned themselves with fibres, whereas on the PHBV flat films and tissue culture plastic control, random orientation was seen. The addition of primary Schwann cells increased neurite length. Average neurite length was calculated from micrograph samples. Scale bar = 100µm.

When comparing samples to figure 4.5 (confocal micrographs of cultured NG108-15 neuronal cells alone), neurites outgrown from NG1080-15 neuronal cells were observed to be longer, supporting the evidence that Schwann cells in co-culture increases the length of neurite outgrowth. Both cell types attached and aligned to the different fibre diameters, whereas cell types were more spread out and sparse on the PHBV films and tissue culture plastic. Visually, neurites outgrown from NG108-15 neuronal cells cultured on PHBV fibres aligned themselves to the fibres, whereas neurite outgrowth was of a more random orientation when cultured on PHBV films and tissue culture plastic. In order to quantify the effect of the addition of Schwann cells in co-culture on NG108-15 neuronal cell differentiation and neurite outgrowth, neurite lengths of neurites expressed from the neuronal cells were measured using the ruler tool on image J (Schneider *et al.*, 2012). 100 neurites were

imaged, per condition, to determine the average neurite length of NG108-15 neuronal cell neurite outgrowth on different PHBV fibre diameters in co-culture with primary Schwann cells.
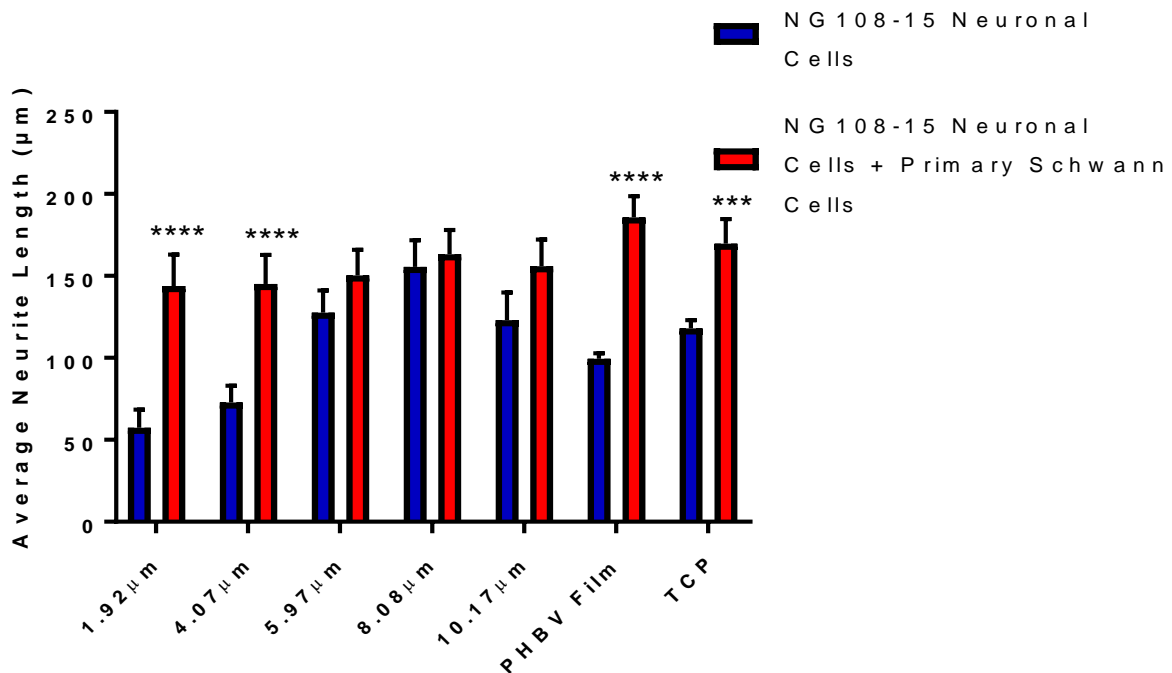
Figure 4.14. Analysis of NG108-15 neuronal cell neurite outgrowth studies comparing neurite lengths in the presence and absence of primary rat Schwann cells. 100 neurites per diameter/sample was measured, using Image J. A two way anova with Sidak's multiple comparisons tests was used to analyse data (Mean ± SD, n=3 independent experiments ***p<0.001 and ****p<0.0001 compared to neuronal cell alone).

Figure 4.14 shows that addition of Schwann cells to a culture of NG108-15 neuronal cells significantly increased neurite length, depending on fibre diameter. The maximum neurite lengths of neurites in co-culture were 143.94 ± 19.01µm, 145.19 ± 17.64µm, 150.34 ± 15.57µm, 163.13 ± 14.79µm and 155.88 ± 16.33µm for 1.92, 4.07, 5.97, 8.08 and 10.17µm fibres respectively. Interestingly, neurite outgrowth lengths from NG108-15 neuronal cells cultured on 1.92 and 4.07µm fibres were significantly higher, when in co-culture, compared to the other fibre diameters. Neurite outgrowth had increased from 57.35 ± 11.15µm to 143.94 ± 19.01µm on 1.92µm PHBV fibres, and from 72.73 ± 10.38µm to 145.19 ± 17.64µm on 4.07µm fibres. This indicated that there was a relationship between fibre diameter and neuronal/Schwann cell co-culture but only on thinner fibres. In single culture of NG108-15 neuronal cells, cultured on PHBV fibres, neurite outgrowth was significantly higher on 5.97, 8.08, and 10.17µm, compared to 1.92 and 4.07µm fibres. This supports a rationale that addition of Schwann cells during nerve regeneration *in vivo*, could increase axon regeneration length if using smaller diameter fibres. However, further work *in vivo* would need to be performed to clarify this. Overall, the longest neurite outgrowth from NG108-15 neuronal cells in co-culture was recorded on the 8.08µm fibres, 163.13 ± 14.79µm, followed

by 10.17μm fibres, 155.88 ± 16.33μm which would indicate that higher fibre diameters were the most efficient for NG108-15 neuronal cell neurite outgrowth in a co-culture system. As no statistical differences were detected between neurite outgrowth lengths in co-culture, this cannot be confirmed.

4.3.7 Cell Viability Study of co-cultures of NG108-15 neuronal cells and primary Schwann cell on different PHBV fibre diameters

To determine cell viability of NG108-15 neuronal cells and primary Schwann cells cultured on PHBV fibres in co-culture, cells were stained for Syto-9 and propidium iodide to visualise live and dead cells. Figure 4.15 shows neuronal cells and Schwann cells cultured together aligned on the PHBV fibres. Although the live/dead cell viability assay can't be used to determine cell phenotypes by colour, cell shape is distinct - Schwann cells have a more spindle like shape and neuronal cells a more circular shape. Overall, there were very little dead cells in any of the conditions, indicating that PHBV fibres support Schwann and neuronal cell proliferation and growth. Higher numbers of live Schwann cells were seen on 1.92μm fibres (figure 4.15A) compared with other fibre diameters. Higher numbers of neuronal cells could be observed on 5.97μm fibres (figure 4.15C). The highest number of dead cells was seen on tissue culture plastic control.

In order to determine cell viability, live versus dead cells, as well as determine which fibre diameter had the highest amount of neuronal and Schwann cell attachment, confocal micrographs were quantified. Figure 4.16A shows that the highest number of live cells was on the tissue culture plastic control and PHBV flat films, 484.66 ± 104.11 cells and 215.50 ± 35.44 cells. The highest number of live cells was on 1.92μm fibres (212.01 ± 96.21 cells), followed by the 8.08μm fibres (131.22 ± 50.38 cells). This coincides with figure 4.12A, where there was a higher number of live primary Schwann cells attached to the 1.92μm fibres, and figure 4.8A which had the highest number of live NG108-15 neuronal cells attached to the 8.08μm fibres. This data also corresponds to figure 4.4C, which saw that 1.92μm fibres had the highest fibre density and surface coverage which would explain and increase in cell attachment.
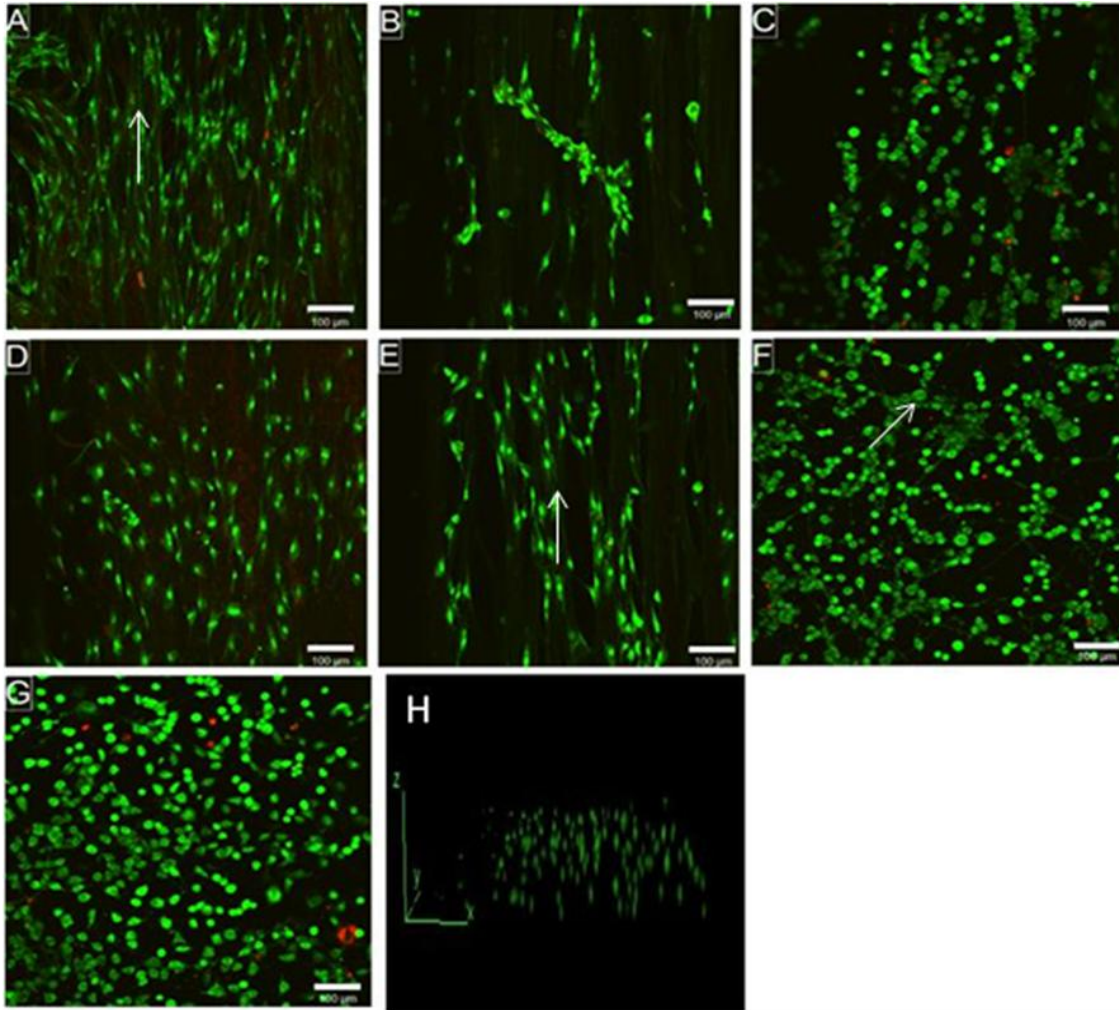
Figure 4.15. Confocal micrographs of primary rat Schwann cells co-cultured with NG108-15 neuronal cells cultured on (A) 1.92µm PHBV fibres, B) 4.07µm PHBV fibres, C) 5.97µm PHBV fibres, D) 8.08µm PHBV fibres, E) 10.17µm, F) PHBV spin coated flat films, G) tissue culture plastic control and H) 3D composite image of neuronal and Schwann cells on fibres. Green cells represent live cells, and red cells represent dead cells. Scale bar = 100µm.
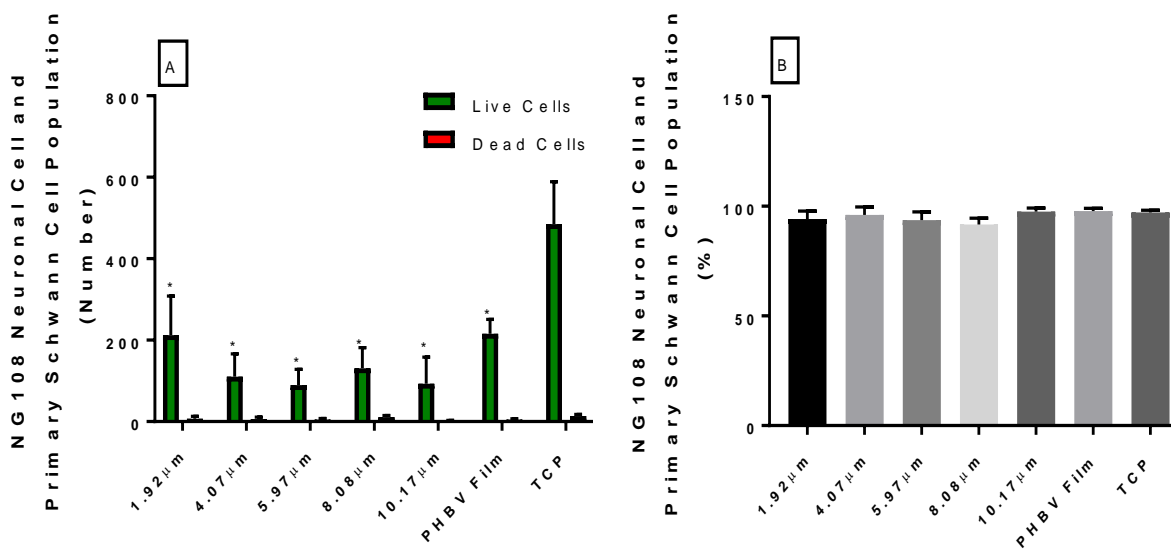
Figure 4.16. Live/dead analysis of co-cultures of NG108-15 neuronal cells and rat primary Schwann cells, cultured on different fibre diameters, PHBV flat film and tissue culture plastic control. A) Number of live cells against dead cells per sample (mean ± SD, n=3 independent experiments *p< 0.05 compared to tissue culture plastic control). B) live/dead analysis expressed as a percentage. A one way anova with Tukey's multiple comparisons tests was used to analyse data (Mean ± SD, n=3 independent experiments P< 0.05). No significant differences were detected between samples.

4.4 Discussion

This chapter reports on the relationship PHBV fibre diameter has on neuronal and Schwann cell response *in vitro*. PHBV was chosen as the fibre material to determine this effect, due to excellent biocompatibility and promoting NG108-15 neuronal cell adherence and proliferation, seen in chapter 2. As well as this, chapter 3 confirmed that aligned fibres of PHBV could be fabricated by electrospinning, as well as fabricating statistically different fibre diameters. Previous literature has shown that different diameters, ranging from nanofibres to microfibers, have different effects on different cell types (Schaub *et al.*, 2016). As previous work on fibre diameter and NG108-15 neuronal cells had been conducted, and published, NG108-15 neuronal cells were chosen for fibre diameter experiments (Daud *et al.*, 2012). NG108-15 neuronal cells are very well characterised and have been shown to behave and respond similarly to primary sensory neurons in specific co-culture conditions with primary Schwann cells (Armstrong *et al.*, 2007; Armstrong *et al.*, 2008).

Electrospinning conditions, to fabricate PHBV fibres, with diameters ranging from 1.92-10.17µm, had been confirmed in chapter 3. Five different fibre conditions were chosen to investigate the effect fibre diameter had on NG108-15 neuronal cell and primary Schwann cell attachment, proliferation and maturation. The largest PHBV fibre diameter fabricated, 10.17µm was chosen for analysis. Wang *et al.* (2010) reported significantly higher Schwann cell migration lengths, and neurite out growth from chick DRGs on 1.325µm PLLA scaffolds compared 0.759µm and 0.293µm fibre scaffolds (H. B. Wang *et al.*, 2010). The small diameter of PHBV fibres,1.92µm, were chosen for investigation. Daud *et al.* (2012) investigated 1, 5 and 8µm PCL fibres for use in creating a 3D peripheral nerve injury model (Daud *et al.*, 2012). As 8µm fibres were the most effective in promoting significantly higher NG108-15 neurite outgrowth length, compared to other diameters, 8.08µm PHBV fibres were also investigated (Daud *et al.*, 2012). Overall, fibres with 2µm increments (1.92, 4.07, 5.97, 8.08 and 10.17µm) fibres were chosen for *in vitro* evaluation. Surface coverage and fibre density were also investigated to ensure that there was a relationship between cell response and fibre diameter, not on the addition of fibres. Analysis confirmed the 1.92µm fibres had the largest surface coverage and fibre density, compared to the other diameters. The highest numbers of live Schwann cells were observed on the 1.92µm which was expected due to the higher fibre density. However, in the case of the NG108-15 neuronal cells, this was the opposite.

It was hypothesised that the larger fibre diameters (6-10μm) would support NG108-15 neuronal cell differentiation more effectively than the smaller diameters, as seen in literature (Gnavi *et al.*, 2015a). The highest numbers of cells bearing neurites were observed on the flat controls, suggesting that a 3D scaffold, did not promote initial neurite outgrowth. Similar to this effect, the number of neurons showing neurites were significantly lower on the fibre scaffolds compared to the 2D flat controls of tissue culture plastic and PHBV film. However, when observing neurite outgrowth length, statistically longer neurite lengths were observed on the 5.97, 8.08 and 10.17μm fibres compared to the 1.92 and 4.07μm fibres and flat controls, with the highest average neurite length detected on the 8.08μm fibres. This data is very similar to the results published by Daud *et al.* (2012). However, of note, average neurite length, number of neurons and percentage of neuronal cells bearing neurites was higher on 8.08μm PHBV fibres, compared to results on 8μm PCL fibres. Classical contact guidance could be observed by NG108-15 neuronal cells when cultured on aligned fibres, compared to the 2D plastic controls, as cells could be seen adhered to the fibre, changing its orientation and neurites growing along the fibres (F. Yang *et al.*, 2005a).

This data reflects work in chapter 2 in which PHBV was more biocompatible compared to PCL, which could be due to its more hydrophilic properties. Average neurite outgrowth length of neurites cultured on 1.92 and 4.07μm PHBV fibres was quite similar, but there was a significant increase in average neurite length from 4.07 to 5.97μm fibres (72.73 ± 10.38μm to 127.54 ± 13.66μm) suggesting a minimum diameter value to promote neurite outgrowth length. No statistical differences were detected between NG108-18 neuronal cell attachment and viability across all fibre diameters, suggesting PHBV is an efficient material in promoting neuronal cell attachment and proliferation. Primary Schwann cells, grown according to the method of Kaewkhaw *et al.* (2012), were seeded onto the fibres, to determine maintained cell phenotype and cell viability on the PHBV fibres. The average Schwann cell length was measured for each diameter, as a marker of Schwann cell morphology, as decreased Schwann cell length indicates immature (or unhealthy) cells, whereas a longer cell length indicates a mature cell and maintained phenotype (Chew *et al.*, 2008; Daud *et al.*, 2012).

Overall, the average Schwann cell length decreased, as the fibre diameter increased, however this result was not significant. It would suggest that Schwann cells prefer a smaller fibre diameter, as seen in the study by Gnavi *et al.* (2015) and Daud *et al.* (2012). The number of live cells on 1.92μm fibres was significantly higher than the other fibre diameters, confirming that Schwann cells attached more effectively on smaller fibre diameters. However, this could also be due to the increased fibre density of the 1.92μm fibres. Previous work has confirmed that Schwann cells mature more efficiently on aligned fibres, compared to random fibres, but most of this work has been performed using nanofibers, and

not microfibers. Although Gnavi *et al.* (2015) used 1.0 and 1.3μm fibres in their study, random nanofibers enhanced primary Schwann cell proliferation and adhesion, versus random microfibers, which would explain the results in this chapter, in which 1.92μm PHBV fibres promote higher Schwann cell attachment, than larger fibre diameters (Gnavi *et al.*, 2015a). However, it is difficult to compare the results in this chapter with other published findings except those by Daud *et al.* (2012) (Chew *et al.*, 2008).

Previous work investigating the effect on aligned fibre diameters on neuronal and Schwann cells has focused mainly on either the culture of cell types individually, or using a DRG *ex vivo* culture model, to replicate a nerve injury model (H. B. Wang *et al.*, 2010). In order to reduce animal work, a co-culture of NG108-15 neuronal cells and primary Schwann cells was established to determine the effect of the different fibre diameters on both cell types. Overall, the highest neurite outgrowth lengths were measured on the 8.08μm fibres, followed by the 5.97 and 10.17μm fibres, although this was not significant.

However, addition of Schwann cells to NG108-15 neuronal cell cultures did significantly increase NG108-15 neuronal cell neurite outgrowth on the 1.92 and 4.07μm fibres. This is consistent with published findings by Armstrong *et al.* (2007) as well as other studies, that confirm that Schwann cells release neurotrophic growth factors and ECM molecules to stimulate neurite outgrowth (Armstrong *et al.*, 2007; Daud *et al.*, 2012). With regards to cell viability, live cell attachment was highest on the 1.92μm fibres, compared to the other fibre diameters, although this was not significant. These results could be due to smaller fibre diameters promoting higher Schwann cell attachment and proliferation as seen in Gnavi *et al.* (2015). But this effect could also be due to the lower amount of NG108-15 neuronal cells added to the co-culture, plus differentiation of NG108-15 neuronal cells is initiated straight away in co-culture, rather than having 2 days to proliferate and attach, in mono-culture. All scaffolds had high cell viability, indicating PHBV fibres, of different diameters, promote NG108-15 neuronal cell and primary Schwann cell attachment, proliferation and differentiation.

Overall, the conclusions of this chapter report that using a higher fibre diameter, of 8.08μm, promotes longer NG108-15 neurite outgrowth, but that a smaller fibre diameter, of 1.92μm, promotes higher Schwann cell attachment and proliferation rate. 8.08μm fibres promoted the longest neurite outgrowth of NG108-15 neuronal cells in co-culture, although this result was not significant compared to the other fibre diameters. 1.92μm fibres promoted the highest number of live attached NG108-15 neuronal cells and primary Schwann cells, but this result was not significant. As 5.97 and 8.08μm fibres appeared to have the greatest effect on NG108-15 neuronal cell outgrowth, these diameters were chosen to fabricate

P(3HO):P(3HB) (50:50), P(3HO-co-3HD):PLLA (50:50) fibres, using PHBV and PCL fibres as a control. Therefore, 5 and 8µm fibres of all four materials / blends were taken forward to chapter 5 for a full *in vitro* analysis with NG108-15 neuronal cells and primary Schwann cells, in single and co-culture. Following this, the materials / blends will be taken forward to *ex vivo* analysis using a rat DRG 3D culture model established in the Haycock laboratory, in order to determine if any of the materials could be used as an internal guidance filler for use with a nerve guide conduit (Behbehani *et al.*, 2018).

Chapter 5: *In Vitro* Analysis of Fibre Blends

5.1 Introduction

The choice of biomaterial, and its chemical composition, is an essential requirement when considering the design of an internal fibre scaffold to aid nerve repair. A fibrous internal guidance scaffold must meet certain criteria in order to successfully promote nerve regeneration (Subramanian *et al.*, 2009). Nerve guide conduits must have the correct degradation rate, and similar mechanical and physical properties, and chemistry to native nerve tissue. NGCs must also allow nutrient transfer, and have the correct surface topography to aid cell adhesion, proliferation and differentiation (Nectow *et al.*, 2012). With regards to the fibrous internal scaffold, the biomaterial of choice must be fabricated from aligned fibres with specific diameters that can be easily reproduced and that are easy to handle and manipulate. Fibres must be able to be threaded into a conduit without losing alignment and maintain structure (Subramanian *et al.*, 2009).

Chapter 2 concluded that polyhydroxyalkanoates are an advantageous choice of material, for peripheral nerve repair, due to their range of different mechanical properties, biodegradability and excellent biocompatibility (Philip *et al.*, 2007). P(3HO-co-3HD), P(3HO) and PLGA had Young's moduli closer to that of rat sciatic nerve. However, P(3HB) and PHBV are more hydrophilic polymers compared to other PHAs, and they promoted NG108-15 neuronal cell adhesion more effectively. Out of all the polyhydroxyalkanoates, P(3HB) has the fastest degradation rate. Therefore, blending materials was performed to achieve a balance of biocompatibility, mechanical and physical properties, as well as the required degradation rate, as is required for the ideal nerve guide conduit (Kehoe *et al.*, 2012).

Research, in nerve tissue engineering, has focused primarily on blending synthetic polymers with natural polymers, such as collagen and gelatine, which has shown that addition of the natural polymer improves cellular adhesion to a synthetic polymer and can promote regeneration (Gnavi *et al.*, 2015b). However, no studies have been published which shows a direct comparison between individual polymers, or blends, for improving nerve regeneration, (except in considering an immortal Schwann cell line (Sangsanoh *et al.*, 2007).) There are many published reviews on current FDA nerve guide conduits, and wraps, in comparison to autografts, which have highlighted the limitations and advantages of using a conduit made of a specific polymer, but again, no study has shown whether one NGC material is more effective than another (Kehoe *et al.*, 2012). This chapter therefore investigated a comparison of different candidate materials, and different blends, to determine if one material or blend

was more effective in promoting neuronal and Schwann cell adherence, proliferation and maturation, than the other. Fibres were fabricated, from each material and blends, by electrospinning, with the same diameters and alignment for a direct comparison. Overall, chapter 3 confirmed that many of the polyesters with FDA approval for peripheral nerve repair could be electrospun into aligned fibres of different diameters. It was also concluded that a softer elastomeric polymer, such as P(3HO), could only be electrospun successfully when blended with a more brittle polymer at a minimum of a 50:50 ratio. P(3HO):P(3HB) (50:50) and P(3HO-co-3HD):PLLA (50:50) were chosen blends to be investigated, from chapter 3, due to ease and reproducibility of electrospinning aligned fibres. Use of these blends was a compromise between biocompatibility and degradation rate. PCL fibres were also fabricated as a control material, as results of *in vitro* analysis using neuronal and Schwann cells have been well documented (Daud *et al.*, 2012). PHBV was also taken forward for *in vitro* analysis due to its performance in initial biocompatibility studies in chapter 2. PHBV is cheaper to fabricate than P(3HB) and P(3HO) and its mechanical properties can be tailored.

Following the data reported in chapter 4, it was concluded that the most effective diameter for NG108-15 neuronal cell differentiation was 8µm. The average neurite length from neuronal cells cultured on 8µm fibres was significantly longer than on fibres 2 and 4µm diameter, and live cell attachment higher on 8µm fibres compared to the other diameters fabricated. 5 and 8µm fibres of all 4 materials / material blends have been fabricated for *in vitro* analysis to determine which material / blend would be the most effective for neuronal cell attachment and differentiation, as well as Schwann cell attachment and proliferation. It is hypothesised that the PHA blends and PHBV will support NG108-15 neuronal cell attachment and differentiation more efficiently than PCL. Although previous work by Lizarraga *et al.* (2015) had investigated the material characteristics of the PHA blends, and P(3HO):P(3HB) (50:50), degradation of the blend had not been investigated. Due to the novelty of the P(3HO-co-3HD):PLLA (50:50) blend, water contact angle was also performed again and compared to the other materials, as well as undergo degradation testing. Mechanical testing of P(3HO):P(3HB) (50:50) and P(3HO-co-3HD):PLLA (50:50) fibres, as well as PHBV and PCL fibres was performed in chapter 6 before *ex vivo* analysis.

5. 2 Methods and Materials

5.2.1 Water contact angle of final blends

As previously described in section 1.2, *methods* section of chapter 2, the water contact angle was determined for the P(3HO-co-3HD):PLLA (50:50) blend. A 10wt% solution of the blend was spin coated (as described in section 1.1- chapter 2) and left to dry. The data was then added to that found in section 2.1 chapter 2.

5.2.2 Degradation studies of final fibre blends

In vitro degradation tests were performed on spin coated films of the P(3HO):P(3HB) (50:50) and P(3HO-co-3HD):PLLA (50:50) in comparison with PCL and PHBV, with known degradation properties. Spin coated films were fabricated as previously described in section 1.2, of the methods section in chapter 2. Glass coverslips were weighed before and after spin coating to determine the weight of the polymer film. Films were placed into a 24 well plate, sterilised with 70% ethanol and washed with PBS before experimentation. 2mL of sterilised PBS was added to each sample, and the pH was recorded (Jenway 310 pH meter). The pH was then taken every 2 weeks up to 24 weeks, to observe the change in pH. In a separate well plate, 1mL of sterilised PBS was added to each sample, and was replaced every week to keep the pH constant at pH 7.04. Samples were weighed every 4 weeks, up to 24 weeks, and were then vacuum dried to calculate the mass of the dried samples. Weight loss (%) was calculated by the following equation:

Weight loss (%)= 100 (M1dry- M2dry) x M1dry

In which M1 is the recorded mass at week 0, and M2 dry is the vacuum dried mass after a certain time point. An average of 3 samples was taken to determine the cumulative weight loss % of the films during degradation. (Haiyan Li and Chang, 2005)

5.2.3   Fabrication of electrospun material fibres and characterisation

Aligned 5 and 8µm fibres of all 4 investigated materials, were fabricated by electrospinning. Figure 1 shows the different electrospinning conditions used to fabricate these diameters, confirmed in chapter 3. Electrospinning was performed using a high-power voltage supply (Genvolt UK), a single syringe pump (WPI-Europe) and a rotating cylindrical collector attached to a motor (IKA Works) (as described in section 1.1, *methods* in chapter 3).

Table 5.1. Electrospinning conditions to fabricate 5 and 8μm fibres of P(3HO):P(3HB) (50:50), P(3HO):PLLA (50:50), PHBV and PCL.

	Material	Solution (%)	Voltage (kV)	Distance (cm)	Flow rate (mL/h)	Collector Speed (xg)	Size of fibres (μm)
A	P(3HO):P(3HB) (50:50)	8	12.5	15	3	134	4.97 ± 0.61
B	P(3HO):P(3HB) (50:50)	8	12.5	10	3	134	7.86 ± 1.13
C	P(3HO-co-3HD):PLLA (50:50)	12	8	20	4	134	4.97 ± 0.74
D	P(3HO-co-3HD):PLLA (50:50)	12	8	15	4	134	7.81 ± 1.77
E	PCL	10	15	20	4	134	5.03 ± 0.13
F	PCL	20	18	20	6	134	8.07 ± 0.07
G	PHBV	14	12	20	3	134	5.07 ± 0.96
H	PHBV	15	10	20	4	134	8.08 ± 1.43

Electrospun fibres were characterised by scanning electron microscopy to confirm fibre diameter and alignment (described in more detail in the materials and methods section in chapter 3, 1.2). The ruler tool in NIH software Image J was used to measure fibre diameter and determine angular variance between individual fibres (Schneider *et al.*, 2012). The number of fibres, per 100μm were counted manually for each batch of electrospun fibres and fibres per μm determined.

5.2.4 Preparation of aligned electrospun fibres for In Vitro Analysis

Electrospun fibres were cut into 25mm x 25mm squared samples, to fit into a 6 culture well plate. Fibres were carefully removed from the foil collector and adhered to the surface with a 10wt% solution of the relative polymer/blend. Fibres were held into position by large medical grade 316L stainless steel cell culture rings (inner diameter = 26mm, outer diameter = 35mm) and a smaller stainless-steel cell culture ring, (inner diameter = 10 mm, outer diameter = 20 mm) was placed into the middle of the sample, to decrease fibre surface area. Samples were sterilised using 70% ethanol for 3 hours, followed by a wash in PBS. Samples were immersed in PBS and left in PBS overnight to ensure all contaminants had been

removed. Before cell seeding, samples were washed again in PBS for 5 minutes (Daud *et al.*, 2012).

5.2.5 NG108-15 neuronal cell culture

See chapter 2, 2.2.6 *Methods* section for details.

5.2.6 Immunolabelling of NG108-15 neuronal cells for β III tubulin

See chapter 4, 4.2.6 *Methods* section for details.

5.2.7 Isolation of rat primary Schwann cells

See chapter 4, 4.2.7 *Methods* section for details.

5.2.8 Co-culture of NG108-15 neuronal cells and rat primary Schwann cells different material fibres with different diameters

See chapter 4, 4.2.8 *Methods* section for details.

5.2.9 Immunolabelling of rat Primary Schwann cells for S100β

See chapter 4, 4.2.9 *Methods* section for details.

5.2.10 Live/Dead analysis of NG108 neuronal cells and primary Schwann cells

See chapter 2, 2.6 *Methods* section for details.

5.2.11 Neurite outgrowth assessments

See chapter 4, 4.2.11 *Methods* section for details.

5.2.12 Assessment of Primary Schwann Cell Morphology and Schwann cell migration length

See chapter 4, 4.2.12 *Methods* section for details.

5.2.13 Statistical Analysis

GraphPad Instat (GraphPad Software, USA) was used to perform statistical tests on data collected. One-way analysis of variance ($p < 0.05$) was conducted to analyse the differences between the data, incorporating Tukey's multiple comparisons test if $p < 0.05$. Data was reported as mean ± SD, $p < 0.05$. Each experiment was performed three independent times with each sample repeated three times as n=3.

5.3 Results

5.3.1 Water contact angles of final fibre blends

Water contact angles of polymers investigated, and polymer blends, were confirmed in chapter 2 (*Results* section 2.1), to determine the surface wettability and hydrophilic / hydrophobic characteristics. Figure 2.1A and B (chapter 2) show water contact angle for PCL, PHBV and P(3HO):P(3HB) (50:50) but not for P(3HO-co-3HD):PLLA (50:50), as this blend was included for *in vitro* testing after the electrospinning results in chapter 3. Figure 5.1, below, shows a graph comparing the water contact values of the two polymers and two blends, with the addition of the P(3HO-co-3HD):PLLA (50:50) blend. The water contact angles of PCL and PHBV are significantly lower than that of the P(3HO):P(3HB) (50:50) and P(3HO-co-3HD):PLLA (50:50), 72 ± 2.12˚ and 67.22 ± 2.72˚ compared to 102.17 ± 1.60˚ and 94.73 ± 6.53˚ respectively.
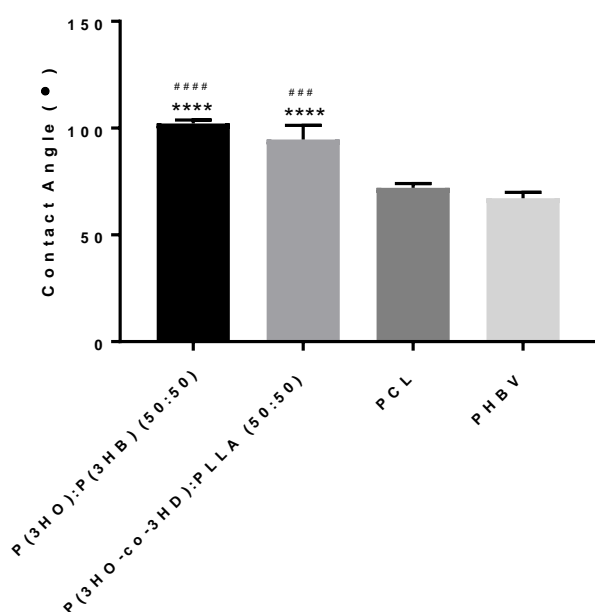

Figure 5.1. Graph to show the average water contact angle recorded on neat polymer and polymer blend spin coated films. A one way anova with Tukey's multiple comparisons tests was used to analyse data (Mean ± SD, n= 3 independently fabricated samples ****p < 0.0001 compared to PHBV, ###p < 0.001and #### p < 0.0001 compared to PCL).

5.3.2 Degradation studies of final fibre blends

Figure 5.2A shows the cumulative weight loss (%) of the polymer films over an incubation time of 24 weeks. Scaffold weight loss increased over the time, in which the highest weight loss after 24 weeks incubation at 37°C was observed in the PHBV films, followed by the PCL films, 105.87 ± 6.96% and 120.05 ± 4.01% respectively. Due to its hydrophobic nature, PCL is known to degrade slowly, up to year, due to little water penetration to the bulk PCL (E Díaz *et al.*, 2014). In contrast, the lowest weight loss, after 24 weeks incubation, was observed in the P(3HO):P(3HB) (50:50) films, of 75.92 ± 11.98%, which also had the lowest initial weight loss of 20.41 ± 14.88% after 8 weeks incubation. Similar data was reported in the study by Basnett *et al.* (2013) which confirmed that after 4 weeks incubation, P(3HO):P(3HB) (50:50) films had a weight loss percentage of 11% (Basnett *et al.*, 2013).

Figure 5.2B shows the change in pH levels of PBS, containing the polymer blends, over 24 weeks incubation at 37°C. The initial pH value of the PBS was 7.41, and over the time, the pH decreased. There was very little change in pH of PBS containing the PHA blends over 24 weeks incubation, maintaining a neutral pH. P(3HO-co-3HD):PLLA (50:50) had the lowest pH of 6.62 ± 0.01 after the 24-week time. However, the lowest drop in pH was recorded from the PCL film of 6.02 ± 0.04. As hydrolytic degradation products of PCL are relatively acidic, such as valeric acid and hexanoic acid, a slight more acidic pH after 24 weeks incubation was expected (Sanchez *et al.*, 2000). Out of the PHA blends, the P(3HO-co-3HD):PLLA (50:50) had the lowest pH, of 6.62 ± 0.14. Due to the acidic degradation products of the PLLA, this result was expected (Elsawy *et al.*, 2017). However, the hydrophobic nature of the P(3HO-co-3HD) decreased the degradation rate, and the release of acidic degradation by products from the PLLA (Renard *et al.*, 2004).
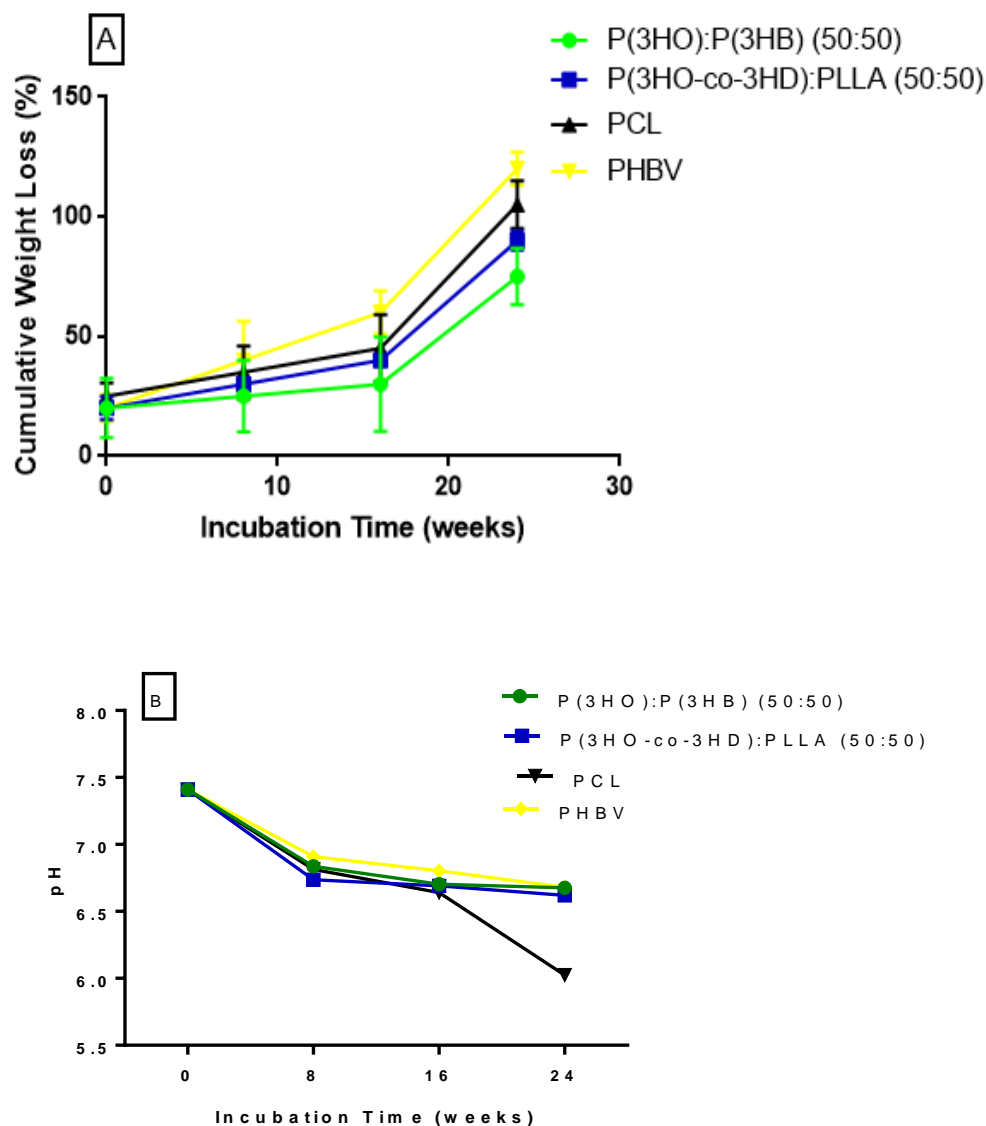
Figure 5.2. Change in A) weight loss % and B) pH of P(3HO):P(3HB) (50:50), P(3HO-co-3HD):PLLA (50:50), PCL and PHBV films incubated for 24 weeks in PBS.

5.3.3 Fabrication of aligned fibres from different materials with different fibre diameters

Electrospinning conditions, in table 5.1, were used to fabricated 5 and 8µm fibres of P(3HO):P(3HB) (50:50), P(3HO-co-3HD):PLLA (50:50), PCL and PHBV. Figure 5.3 shows scanning electron micrographs of fibres fabricated from these conditions to be used for *in vitro* testing. Fibre fabricated appeared and aligned, and differences in fibre diameter could be seen between the material types.
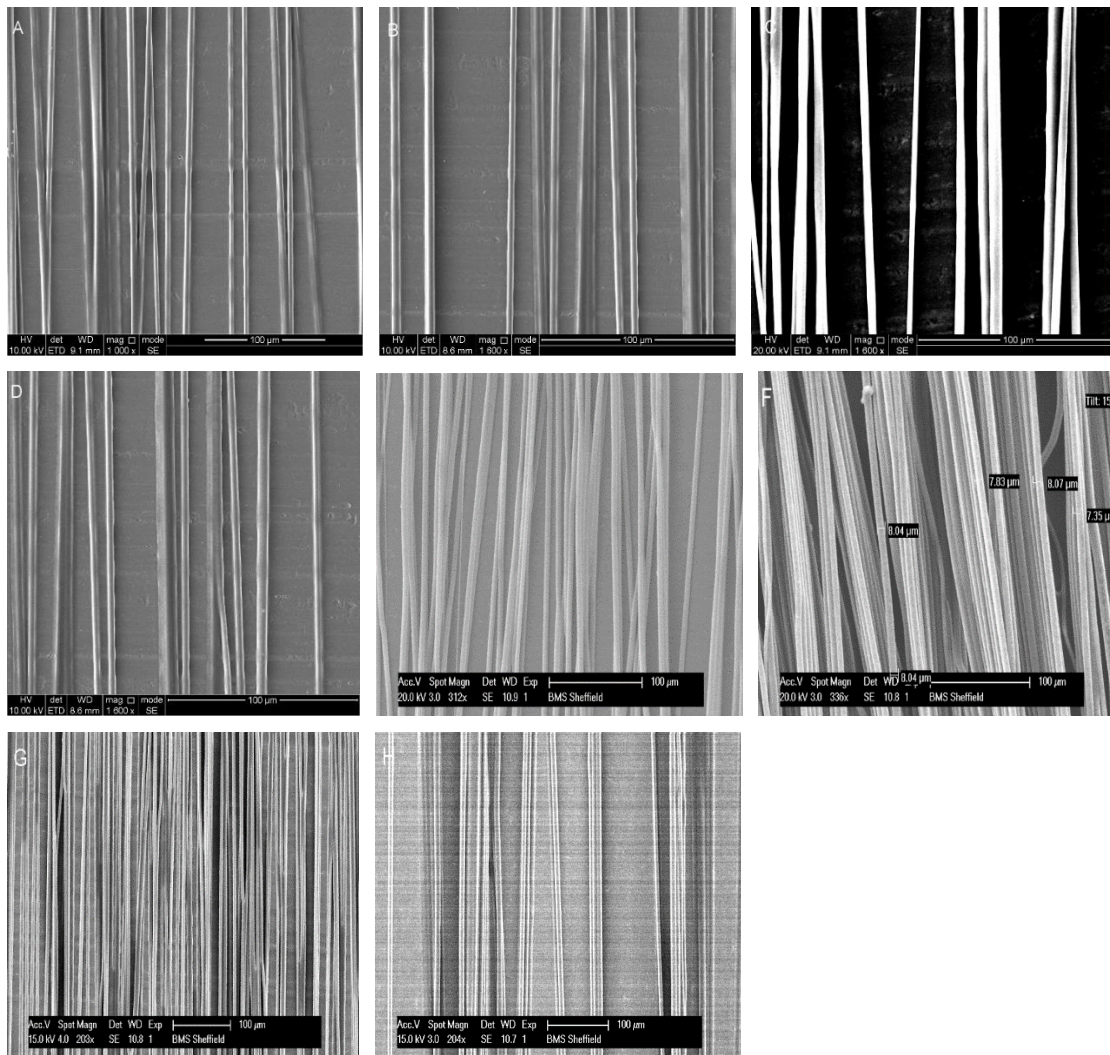
Figure 5.3. Scanning electron micrographs of (A) P(3HO):P(3HB) (50:50) 5μm fibres, (B) P(3HO):P(3HB) (50:50) 8μm fibres, (C) P(3HO-co-3HD):PLLA (50:50) 5μm fibres, (D) P(3HO-co-3HD):PLLA (50:50) 8μm fibres, (E) PCL 5μm fibres, (F) PCL 8μm fibres and (G) PHBV 5μm fibres, (H) PHBV 8μm fibres and (I) Tissue culture plastic. Scale bar =100μm.

To confirm the correct fibre diameter of each material manufactured, fibre diameter was determined by measuring each fibre from micrographs taken using the ruler tool on Image J (Schneider *et al.*, 2012). Figure 5.4A concluded that 5 and 8μm fibres of all material types had been fabricated, and that there was very little variance between individual fibre diameters measured, due to low standard deviation. It was also confirmed that the 8μm fibres, of each material type, were statistically higher than the 5μm fibres fabricated for each material/material blend.

A

Average Fibre Diameter (μm)

P(3HO):P(3HB) (50:50) 5 μm
P(3HO):P(3HB) (50:50) 8 μm
P(3HO-co-3HD):PLLA (50:50) 5 μm
P(3HO-co-3HD):PLLA (50:50) 8 μm
PCL 5 μm
PCL 8 μm
PHBV 5 μm
PHBV 8 μm

B

Frequency

P(3HO):P(3HB) (50:50) 5 μm
P(3HO):P(3HB) (50:50) 8 μm
P(3HO-co-3HD):PLLA (50:50) 5 μm
P(3HO-co-3HD):PLLA (50:50) 8 μm
PCL 5 μm
PCL 8 μm
PHBV 5 μm
PHBV 8 μm

Angular Difference (°)

C
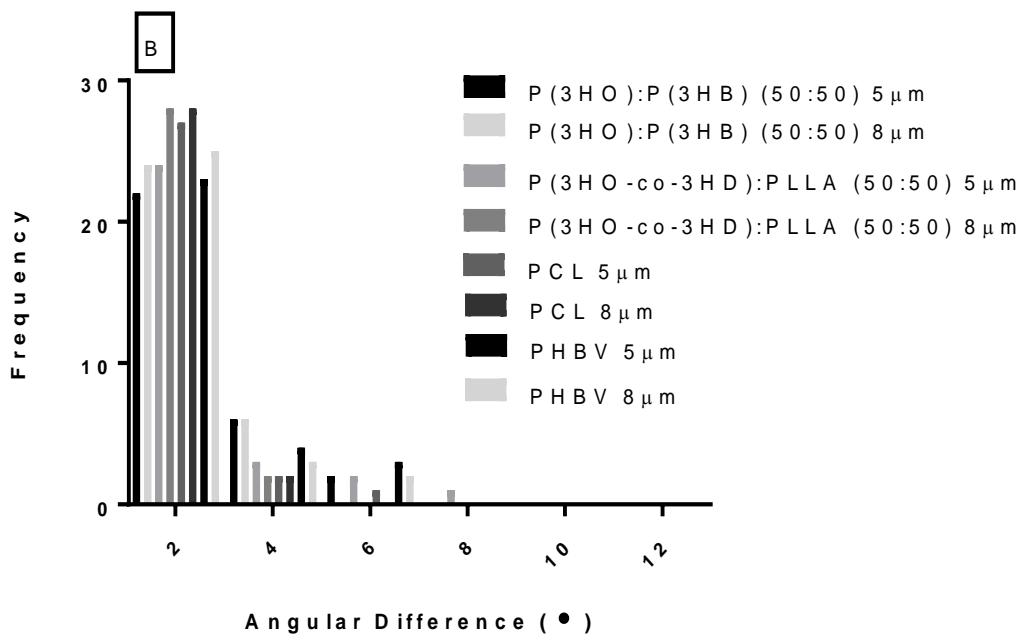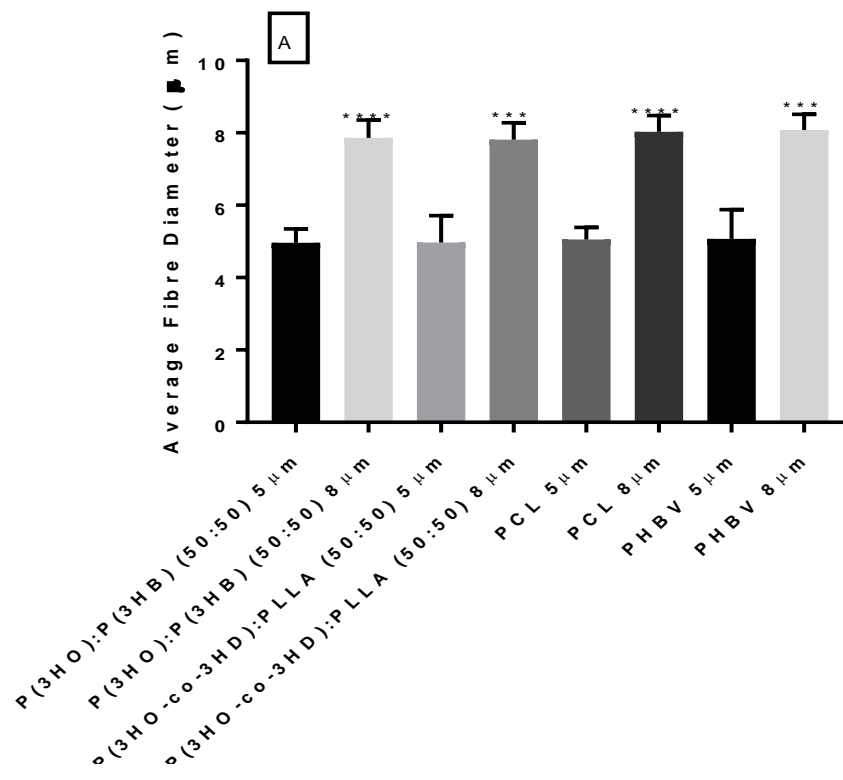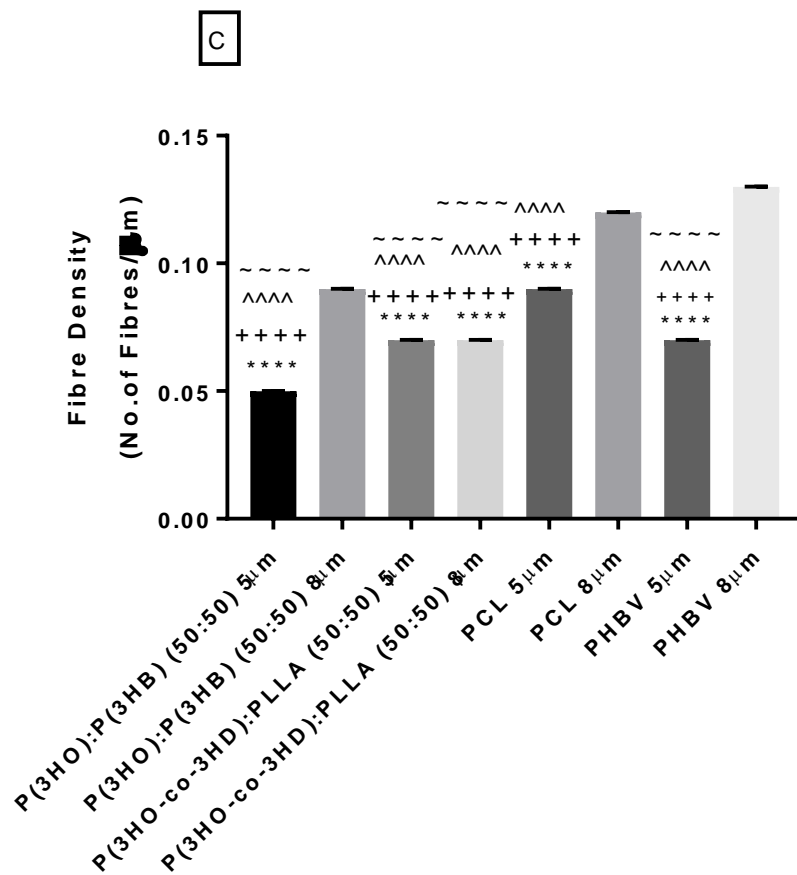
Figure 5.4. A) Average fibre diameter of PHA polymers. An average of 30 fibres was assessed for each fibre condition and mean of the diameter presented. A two way anova with Sidak's multiple comparisons tests was used to analyse data (mean ± SD, n= 3 independently fabricated samples ***p < 0.01 compared to 5µm fibres, ****p < 0.0001 compared to 5µm fibres). B) Histogram to show the angular variance of 5 and 8µm fibres of the 3 different material blends compared to PCL fibres. C) Surface coverage of fibres was determined by the fibre density. Fibres per µm was conducted by counting the number of fibres per 100µm. A one way anova with Tukey's multiple comparisons tests was used to analyse data (****p < 0.0001 compared to PHBV 8µm fibres, ++++p < 0.0001 compared to PCL 8µm fibres, ^^^^p < 0.0001 compared to PCL 5µm fibres and ~~~~p < 0.0001 compared to P(3HO):P(3HB) (50:50) 8µm fibres. Per independently electrospun batch of fibres, 30 fibres were measured. (n=3)

Fibre alignment was also confirmed by determining the angular variance between each fibre, per condition. Figure 5.4B confirmed all fibres were aligned, as over 70% of fibres were measured in the 0-2° category. The most aligned fibres were the PCL fibres, 8µm P(3HO-co-3HD):PLLA (50:50) fibres and 8µm PHBV fibres. The least aligned fibres were the 5µm P(3HO):P(3HB) fibres. Figure 5A and B confirmed that fibres fabricated for *in vitro* analysis were the correct diameter and were aligned, and the conditions fabricated in chapter 3 are reproducible. Surface coverage of the fibres was determined by calculating the fibre density. The highest fibre density, number of fibres per µm, was calculated for the 8µm PCL, PHBV and P(3HO):P(3HB) fibres and PCL 5µm fibres, which corresponded with the SEM micrographs in figure 5.3.

5.3.4 NG108-15 neuronal cell differentiation on aligned fibres

Figure 5.5 shows confocal micrographs of NG108-15 neuronal cells, cultured on the fibres after 6 days in culture. Cells were immunolabelled for the cell nucleus (DAPI - blue) and neurite outgrowth (βIII tubulin - red). Neurites extended from NG108-15 cells on all samples and long neurites could be visualised aligning themselves to the fibres, compared to the tissue culture plastic control, in which neurites grew out in a random manner (see arrows). Longer neurites could be seen on the 8μm fibre sizes of all samples. Confocal micrographs were quantified to determine the percentage of neurite bearing cells per sample, to calculate the average number of neurites per neuron and calculate the average neurite length per sample. Three fields of view per sample, per independent experimental run, were analysed to calculate the percentage number of neurite bearing cells. Cells were counted manually by cell counter software in NIH Image J (Usaj *et al.*, 2010). The highest percentage of neurite bearing cells (figure 5.6A) per sample, were detected on 5μm PCL fibres, 8μm and 5μm P(3HO):P(3HB) (50:50) fibres, and the P(3HO-co-3HD):PLLA 5μm fibres, 68.66 ± 39.37%, 67.88 ± 6.91%, 66.86 ±6.78% and 66.21 ± 9.55% respectfully. No statistical differences were detected between the fibre samples suggesting no trend between fibre size and neurite bearing cell percentage. However, the percentage of neuronal cells expressing neurites on the 5μm PCL fibres, 8μm and 5μm P(3HO):P(3HB) (50:50) fibres, and the P(3HO-co-3HD):PLLA 5μm was statistically higher than the percentage of neurite bearing neuronal cells cultured on the tissue culture plastic control.

Figure 5.5. Immunolabelled confocal micrographs of NG108-15 neuronal cells cultured on (A) P(3HO):P(3HB) (50:50) 5µm fibres, (B) P(3HO):P(3HB) (50:50) 8µm fibres, (C) P(3HO-co-3HD):PLLA (50:50) 5µm fibres, (D) P(3HO-co-3HD):PLLA (50:50) 8µm fibres, (E) PCL 5µm fibres, (F) PCL 8µm fibres and (G) PHBV 5µm fibres, (H) PHBV 8µm fibres and (I) Tissue culture plastic control and J) 3D composite image of neuronal cells on fibres. Neuronal cell nuclei were labelled with DAPI (blue) and neurite extension labelled for βIII tubulin (red) to conduct NG108-15 neuronal cell differentiation studies. Scale bar = 100µm.

Analysis of samples from confocal micrographs was performed to calculate the average number of neurites present per NG108-15 neuronal cell. Figure 5.6B concluded that NG108-

15 neuronal cells cultured on 5μm P(3HO-co-3HD):PLLA (50:50) fibres, and 8μm P(3HO-co-3HD):PLLA (50:50) fibres had the highest average of neurites shown per neuron, 1.63 ± 0.19 neurites per neuron and 1.31 ± 0.06 neurites per neuron. The lowest average numbers of neurites per neuron were from NG108-15 neuronal cells cultured on 8μm PCL fibres. However, no statistical differences were observed independent of fibre diameters. This indicates that material type, and fibre diameter does not influence initial NG108-15 neuronal cell neurite outgrowth.
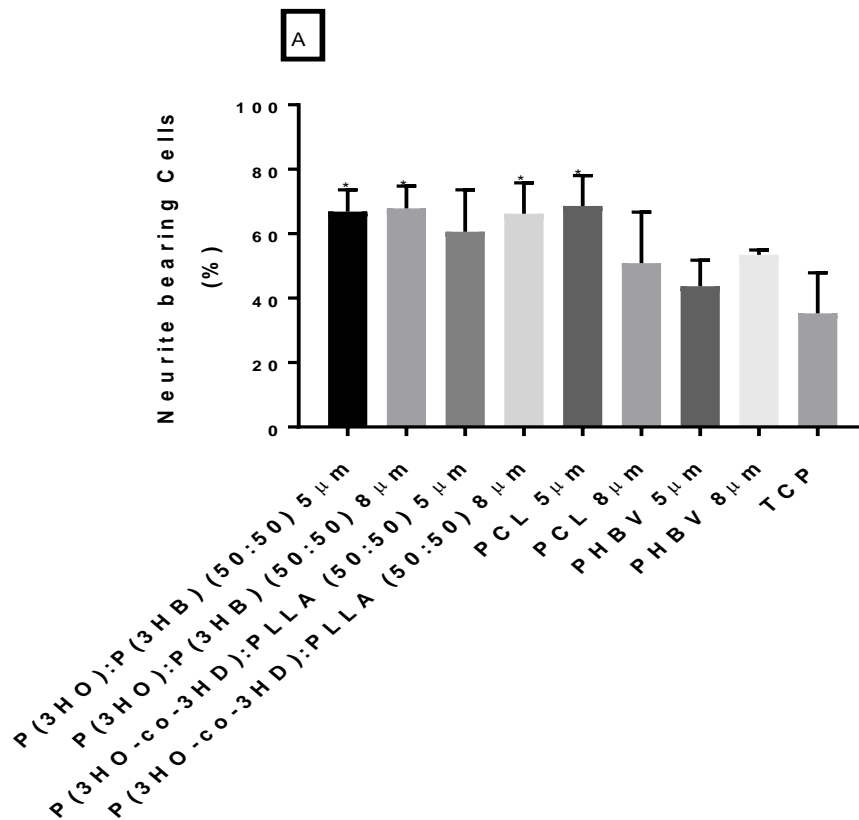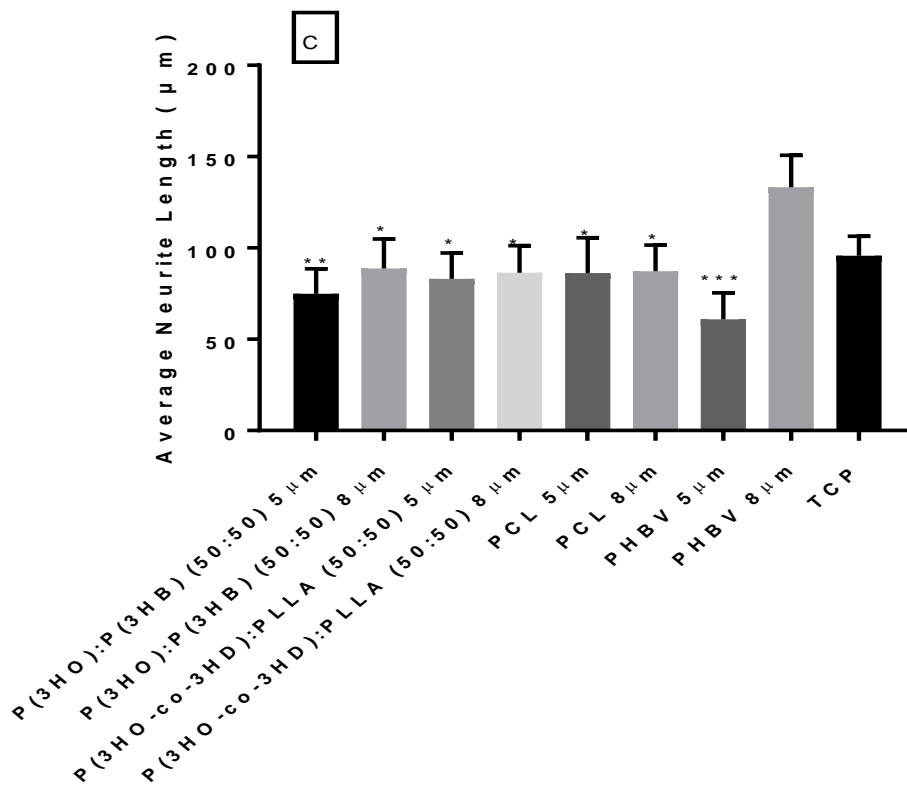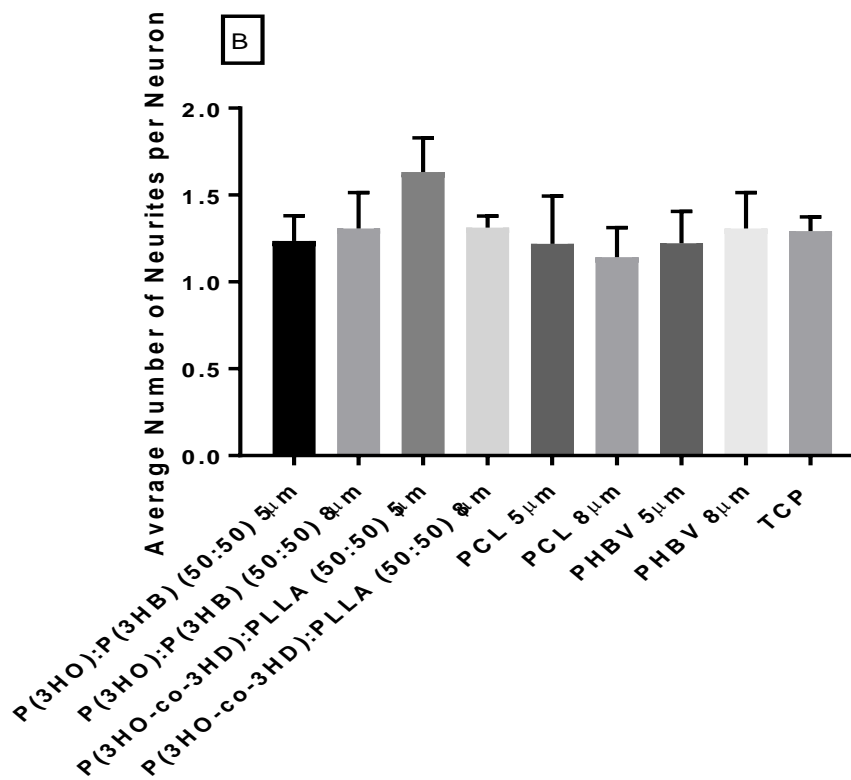
Figure 5.6. Analysis of NG108-15 neuronal cell differentiation studies on candidate fibres and polymer films. A) Neurite bearing NG108-15 neuronal cells after 6 days in culture, expressed as a percentage. A one way anova with Tukey's multiple comparisons tests was used to analyse data (Mean ± SD, n=3 independent experiments, *p<0.05 compared to TCP) (B) The average number of neurites expressed per neuron. A one way anova with Tukey's multiple comparisons tests was used to analyse data (Mean ± SD, n=3 independent experiments, no statistical difference detected) and (C) The average neurite length measured per sample.100 neurites per diameter/sample were measured, using Image J, to determine the average neurite length. A one way anova with Tukey's multiple comparisons tests was used to analyse data (Mean ± SD, n=3 independent experiments, *p < 0.05, **p < 0.01 and ***p < 0.001 compared to 8µm PHBV fibres).

To calculate average neurite length per sample, 100 neurites per condition were measured, using the neuron tracer plugin, Neuron J, in NIH Image J software (Popko *et al.*, 2009). The average neurite length was longer on the 8µm PHBV fibres, 133.32 ± 17.38µm, which was statistically higher than for all other fibre material blends and fibre diameters. Overall, the average neurite was longer on 8µm fibres than on 5µm, but there was minor difference in average neurite length on P(3HO-co-3HD):PLLA (50:50) 5 and 8µm fibres or 5 and 8µm PCL fibres, 83.03 ± 14.23µm, 86.39 ± 14.83µm, 86.30 ± 19.29µm and 87.28 ± 14.28µm respectively. All materials and fibre diameters supported NG108-15 neuronal cell adhesion and cell differentiation. However, significantly longer neurites grew on the 8µm fibres.

5.3.5 NG108-15 neuronal cell viability on different material aligned fibres with different diameters

NG108-15 neuronal cells were labelled with Syto-9 and propidium iodide to visualise the average number of live and dead cells on each scaffold by confocal microscopy for each material type and fibre diameter, to determine cell viability.
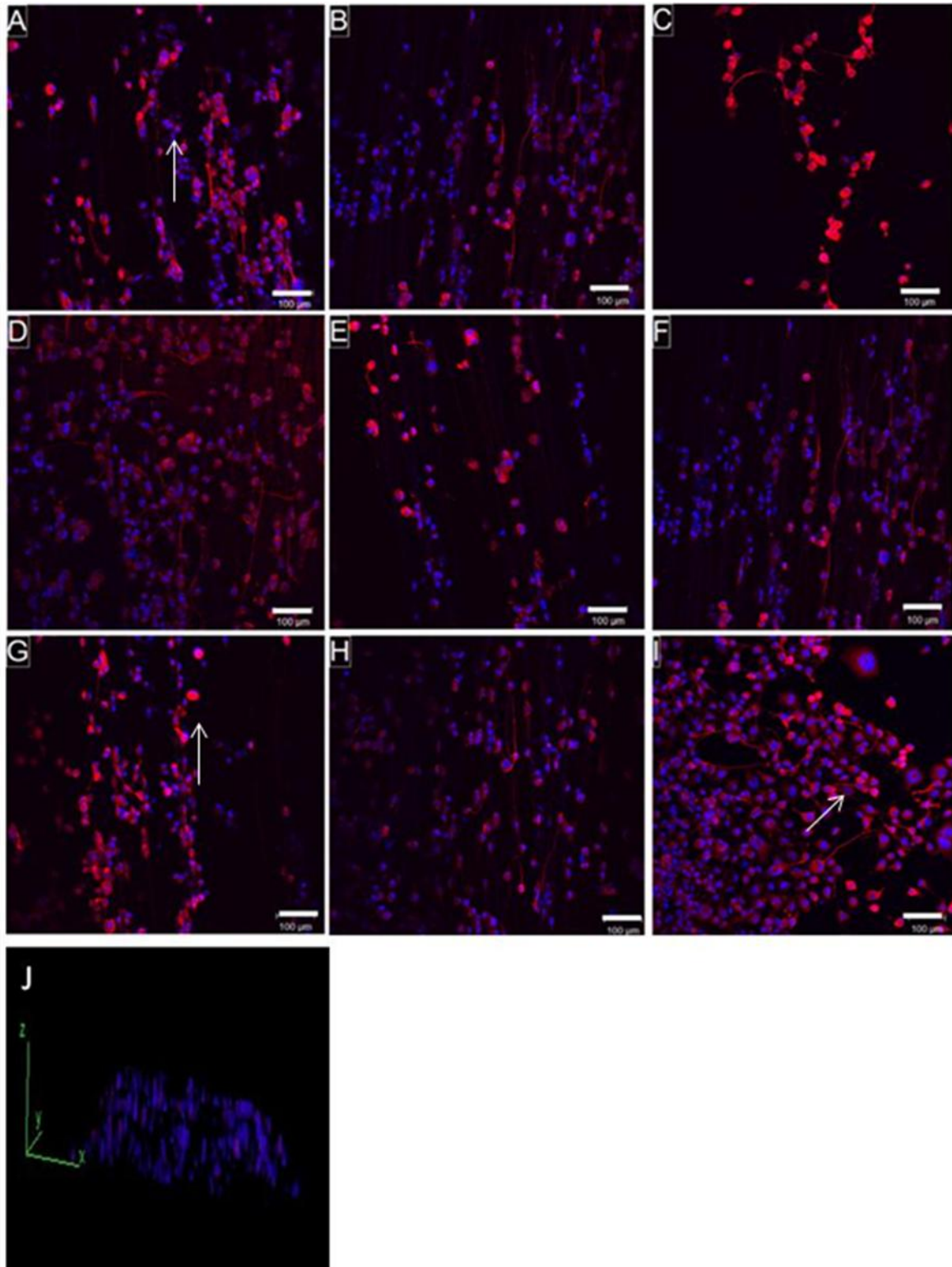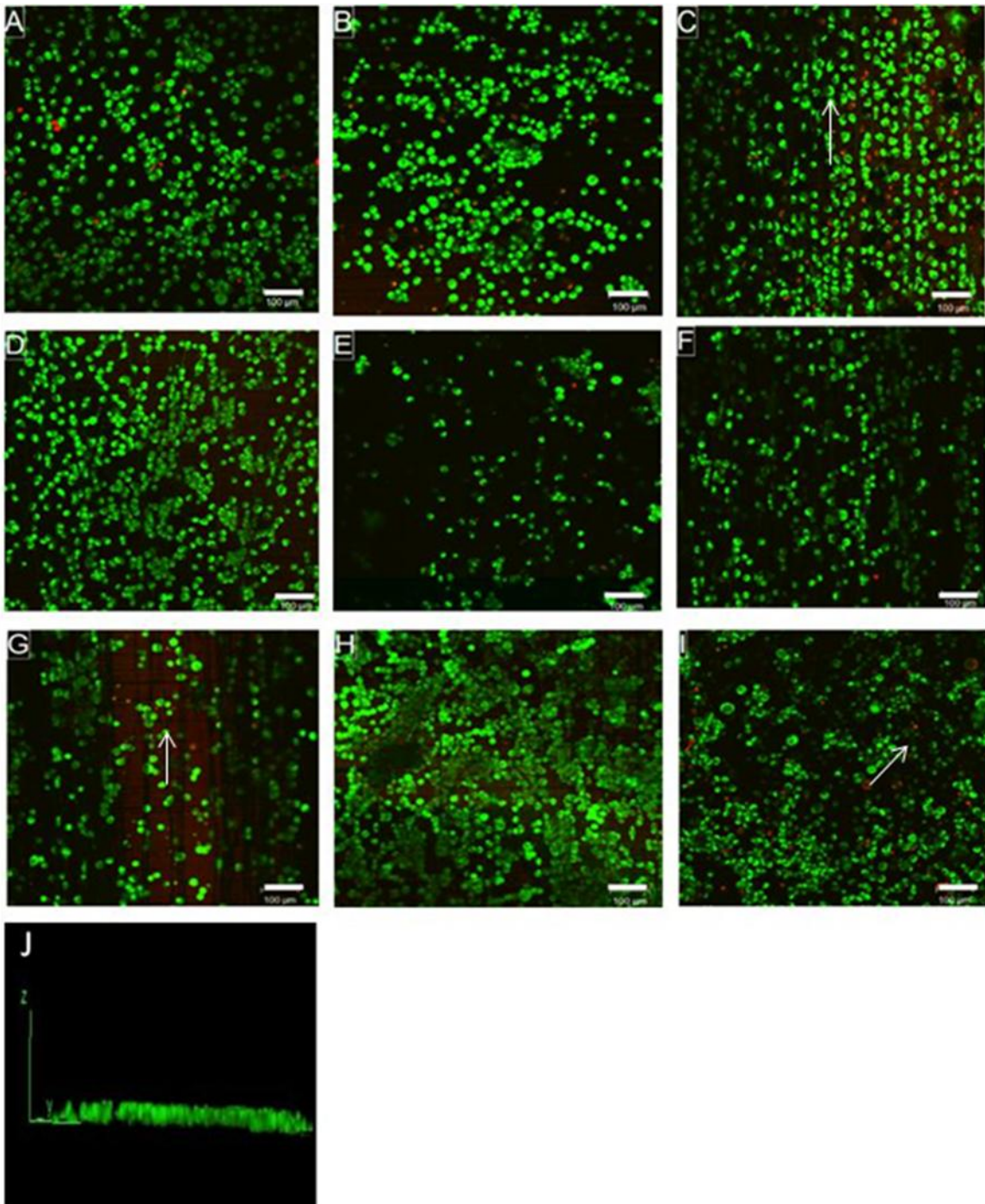
Figure 5.7. Live/dead confocal micrograph analysis of NG108-15 neuronal cells cultured on (A) P(3HO):P(3HB) (50:50) 5µm fibres, (B) P(3HO):P(3HB) (50:50) 8µm fibres, (C) P(3HO-co-3HD):PLLA (50:50) 5µm fibres, (D) P(3HO-co-3HD):PLLA (50:50) 8µm fibres, (E) PCL 5µm fibres, (F) PCL 8µm fibres and (G) PHBV 5µm fibres, (H) PHBV 8µm fibres, (I) Tissue culture plastic and J) 3D composite image of neuronal cells on fibres. Neuronal cells were labelled with Syto-9 (green) and propidium iodide (red) for live and dead cells respectfully. Scale bar =100µm.

Figure 5.7 shows confocal micrographs of live and dead NG108-15 neuronal cells cultured on each material type and fibre diameter. NG108-15 neuronal cells align themselves to the fibres, whereas cells adhered and proliferated in a random orientation on the tissue culture plastic. Visually, there is a higher number of live cells on the P(3HO-co-3HD):PLLA (50:50), PHBV and the P(3HO):P(3HB) (50:50) fibres compared to the PCL fibres. Micrographs were

143

quantified to determine the average number of live cells versus dead cells (figure 5.8A). The highest number of live cells were found on the tissue culture plastic, 660.67 ± 135.60 cells. With regards to the fibre samples, the highest number of live cells were found on the 8μm and 5μm PHBV fibres, followed by the P(3HO-co-3HD):PLLA (50:50) 8μm fibres, 564.56 ± 215.69 cells, 427.33 ± 198.31 cells and 431.55 ± 153.81 cells respectfully. The highest number of dead cells was found on the P(3HO):P(3HB) 8μm fibres, 20.33 ± 7.84 cells. Overall, each material type and fibre diameter had a statistically higher number of live cells attached, compared to the 5μm P(3HO):P(3HB) and 8μm PCL fibres. Overall it is suggested that the PHBV fibres support NG108-15 neuronal cell attachment and proliferation the most efficiently.

When cell viability was calculated for each sample, (figure 5.8B) there were no significant differences detected between data sets and all samples had above 90% viability of live cells. Percentage viability of samples were 96.97 ± 4.17%, 94.63 ± 7.84%, 94.88 ± 4.16%, 98.63 ± 2.048%, 99.10 ± 2.58%, 97.57 ± 4.37%, 97.03 ± 1.75% and 96.94 ± 1.63% for P(3HO):P(3HB) (50:50) 5μm fibres, P(3HO):P(3HB) (50:50) 8μm fibres, P(3HO-co-3HD):PLLA (50:50) 5μm fibres, P(3HO-co-3HD):PLLA (50:50) 8μm fibres, PCL 5μm fibres, PCL 8μm fibres, PHBV 5μm fibres and PHBV 8μm fibres respectfully. This indicates that having a larger fibre diameter increases the amount of cell adhesion, with regards to PHBV and the PHA blends, and that the polyhydroxyalkanoates increase cell adhesion and proliferation more than PCL.
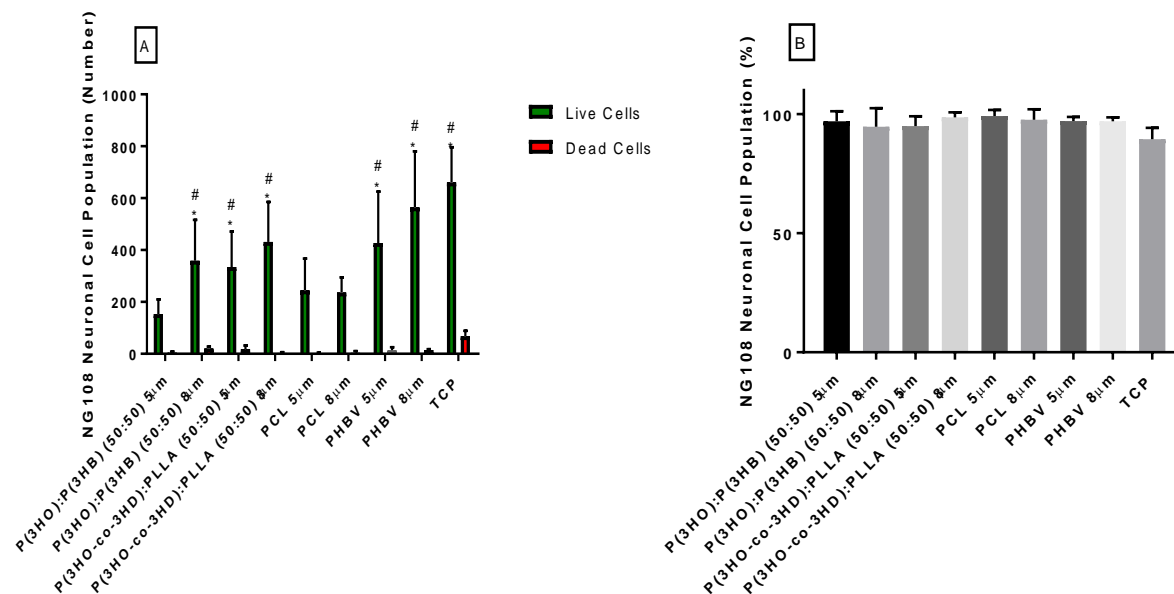
Figure 5.8. Live/dead analysis of neuronal cells on electrospun fibres expressing the average total number of live versus dead cells. A one way anova with Tukey's multiple comparisons tests was used to analyse data (Mean ± SD, n=3 independent experiments, *p < 0.05 compared to 8μm PCL fibres, #p < 0.05 compared to 5μm PCL fibres). Cell viability was also expressed as a percentage (B). (Mean ± SD n=3 independent experiments). No significant differences were seen.

5.3.6 Primary Schwann cell culture on different material aligned fibres with different diameters

60,000 rat primary Schwann cells were cultured on fibrous scaffolds for 6 days. Samples were labelled with DAPI, to visualise the cell nucleus, and S100, to visualise the Schwann cell body. Figure 5.9 shows confocal micrographs taken of primary Schwann cells cultured onto the different material fibres, and different diameters. All Schwann cells stained positively for S100β, and could be seen aligning themselves to the fibres, and some elongation of cells over fibres. Higher numbers of Schwann cells were seen on tissue culture plastic (figure 5.9I), compared to fibrous samples. All fibre samples supported Schwann cell attachment, and there appeared to be less Schwann cells attached to 8µm fibres compared to 5µm.
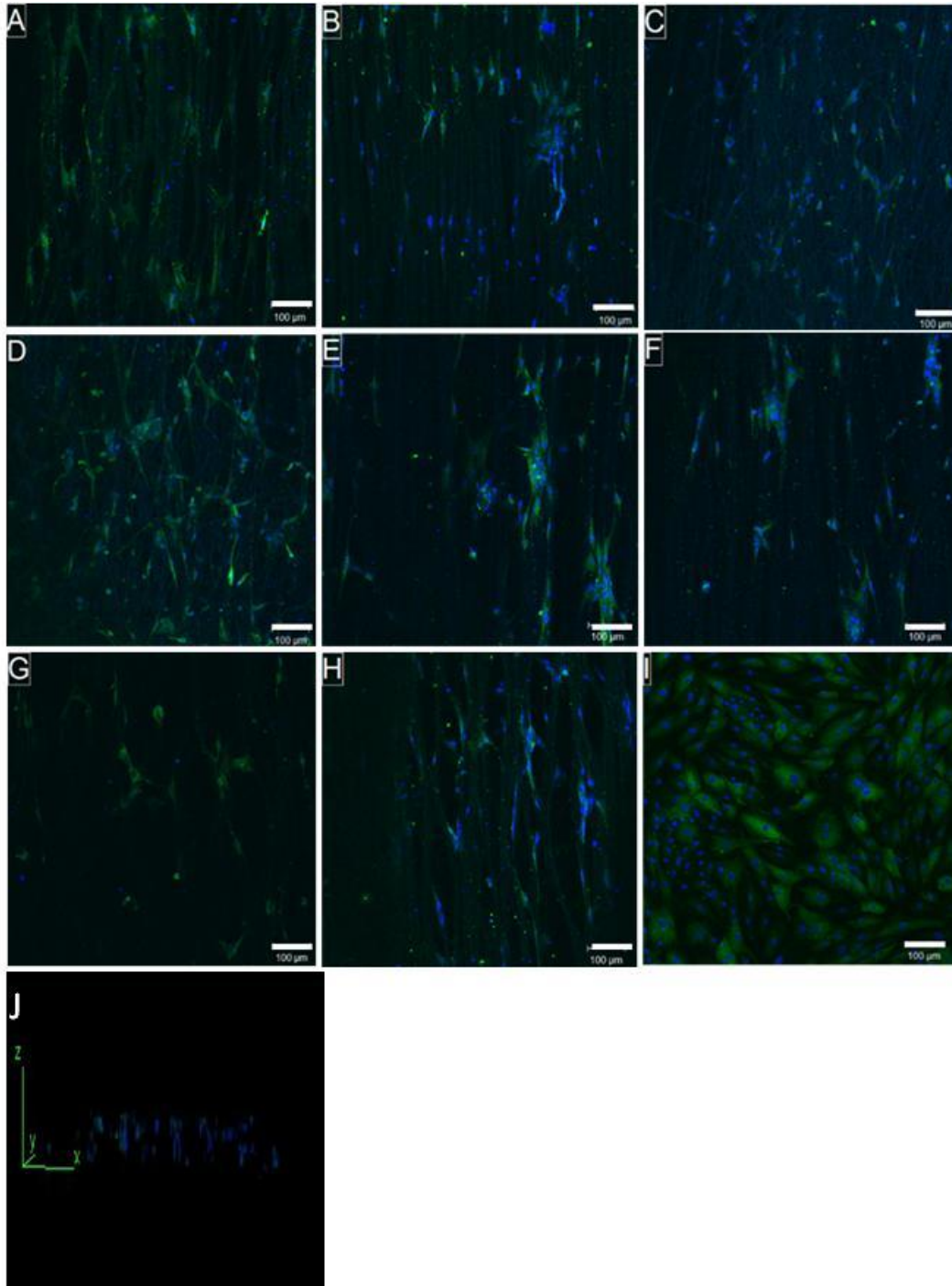
Figure 5.9. (A) P(3HO):P(3HB) (50:50) 5μm fibres, (B) P(3HO):P(3HB) (50:50) 8μm fibres, (C) P(3HO-co-3HD):PLLA (50:50) 5μm fibres, (D) P(3HO-co-3HD):PLLA (50:50) 8μm fibres, (E) PCL 5μm fibres, (F) PCL 8μm fibres and (G) PHBV 5μm fibres, (H) PHBV 8μm fibres, (I) Tissue culture plastic and J) 3D composite image of Schwann cells on fibres. Cell nuclei were labelled with DAPI (blue) and Schwann cell bodies labelled with S100 (green). Scale bar =100μm.

To confirm that Schwann cells had maintained their differentiation phenotype, the average Schwann cell length was calculated, as a Schwann cell morphology marker. Schwann cells were measured using the ruler tool on NIH software Image J and 100 Schwann cells were measured per condition (Schneider *et al.*, 2012). There were no significant differences detected between data sets. The highest average Schwann cell length was found on the PHBV 8μm fibres, followed by the P(3HO):P(3HB) (50:50) 5μm fibres and the tissue culture

plastic control, 82.60 ± 1.98µm, 80.49 ± 19.15µm and 80.42 ± 25.13µm respectively. Overall, it was observed that average Schwann cell length was lower on 8µm fibres, compared to 5µm fibres of the same material. However, average Schwann cell length was longer on PHBV 8µm fibres, compared to 5µm fibres. This indicates a positive relationship between fibre diameter and Schwann cell morphology and indicates a retained Schwann cell morphology.
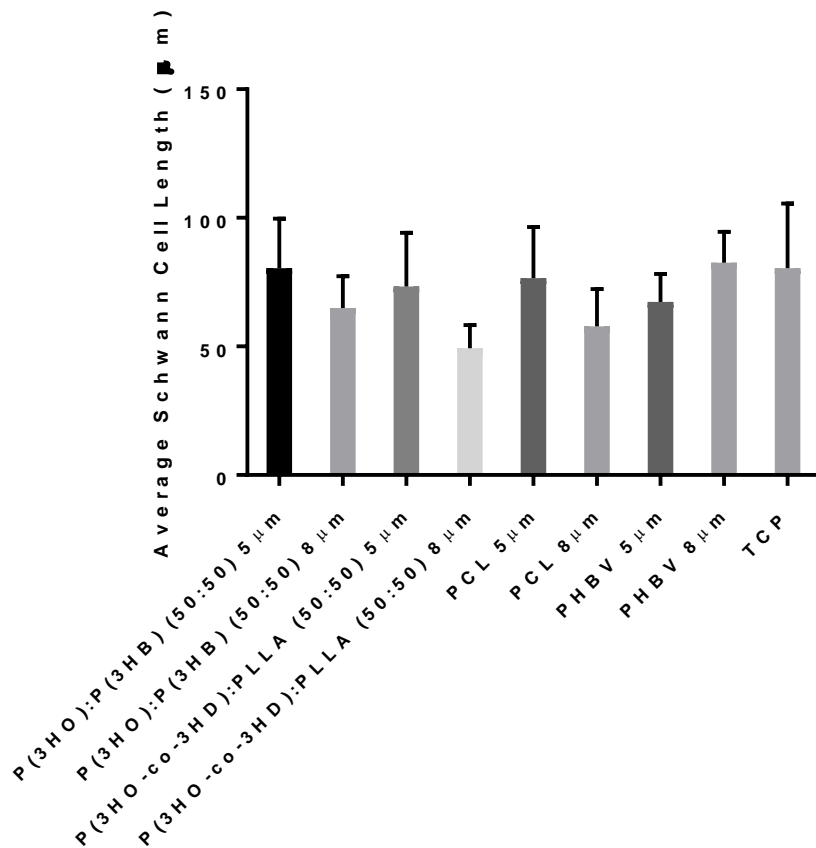
Figure 5.10. Average Schwann cell length for each material fibre size to determine maintained Schwann cell phenotype. A one way anova with Tukey's multiple comparisons tests was used to analyse data (Mean ± SD n=3 independent experiments). No statistical differences were detected between samples.

5.3.7 Rat primary Schwann cell viability on different material aligned fibres with different diameters

Figure 5.11 shows confocal micrographs of Schwann cells labelled with Syto-9 and propidium iodide to determine cell viability on the fibrous scaffolds. Schwann cells appear to align themselves to individual fibres but adhere in a more random orientation on the tissue culture plastic. The highest number of Schwann cells was seen on tissue culture plastic control. The highest number of attached cells was seen on 5µm fibres, compared to 8µm, suggesting a relationship between fibre diameter and Schwann cell attachment.
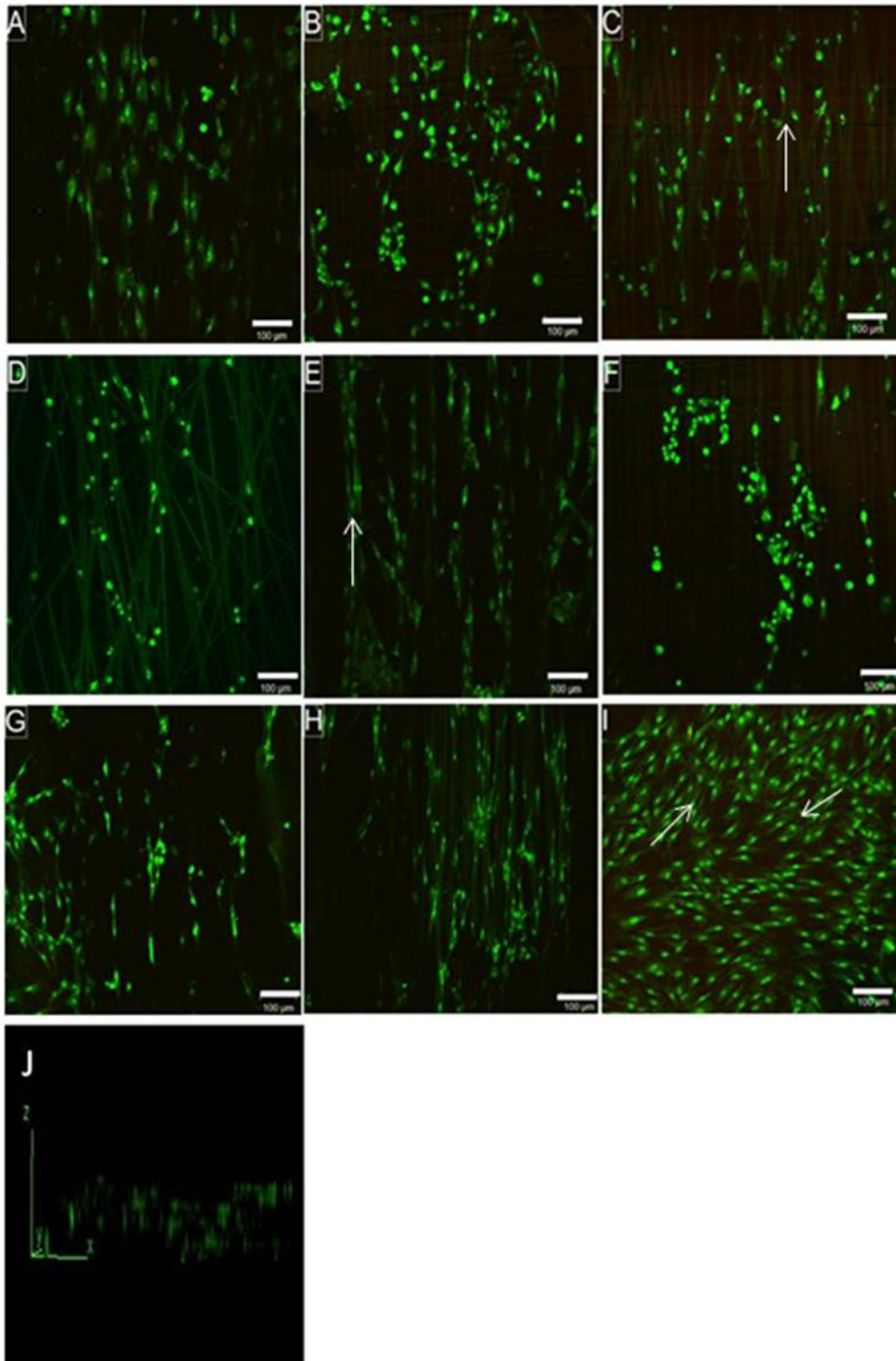
Figure 5.11. Live/dead confocal analysis of rat primary Schwann cells cultured on (A) P(3HO):P(3HB) (50:50) 5μm fibres, (B) P(3HO):P(3HB) (50:50) 8μm fibres, (C) P(3HO-co-3HD):PLLA (50:50) 5μm fibres, (D) P(3HO-co-3HD):PLLA (50:50) 8μm fibres, (E) PCL 5μm fibres, (F) PCL 8μm fibres and (G) PHBV 5μm fibres, (H) PHBV 8μm fibres, (I) Tissue culture plastic and J) 3D composite image of Schwann cells on fibres. Schwann cells were labelled with Syto-9 (green) and propidium iodide (red) for live and dead cells respectively. Scale bar = 100μm.

The highest number of live cells were found on the tissue culture plastic. With regards to the fibres, the highest number of live cells were found on 5μm PHBV fibres, followed by the 8μm

fibres, 136.30 ± 19.52 cells and 134.67 ± 17.68 cells respectfully. The number of live cells on the 5µm PCL fibres and 5µm P(3HO):P(3HB) (50:50) fibres were 133.33 ± 18.91 cells and 102.44 ± 20.16 cells respectfully (Figure 5.12B). Statistical differences were detected between data sets, in which all fibres, apart from 8µm PCL fibres and 5µm P(3HO-co-3HD):PLLA (50:50) fibres, had significantly higher numbers of live cells attached compared to 8µm P(3HO-co-3HD):PLLA (50:50) fibres. Live Schwann cell number was higher on the PHBV fibres, PCL fibres and P(3HO):P(3HB) (50:50) fibres compared to P(3HO-co-3HD):PLLA (50:50) fibres which could suggest that this blend does not support the proliferation of rat Primary Schwann cells as efficiently.

Figure 5.12B confirmed that cell viability of Schwann cells cultured on 5 and 8µm PHBV fibres, 8µm P(3HO):P(3HB) (50:50) fibres, 5µm PCL and P(3HO-co-3HD):PLLA (50:50) fibres was significantly higher than cell viability of Schwann cells cultured on 8µm PCL fibres, which was 85.05 ± 4.87%. Schwann cell viability was also low on P(3HO-co-3HD):PLLA (50:50) 8µm fibres which was 87.47 ±10.78%. All other materials and fibre diameters had a cell viability over 90% confirming all fibrous scaffolds supported Schwann cell adherence and proliferation.
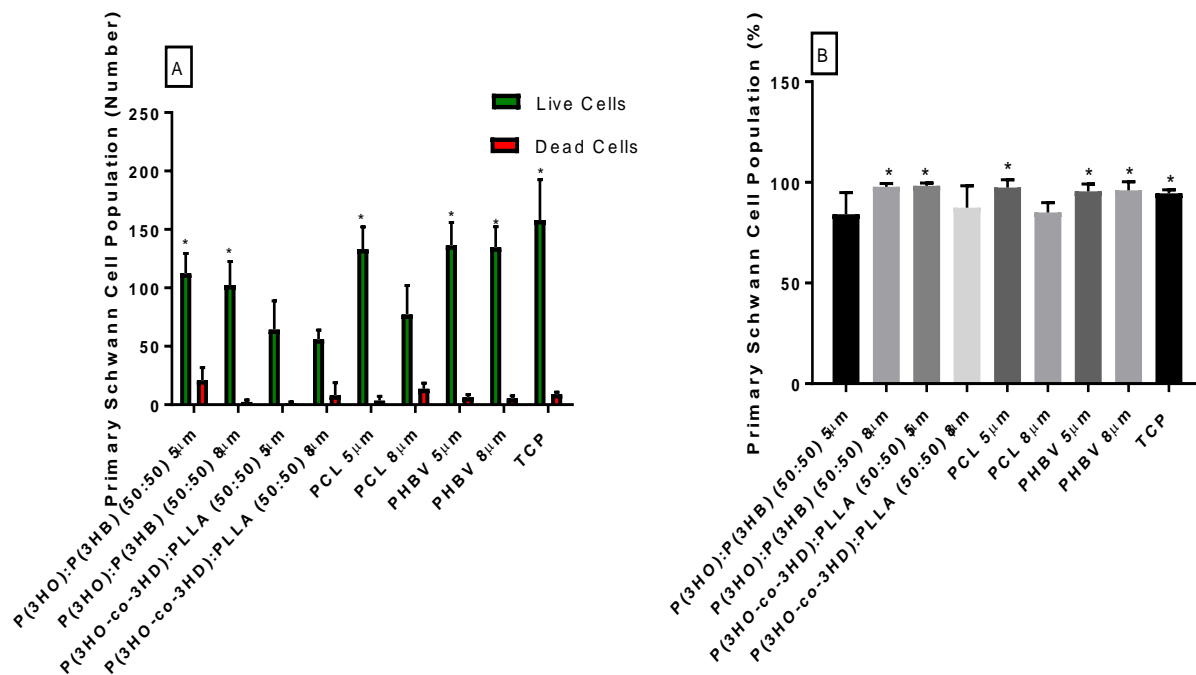
Figure 5.12. Live/dead analysis of rat primary Schwann cells on aligned fibres expressing the average total number of live versus dead cells. A one way anova with Tukey's multiple comparisons tests was used to analyse data (Mean ± SD, n= 3 independent experiments, *p<0.05 in comparison to 8µm P(3HO-co-3HD):PLLA (50:50) fibres). No significant differences were detected between data sets of polymer flat films. Cell viability was also expressed as a percentage (B) (Mean ± SD n=3 independent experiments, *p<0.05 in comparison to 8µm PCL fibres).

Overall PHBV supported Schwann cell proliferation, on both diameters (figure 5.12). Higher numbers of Schwann cells adhered to PCL than P(3HO):P(3HB) (50:50), but from Schwann

cell *in vitro* analysis, P(3HO-co-3HD):PLLA (50:50) did not undergo *ex vivo* and *in vivo* analysis as primary Schwann cells did not adhere to the blend. It could be concluded fibres, of 5µm diameter, do support Schwann cell proliferation, phenotype and elongation more efficiently than 8µm fibres.

5.3.8 Rat primary Schwann cell and NG108-15 neuronal cell co-culture differentiation on different material aligned fibres with different diameters

A co-culture of Schwann cells and neuronal cells was established to investigate the effect of fibre diameter and material type, on cells, as well as their interaction between one another. After culture, cells were labelled for βIII-tubulin (neurite outgrowth-red), DAPI (cell nucleus-blue) and S100β (Schwann cell marker-green). From the confocal micrographs in figure 5.13, longer neurites are expressed from NG108-15 neuronal cells, when co-cultured with rat primary Schwann cells, compared to single NG108-15 neuronal cell culture (figure 5.3). The longest neurites appear to be expressed by NG108-15 neuronal cells cultured on 5 and 8µm fibres, figure 5.13G and H, compared to the other materials.

Confocal micrographs were then quantified to determine the average neurite length expressed per condition in co-culture compared to mono-culture (figure 5.14). Overall, the addition of Schwann cells to NG108-15 neuronal cell culture increased average neurite length. This observation was significant with regards to PHBV fibres, in which the average length of neurites extending from neuronal cells cultured on 5µm PHBV fibres, significantly increased with the addition of primary Schwann cells. The smallest increase in average neurite length was seen on the P(3HO):P(3HB) (50:50) 8µm, in which the average neurite length increased from 88.72 ± 26.24µm to 97.17 ± 28.68µm.

Figure 5.13. Immunolabelled confocal micrographs of NG108-15 neuronal cells co-cultured with rat primary Schwann cells, on (A) P(3HO):P(3HB) (50:50) 5µm fibres, (B) P(3HO):P(3HB) (50:50) 8µm fibres, (C) P(3HO-co-3HD):PLLA (50:50) 5µm fibres, (D) P(3HO-co-3HD):PLLA (50:50) 8µm fibres, (C) PCL 5µm fibres, (F) PCL 8µm fibres and (G) PHBV 5µm fibres, H) PHBV 8µm fibres, I) Tissue culture plastic control and J) 3D composite image of neuronal and Schwann cells on fibres. Neuronal and Schwann cell nuclei were labelled with DAPI (blue) and neurite extensions labelled for β III tubulin (Cell marker-red) to conduct NG108-15 neuronal cell differentiation studies. Scale bar = 100µm.
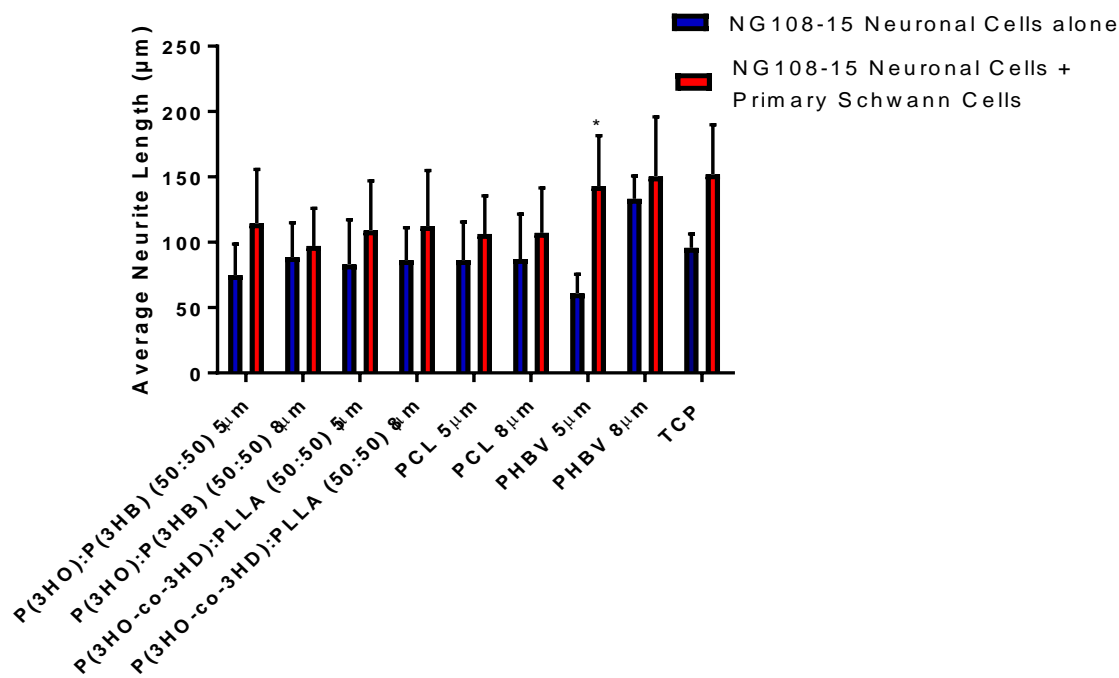
Figure 5.14. Analysis of NG108-15 neuronal cell neurite outgrowth studies comparing neurite lengths to culture with and without rat primary Schwann cells. The average neurite length measured per diameter and controls. 100 neurites per diameter/sample were measured, using Image J, to determine the average neurite length. A two way anova with Sidak's multiple comparisons tests was used to analyse data (Mean ± SD, n=3 independent experiments *p<0.05 compared to neuronal cell alone).

Previous studies have shown that the addition of rat primary Schwann cells, to the culture of NG108-15 neuronal cells, does increase the average neurite length of neurites expressed by NG108-15 neuronal cells (Daud *et al.*, 2012). The effect of Schwann cells on neuronal cell culture, was significant for the 5µm PHBV fibres. In mono-culture, the average length of neurites presented by neuronal cells cultured on 5µm was significantly lower. However, figure 5.12 showed that PHBV fibres supported the highest amount of Schwann cell attachment and higher numbers of live Schwann cells. Therefore, the addition of Schwann cells has influenced NG108-15 neuronal cell differentiation on this material and fibre diameter, confirming an interaction between the two cell types.

5.3.9 Cell viability of co-cultures of NG108-15 neuronal cell and rat primary Schwann cell viability on polymer films and aligned fibres

Cell viability of NG108-15 neuronal cells in co-culture with primary Schwann cells was assessed by labelling cells with Syto-9 (live cell stain) and propidium iodide (dead cell stain). The stain does not distinguish between cell type but due to Syto-9 staining the whole cell body and shape of cells was seen sufficiently to identify cell viability of different cell types. NG108-15 neuronal cells are more circular, whereas primary Schwann cells elongate into a

more spindle like morphology. Figure 5.15 shows confocal micrographs taken of both cell types cultured on different material blends with different fibre diameters. Very few dead cells can be seen on all fibre samples, indicating the material blends are not toxic to both cell types, as quantified in figures 5.12 and 5.8. Neuronal cells and Schwann cells align themselves to the fibres, where as they are more randomly orientated on the flat tissue culture plastic control.

All material blends support NG108-15 neuronal cell and primary Schwann cell attachment and proliferation. Higher numbers of attached cells appear to be on 5µm fibres of each material or material blend, compared to 8µm fibres. To determine the total number of live cells attached to the fibres, per field of view, micrographs were quantified.
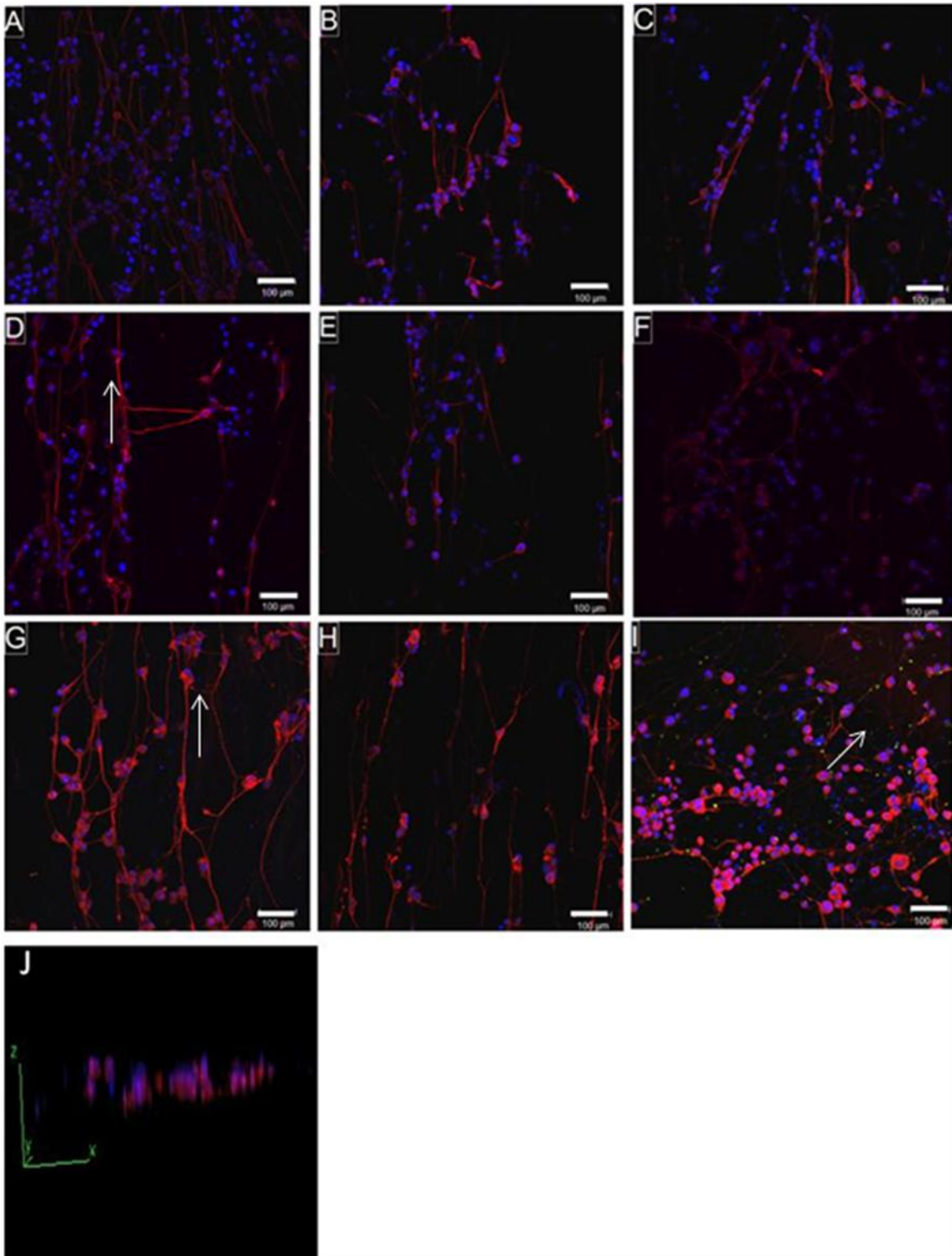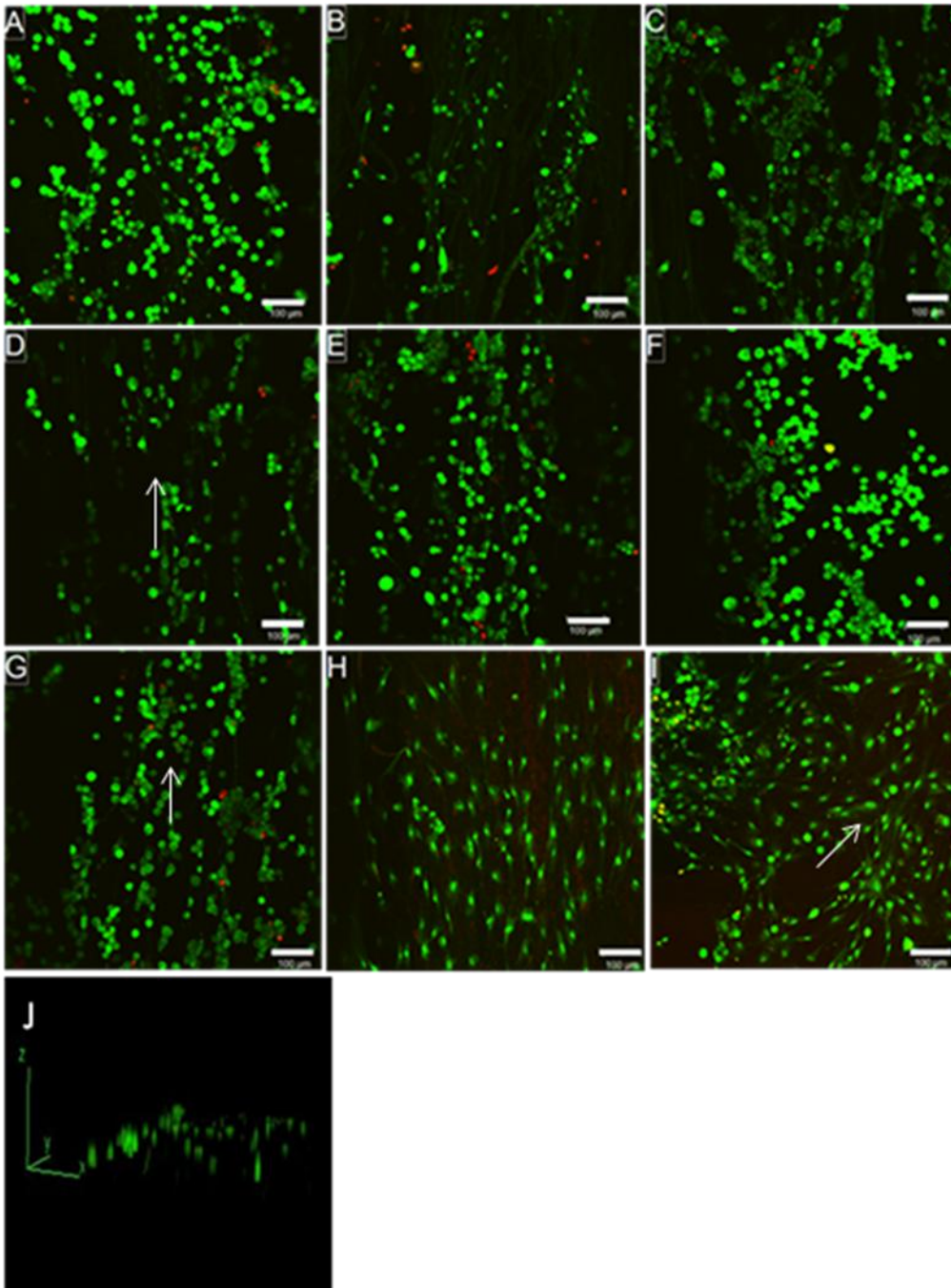
Figure 5.15. Live/dead confocal analysis of NG108-15 neuronal cells co-cultured with rat primary Schwann cells cultured on (A) P(3HO):P(3HB) (50:50) 5µm fibres, (B) P(3HO):P(3HB) (50:50) 8µm fibres, (C) P(3HO-co-3HD):PLLA (50:50) 5µm fibres, (D) P(3HO-co-3HD):PLLA (50:50) 8µm fibres, € PCL 5µm fibres, (F) PCL 8µm fibres and (G) PHBV 5µm fibres, H) PHBV 8µm fibres, I) Tissue culture plastic control and J) 3D composite image of neuronal and Schwann cells on fibres. Neuronal and Schwann cells were labelled with Syto-9 (green) and propidium iodide (red) for live and dead cells respectfully. Scale bar = 100µm.

The highest number of live cells were detected on tissue culture plastic 484.67 ± 34.10 cells, which was statistically larger than all the fibre samples. Overall, the highest number of live cells on the fibrous samples were on the P(3HO):P(3HB) (50:50) 8µm fibres, 269.55 ± 1.12 cells, followed by the 5µm PCL fibres, 260.33 ± 81.85 cells. The highest number of dead cells was found on the tissue culture plastic, followed by the 8µm PHBV fibres, 13.67 ± 4.18 cells and 11.22 ± 3.46 cells respectfully. As statistical differences were not detected between

fibre samples, it could not be concluded that one material type, or fibre diameter, was the most effective for supporting neuronal and Schwann cell attachment and proliferation. The number of live cells attached did decrease when cultured on 8µm compared to 5µm fibres, but this trend could not be seen for P(3HO):P(3HB) (50:50) fibres. Overall, P(3HO):P(3HB) (50:50) and PCL fibres supported higher cell proliferation compared to P(3HO-co-3HD):)PLLA (50:50) and PHBV.

With regards to cell viability, no significant differences were detected between data sets (figure 5.16B). The highest percentage of live cells, against dead cells, was found on NG108-15 neuronal cells cultured on 8µm PCL fibres, followed by 8µm P(3HO-co-3HD):PLLA (50:50) fibres, 98.58 ± 2.00% and 98.07 ± 1.90% respectfully. Cell viability for all material blends and fibres was above 95% indicating that all materials were biocompatible and supported the attachment and proliferation of NG1080-15 neuronal cells and rat primary Schwann cells. The cell viability of cells cultured on the 5µm P(3HO):P(3HB) fibres and the 8µm P(3HO-co-3HD):PLLA and PCL fibres, increased in co-culture, compared to the mono-culture of primary Schwann cells (figure 13B). This confirms that the relationship between primary Schwann cells and neuronal cells is beneficial to both cell types.
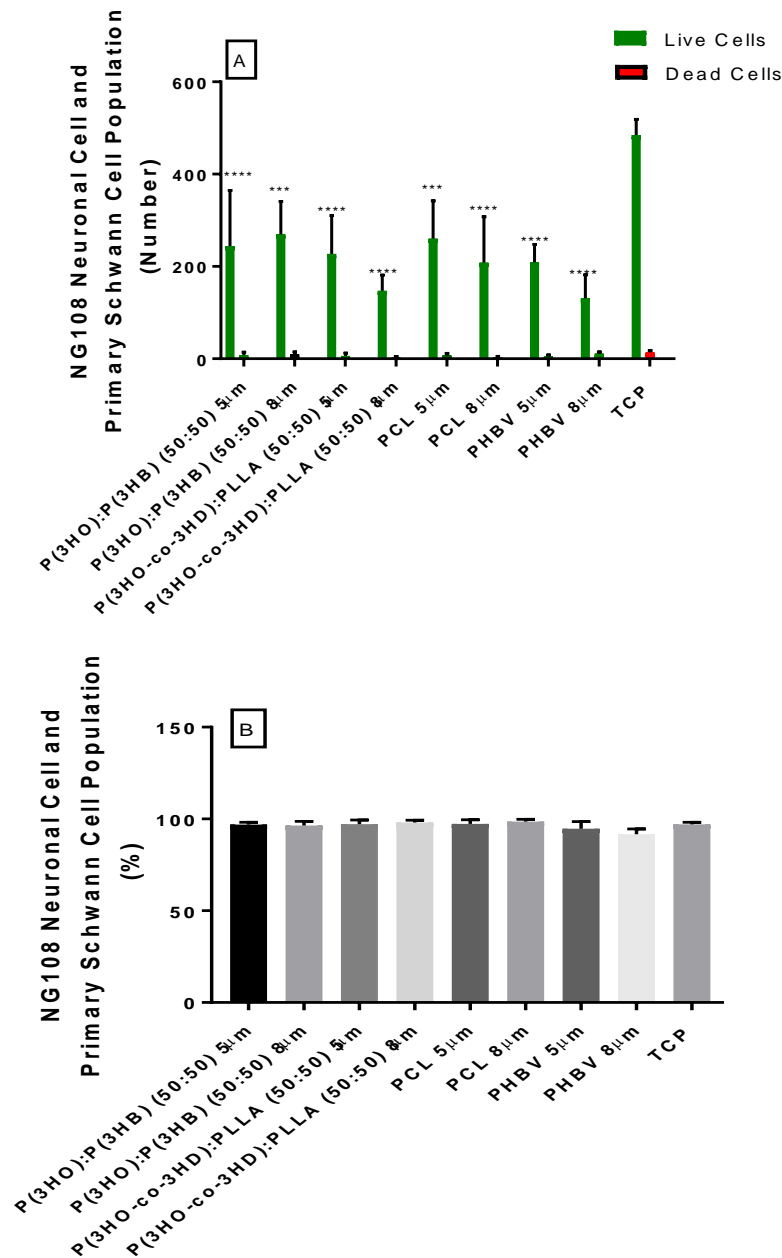
Figure 5.16. (A) Live/dead analysis of NG108-15 neuronal cells and rat primary Schwann cells on material fibres expressing the average total number of live cells versus dead cells. A one way anova with Tukey's multiple comparisons tests was used to analyse data (Mean ± SD n=3 independent experiments, experiments ***p<0.001, ****p<0.0001 compared to TCP). Cell viability was also expressed as a percentage (B). (Mean ± SD n=3 independent experiments). There were no significant differences detected through any of the data analysis.

5.4 Discussion

In this chapter, it was hypothesised that material composition would had an effect on neuronal and Schwann cell attachment and differentiation, favouring the PHA blends.

NG108-15 neuronal cell neurite outgrowth was significantly higher when cells were cultured on the 8μm PHBV fibres, compared to the other polymer blends and fibre diameters. NG108-15 neuronal cell adherence and proliferation was significantly lower when cells were seeded onto PCL 5 and 8μm fibres, compared to the other polymers and fibre diameters. However, a

156

significantly lower amount of viable Schwann cells adhered to both the 5 and 8μm P(3HO-co-3HD):PLLA (50:50) fibres, compared to the other blends. The addition of primary Schwann cells, to NG108-15 neuronal cell culture, significantly increased neurite length of neuronal cells adhered to PHBV 5μm fibres.

Fibre density and surface coverage of the fibres played a crucial role in this study. For all the material blends, bar P(3HO-co-3HD):PLLA (50:50), the 8μm fibres had the largest fibre densities, which could account for the increased cellular adhesion in some experiments. This was certainly the case in figure 5.8, in which there were higher numbers of live attached cells to the 8μm fibres of P(3HO):P(3HB) (50:50), P(3HO-co-3HD):PLLA (50:50) and PHBV, but was not the case for the 8μm PCL fibres. However, an increased fibre density did not appear to increase primary Schwann cell attachment in figure 5.12, or when neuronal and Schwann cells were co-cultured together (figure 5.16).

Overall, all the polymer blends supported the proliferation and maturation of NG108-15 neuronal cells and rat primary Schwann cells, in single culture and co-culture. Due to the lack of success electrospinning P(3HO-co-3HD):PLLA (95:5), the amount of PLLA was increased, P(3HO-co-3HD):PLLA (50:50) could be electrospun into fibres. Water contact angle was determined for the new P(3HO-co-3HD) blend and compared with the P(3HO):P(3HB) (50:50) film, PCL and PHBV films. Overall, data concluded that both the P(3HO):P(3HB) and P(3HO-co-3HD):PLLA (50:50) blends were hydrophobic due to the presence of long aliphatic chains in the P(3HO) (Lorena R. Lizarraga-Valderrama *et al.*, 2015).

Figure 5.1 also suggests that the P(3HO-co-3HD) and P(3HO), in their respective blends, are at the surface of the polymer film, by the increase in contact angle in blend form compared to individual polymers. Multiphase systems are formed when polymers are blended together due to the immiscibility of the polymers used and differences in molecular weight (Martinova and Lubasova, 2012). P(3HO) has a higher molecular weight of 677 kDa compared to P(3HB) at 452 kDa, and P(3HO-co-3HD) has a higher molecular weight, of 350kDa compared to PLLA. As previously discussed, molecular weight of the polymer is a crucial parameter when electrospinning, effecting surface tension, conductivity and solution viscosity (Bhardwaj and Kundu, 2010). Therefore, when these blends are electrospun, it is likely that the higher molecular weight polymer of the blend is sitting at the surface of the fibre. Future work would be to analyse the water contact angle of the fibres and XPS analysis to determine which of the PHAs in the P(3HO):P(3HB) (50:50) blend sits at the top of the fibre.

Polyhydroxyalkanoates degrade very slowly via hydrolytic degradation but it has been previously reported that PHA blends and co-polymers, containing higher amounts of P(3HB), degrade quicker by hydrolytic degradation, due to the hydrophilic nature of P(3HB). The

monomer of P(3HB) contains four carbon atoms, compared to the eight carbon atoms in the monomer of P(3HO), which accounts for its hydrophilic properties (Basnett *et al.*, 2013). The increased hydrophobicity of the P(3HO):P(3HB) (50:50) blend was observed in figure 2.2. In contrast, the rate of weight loss in the P(3HO-co-3HD):PLLA (50:50) blend was much higher, compared to the P(3HO):P(3HB) (50:50) blend. Although the high amount of P(3HO-co-3HD) accounted for the hydrophobic nature, as seen in figure 2.2, the rate of weight loss was increased to the addition of the polyester PLLA. The addition of PLLA to polymer blends has been reported to increase degradation rate due to random cleavage of the ester bond (Elsawy *et al.*, 2017). Renard *et al.* (2004), reported that the addition of PLLA to P(3HO) did not significantly increase degradation rate, compared to blending it with P(3HB) and PHBV. Therefore, the addition of the P(3HO-co-3HD) to PLLA must have a different effect on hydrolytic degradation. The hydrophobic nature of the P(3HO):P(3HB) and P(3HO-co-3HD):PLLA (50:50) blends, and slow degradation rate, also had an effect on the pH of PBS containing degradation properties, and slowed down the release of acidic by products from the PLLA (Elsawy *et al.*, 2017). PHBV had a higher rate of weight loss, over 24 weeks incubation, due to the hydrophilic nature of the hydroxybutyrate monomer in its structure (Suwantong *et al.*, 2007). PHBV degrades via random chain scission during hydrolytic degradation, producing carboxylic acid end group degradation products, which accounted for the decrease in pH over the time period (Haiyan Li and Chang, 2005). Data reported for the degradation rate of PCL, and the acidic nature of its degradation products, was similar to that reported in literature (E Díaz *et al.*, 2014). Overall, the PHA blends would be suitable for use as an internal fibrous scaffold guide for a nerve guide conduit, treating a long gap injury, due to their slower degradation rates, and therefore, the slower release of acidic degradation products.

Both PHA blends, and PCL fibres had a significantly higher percentage of neurite bearing cells compared to the tissue culture plastic control, but no significant differences were detected between fibres. This was also the same for the average number of neurites expressed per neuron. However, in NG108-15 neuronal cell culture, alone, the longest average neurite lengths were found on NG108-15 neuronal cells cultured on 8µm PHBV fibres, which was significantly higher than all the other material blends and fibre diameters. Although neurite length was higher on the 8µm compared to the 5µm fibres, the only significant difference was between the 5 and 8µm PHBV fibres. This would indicate that PHBV, and 8µm fibres are the more efficient in promoting NG108-15 neuronal cell differentiation and neurite outgrowth. When observing NG108-15 neuronal cell viability on the fibrous scaffolds, both PHA blends and PHBV fibres had a significantly higher number of attached live cells, compared to the PCL fibre, which indicates that PHAs increase cell

adhesion and proliferation compared to PCL, regardless of fibre diameter. It is difficult to compare these results to other published studies, as there is little research on comparison of materials when in fibrous form, using NG108-15 neuronal cells. However, Lizarraga *et al.* (2015) did compare PHA solvent casted films with PCL films. P(3HB), P(3HB):P(3HO) 50:50 and 75:25 solvent casted films did promote increased NG108-15 neuronal cell attachment, proliferation, and differentiation, compared to PCL films (Lorena R. Lizarraga-Valderrama *et al.*, 2015).

In comparison to the neuronal cell data, rat primary Schwann cell proliferation was favourable on the PCL fibres, PHBV fibres and P(3HO):P(3HB) (50:50) fibres, but numbers of attached live cells were significantly lower on the P(3HO-co-3HD):PLLA fibres. No significant differences were detected when determining the average Schwann cell length, which would indicate that the Schwann cell phenotype was maintained on all fibre blends. Suwantong *et al.* (2007) showed good Schwann cell line RT4-D6P2T cell viability between P(3HB) fibres and PHBV fibres, compared to their flat film counterparts (Suwantong *et al.*, 2007). The study used the same Schwann cell line to assess cell viability on PCL, PHBV, PLLA and P(3HB) films and fibrous scaffolds, to determine the effect of the material. After 5 days of culture, cell viability was highest on the PHBV films, followed by PCL, PLLA and P(3HB) (Sangsanoh *et al.*, 2007). This study would indicate that PLLA is not toxic to Schwann cell lines, and other studies have published data indicating PLLA does support primary Schwann cell proliferation and migration (H. B. Wang *et al.*, 2009). Therefore, the decrease in Schwann cell attachment on the P(3HO-co-3HD):PLLA (50:50) fibres must be down to the P(3HO-co-3HD) component, in which little data on P(3HO-co-3HD) has been published for nerve tissue engineering. The hydrophobic nature of P(3H0-co-3HD) is the most likely reason for this observation as seen figure 2.1.

A co-culture of NG108-15 neuronal cells and primary Schwann cells was established, to determine the effect of the addition of Schwann cells to NG108-15 neuronal cell neurite outgrowth on the fibres, as performed and discussed in chapter 4. However, in this chapter, it was important to determine if the material/blend would have an effect on both cell types in co-culture, either inhibiting or promoting the excretion of neurotrophic growth factors and ECM proteins from Schwann cells (Armstrong *et al.*, 2007). Overall, the addition of primary Schwann cells did increase the average length of neurites expressed per neuronal cell, but this result was only significant on the 5μm PHBV fibres. NG108-15 neuronal cell neurite length was highest on the 5 and 8μm PHBV fibres, compared to the other materials/blends, which were all quite similar. This result indicates that PHBV was more efficient in supporting both cell type attachment and differentiation. When observing the number of live NG108-15

neuronal cells and Schwann cells on the fibres, cell numbers were less on the 8µm fibres compared to their 5µm counterparts, although this was not significant. The lowest numbers of live cells attached to fibres were detected on the 8µm PHBV and P(3HO-co-3HD):PLLA (50:50) fibres. However, all fibre scaffolds had a cell viability of above 95% indicating that all fibre materials promoted NG108-15 neuronal cell and primary Schwann cell proliferation and attachment. Difficulty is had in comparing the results of neuronal and Schwann cell growth from this chapter to published research, due to novelty of the two PHA blends. Material type, and fibre diameter, on DRG neurite outgrowth and Schwann cell migration, will be determined in chapter 6 to conclude if one material blend, or fibre diameter, promotes longer Schwann cell migration and neurite outgrowth.

In conclusion it was found that blending specific materials with one another does has a significant effect on NG108-15 neuronal cell and primary Schwann cell proliferation and differentiation, regardless of fibre diameter. The most effective material for supporting NG108-15 neuronal cell differentiation by *in vitro* analysis were PHBV fibres. However, P(3HO):P(3HB) (50:50) would also be a material of choice of for fabricating fibres for use with a nerve guide conduit, as both materials / blends promoted Schwann cell attachment, proliferation and native cell phenotype. It was also found that polyhydroxyalkanoates supported an increase in NG108-15 neuronal cell differentiation compared to PCL. However, Schwann cells did not adhere to P(3HO-co-3HD) compared to the other materials. Therefore, this material would not be effective for use as an intraluminal fibrous scaffold with a nerve guide conduit. Very little cell death was detected on all fibrous scaffolds.

Future investigational work for this chapter would involve looking at neuronal and Schwann cell differentiation on the fibres. This would include using PCR to look at genetic changes, and staining for proteins expressed by the cells when forming focal adhesions, such as fibronectin and vitronectin (Curran *et al.*, 2005).

PCL, PHBV and P(3HO):P(3HB) (50:50) 5 and 8µm fibres will be analysed in chapter 6 using an *ex vivo* DRG model. Previous work investigating the effect of aligned fibre diameters on neuronal and Schwann cells has focused on explanting whole DRGs onto fibres to replicate a nerve injury model (H. B. Wang *et al.*, 2010). An *ex vivo* DRG testing model was developed in the Haycock group and recently published by Behbehani *et al.* Here, fibres were threaded in to polyethylene glycol tubes fabricated by microstereolithography. Rat DRGs were explanted and placed onto conduits. After culture, scaffold were assessed for DRG neurite outgrowth and Schwann cell migration (Behbehani *et al.*, 2018). The DRG ex vivo model is an advantageous model when considering the 3Rs (Replacement, Refinement and Reduction), in which the model reduces the amount of

animal experimentation for *in vivo* investigations (Tannenbaum and Bennett, 2015). By removing the dorsal root ganglion body, and trimming the nerve roots, this replicates a 3D peripheral nerve injury model and 25-35 conduits containing fibres can be investigated in one experimental run (Daud *et al.*, 2012). This model will determine the most efficient material blend, and fibre diameter, for enhancing DRG neurite outgrowth and Schwann cell migration, in which the best will be taken forward to in vivo testing.

Chapter 6: *Ex Vivo* Analysis of Fibre Blends Using Organotypic DRG Explant Culture

6.1 Introduction

Chapter 5 concluded that 5 and 8µm fibres manufactured from PHBV, PCL or P(3HO):P(3HB) (50:50) had the most potential for use as an intraluminal fibrous guidance scaffold in a nerve guide conduit. P(3HO-co-3HD):PLLA (50:50) was not taken forward for *ex vivo* analysis due to its poor primary Schwann cell viability, loss of alignment during *in vitro* cell culture, as well as difficulties threading the fibre mats into NGCS, and fibres losing alignment. PHBV maintained good neuronal and Schwann cell viability, as well as promoting NG108-15 neuronal cell differentiation and higher average neurite lengths than PCL and P(3HO):P(3HB) (50:50). This result was also seen by Sangsanoh *et al.* (2007) in which PHBV had a higher RT4-D6P2T Schwann cell viability after 5 days of culture compared to P(3HB) and PCL (Sangsanoh *et al.*, 2007). Although primary Schwann cell culture on fibres can indicate whether a material supports cell growth and maintains cell phenotype, it does not indicate how the Schwann cells will behave on the material *in vivo*. This is also true of using the NG108-15 neuronal cell line. Although NG108-15 neuronal cells are well characterised and used extensively in *in vitro* research, they are a proliferative hybrid cancer cell line, and do not mimic the regeneration rate of a regenerating axon *in vivo* (Armstrong *et al.*, 2007; Schaub *et al.*, 2016). Even as a co-culture, the behaviour of neuronal cell lines and primary Schwann cells are not comparable to *in vivo* nerve injury models, and only give researchers a small indication of the *in vivo* environment (Ziats *et al.*, 1988).

Therefore, a primary nerve injury model such as an *ex vivo* organotypic DRG explant model, could benefit research into improving nerve repair devices, by more closely mimicking a regenerating nerve. Dorsal root ganglia are a collection of sensory neurons which are located on each side of the spinal cord, in the dorsal intervertebral foramen (Sleigh *et al.*, 2016). Neuronal cell bodies, of the sensory aspect of the peripheral nervous system, are located in the ganglia, and axon extensions from the neuronal cell body innervate sensory receptors such as those in skin and muscles (Romero-Ortega, 2013). Dorsal root ganglia can be used *in vitro* as a primary cell peripheral nerve injury model for assessing different materials, conduit designs, and additional factors that could be used to improve the rate and efficiency of regenerating nerves after injury (Schaub *et al.*, 2015). They contain a mixture of neuronal cells, glial cells, supporting connective tissue, and single primary neurons can be

cultured *in vitro* by dissociation (Rodríguez *et al.*, 2004). However, when dissociating dorsal root ganglia connections between neuronal and glial cells, as well as the supporting connective tissues are lost (Rodríguez *et al.*, 2004). By cutting the nerve roots away from the DRG body, after removal of explants from the dorsal intervertebral foramen, ganglia regenerate and repair *in vitro* (Pateman *et al.*, 2015). Neurite outgrowth extensions and Schwann cell migration lengths can be measured to assess if certain conditions can improve the rate and distance of regeneration, whilst keeping the connections in place between the neuronal, glial cells and supporting tissue (Rodríguez *et al.*, 2004; Pateman *et al.*, 2015). As a primary sensory neuron, the rate of neurite outgrowth and regeneration is comparable to that of an *in vivo* model (Daud *et al.*, 2012). Using organotypic DRG explant culture as a peripheral nerve injury model also addresses the 3Rs principles, as one rat spinal column contains 30-35 DRG explants. This model is used as a high through put method to screen materials for use in peripheral nerve repair, greatly reducing the amount of animals used if the testing conduits *in vivo* (Tannenbaum and Bennett, 2015).

Kim *et al.* (2008) report on the culture of rat DRGs on aligned and random poly(acrylonitrile-co-methylacrylate) films, which saw that neurite out growth and Schwann cell length was significantly higher on the aligned fibres compared to the randomly orientated fibres (Kim *et al.*, 2008). When both random and aligned scaffolds were implanted in vivo, aligned fibres promoted axon regeneration over a 17mm gap, in rat sciatic nerve, whereas random fibres did not (Kim *et al.*, 2008). Therefore, the DRG injury model gives a better indication of what is happening *in vivo*, compared to using an immortal neuronal cell line and analysis of compounds/ growth factors/ materials for use in peripheral nerve repair should be assessed using a DRG culture model before using in animal research. As well as use in nerve injury models for tissue engineering, DRGs can also be used as a model to understand the pathophysiological changes, and the mechanisms involved, that lead to neuropathic pain after injury and inflammation (Repić *et al.*, 2016).

Electrospun fibres with varying diameters and alignment have been investigated using DRGs as an *in vitro* peripheral nerve injury model. Corey *et al.* (2007) reported that rat DRG neurite outgrowth was 20% longer on aligned PLLA nanofibres, and Schwann cell migration was also further, compared to randomly orientated fibres PLLA fibres (Corey *et al.*, 2007). With regards to fibre diameters, neurite outgrowth and Schwann cell migration, from chick DRGS, cultured on 1.3μm PLLA aligned fibres, was significantly higher than 0.7 and 0.2μm fibres, as well as more guided (H. B. Wang *et al.*, 2010). Wen *et al.* (2006) reported that rat DRG neurite outgrowth, and Schwann cell migration, was significantly higher on 5 and 30μm fibres, compared to 100, 200 and 500μm polypropylene fibre filaments which suggested that optimum fibre diameters for DRG culture were between 0.7μm and 30μm, fibres in the

micrometer range, not nanometer range (Wen and Tresco, 2006). However, both Yao *et al.* (2009) and Daud *et al.* (2012) concluded that DRG neurite outgrowth, and Schwann cell migration, was highest on 0.8 and 1µm fibres, compared to 3.7, 5, 5.9, 8 and 8.8µm aligned PCL fibres, although this result was not significant (L. Yao *et al.*, 2009; Daud *et al.*, 2012). These results suggest that there is not an optimum diameter, from 0.8-8.8µm, that is more efficient in promoting DRG neurite outgrowth and Schwann cell migration. However, as both studies used PCL as a material of choice for fibre fabrication, there is no published data suggesting that one material, or material blend, is more efficient in promoting DRG neurite outgrowth and Schwann cell migration that the other.

Following on from *in vitro* analysis, this chapter investigated the effects of rat DRG neurite outgrowth and Schwann cell migration lengths, when cultured on aligned 5 and 8µm PHBV, P(3HO):P(3HB) (50:50) and PCL fibres. However, unlike previous studies, ex vivo DRG culture was performed differently. In previously reported studies dorsal root ganglia were dissected from spinal columns, trimmed and explanted onto fibres which were held down in cell culture well plates (Daud *et al.*, 2012). Therefore, an *ex vivo* DRG fibre testing model was developed by Behbehani *et al* (2018), in which fibres were threaded into a nerve guide conduit, replicating a structured NGC device which would be implanted *in vivo*. The DRG explant was placed on top of the fibres in the tube, in which DRG neurite outgrowth mimics the regenerating nerve after injury. Both the conduit material, and fibre material/diameter, can be assessed using this method before more detailed *in vivo* investigation (Behbehani *et al.*, 2018). It is hypothesised that the P(3HO):P(3HB) (50:50) blend will support further DRG neurite outgrowth and Schwann cell migration lengths due to results confirmed in chapter 5.

The *ex vivo* DRG model is a combination of methodologies used in the publications by Pateman *et al.* and Daud *et al*. Pateman *et al*. fabricated hollow NGC tubes from polyethylene glycol (PEG) NGC tubes using microstereolithography, an additive manufacturing technique with a laser to polymerize a liquid polymer into a 3D solid structure with specific detail (Pateman *et al.*, 2015). Microstereolithography was used to 3D print PEG tubes with specific diameters, and wall thickness required for *in vivo* analysis. There has been a great increase in the use of 3D printing, of biomaterials, for applications in tissue engineering. 3D printing can be used to fabricate custom made medical devices for patients, in which the macro, micro and nanoarchitecture can be controlled and designed for a specific application (Chia and Wu, 2015). 3D printing has been used in nerve tissue engineering, to print moulds to manufacture NGCs with channels, hollow, and a bifurcating structures in the paper by Hu *et al.* (2016) using cryo Gelatin methacryloyl (GelMA) (Yu Hu *et al.*, 2016). CryoGelMA tubes and structures were shown to degradable, as well as

biocompatible to adipose derived stem cells (ASCs). When cryoGelMA tubes were implanted, tubes seeded with ASCs increased the diameter of regenerating nerve fibres similar to the autograft, compared to nerve fibres diameter of fibres in the hollow cryoGelMA tubes alone (Yu Hu *et al.*, 2016). Johnson *et al.* (2015) were also able to 3D print methacrylated gelatine hydrogel and silicone bifurcating pathways by 3D structured light scanning, in order to fabricate tailored and custom made nerve guide devices, with personalised anatomical geometries and topographical guidance cues (B. N. Johnson *et al.*, 2015). Recent advances in 3D printing, have seen the incorporation of pores into tissue engineering scaffolds, without the use of a porogen (D. W. Johnson *et al.*, 2013). Owen *et al.* (2016) have incorporated pores into emulsion templated scaffolds for use in bone tissue engineering, and as seen in the publication by Johnson *et al* (2013) pores have been incorporated into tube structures for nerve tissue engineering (D. W. Johnson *et al.*, 2013; Owen *et al.*, 2016).

Using the method described in Pateman *et al.* (2015), hollow PEG tubes were manufactured and PHBV, P(3HO):P(3HB) (50:50) fibres, of 5 and 8µm, were threaded into the tubes (Pateman *et al.*, 2015). Using the 3D ex vivo DRG model, their potential for use as an internal guidance scaffold within a nerve guide tube was assessed. PCL fibres, of 5 and 8µm, were also assessed using DRG culture in this chapter as a control material, which has previously been assessed by (Daud *et al.*, 2012). The work in this chapter was part of the Neurimp project and was a collaboration in which parts of the work were performed by Dr Adam Glen (microCT imaging at The University of Sheffield) and by Miss Mehrie Behbehani (some of the DRG confocal images and data analysis, PhD student at The University of Sheffield). The results from this chapter informed the blend of materials and diameters to be used for *in vivo* experiments, which are ongoing (NEURIMP). The results of the *ex vivo* model are below.

6.2 Methods

6.2.1 Fabrication of electrospun fibres

5 and 8µm PCL, PHBV and P(3HO):P(3HB) (50:50) fibres were fabricated by electrospinning using the same conditions in the *methods* section, 1.1, in chapter 5. Fibres were analysed by scanning electron microscopy to confirm alignment and the correct fibre diameter. Fibres were removed from the foil collector and threaded into hollow tubes for *ex vivo* analysis.

6.2.2 Determining density of fibres

Before threading fibres in conduits, the density and thickness of the fibre mats was determined for each fibre diameter, to ensure the correct filling of the conduits. Both 5 and 8μm fibres, of PCL, PHBV and P(3HO):P(3HB) (50:50), were electrospun for 5, 10, 15 and 20 minutes and the matts peeled off foils. The timed electrospun mats were threaded into 5mm PEG conduits using a Hamilton 80300 Standard Microliter Syringes, 10 uL, Cemented-Needle, 1/ea, with a needle gauge of 26S. The fibres were laser cut into the correct length and tightly wrapped around the Hamilton syringe with the fibres parallel to the needle and placed into the conduit. 5mm PEG tubes containing the fibres were then imaged using MicroCT, to determine the correct electrospinning time, as well as confirm fibre alignment was maintained throughout the tube using the threading technique.

6.2.3 Mechanical testing of fibres for threading

Dry electrospun fibre samples were cut into 10mm x 8mm square samples for testing. Fibres were positioned vertically and were clamped to a tensiometer (BOSE Electroforce test instruments, Minnesota, USA) using a 405N load cell. The thickness of the fibre samples was recorded before testing to calculate the area. An extension rate of 0.2mm/s was used and a maximum extension of 8 mm. The ultimate tensile strength (UTS) and Young's modulus (YM) was calculated for each material and each fibre diameter (Owen *et al.*, 2016).

6.2.4 Fabrication of hollow tube conduits

Hollow PEG tubes were fabricated by the methods in Behbehani *et al.* (2018) and Pateman *et al.* (2015). Hollow tube 3D conduits were fabricated using Polyethylene glycol diacrylate (PEG) (Mn = 575, Sigma, Poole, U.K.) by microstereolithography. Polyethylene glycol diacrylate liquid pre-polymer was mixed with 4wt% diphenyl-(2,4,6-trimethylbenzoyl)-phosphineoxide/2-hydroxy-2-methylpropiophenone 50/50 photoinitiator (Sigma) and stored in a light blocking glass vial. To fabricate tubes, a cross sectional image of a tube was fabricated using Paint Software and uploaded to a Digital Micromirror Device (DMD) (Texas Instruments Incorporated, USA) using ALP-3 Basic version 1.0.03 (ViALUX, GmbH). The image was created to fabricate a tube with a 1.2 mm internal diameter, and a 250 μm wall thickness, (dimensions provided by an external collaborator on the Neurimp project, which allows for nerve swelling). A 405nm laser (Vortran Laser Technology Inc, USA), at 100mW power, was then projected onto the DMD image, and reflected off using a variety of mirrors and spatial filters onto the liquid pre-polymer, which was contained in a wide glass container

on a motorized z-axis translation stage (Thorlabs Ltd, UK, associated software: APT software) (Pateman *et al.*, 2015).
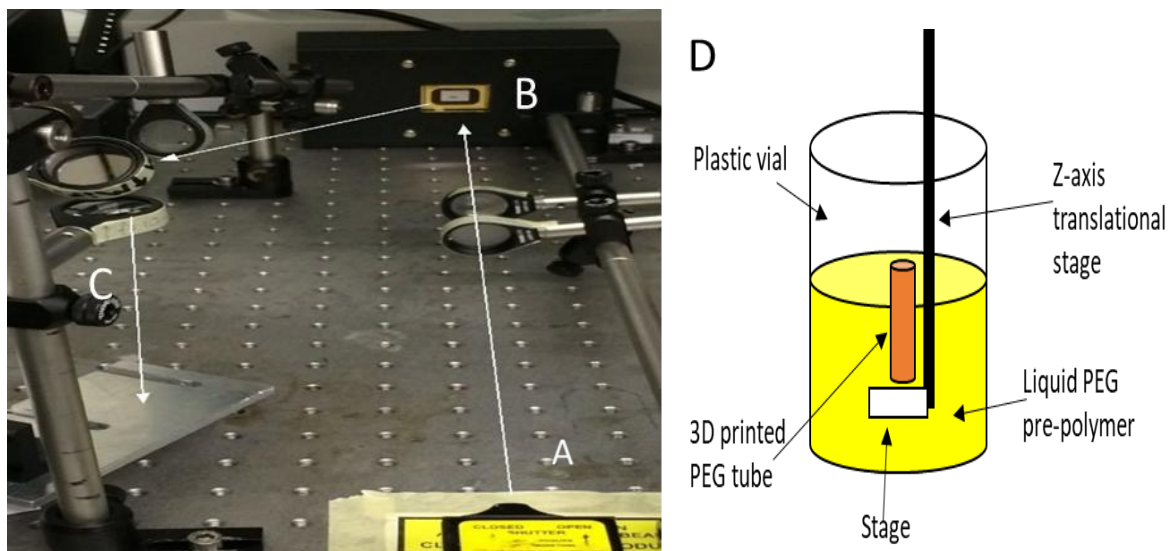
Figure 6.1. Image to show the microstereolithography set up. A) A 405nm laser is lined up to focus laser light onto B) the Digital Micromirror Device (DMD). A 2D cross sectional area image of the shape of the structure to be printed is created in paint computer software and is uploaded to the DMD. The laser is then reflected onto a z-axis translational stage, C), to create a 3D structure, the white arrows represent the pathway of the laser. D) An image to show the vial of liquid polymer. The laser DMD image is focused onto the stage at the top of the liquid polymer. The z-axis motorised stage lowers and layer by layer a tube is printed.

An L shaped copper piece was fabricated, to be used as a holder stage, and connected to the z-axis translation stage. To produce conduits, the laser power was turned on at a power of 100mW. The Z stage was then turned on, and the stage moved downwards at a speed of 0.05mm/s. As the stage moved, the PEG liquid pre-polymer was polymerised into a bulk material structure using the 405nm laser. Once a 5mm length conduit was fabricated, the laser was turned off by a shutter, and the structure raised out of the liquid PEG using the z-axis translation stage. Conduits were analysed using scanning electron microscopy, to confirm the correct internal diameter and wall thickness. Conduits were washed using isopropyl alcohol (IPA, Fisher Scientific UK) and left in IPA for 7 days before cell culture experiments, to ensure complete removal of contaminants. For further detail see the methods published by (Pateman *et al.*, 2015).

6.2.5 Threading of microfibres into hollow conduits

Fibre mats for each material blend, and diameter were then manufactured, using the conditions in the methods section, 1.1, in chapter 5. Fibres were then wrapped tightly around

the Hamilton syringe and placed into the 5mm PEG conduits. Conduits were then analysed using microCT to confirm fibre alignment throughout the tube before *ex vivo* analysis.
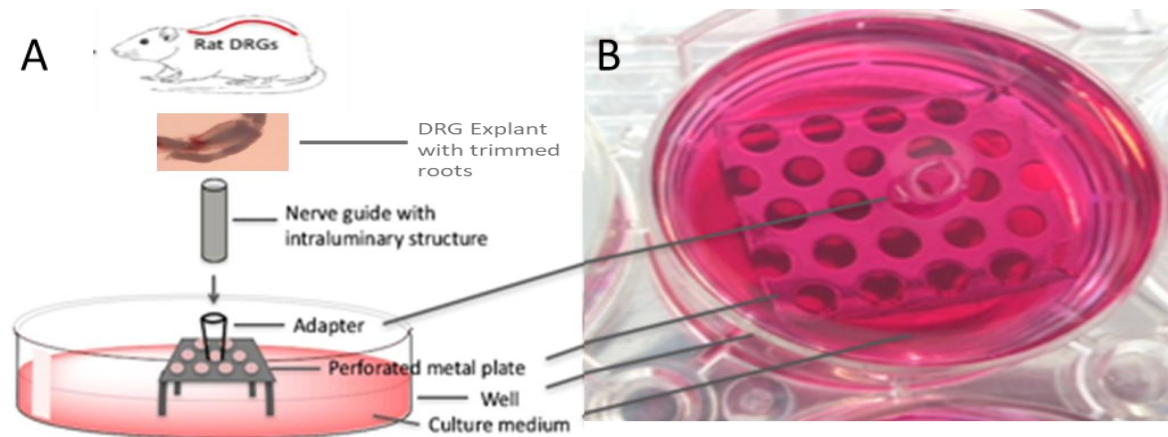
Figure 6.2. Image from (Behbehani *et al.*, 2018). A) DRGs are removed from rat spinal columns and placed onto the top of a hollow PEG conduit. B) The conduit is held in place by a sterilise pipette placed into a cell culture stainless steel grid, placed in a well place. Culture media is added to the well plate, filling the conduit.

6.2.6 Design of the ex vivo testing setup and preparation for DRG culture

An *ex vivo* 3D culture testing model had been designed and developed by Behbehani *et al.* (2018) to analyse the fibre material blends in PEG conduits using NG108-15 neuronal cells, and Dorsal root ganglion explants. Fibres were threaded into tubes, and placed upright into a sterile stainless steel grid (Behbehani *et al.*, 2018). The metal grid was placed in a 6 well plated and filled with culture medium (see figure 6.2). Before DRG culture, tubes containing fibres were sterilised using 70% ethanol for 3 hours. Samples were washed with PBS and left overnight in PBS to ensure the complete removal of contaminants and ethanol.

6.2.7 Dorsal root ganglion explant isolation and culture

The protocol by Sleigh *et al.* (2016) was adapted for the removal of Dorsal root ganglion from 4 week old male Wistar rats, which were sacrificed in accordance to the Animals (Scientific Procedures) Act 1986 via Schedule 1. The spinal column was dissected out and trimmed to expose the spinal cord, nerve roots and dorsal root ganglia (see figure 6.3). DRGs were pulled out of the spinal column using fine forceps and placed into a petri dish containing DMEM medium. Using a dissection microscope, DRG roots were trimmed off, and the explants were placed onto the top of hollow tubes containing fibres (see figure 6.2) (Sleigh *et al.*, 2016). Dry DRG explants were incubated for 30 minutes, to attach, before the addition of supplemented DMEM medium, to the fill the well. Supplemented DMEM medium was added to the well drop wise once the medium reached the top of tube and the DRG

explants. Samples were incubated at 37°C and 5% CO_2, for 21 days and the culture media was changed every 5 days. Cell migration and Neurite outgrowth was determined for each condition, and experiments were repeated 3 times (n=3).
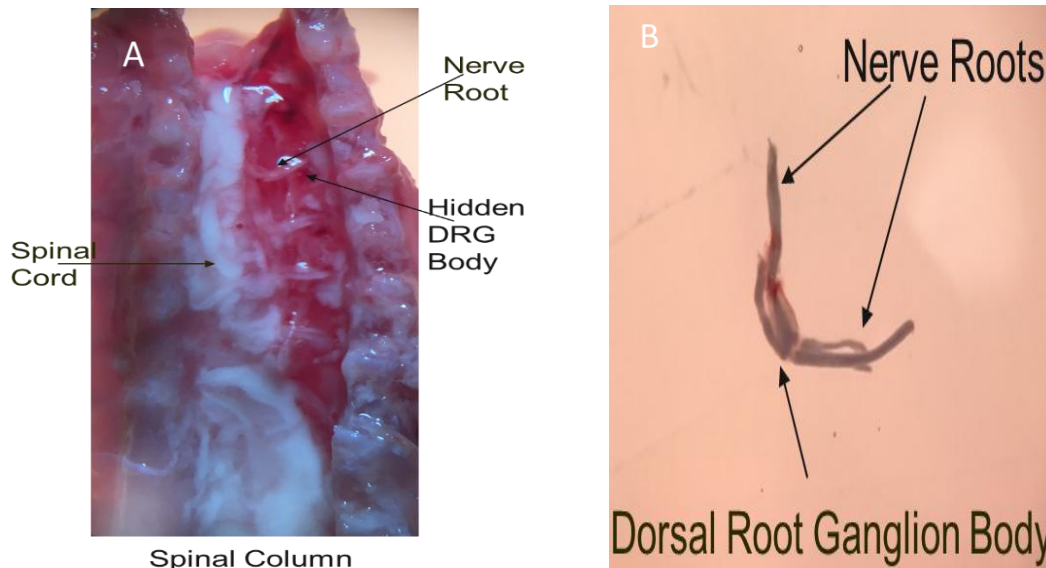
Figure 6.3. Images of A) rat dorsal root ganglia in the spinal column and B) An image of a DRG removed from the spinal column showing the body and axon extensions (nerve roots).

6.2.8 *Immunolabelling of DRG explants for β III tubulin and S100*

Immunolabelling was performed as per the methods in Daud *et al.* (2012). To image DRG explants on the fibres, the conduit was picked up, using a sharp pair of forceps, and placed on its side in culture medium. Fibres, containing the DRG body, were floated out of the conduit and onto a glass slide for labelling and imaging. Fibres and DRGs, were washed three times with PBS before being fixed with 3.7% paraformaldehyde for 20 minutes. After washing with PBS, samples were permeabilized with 0.1% Triton X-100 for 30 minutes and washed with PBS. Unreactive binding sites were blocked with 3% bovine serum albumin (BSA) for 30 minutes and incubated, at 4°C for 48 hours, with a mouse anti-β III-tubulin antibody (1:500) (Promega, UK) and a rabbit-anti S100 antibody (Schwann cell Marker) (1:100) (Dako, Denmark), both diluted in 1% BSA. After washing with PBS three times, samples were incubated at room temperature, for 90 minutes, with a Texas Red-conjugated anti-mouse IgG antibody (1:100) (Vector Labs, USA) and a FITC-conjugated secondary anti-rabbit IgG antibody (1:100) (Vector Labs, USA) both diluted in 1% BSA. Cells were washed with PBS and cell nuclei were labelled with 4,6-diamidino-2-phenylindole dihydrochloride (DAPI) (Sigma Aldrich) (1:500 dilution in PBS) at room temperature for 15 minutes, followed by dropping PBS onto samples for imaging. Fibre samples were imaged using an upright Zeiss LSM 510 confocal microscope and three fields of view were imaged for each sample, the top, the middle and the bottom. A helium-neon laser (543 nm) was used to image Texas

Red excitation (λex = 589nm / λem = 615 nm), an argon ion laser to visualise FITC (λex = 493 nm / λem = 528 nm) and a Ti:sapphire laser (800 nm) was used to image DAPI (λex= 358 nm / λem = 461 nm) (Daud *et al.*, 2012).

6.2.9   Neurite outgrowth and Schwann cell migration determination from DRG explants
Three selected fields of view, for each fibre sample, were imaged using an upright Zeiss 510 confocal microscope. Neurite outgrowth length was traced and determined by using the Neuron J plugin tool on NIH software Image J (Popko *et al.*, 2009). Neurites were measured from the tip of the neurite, to the DRG body, and all neurites expressed from DRG bodies were measured. Schwann cell migration, from Dorsal root ganglion body explants, was measured using the ruler tool on Image J NIH software (Schneider *et al.*, 2012). The length was measured from the DRG body, to the tip of the Schwann cell body. 100 Schwann cell lengths, per sample, were measured to calculate the average Schwann cell migration length (Daud *et al.*, 2012).

6.2.10 Statistical analysis
GraphPad Instat (GraphPad Software, USA) was used to perform statistical tests on data collected. One-way analysis of variance ($p < 0.05$) was conducted to analyse the differences between the data, incorporating Tukey's multiple comparisons test if $p < 0.05$. Data was reported as mean ± SD, $p<0.05$. Each experiment was performed three independent times with each sample repeated three times as n=3.

6.3 Results

6.3.1   Fabrication of electrospun fibres for threading into tubes
As seen in the methodology section of chapter 5, section 1.1, PHBV, PCL and P(3HO):P(3HB) (50:50) 5 and 8μm fibres were produced using the conditions in table figure 1 chapter 5. To determine the correct time of spinning, P(3HO):P(3HB) (50:50) 5 and 8μm fibres were electrospun for 4 different time points: 5, 10, 15 and 20 minutes. Figure 6.4A shows microCT images of P(3HO):P(3HB) (50:50) fibres of 5μm (figure 4A-D) and 8μm (figure 6.4E-H) electrospun for 5-20 minutes and threaded into 5mm PEG tubes. Figure 6.4A-D shows that, for 5μm fibres, 15-20 minutes electrospinning is the optimum time to create electrospun fibrous mats that fill the tube, however, in figure 6.4D (20mins), fibres appeared more aligned throughout. For 8μm fibres, 15 minutes electrospinning was adequate to fill the PEG tube, and fibres were aligned throughout. These times ensured that

the correct density of fibres filled the conduits fully, as well as maintained fibre alignment throughout the conduit (microCT images in figure 6.4 were kindly imaged by Dr Adam Glen).
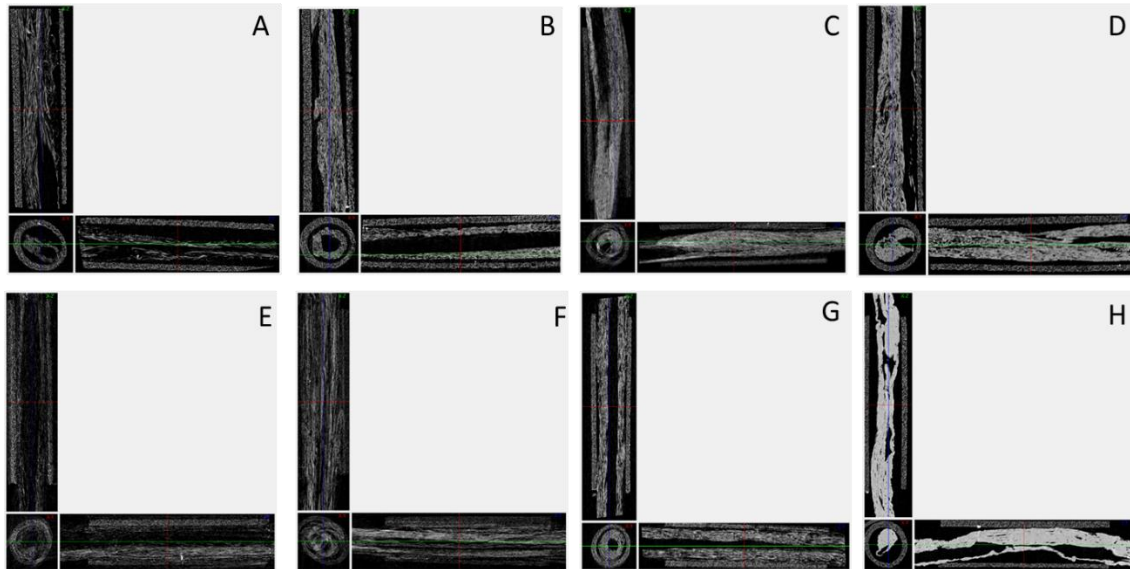
Figure 6.4. A)MicroCT images of 5µm P(3HO):P(3HB) (50:50) fibres electrospun for A) 5 minutes, B) 10 minutes, C) 15 minutes and D) 20 minutes. 8µm P(3HO):P(3HB) (50:50) fibres were also spun for E) 5 minutes, F) 10 minutes, G) 15 minutes and H) 20 minutes. MicroCT images were taken and rendered by Dr Adam Glen.

After determining the correct electrospinning time, 5 and 8µm of P(3HO):P(3HB) (50:50), PCL and PHBV were electrospun for 20 and 15 minutes. Alignment of fibres, and diameter of fibres, was determined for each material/blend using scanning electron microscopy. Fibre mat thickness was also confirmed using scanning electron microscopy to ensure the correct amount and thickness of fibres were being threaded. Figure 6.5A and B shows electron micrographs of 5 and 8µm P(3HO):P(3HB) (50:50) fibres, electrospun for 15 and 20 minutes, respectively, and the thickness of these mats fabricated. Thickness was confirmed by measuring fibre mats with a micrometer, and by scanning electron microscopy measurements. Overall, the thickness of the 5µm fibre mats was between 75.83 ± 8.10µm and 81.8 ± 8.17µm. The thickness of the 8µm fibres were between 102.80 ± 7.43µm and 109.80 ± 7.43µm. The thickness of the 8µm fibre mats were significantly higher than the 5µm fibre mats. After manufacture of fibre mats for threading, average fibre diameter was also confirmed by measuring the diameter of the fibres using the ruler tool on image J (figure 6.4D)(Schneider *et al.*, 2012). Diameters confirmed were 4.96 ± 0.67µm, 5.05 ± 0.34µm and 5.07 ± 0.81µm for the 5µm P(3HO):P(3HB) (50:50), PCL and PHBV mats respectfully. The diameters confirmed for the 8µm P(3HO):P(3HB) (50:50), PCL and PHBV mats were 8.13 ± 0.78µm, 8.03 ± 0.45µm and 8.08 ± 0.43µm respectfully. The average diameter of the 8µm fibre mats for all materials was significantly higher than their 5µm counterparts.
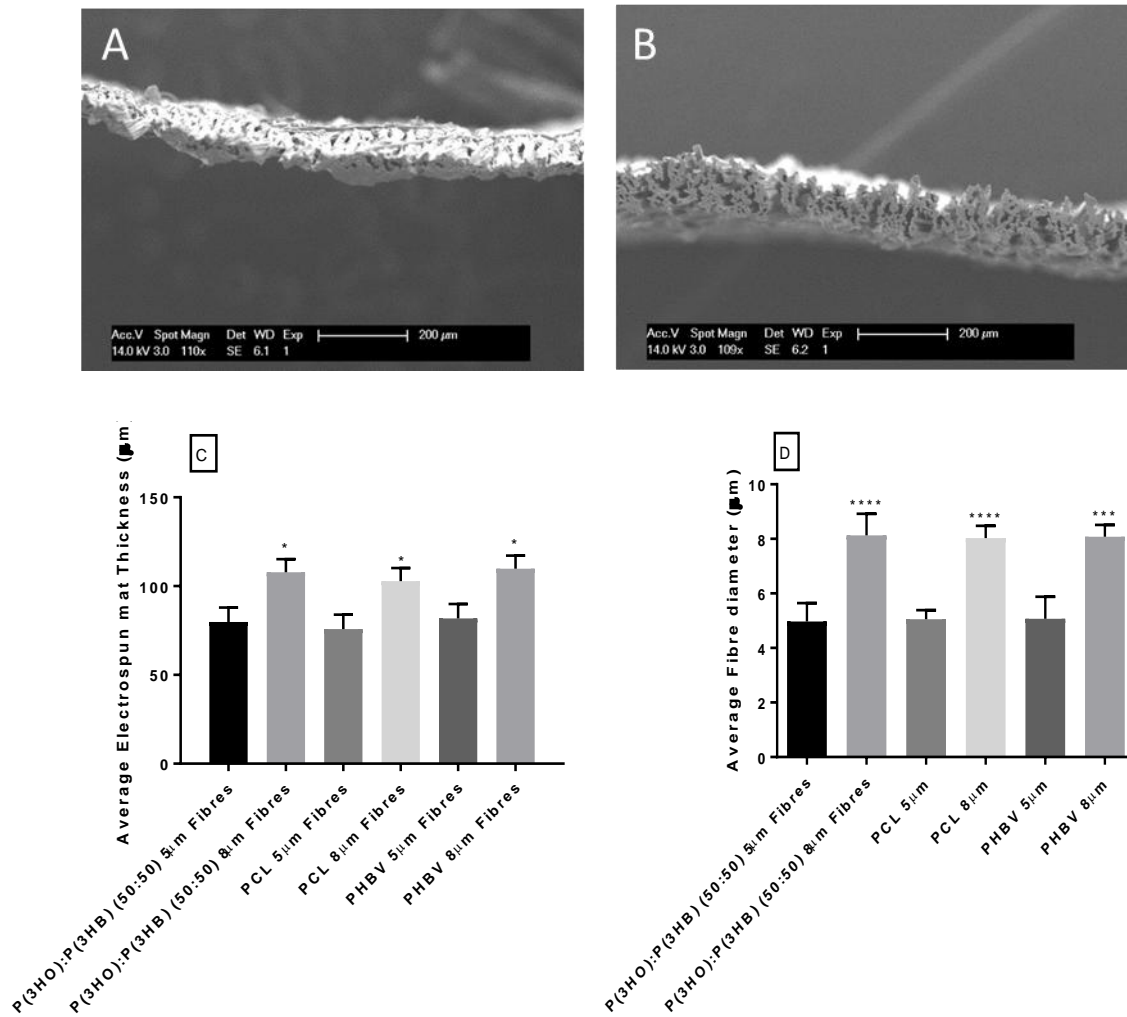
Figure 6.5. Scanning electron micrographs were taken of the 5µm (A) and 8µm (B) fibres of P(3HO):P(3HB) (50:50) to measure matt thickness. C) Graph to show the thickness of electrospun mats fabricated were similar for each material. A two way anova with Sidak's multiple comparisons tests was used to analyse data (Mean ± SD, n= 3 independently fabricated samples *p < 0.05 compared to 8µm fibres) and D) Graph to show confirm fibre diameter of each electrospun mat fabricated. A two way anova with Sidak's multiple comparisons tests was used to analyse data (Mean ± SD, n= 3 independently fabricated samples ***p < 0.001 and ****p < 0.0001 compared to 8µm fibres).

6.3.2 Mechanical testing of fibres

Mechanical data of material electrospun fibres, of different diameters, is shown in table 6.1. With regards to Youngs modulus, 8µm PHBV fibres, spun for 10 minutes, was the closest to native rat sciatic nerve, 0.61 ± 0.31 MPa compared to 0.57-0.58 MPa, respectively (Borschel *et al.*, 2003). However, when looking at tensile strength, P(3HO-co-3HD):PLLA and PCL 5 and 8µm fibres were closer to native nerve than the other materials and fibre diameters. In chapter 2, table 2.1, P(3HO) and P(3HO-co-3HD) were chosen to be blended with stiffer materials, such as P(3HB), due to their low Youngs modulus and elastomeric properties (Rai *et al.*, 2011). However, when manufactured into fibres, P(3HO):P(3HB) (50:50), and P(3HO-co-3HD):PLLA (50:50) had a higher Young's modulus than PHBV and PCL fibres. Overall,

PHBV 8µm would be the suggested internal filler for a nerve guide conduit based on the mechanical properties.

Table 6.1.Table to show the ultimate tensile strength (σ, MPa), percentage elongation at failure ($\varepsilon_{failure}$, %) and the Young's modulus (E, MPa) of the electrospun fibre materials and different fibre diameters.

Material Fibres and Size	σ, MPa	E, MPa
P(3HO): P(3HB) (50:50) 5µm	2.69 ± 0.27	7.45 ± 0.36
P(3HO): P(3HB) (50:50) 8µm	4.40 ± 0.83	6.75 ± 0.05
P(3HO-co-3HD): PLLA (50:50) 5µm	0.73 ± 0.07	3.18 ± 0.09
P(3HO-co-3HD): PLLA (50:50) 8µm	0.85 ± 0.20	2.14 ± 0.05
PCL 5µm	2.09 ± 0.16	2.18 ± 0.18
PCL 8µm	2.53 ± 0.49	1.87 ± 0.25
PHBV 5µm	0.54 ± 0.05	1.10 ± 0.35
PHBV 8µm	0.62 ± 0.01	0.61 ± 0.31
Rat Sciatic Nerve	1.4-2.7	0.57-0.58

6.3.3   Fabrication of polyethylene glycol hollow tubes

Hollow polyethylene glycol tubes were created using microstereolithography. 5mm tubes were printed, having a wall thickness of 250µm and an internal diameter of 1.1mm (Daud *et al.*, 2012). Figure 6.6 shows scanning electron micrographs of hollow PEG tubes fabricated by microstereolithography, with a lack of porosity. In figure 6.6A, lines can be seen down the conduit from printing. This is due to the high resolution of the digital micromirror device (DMD), which has printed the pixels of the uploaded paint image. This can be seen more clearly in figure 6.6B. However, it is possible that the printing of pixels, and subsequent lines down the outside and inside of the conduit, may benefit nerve regeneration, by providing additional guidance, to the regenerating nerve and Schwann cell migration due to creating a rough surface topography. Melissinaki *et al.* (2011) reported that NG108-15 and PC12 neuronal cells align along 10µm PLLA lines printed by 2-photon polymerisation, and it is well reported that aligned electrospun fibres provide guidance for neuronal and glial cells (Melissinaki *et al.*, 2011; Daud *et al.*, 2012). As seen in Pateman *et al.* (2015), hollow PEG tubes printed using the 405nm laser microstereolithography set up in the laboratory, did promote nerve regeneration, *in vitro* and *in vivo*, and was comparable to an autograft when observing number of unique axons at the end distal end of the injury (Pateman *et al.*, 2015). 3D printing of PEG tubes is relatively straightforward compared to other biodegradable polymers, which was why the material was chosen for the *ex vivo* DRG testing model. Figure 6.6C also confirms that any length tube can be fabricated by microstereolithography, which confirms the potential of this set up for printing hollow, or structural, tubes out of other

photocurable biodegradable polymers for use in peripheral nerve repair (Pateman *et al.*, 2015).
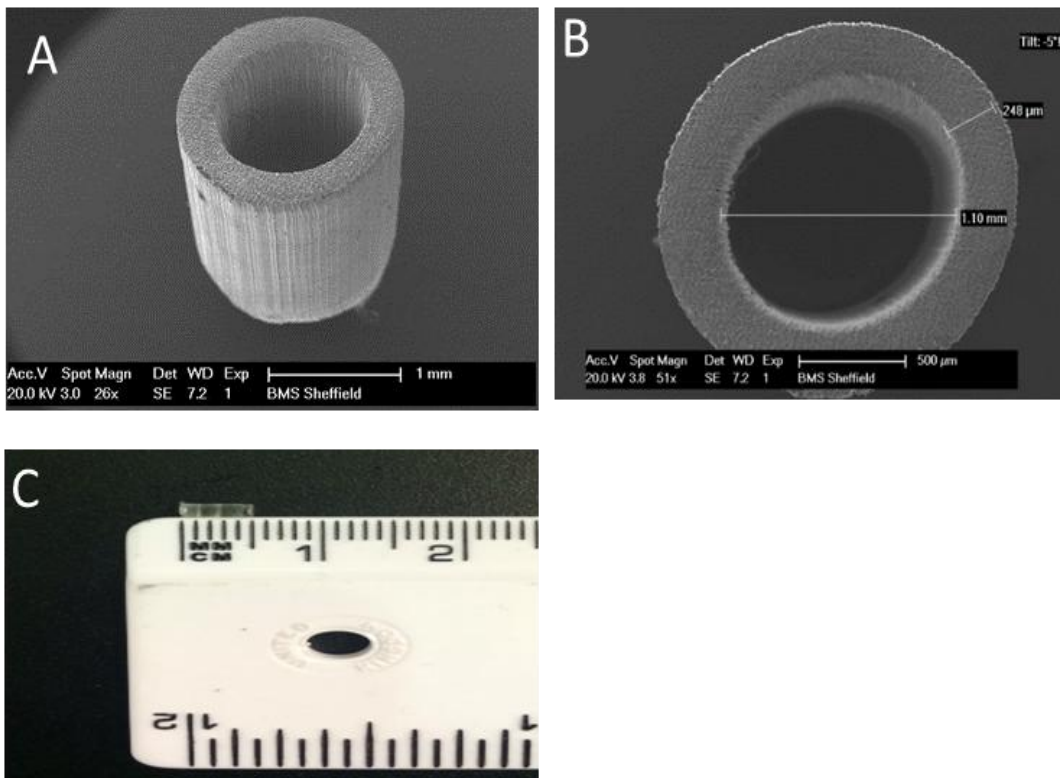
Figure 6. 6. Scanning electron micrographs and image of A) hollow PEG tube printed by microstereolithography, B) the accuracy in dimensions that the set up can print and C) an image to demonstrate the sizes of tubes that can be printed.

6.3.4 Threading of microfibres into hollow conduits and confirmation of fibre alignment

Threading of microfibers was performed by the *methods* in section 1.4 using a Hamilton syringe. Fibres were wrapped around the needle of the syringe parallel to their orientation, to maintain fibre alignment inside the tube. Fibres were placed inside, and the tube was pinched by hand to remove the needle. This was found to be the most efficient for maintaining fibre alignment throughout the tube, although the small circular empty space was always left (as seen in microCT images). Before *ex vivo* DRG culture, conduits containing fibres were imaged by microCT to confirm fibre alignment throughout the 5mm PEG tubes. Figure 6.7 shows microCT images of the different fibres, with different fibre diameters, threaded into 5mm PEG tubes. Figure 6.7A-D images were taken by Dr Adam Glen, who also oversaw imaging of figure 6.7E and F. When electrospinning P(3HO):P(3HB) (50:50) and PHBV fibres, they form a mat of fibres, whereas PCL fibres resemble a cotton thread. When threading the polyhydroxyalkanoate fibre mats, a circular 'tube' of dense fibres was formed leaving a small circular space, seen on the microCT images. This could be beneficial to aiding nerve regeneration, as the internal fibre tube mat would provide extra guidance, without blocking the regenerating nerve. PCL fibres could be threaded through the

tube using a sewing needle. Therefore, fibres were more distributed through the cross sectional image of the PEG tubes, and more distributed throughout the tube. Interesting, the 5µm P(3HO):P(3HB) (50:50) and PHBV fibres, did fill the middle of the tube more than the 8µm fibres, which were densely compacted at the edges of the tubes, rather than filling the middle, which could be due to the threading technique and thicker electrospun mat (as seen in figure 6.4E). Overall, microCT did confirm that all individual fibres did maintain their alignment, and that PCL fibres maintained alignment throughout the entire tube. It was noticed that the 5µm P(3HO):P(3HB) (50:50) fibres did lose a little alignment further down the PEG tube, which could be due to elastomeric nature of the P(3HO) in the blend (Lorena R. Lizarraga-Valderrama *et al.*, 2015). Overall, microCT could confirm the alignment of fibres throughout the 5mm tubes, and that the threading techniques ensured that the fibres could be threaded right to the end of the tube.
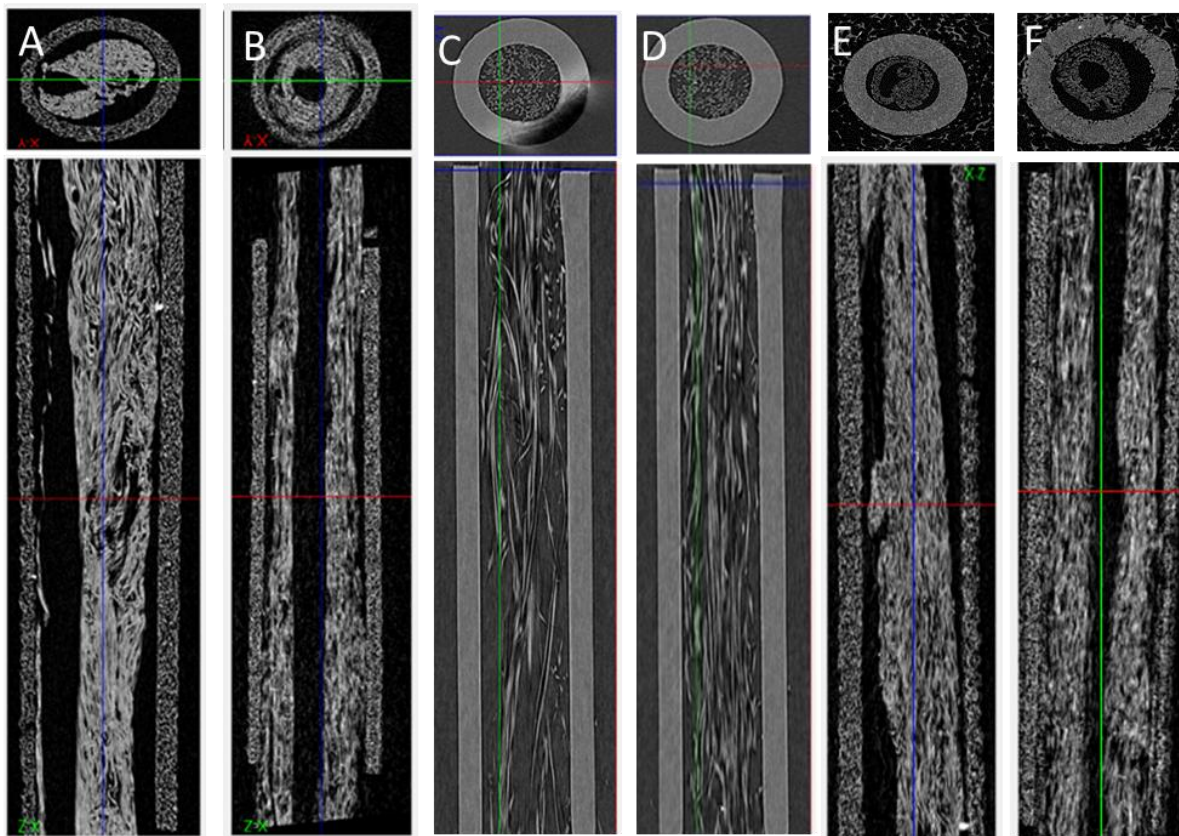
Figure 6.7. MicroCT images of A) 5µm P(3HO):P(3HB) (50:50) fibres, B) 8µm P(3HO):P(3HB) (50:50) fibres, C) 5µm PCL fibres, D) 8µm PCL fibres, E) 5µm PHBV fibres and F) 8µm PHBV fibres threaded into 5mm polyethylene glycol tubes (Images A-D taken by Dr Adam Glen in collaboration with the Neurimp project).

6.3.4   Dorsal root ganglion explant culture on fibres

To observe the effect of fibre diameter, and material type, on primary neuronal and Schwann cells, dorsal root ganglion bodies were isolated from the spinal column and explanted on top of the fibres, which had been threaded into 5mm hollow PEG tubes. DRG explants were left

in culture for 21 days, before the fibres were removed from conduits containing the explants. Explants, on fibres, were labelled with DAPI, β III tubulin and S100 to identify and measure Schwann cell migration and neurite extension length.
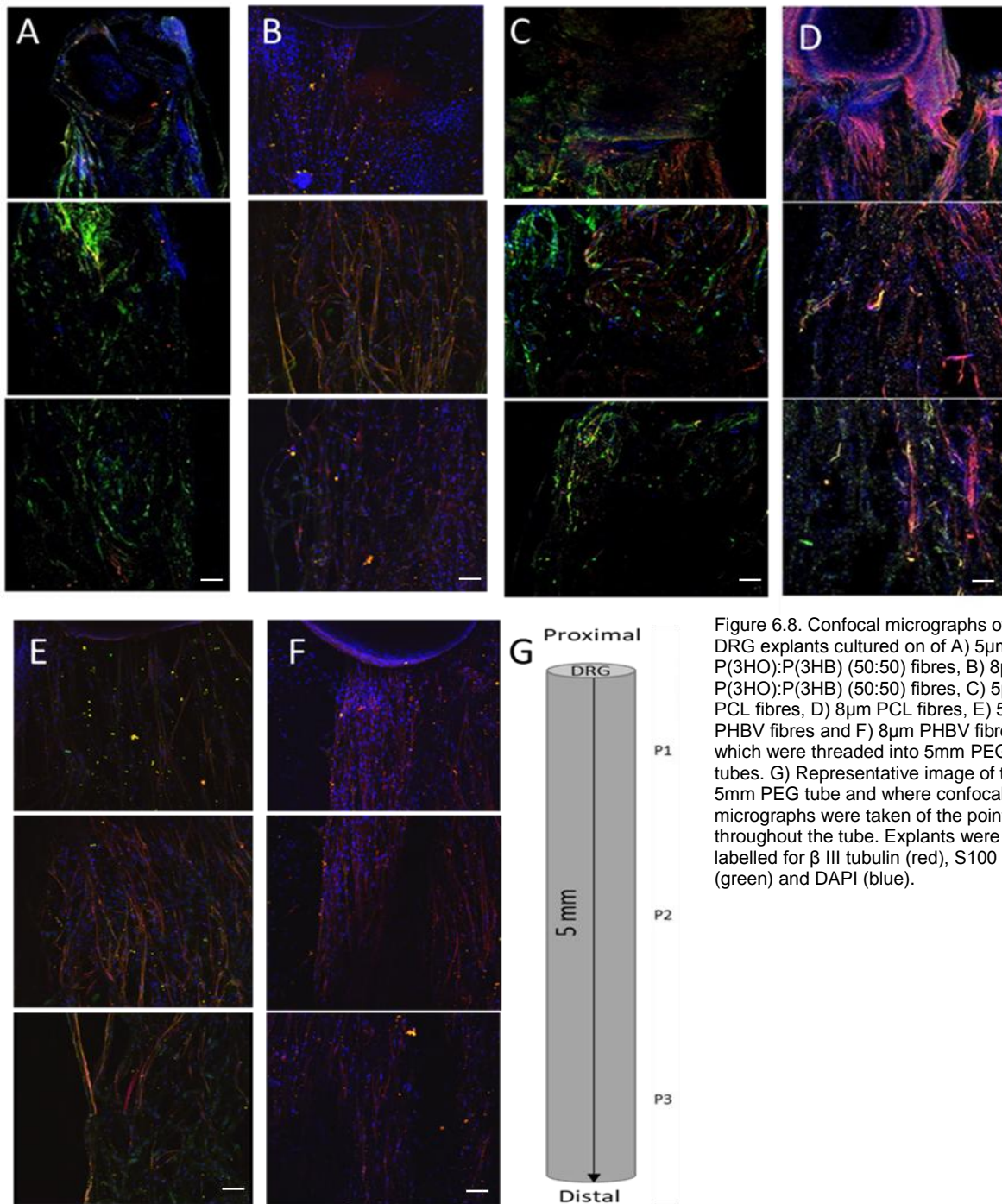
Figure 6.8. Confocal micrographs of DRG explants cultured on of A) 5μm P(3HO):P(3HB) (50:50) fibres, B) 8μm P(3HO):P(3HB) (50:50) fibres, C) 5μm PCL fibres, D) 8μm PCL fibres, E) 5μm PHBV fibres and F) 8μm PHBV fibres, which were threaded into 5mm PEG tubes. G) Representative image of the 5mm PEG tube and where confocal micrographs were taken of the points throughout the tube. Explants were labelled for β III tubulin (red), S100 (green) and DAPI (blue).

Figure 6.8 shows confocal micrographs of fibres removed from conduits, which had been immunolabelled for neuronal cell and Schwann cell markers. Images 6.A, C and D were taken by Miss Mehrie Behbehani and measuring of Schwann cell migration and axon regeneration length was performed.

Overall, it was observed that Schwann cell migration preceded axon migration, or that axon regeneration followed Schwann cell migration. Schwann cells could be seen present on all images taken at position 3 of the conduit (approximately 4mm along the tube), indicating that fibres did not inhibit Schwann cell migration. It was observed that fibre alignment was lost during DRG culture due fluid interactions of the culture medium. Therefore, if tubes containing fibres were to be implanted *in vivo*, fibres would have to be sutured/fixed to the dorsal and proximal end of the distal nerve to maintain alignment. Confocal micrographs were quantified to determine the average Schwann cell migration and axon regeneration lengths, and figure 6.9 confirmed that the highest Schwann cell migration and axon regenerations lengths were observed on the tissue culture plastic (not pictured in figure 6.8) in which Schwann cell migration length was significantly higher than that of the fibre samples, except 5µm PHBV fibres.

The highest average Schwann cell migration length was observed on 5µm PHBV fibres followed by the 5µm P(3HO):P(3HB) (50:50) fibres, which were measured at 4027.67 ± 126.3µm and 3943.58 ± 386.63µm respectively. The average Schwann cell migration length measured on the 5µm PHBV fibres, was significantly higher than the migration length of the 8µm P(3HO):P(3HB) (50:50), PCL and PHBV fibres, which would indicate that 5µm fibres are more effective in directing Schwann cell migration from DRG explants than 8µm fibres. The increase in Schwann cell migration length on PHA fibres, could also be down to the fibres maintaining alignment in culture medium, in the PEG tubes, as electrospun PHA fibres form a mat, whereas the PCL fibres are more threadlike. The more elastomeric properties of P(3HO) in the P(3HO):P(3HB) (50:50) blend and the addition of the hydroxyvalerate monomer to P(3HB) in PHBV cause the formation of the mat, and cause the fibres to stick together (Scandola *et al.*, 1997; Basnett *et al.*, 2013).

Similar results were also observed in neurite outgrowth length, in which the highest neurite outgrowth lengths were seen on 5µm P(3HO):P(3HB) (50:50) fibres followed by the 5µm PHBV fibres, 2502.69 ± 112.63µm and 2482.67 ± 113.32µm respectfully. Both PHA 5µm fibres significantly increase neurite outgrowth length from DRG explants when compared to 8µm PCL fibres, but no other statistical differences were detected between samples. What this result suggests is that DRG neurite outgrowth length is longer when cultured on material fibres, of certain diameters, that promote the furthest Schwann cell migration from the explant, which in this case is the on 5µm P(3HO):P(3HB) (50:50) fibres followed by the 5µm PHBV fibres. Overall, this data would suggest that 5µm fibres are the most efficient for Schwann cell migration and neurite outgrowth from DRG explants.
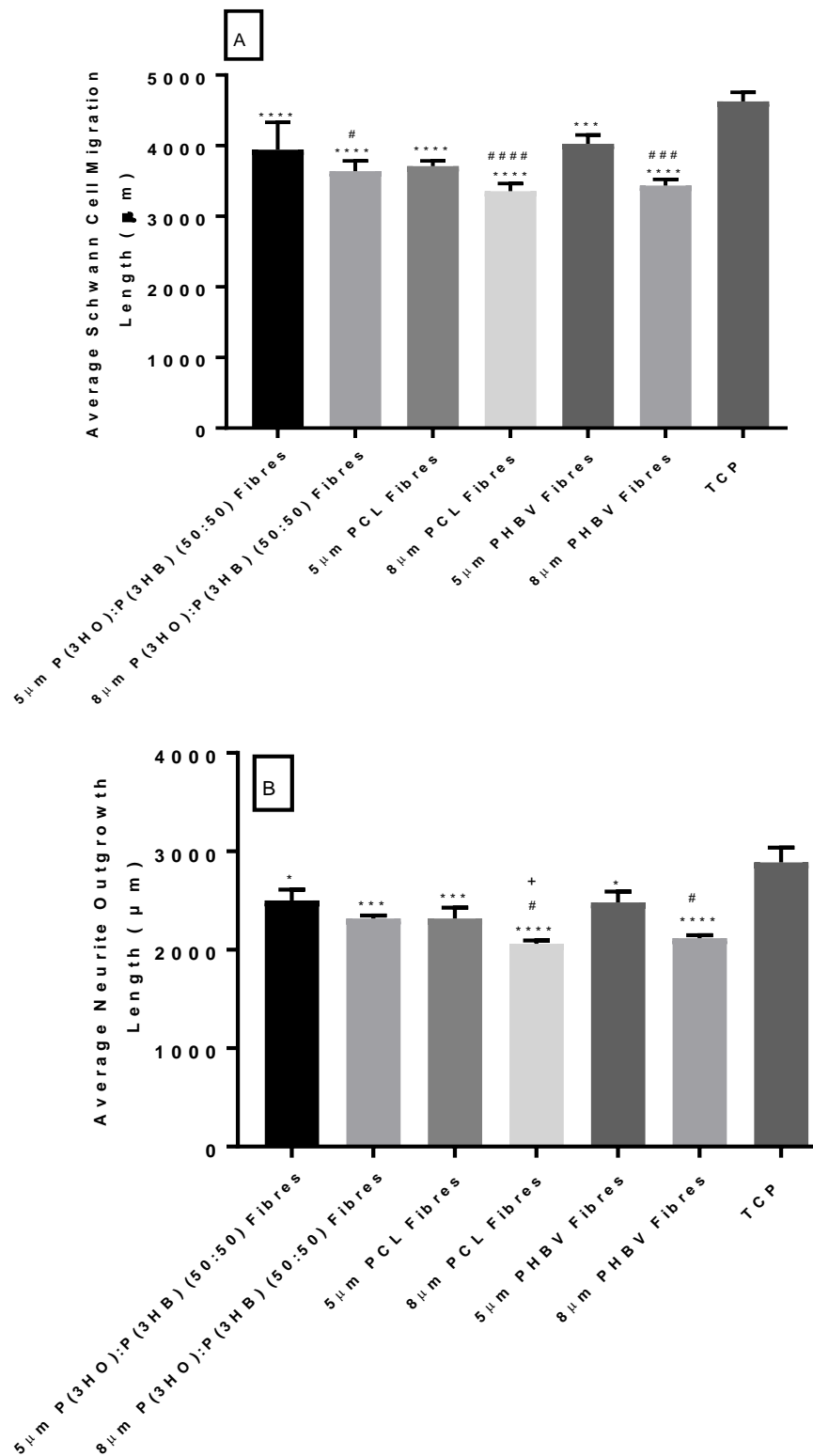
Figure 6.9. A) Graph to show the average Schwann cell migration length for the different materials and fibre diameters. A one way anova with Tukey's multiple comparisons tests was used to analyse data (Mean ± SD, n=3 independent experiments, ***p < 0.001 and ****p < 0.0001 compared to TCP, #p < 0.05, ###p < 0.001 and ####p < 0.0001 against 5µm PHBV fibres. B) Graph to show the average neurite outgrowth regeneration length for the different conditions. A one way anova with Tukey's multiple comparisons tests was used to analyse data (Mean ± SD, n=3 independent experiments, *p < 0.05, ***p < 0.001 and ****p < 0.0001 compared to TCP, #p < 0.05 compared to 5µm P(3HO):P(3HB) (50:50) fibres, +p < 0.05 compared to 5µm PHBV fibres).

6.4 Discussion

The main findings of this chapter were that average neurite outgrowth length and Schwann cell migration lengths were significantly higher on 5µm P(3HO):P(3HB) and PHBV fibres, compared to 8µm PCL and PHBV fibres. Overall, neurite outgrowth length and Schwann cell migration increased when cell were cultured on 5µm compared to 8µm fibres, and on PHA blends compared to the PCL fibres. Previous work using DRG explants had been successful for use as an *ex vivo* primary nerve injury model. Daud *et al.* (2012) had placed DRG explants onto 1, 5 and 8µm fibres, which concluded that Schwann cell migration length was always further than the neurite outgrowth length, also seen in figures 6.9A and B in this chapter. Daud *et al.* (2012) also concluded that smaller fibres, of 1µm supported Schwann cell migration and DRG neurite outgrowth more efficiently than the 5 and 8µm fibres, however this was not significant (Daud *et al.*, 2012). Pateman *et al.* (2015) also cultured DRG explants onto 3D printed PEG tubes, and observed, after 14 days of culture, that Schwann cells migrated 9.5mm either side of the DRG body (Pateman *et al.*, 2015). However, as PEG tubes were later implanted *in vivo*, DRG experiments were not quantified in the publication. The 3D *ex vivo* DRG testing model was developed in collaboration with Miss Mehrie Behbehani and Dr Adam Glen, which is a combination of the work fabricated by Daud *et al.* (2012) and Pateman *et al.* (2015). Using the microstereolithography set up, polyethylene glycol could be 3D printed into hollow tubes, 5mm in length with a 1.1mm internal diameter and a 250µm wall thickness, although these dimensions can be changed by changing the image of the DMD image. Currently, the microstereolithography set up in the Claeyssens laboratory has a resolution of 50µm, and work is currently undergoing to decrease the resolution even further to allow for the printing of NGCs with internal structures and channels (Pateman *et al.*, 2015).

Previous work had concluded that the optimum time to electrospin 5 and 8µm fibres was 15 and 20 minutes respectfully, to produce thick mats of fibres that could be threaded into a hollow tube and provide the correct filling density. Conditions to fabricate 5µm fibres produced electrospun fibre mats with a thickness of 75µm, whereas 8µm fibres fabricated mats of 102µm. PHBV and P(3HO):P(3HB) (50:50) fibre mats were more sheet like, in which they could be peeled off the collector material easily. PCL fibres were more threadlike, and filled the tube more sporadically when threaded, before DRG culture. The PHA fibres filled the tube more densely, in which 8µm were denser around the walls of the PEG tubes, leaving an unfilled hole in the middle of the tube. The microCT data (figure 6.7), provided by Dr Adam Glen, interestingly provided 3 different threading appearances, (sporadic- PCL fibres, dense middle- 5µm PHA fibres and densely filled outer- 8µm PHA fibres) which

provided another variable for the DRG explant culture, as well as material type and fibre diameter. Mechanical data would suggest that 5 and 8µm fibres would be the most suitable as an internal filler material, due to having a similar Young's modulus and tensile strength to native rat sciatic nerve (Borschel *et al.*, 2003). Increasing fibre diameter decreases Young's modulus due to decreasing fibre density.

After DRG explant culture for 21 days, fibres, containing the DRG body and cells, were carefully removed from the tubes, before staining and imaging. Confocal microscopy images were taken in three positions to observe neurite outgrowth and Schwann cell migration length, at the distal end, middle and proximal end of the tube. When removing the fibres from the tubes, it was observed that during exposure to the culture medium, the PHA fibres had retained their shape and dense structure, whereas the PCL fibres had lost some alignment during DRG culture. Overall, Schwann cells could be visualised at the distal end of the tube (p3) for all fibre samples, although were less so on the PHBV and PCL 8µm fibres. Quantification of images confirmed that the 5µm PHBV and P(3HO):P(3HB) (50:50) fibres supported the furthest Schwann cell migration rate. This would appear to indicate that Schwann cell migration is more efficient on PHA fibres, of 5µm diameter, which filled the PEG tubes more densely than the other materials and the 8µm fibres. The tissue culture plastic control had the longest Schwann cell migration lengths. This could be due to the space available on the culture well plate, and perhaps some of the fibres inside the tubes had become entangled and were inhibiting Schwann cell migration.

Neurite outgrowth rate from DRG explants on the fibre scaffolds was measured from 0.10-0.11mm, with the highest rates recorded on the 5µm PHBV and P(3HO):P(3HB) (50:50) fibres. The rate of nerve regeneration in humans has been reported to be 1mm/day so compared to this the regeneration rate is much slower (Belkas *et al.*, 2004b). However, it has been reported that the rate of nerve regeneration in rats can be up to 1.9mm/day due to the faster rate of the fibrin cable formation after injury, and the increased rate of the fibrin cable degradation afterwards (Kaplan *et al.*, 2015). Of note, the tissue culture plastic control had the longest neurite outgrowth extension lengths. This could be due to the fibres inhibiting neurite outgrowth length when inside the conduit in a wet environment. Both the tissue culture plastic control and fibres were in a static culture model, and cells cultured on the TCP surface had access to oxygen and nutrients, that cells inside the conduit did not. This is also explained by the lack of porosity the PEG tubes have, which have been inhibiting oxygen and nutrient delivery. These results would suggest applying dynamic culture conditions to the 3D DRG explants *ex vivo* model, such as culture in a perfusion bioreactor system, which would allow a continual flow of both oxygen and nutrients for cells inside the conduit and the plastic control. Studies have shown that the addition of flow improves cell viability and

differentiation (Miranda-Azpiazu *et al.*, 2018). Further work could also include fabricating pores into the PEG tubes before conducting analysis. This could be done using porogens, such as plastic, salt, or sugar, but recent work using HIPEs has fabricated PCL nerve guide conduits with pores without the use of a porogen (D. W. Johnson *et al.*, 2013). Therefore, although the DRG *ex vivo* model is a good indication to determine optimum fibre diameters, density and material type, axon regeneration rate is still not comparable to *in vivo* data. Future work would include repeating the *ex vivo* DRG explants culture using a bioreactor or perfusion system to circulate culture medium through the nerve guide conduits containing fibres to ensure constant supply of oxygen and nutrient. Dissociated neurons, from DRG explants, could also be cultured onto fibres to observe and measure neurite outgrowth, per neuron, on different fibre diameters and the different materials, as well as the interaction of neurons with primary Schwann cells. However, Schwann cell migration cannot be measured from DRG explant dissociation, in which it can be measured from DRG whole explant culture. From this data, the P(3HO):P(3HB) (50:50) blend was chosen for in vivo work. 5 and 8µm fibres were fabricated from previous conditions and threaded into hollow tubes (material blend undergoing patent for Neurimp project) of 10mm, 14mm and 19mm length. A 2mm gap either side of the fibres was allowed for suturing tubes to the proximal and distal stumps of a rat sciatic nerve injury. Overall, fibres were cut into 6mm, 10mm and 15mm sections before threading to test a short, medium and long gap injury.

Chapter 7: Aminosilanes and their use in Peripheral Nerve Repair

7.1 Introduction

Current research in peripheral nerve repair focuses primarily on improving nerve guide conduits (NGCs) by several different ways. This could be changing the material of the conduit, or conduit design, adding intraluminal guidance cues, such as electrospun fibres, or by the addition of biological coatings (W. Daly *et al.*, 2012). Coatings can be used to improve the biocompatibility of biodegradable synthetic polymers, such as PLLA, PLGA and PCL (J. H. Bell and Haycock, 2012). Natural biopolymers such as chitosan and silk offer excellent biocompatibility and offer similar mechanical properties, and topography, to the native nerve tissue. However, there is often batch to batch variation in manufacture, as well as difficulties in fabricating the materials into nerve guide conduits (Arslantunali *et al.*, 2014b). Synthetic biodegradable polymers offer controllable degradation rates and mechanical properties, and can be processed into NGCs via a number of manufacturing methods (Nectow *et al.*, 2012). However, they are often less biocompatible than natural polymers due to surface characteristics such as wettability and topography (Arslantunali *et al.*, 2014b).

Coatings can be added to synthetic polymers, to improve their biocompatibility, in a number of different ways. Natural coatings, such as collagen and laminin, have been shown to improve the biocompatibility of biodegradable polymers, for use in peripheral nerve tissue engineering, due to the addition of natural topographical cues found in the extracellular matrix. Collagen is already used in the FDA approved NGCs Neuragen ® and Neuro*flex* ™ (Kehoe *et al.*, 2012), and laminin has been shown to promote an increase in Schwann cell proliferation when coated onto tissue culture plastic and P(3HB) mats. A study by Armstrong *et al.* (2007) coated extracellular matrix proteins laminin, collagen and fibronectin onto tissue culture plastic and P(3HB) mats and concluded that laminin not only increased Schwann cell proliferation, but significantly increased the length of neurites extending from NG108-15 neuronal cells, when co-cultured with primary Schwann cells. Fibronectin was reported as having a similar effect to laminin, but collagen coatings did not increase Schwann cell attachment, or neurite length of NG108-15 neuronal cells (Armstrong *et al.*, 2007). Laminin addition mimics the extracellular matrix, providing a more native surface topography and biochemical characteristics for nerve repair, improving regenerative outcomes of the conduit (W. Daly *et al.*, 2012). However, the use of natural ECM coatings can be costly, and there is also batch to batch variation during manufacture, plus the potential to illicit an immune

response. Therefore, the use of synthetic coatings such as plasma polymers or aminosilanes offer a more scalable solution, repeatable and cheaper alternative (Chua *et al.*, 2002).

Surface functionalisation by plasma polymerisation is a controllable, reproducible technique used to alter the surface characteristics of a biomaterial, without altering the bulk properties of the material (Minati *et al.*, 2017). Plasma consists of ions, electrons, radicals, neutrons and photons in a partially ionized gas (Yasuda *et al.*, 1989). The principle behind plasma polymerisation is to use a radio frequency to ionise a plasma source into a gaseous discharge of ions and other reactive species under a vacuum (Poncin-Epaillard and Legeay, 2003). Depending on the plasma monomer and surface species used, the gas covers the biomaterial surface, creating a functionalised coating, which can indirectly influence cell attachment, and responses thereafter e.g. proliferation by controlling chemical composition (J. H. Bell and Haycock, 2012). Surface modification by plasma polymerisation is used in tissue engineering and peripheral nerve tissue engineering to improve the biocompatibility of nerve guide conduits, by the addition of coatings that improve nerve regeneration. In a study by Buttiglione *et al.* (2007) plasma coated surfaces with polyethylene terephthalate (PET), a relatively inert polymer, acrylic acid or allylamine, and cultured SH-SY5Y neuroblastoma cells upon them (Buttiglione *et al.*, 2007).

Acrylic acid coats surfaces with carboxylic groups, whereas allylamine causes an increase in surface amino groups. It was found that addition of amine groups to the PET surfaces caused an increase in SH-SY5Y cell attachment and proliferation, and that addition of carboxyl groups onto the PET surface increased SY5Y cell number - but more importantly the expression of neurofilament-200, and an increase in cell differentiation (Buttiglione *et al.*, 2007). Air plasma surface modification was used to treat PLA nerve guide conduits in a study by Ni *et al.* (2010) to graft polysaccharides and growth factors on the surface. After air plasma surface modification of PLA, conduits were grafted with either chitosan or chitosan plus gold nanoparticles to provide a change in surface microstructure, plus fibroblast growth factor 1 (FGF1). 12mm long conduits were implanted into a 10mm rat sciatic nerve defect, with 1mm overlapping each end of the conduit. Overall, addition of air plasma treated PLA conduits, with the addition of chitosan, increased the number of myelinated axons significantly. An increase in the number of blood vessels was observed, and there was a significant increase in the area of regenerated nerve, per mm^2, when comparing with air plasma treated PLA conduits grafted with chitosan when compared to the silicon control (Ni *et al.*, 2010). The study shows the promise of treating conduits with air plasma surface modification techniques, in order graft peptides and growth factors to increase the nerve regenerative properties of conduits.

As well as functionalising conduits, surface modification techniques can also be applied to internal guidance cues such as electrospun fibres fabricated from polyesters. The study by Prabhakaran *et al.* (2008) air plasma treated PCL fibres, and seeded Schwann cells onto untreated PCL fibres, air plasma treated PCL fibres, and PCL/collagen fibres, fabricated by electrospinning. Schwann cell proliferation was significantly higher on-air plasma treated PCL fibres, compared to untreated PCL fibres, confirming the addition of oxygen groups to the surface of the PCL fibres increases Schwann cell attachment and proliferation (Prabhakaran *et al.*, 2008).

Although there is much promise with regards to surface modification using plasma polymerisation as a method of coating biomaterials, there are many disadvantages to the process. Although it is a cost-effective method, compared to using ECM proteins, plasma polymerisation can sometimes be costly, due to coating under high vacuums, and upscaling the process to an industrial application would be costly (Ratner, 1992). Therefore, a simpler, more cost-effective coating technique would be advantageous on an industrial scale.

Silanization is cost effective, quick, scalable technique to introduce a reactive group to a substrate, such as glass or polymer, which changes the surface topography and surface energy (Taglietti *et al.*, 2014). Differences in surface chemistry and topography have been shown to control initial cell attachment events such as focal adhesion and integrin binding, by variations in chemistry and topography (Fawcett *et al.*, 2017). Silanes are used as a coupling agent, to attach a reactive group, such as an amine, hydroxyl or carboxylic acid reactive group, onto a substrate. Different modified silane chains can be applied to glass surfaces by dip coating, a very simple technique, to deposit an even deposition of a chemical group due to surface OH groups present on substrates such as glass (Metwalli *et al.*, 2006). Due to the simplicity of this technique to attach a reactive group to a substrate, research has been done to look at the effects different reactive groups have on different cell types, as well as looking at differences in silane chain length.

Different reactive groups have been shown to promote the differentiation of human mesenchymal stem cells down different differentiation pathways, without the need of biological supplements, such as cytokines and growth factors (Curran *et al.*, 2006). Surfaces containing an amine group ($-NH_2$) can promote human mesenchymal stem cells down an osteogenic pathway. In contrast, surfaces containing carboxyl (-COOH) groups promoted human mesenchymal stems cells down a chondrogenic pathway (Curran *et al.*, 2005). Surfaces containing methyl, hydroxyl and silane end groups maintained mesenchymal stem cell proliferation and phenotype but did not have any influence on differentiation.

Overall, amine modified surfaces are reported to have the greatest influence on viable cell attachment and proliferation. This research highlights the importance that surface chemistry, topography and energy has alone on cell attachment, proliferation and differentiation, and that differentiation can be achieved without the need of costly supplements to add to cell culture medium (Curran *et al.*, 2006). As well as the effect different reactive groups have on human mesenchymal stem cells, amine and carboxyl groups can influence primary human osteoblasts and osteoprogenitor cells (Verrier *et al.*, 2002). A study by Fawcett *et al.* (2017) confirmed that amine modified substrates increase the osteoinduction of primary human osteoblast-like cells, but that topography and surface roughness had a significant impact in the amount of calcified nodule formation and cell attachment (Fawcett *et al.*, 2017). It also confirmed that changing the silane chain length changes the surface topography and surface roughness of the modified layer, as well as the deposition of the chemical group (Verrier *et al.*, 2002).

It has also be reported that biodegradable polymers used in peripheral nerve tissue engineering, such as PLGA and PLLA, have been modified by silane modification for other applications, such as promoting chondrogenesis and osteogenesis differentiation from mesenchymal stem cells in a 2D and 3D environment (Richardson *et al.*, 2006). This highlights that silane modification is a simple technique, to apply a reactive chemical group to a substrate, polymer or glass, in a reproducible, cost effective and scalable way (Curran *et al.*, 2013). As it can be applied to biodegradable polymers, it can be a useful technique in peripheral nerve tissue engineering and nerve repair. Challenges in nerve repair using nerve guide conduits, such as a reduction in biocompatibility using synthetic materials can be overcome using silane modification to apply chemical groups that enhance and increase Schwann cell proliferation and nerve regeneration.

However, using silane modification in peripheral nerve repair has not been previously reported. Therefore, the aim of this chapter was to study aminosilane modification, and its potential value for peripheral nerve repair. Although Buttiglione *et al* .(2007) reported that the addition of amine groups to PET surfaces only enhanced cell attachment, and not SH-SY5Y cell differentiation, the use of proteins such as laminin does have a significant effect in increasing Schwann cells addition and proliferation (Armstrong *et al.*, 2007). As well as investigating the effect of amine surface modification on neuronal and Schwann cells, the effect of silane chain length was also considered. Initial studies have been shown to suggest changing the silane chain length can be used as a techniques to control the deposition of the reactive group, and it has been reported that changing the silane chain length does change the topographical profile of the modified layer (Curran *et al.*, 2011). It is hypothesised that

the addition of the aminosilanes will have an effect on NG108-15 neuronal cell adherence and differentiation, and that the chain length may have an effect on this. Glass coverslips were modified with two different aminosilane chain lengths to investigate the responses of NG108-15 neuronal cells and primary Schwann cells cultured on the different silane chain lengths. Cell viability and maturation of neuronal and Schwann cells cultured on the different silane chain lengths was investigated.

7.2 Materials and Methods

7.2.1 Preparation and modification of borosilicate glass coverslips

Coverslips were prepared as per the methods in Curran *et al.* (2005). Glass coverslips (Φ=13mm diameter, 22 x 22 mm Borosilicate Glass Co. UK) were washed with 5% sodium hydroxide solution in ultrasonic bath for 15 minutes, followed by immersed in concentrated nitric acid for 30 minutes. All the coverslips were then rinsed with ultra-pure water for 4 times, dried at 120 °C and stored in a vacuum desiccator prior to surface modification. For aminosilane modification, clean coverslips were immersed into 3% aminosilanes (SC: 3-Aminopropyl triethoxysilane; LC: 11-Aminoundecyltriethoxysilane) isopropanol solution for 2 hours, washed with toluene and isopropanol 4 times each, and then dried overnight. Control and modified glass coverslips were sterilized by washing with 70% ethanol for 30 minutes, washed 3 times with PBS (5mins) before leaving in PBS overnight to ensure the removal of contaminants. Coverslips were washed again with PBS for 5 minutes before cell culture experiments (Curran *et al.*, 2005).

7.2.2 Water contact angle measurement

Water contact angle was performed as per the methods in Curran *et al.* (2005). Dynamic contact angles of the samples in deionised purified water were measured using a Dynamic Contact Angle Tensiometer (CDCA 100, Camtel Ltd., Royston, Herts, UK) at 22 ± 0.5 °C. Briefly, two samples were tightly stuck together on the unmodified side. Each sample was immersed into the wetting solution (deionised pure water) at a rate of 0.060 mm/s. The wetting force at the solid/liquid/vapour interface was recorded by an electrobalance as a function of time and immersion depth and was converted into an advancing contact angle. The values reported for dynamic advancing angles of modified glass coverslips are mean and standard deviations of n = 4 (Curran *et al.*, 2005).

7.2.3 X-Ray photoelectron spectroscopy (XPS) for elemental analysis

X-ray photoelectron spectroscopy (XPS) was carried out as per the methods in Curran *et al.* (2005). A Kratos Axis Ultra DLD spectrometer (Kratos, Telford, UK) was used, with a monochromated AlKα x-ray (1486.6eV) source operating at a power of 150W (voltage: 15 kV, current: 10 mA). All spectra were recorded using a "slot" aperture and spectra were recorded below 5 x 10-8 Torr on three spots on each sample. A magnetic immersion lens was used to charge neutralise the samples. Binding energy (BE) positions were further charge corrected by calibrating the C-C/C-H component to 285.0 eV. A pass energy of 160 eV and 20 eV were used to record the wide energy survey spectra (1-1300 eV) and the high-resolution spectra respectively. The relative atomic % concentration (at. %), was calculated using CasaXPS version 2.3.15 software (Casa software, UK). A total of three repeats per sample were analysed. Data are reported as average values ± standard deviation (Curran *et al.*, 2005).

7.2.4 Atomic force microscopy (AFM) of aminosilane modified glass coverslips

AFM imaging was carried out as per the methods in Curran *et al.* (2005). Using a commercial AFM (NanoScope VIII MultiMode AFM, Bruker Co., Santa Barbara, CA, USA) equipped with 150 x 150 x 5 µm scanner (J-scanner). The ScanAsyst mode was applied using silicon probe (Bruker RTESPA-150A, nominal frequency of 150 kHz, nominal spring constant of 5N/m) with a scan resolution of 256 samples per line at a scan rate of 0.6Hz. 3 images of 1.4µmx1.4µm were obtained for each sample. In total, 3 separate samples per chain length were imaged. All post-image analysis was carried out using Bruker NanoScope Analysis software v1.5. Root mean square (Rq) was determined using the Particle Analysis feature within the software (Curran *et al.*, 2005).

7.2.5 NG108-15 neuronal cell culture

See chapter 2, 1.4 *Methods* section for details.

7.2.6 Isolation and culture of primary Schwann cells

See chapter 4, 4.2.7 *Methods* section for details.

7.2.7 Isolation and dissociation of dorsal root ganglion bodies

Dorsal root ganglia were dissected as per the methods in Daud *et al.* (2012). 4 week old Male Wistar rats were sacrificed in accordance with the Animal Scientific Procedures Act (1986) by an approved schedule 1 method. The spinal column was removed, and any excess tissue trimmed away. The spinal column was then cut, along the middle of the rib cage, and the spinal cord was pushed to one side, with a pair of forceps, to expose the

dorsal root ganglion bodies and the nerve roots. The dorsal root ganglia were gently pulled out of the tissue using a sharp pair of forceps, and placed into a dish of warmed F12 medium, supplemented with penicillin, streptomycin, and amphotericin B. Approximately 25-32 DRGs could be removed per spine. Using a dissection microscope, the nerve roots were trimmed from the DRG bodies, using a scalpel, and the DRG bodies were washed with sterile PBS (Daud *et al.*, 2012).

Dissociation of DRGs into primary neurons and Schwann cells was performed as per the methods by de Luca *et al.* and the PhD thesis written by Dr Juliet Bell. Explants were incubated for 1 hour at 37°C in 1.25mg/mL of collagenase in F12 medium. The medium was removed and replaced with fresh collagenase in F12 for a further 45 minutes of digestion. DRGs were incubated for 30 minutes at 37°C in 2.5mg/ml trypsin/EDTA in F12 medium. The medium was removed carefully and washed with fresh F12 medium (Juliet Bell, 2013; de Luca *et al.*, 2015). It was removed leaving around 100µL and the explants. Once the DRG bodies had settled at the bottom of the plastic universal tube, they were mechanically dissociated by aspirating them vigorously, for 5 minutes, using a glass pipette. This was repeated three times, and the mixture was filtered through a 40µm cell strainer, before being centrifuged for 1500rpm for 5 minutes. Medium was removed carefully to leave around 200µL of supernatant and the cell pellet. The cell pellet and supernatant were aspirated, using a pipette, and carefully pipetted down a premade layer of 3% bovine serum albumin (BSA) in PBS (Juliet Bell, 2013; de Luca *et al.*, 2015).

F12 medium was then added and the mixture centrifuged at 1900rpm for 10 minutes. The supernatant was removed, and the cell pellet was re-suspended in Schwann cell medium (Dulbecco's Modified Eagle Medium D-valine (PAA), supplemented with 2 mM glutamine, 10µL/mL of N2 Supplement, 5 mM forskolin, 1% FCS, 1% penicillin/streptomycin and 0.25% amphotericin B) (Juliet Bell, 2013; de Luca *et al.*, 2015). The D-valine supplemented medium inhibits fibroblast growth and to allow for primary cell attachment. 200µL of cell solution was added to each coverslip. Each spinal column was used for 9 coverslips, and the amount of medium added the cell pellet was adjusted accordingly. After 1 day in culture, medium was changed to F12 (containing 2 mM glutamine, 1% penicillin/streptomycin and 0.25% amphotericin B) supplemented with the addition of 100ug/mL (w/v) BSA, 10µL/mL of N2 and 77ng/mL of nerve growth factor (NGF). Cells were left in culture for 7 days, and medium changed at day 4 (Juliet Bell, 2013; de Luca *et al.*, 2015).

7.2.8 Immunolabelling of NG108 neuronal cells for βIII tubulin
See chapter 4, 4.2.6 *Methods* section for details.

7.2.9 Immunolabelling of primary Schwann cells for S100β, P75 NGFR and GFAP

Primary Schwann cells were labelled as per the methods in Daud *et al.* (2012). Primary Schwann cells, were also fixed with 3.7% paraformaldehyde for 20 minutes, and incubated at 4°C with either a polyclonal rabbit anti-S100β (Schwann cell marker for Schwann cell cultures, co-cultures or DRG samples) (1:250) (Dako, Denmark) a mouse monoclonal IgG1 anti-GFAP (1:250), or rabbit polyclonal IgG anti-p75NGFR antibody (1:250), diluted in 1% BSA in PBS overnight. After washing with PBS, cells were then incubated with a FITC-conjugated secondary anti-rabbit IgG antibody (1:100 dilution in 1% BSA for S100 and p75 staining) USA) and Texas Red anti-mouse IgG1 antibody (for GFAP staining) for 90 minutes. Samples were washed with PBS once, and then incubated at room temperature with 4′,6-diamidino-2-phenylindole dihydrochloride (DAPI) (Sigma Aldrich) (300 nM) for 30 minutes, to stain the cell nuclei. DAPI was removed and samples immersed in PBS for imaging with an upright Zeiss LSM 510 confocal microscope, using a helium-neon laser (543 nm) for Texas Red excitation (λex = 589nm / λem = 615 nm), an argon ion laser (488 nm) for FITC excitation (λex= 495 nm / λem = 521 nm) and a Ti:sapphire laser (800 nm) was used to image DAPI (λex= 358 nm / λem = 461 nm) for visualising nuclei (Daud *et al.*, 2012).

7.2.10 Immunolabelling of co-cultures of primary Schwann cells and neurons dissociated from dorsal root ganglion bodies

DRGs were immunolabelled as per the methods in Pateman *et al.* (2015). Primary Schwann cells and neurons were fixed with 3.7% paraformaldehyde for 20 minutes and the cells were permeabilized with 0.1% Triton X-100 for 45 minutes. Unreactive binding sites blocked with 3% bovine serum albumin (BSA) for 30 minutes and the cells were incubated, for 48 hours, with a mouse anti-β III-tubulin antibody (neuronal cell marker for NG108-15 neuronal cells and neurites) (1:250) (Promega, UK) and polyclonal rabbit anti-S100β (Schwann cell marker for Schwann cell cultures, co-cultures or DRG samples) (1:250) (Dako, Denmark) diluted in 1% BSA at 4 ºC. After a wash in PBS, cells were incubated at room temperature, for 90 minutes, with Texas Red-conjugated anti-mouse IgG antibody (1:250, Vector Labs, USA) and with a FITC-conjugated secondary anti-rabbit IgG antibody (1:250 Vector Labs USA) diluted in 1% BSA. After washing samples once with PBS, cells were incubated with 4,6-diamidino-2-phenylindole dihydrochloride (DAPI) (Sigma Aldrich) (300 nM) for 30 minutes, at room temperature. Before imaging, samples were immersed in PBS. Samples were imaged with an upright Zeiss LSM 510 confocal microscope, using a helium-neon laser (543 nm) for Texas Red excitation (λex = 589nm / λem = 615 nm), an argon ion laser (488 nm) for FITC excitation (λex= 495 nm / λem = 521 nm) and a Ti:sapphire laser (800 nm) was used to image DAPI (λex= 358 nm / λem = 461 nm) (Daud *et al.*, 2012; Pateman *et al.*, 2015)

7.2.11 Live/Dead analysis of NG108-15 neuronal cells and primary Schwann cells

See chapter 2, 2.2.6 *Methods* section for details.

7.2.12 Neurite outgrowth and primary Schwann cell morphology assessment

See chapter 4, 4.2.11 and 4.2.12 *Methods* section for details.

7.2.13 Statistical analysis

GraphPad Instat (GraphPad Software, USA) was used to perform statistical tests on data collected. One-way analysis of variance ($p < 0.05$) was conducted to analyse the differences between the data, incorporating Tukey's multiple comparisons test if $p < 0.05$. Data was reported as mean ± SD, $p<0.05$. Each experiment was performed three independent times with each sample repeated three times as n=3.

Results

7.3.1 Water contact angle

Contact angle results proved that addition of aminosilanes to the glass substrates affected the hydrophilic/hydrophobic properties of the base substrates. Both short and long chain length silanes grafted to the glass substrates and made the surfaces more hydrophobic, as shown by an increase in contact angle (Figure 7.1). This is due to the methylene (CH_2) bridges in the silane molecules.
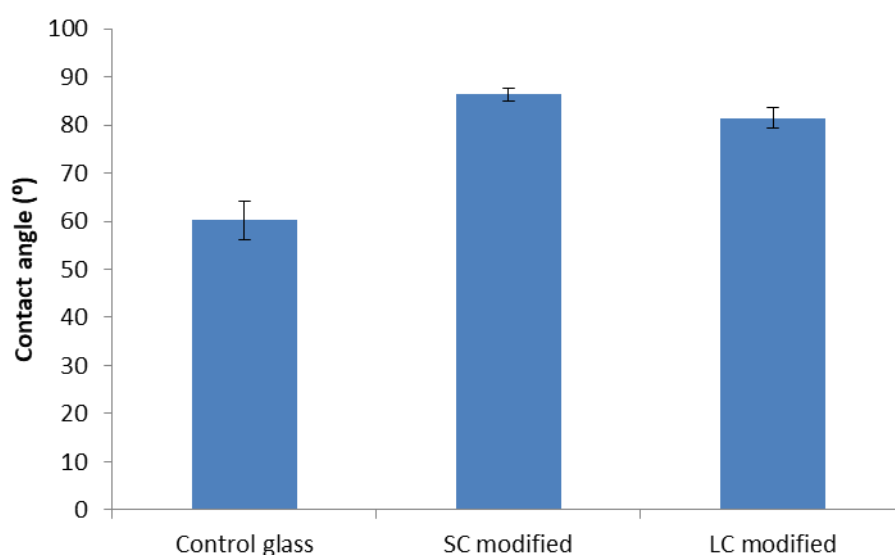

Figure 7.1. Contact angle of glass (control), short chain and long chain aminosilanes modified surfaces.

7.3.2 X-Ray photoelectron spectroscopy (XPS) for elemental analysis

Table 7.1 confirmed that all aminosilane modified surfaces were enriched with carbon and nitrogen elements and decreased silicon and oxygen contents. This result showed that aminosilanes were chemical grafted onto the glass substrates successfully.

Table 7.1. Elemental composition of surfaces by XPS characterisation.

Substrate	% Elemental Composition			
	C	Si	O	N
Glass	19.86±2.48	26.75±1.03	53.17±1.18	0
Short Chain	58.61±0.83	12.65±0.51	20.25±0.63	8.48±0.41
Long Chain	63.53±1.29	13.07±0.57	22.05±0.74	1.35±1.32

7.3.3 Atomic force microscopy (AFM) of aminosilane modified glass coverslips

AFM analysis of the modified surfaces proved that varying the chain length of silane resulted in changes in the nanotopographical profiles, most significantly with long chain modified surface. Representative AFM micrographs and associated analysis of control (unmodified glass), short chain modified and long chain modified are shown in figure 7.2. Correlation of both qualitative (figure 7.2A-C) and quantitative results (figure 7.2D) clearly shows that the topographical profiles of the substrates changed after aminosilane modification. The roughness of clean glass (unmodified control) in 1.4µm x 1.4µm area was 0.464 ± 0.001 nm; after short chain aminosilane modifications, the roughness value reduced to 0.358 ± 0.001 nm; and after long chain aminosilane modifications, it increased to 0.646 ± 0.008 nm. To analyse the uniformity / homogenous distribution of the nano features across the modified surface, the roughness of scan size from 100nm x 100nm to 1.4µm x 1.4µm from centre to outside was measured. Figure 7.2D shows that although long chain aminosilane modified surfaces were rougher, consistent roughness was achieved. For short chain aminosilane modified surfaces (and clean glass), the roughness varied over larger areas, demonstrating a patchy / heterogeneous nanotopographical profile. This was further evidenced at least qualitatively by in topography images (figure 7.2A-C). This demonstrated short chain aminosilane modified surfaces had a patchy pattern; whereas long chain aminosilane modified surfaces had a more consistent roughness. These results revealed that the long chain modified surface was much more uniform with a consistent sub-micron scale structure, compare to short chain modified surface.
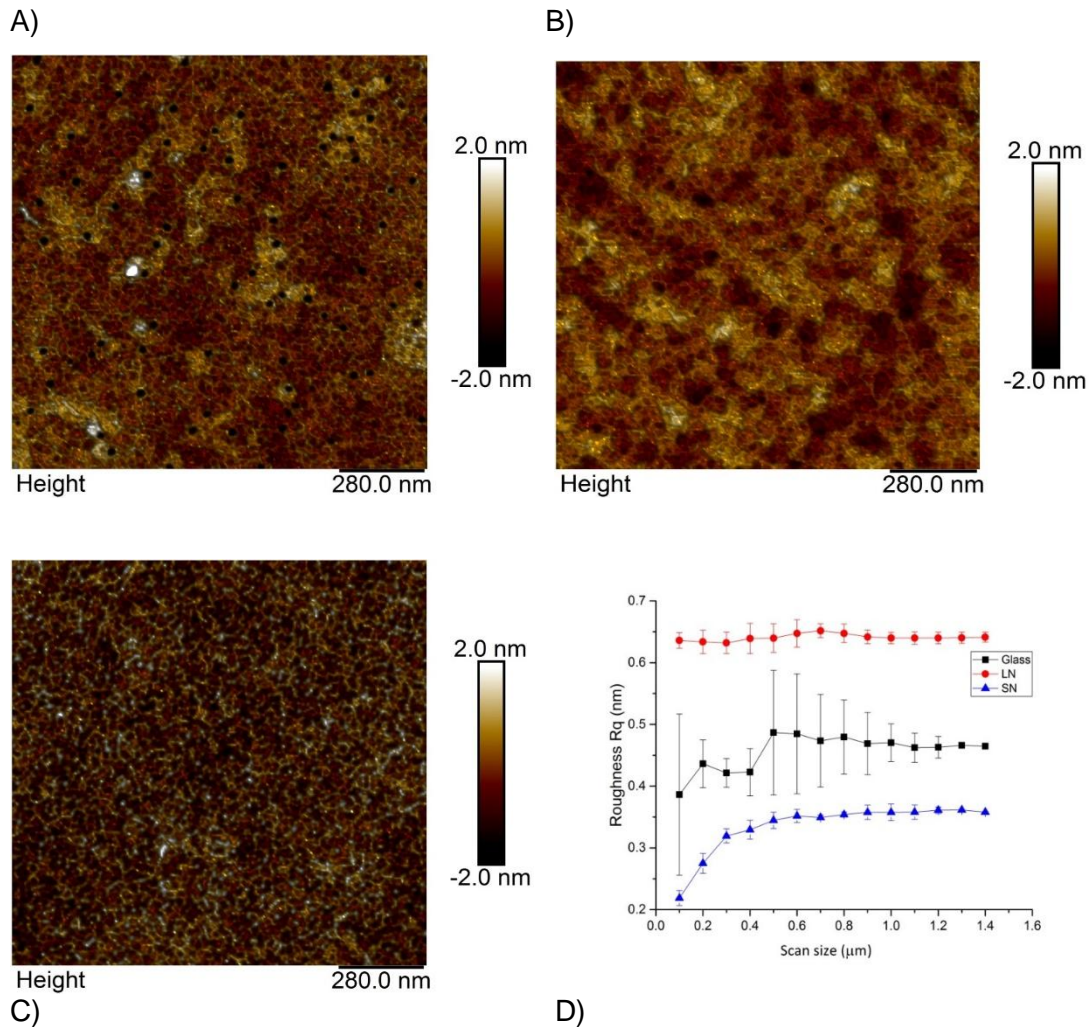
Figure 7.2. AFM analysis with scan size 1.4µm x 1.4µm. (A) Clean glass control; (B) Short chain aminosilane (SC) modified glass; (C) Long chain aminosilane (LC) modified glass. (D) The roughness of clean glass, SC and LC modified surface vs the scan size for 100nm to 1400nm.

7.3.4. The effect of different chain length modified aminosilane coverslips on NG108-15 neuronal cell differentiation

To determine whether aminosilanes could support neuronal cell growth, NG108-15 neuronal cells were cultured on plain glass controls, short, and long chain modified aminosilane coverslips for 6 days, and immunolabelled against βIII tubulin (red) to confirm and visualise neurite outgrowth, and the cell bodies labelled with DAPI (blue). Representative confocal images (figure 7.3) shows that modified aminosilane surfaces supported growth of NG108-15 neuronal cells, as well as maturation. Visually, higher numbers of neurites, and longer neurites could be seen by neuronal cells cultured on long chain modified aminosilane coverslips, compared to the short chain modified coverslips.
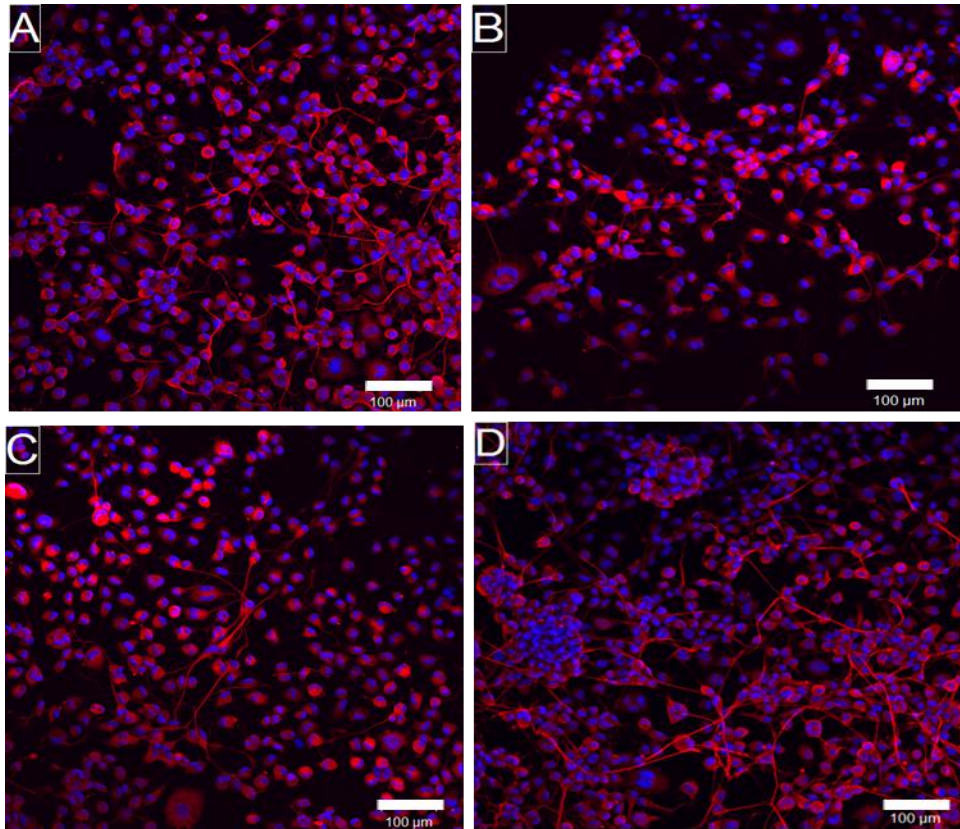
Figure 7.3. Confocal microscopy images of NG108-15 neuronal cells immunolabelled against β III tubulin (red) and cell nuclei (blue). Cells were stained after 6 days in culture on A) plain glass coverslips, B) short chain aminosilane modified glass coverslips, C) Long chain aminosilane modified glass coverslips, and D) Tissue culture plastic control. From confocal images average neurite length, average number of neurites per neuron, and the percentage of neurite bearing cells was determined. Scale bar= 100µm.

Figure 7.4A shows that NG108-15 neuronal cells cultured on long chain modified aminosilane coverslips had the highest percentage of cells bearing neurites (73.56 ± 12.16%) followed by the short chain modified aminosilane coverslips (68.22 ± 15.57%). The percentage of neuronal cells growing neurites on the plain glass control and the tissue plastic controls were 67.98 ± 10.52% and 61.75 ± 8.80% respectfully. Figure 7.4B calculated the average number of neurites growing per neuron to observe a relationship between aminosilane length and neurite outgrowth. The highest average number of neurites, per neuron, was detected on neuronal cell cultured on long chain modified aminosilane coverslips followed by cells cultured on the plain glass control, 1.58 ± 0.06 and 1.47 ± 0.09 respectively. The average number of neurites per neuron detected on the long chain aminosilane modified coverslips was significantly higher than the average number of neurites detected on cells cultured on short chain aminosilane modified coverslips and the tissue culture plastic control, 1.42 ± 0.05 and 1.31 ± 0.09 neurites per neuron respectfully. This does confirm a relationship between aminosilane chain length and NG108-15 neuronal cell differentiation and maturation.

From confocal microscopy image data (figure 7.3), the highest average neurite length was found to be on NG108-15 neuronal cells cultured on the tissue culture plastic control, followed by the long chain modified aminosilane coverslips, 117.02 ± 9.12µm and 98.58 ± 5.51µm respectively. Statistical analysis confirmed significant differences between average neurite lengths on the tissue plastic control versus long chain and small chain modified aminosilane coverslips, and the plain glass control. Significant differences were detected between average neurite lengths on the long chain aminosilane modified coverslips, versus the short chain modified aminosilane coverslip and the plain glass control. The average neurite length of neurites measured on the plain glass control and the short chain aminosilane modified coverslips were 77.08 ± 5.60µm and 71.80 ± 6.49µm respectively. The increase in average neurite length confirms that the addition of aminosilanes onto glass substrates is correlated with an increase in neurite length. The long chain aminosilane was more effective than the short chain aminosilane. This could be due the increase in hydrophilicity of the long chain aminosilanes, compared to the short chain aminosilanes (figure 7.1). Long chain aminosilanes are also rougher, with a homogenous coating compared to the short chain aminosilanes (Figure 7.2D).
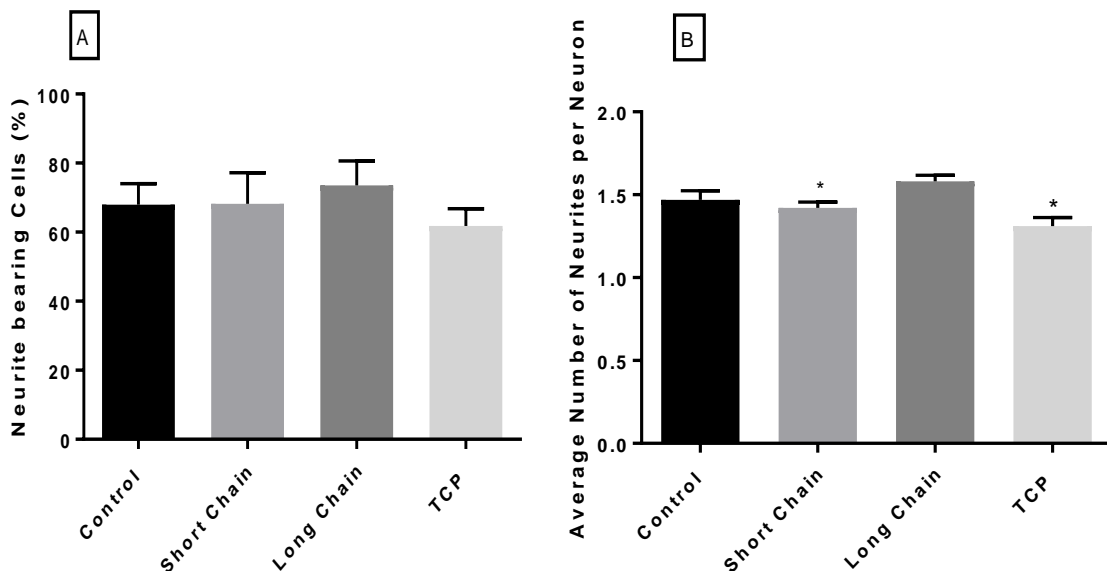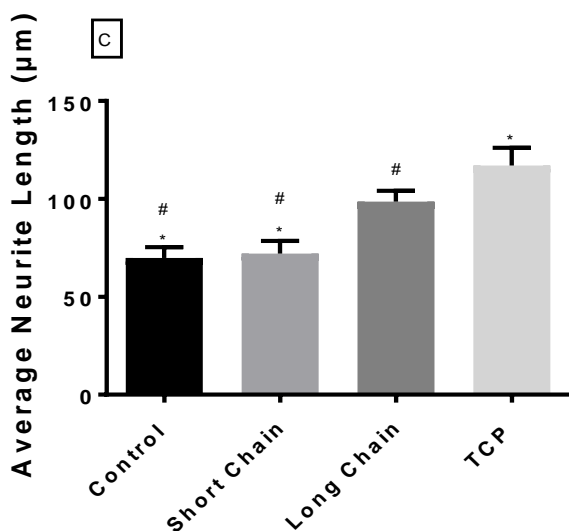
Figure 7.4. Analysis of NG108-15 neuronal cell differentiation studies on different chain length aminosilane modified glass coverslips, plain glass and tissue culture plastic control. A) The percentage of neurite bearing NG108-15 neuronal cells after 6 days in culture. B) The average number of neurites expressed per neuron. A one way anova with Tukey's multiple comparisons tests was used to analyse data (mean ± SD, n=3 *p<0.05 against long chain. C). The average neurite length per condition after 6 days in culture. A one way anova with Tukey's multiple comparisons tests was used to analyse data (mean ± SD, n=3 *p<0.05 against long chain, # p<0.05 against TCP). 100 neurites per condition were measured, using Image J, to determine the average neurite length. For graphs B) and C), each cell per field of view was counted for the sample. (Mean ± SD, n=3 independent experiments p<0.05)

7.3.5. NG108-15 neuronal cell viability on modified aminosilane coverslips

Figure 7.5 shows representative micrographs of NG108-15 neuronal cells cultured onto short and long chain aminosilane modified coverslips, plain glass control and tissue culture plastic. Visually, higher numbers of live cells can be seen on long chain aminosilane modified coverslips, and the plain glass control, compared to the short chain aminosilane modified. Images were quantified to determine the total number of live and dead cells cultured on the different conditions, as well as cell viability as a percentage of live versus dead cells. Figure 7.6 shows that the highest number of live cells were seen on the tissue culture plastic control, followed by the plain glass control, 580.78 ± 190.31 cells and 323.37 ± 52.66 cells respectively. The numbers of live cells on the short and long chain aminosilane modified coverslips were 268.07 ± 16.23 and 288.89 ± 66.74 cells respectively. No significant differences were detected between samples. Cell viability was expressed as a percentage, in which all samples had a cell viability higher than 95%. Cell viabilities were 96.75 ± 1.65%, 98.34 ± 0.23%, 95.71 ± 1.44% and 98.57 ± 0.93% for the plain glass control, short and long chain aminosilane modified coverslips, and the tissue culture plastic control. No significant differences were detected between conditions. This confirms that all samples were biocompatible, and supported the growth of NG108-15 neuronal cells. This also potentially shows that the addition of aminosilanes, does not have a significant affect in NG108-15 neuronal cell proliferation, compared to the other surfaces, but that there is an affect on NG108-15 neuronal cell maturation and differentiation.
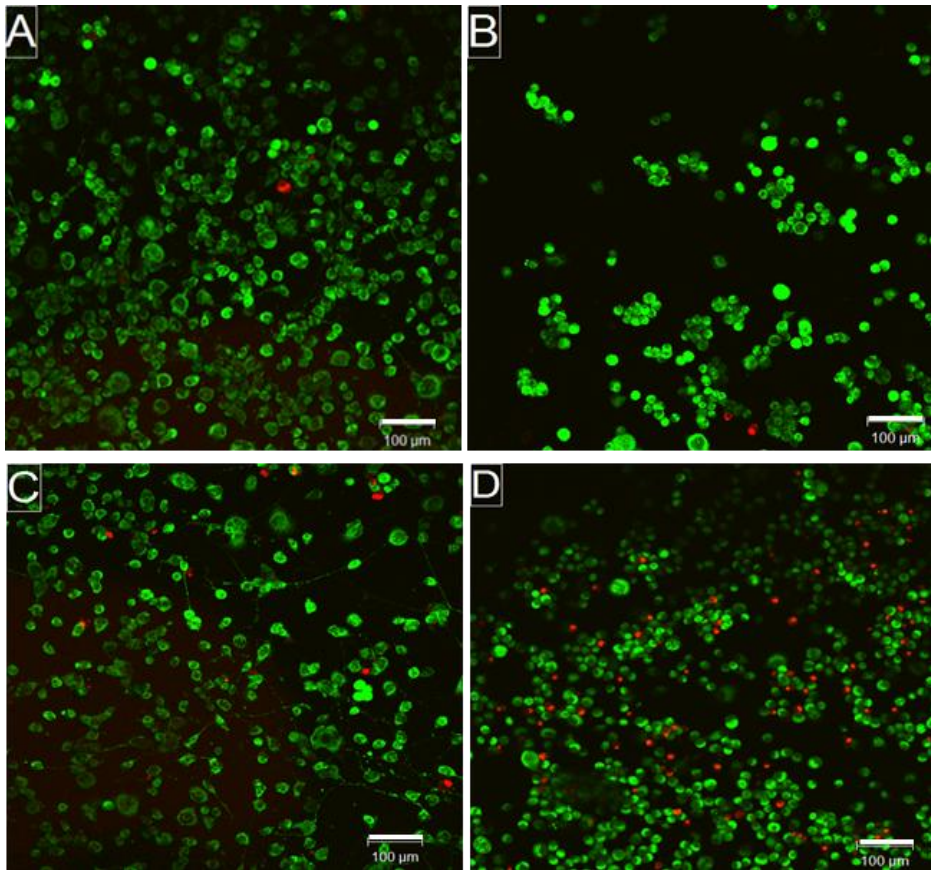
Figure 7.5. Confocal micrographs of the live/dead assay to assess cell viability. Green cells represent live cells, and red cells represent dead cells. NG108-15 neuronal cells were cultured on A) plain glass coverslips, B) short chain aminosilane modified coverslips C) long chain aminosilane modified coverslips and D) tissue culture plastic control. Scale bar = 100μm.
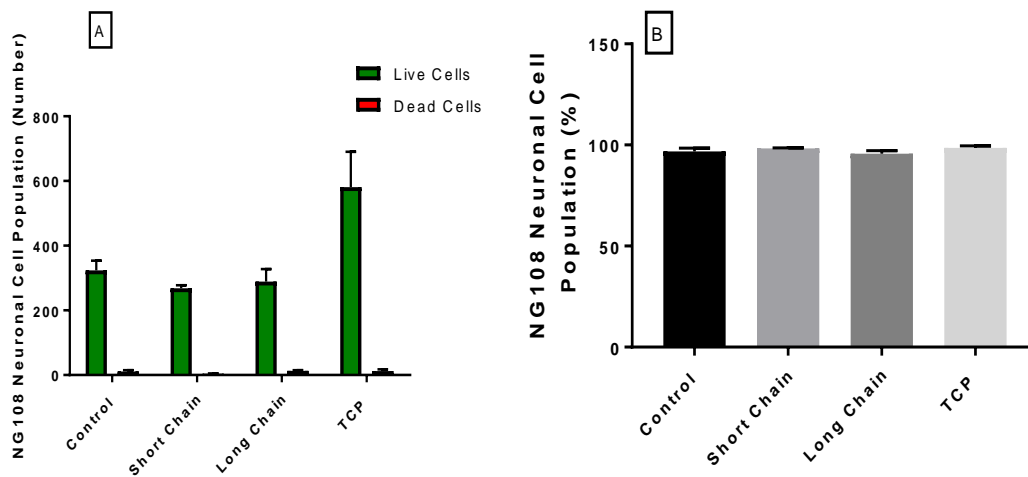
Figure 7.6. Live/dead analysis of NG108-15 neuronal cells cultured on different aminosilane modified glass coverslips and controls. A) Number of live cells against dead cells per sample and B) live/dead analysis expressed as a percentage. A one way anova with Tukey's multiple comparisons tests was used to analyse data (Mean ± SD, n=3 independent experiments P< 0.05)

7.3.6. Primary Schwann cell culture on modified aminosilane coverslips

Primary Schwann cells were cultured onto different chain length aminosilane modified glass coverslips for 7 days, before being immunolabelled against S100β, p75 and GFAP. Figure 7.7 shows that all cells stained positively for the various proteins, and that visually, lower numbers of Schwann cells could be seen on the plain glass control, compared to the aminosilane modified coverslips and the tissue culture plastic control. The presence of healthy Schwann cells is confirmed by the positive staining of S100β, and the presence of putative Schwann cells, by the positive staining of P75 (Zilic *et al.*, 2015). Schwann cells stained positively for GFAP after 7 days in culture on different modified aminosilane coverslips and the positive staining of all three Schwann cell markers confirmed a maintained phenotype (Chew *et al.*, 2008).

7.3.7. The effect of different chain length aminosilanes on the phenotype of primary Schwann cells

To confirm a maintained phenotype quantitatively, the average cell length, of Schwann cells cultured onto the different aminosilane modified surfaces, was determined. No significant differences detected between data sets and Schwann cells cultured on the aminosilane modified coverslips had longest average Schwann cell lengths, 87.5 ± 9.76µm and 83.4 ± 15.68µm, on the long and short chain aminosilane coverslips. This was compared to the plain glass and tissue culture plastic control, which had average Schwann cell lengths of 79.17 ± 13.41µm and 74.13 ± 10.89µm (figure 9). A longer thinner Schwann cell length indicated a maintained cell phenotype and retaining function. This indicates that the aminosilane groups supported Schwann cell growth and function and did not cause a loss of viability.
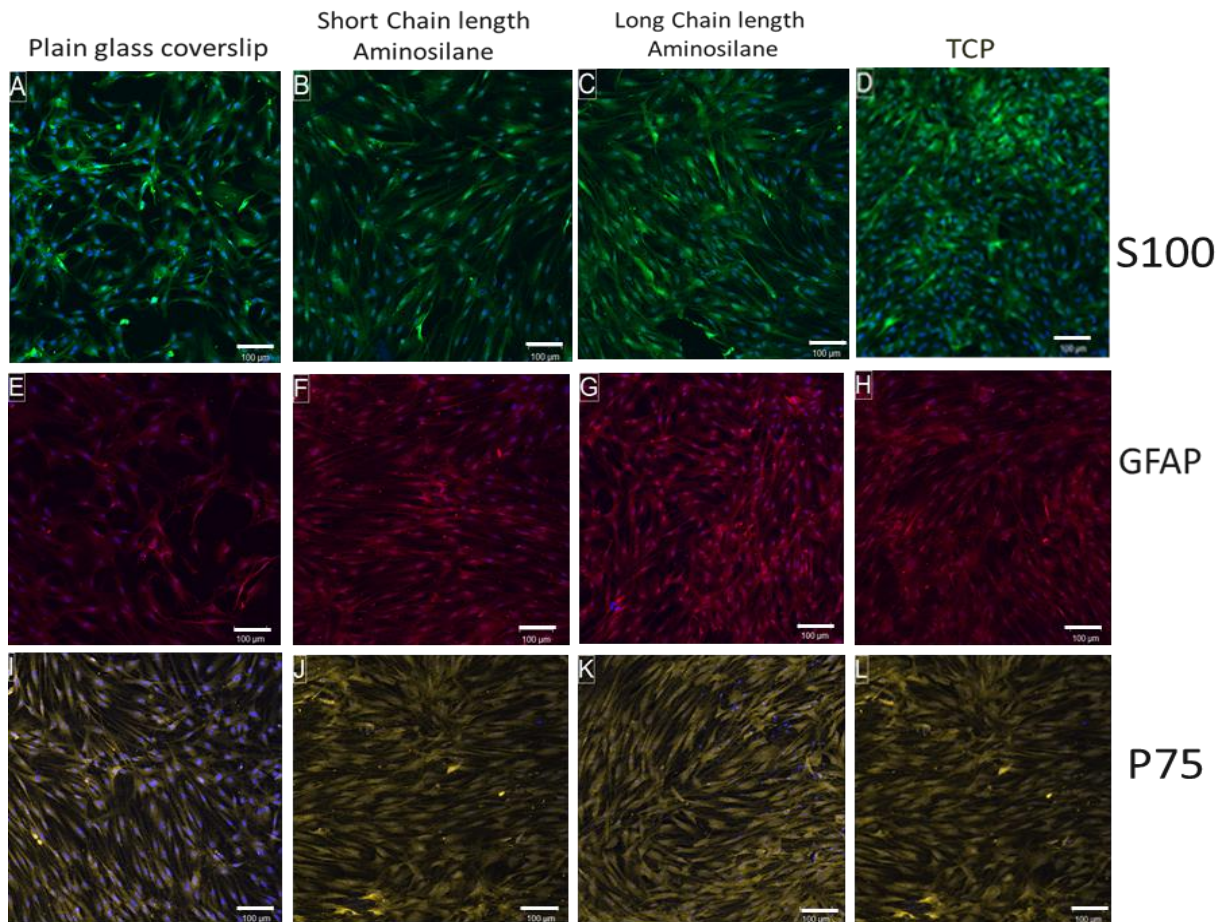
Figure 7.7. Confocal microscopy images of primary Schwann cells immunolabelled for S100β (green), GFAP (red) and P75 (yellow) after 6 days of culture on different chain length aminosilane modified glass coverslips. Schwann cells were stained for S100β on A) plain glass coverslips B) short chain aminosilane modified coverslips C) long chain aminosilane modified coverslips and D) tissue culture plastic control, stained for GFAP on E) plain glass coverslips F) short chain aminosilane modified coverslips G) long chain aminosilane modified coverslips and H) tissue culture plastic control and P75 on I) plain glass coverslips J) short chain aminosilane modified coverslips K) long chain aminosilane modified coverslips and L) tissue culture plastic control. Schwann cells were immunolabelled against these proteins to confirm maintained Schwann cell phenotype.
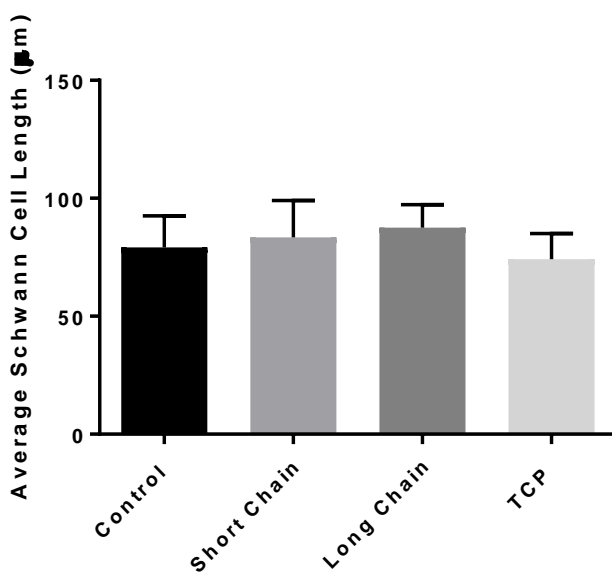
Figure 7.8. To determine maintained Schwann cell phenotype, an average of 300 Schwann cell lengths, per condition, was measured tip-tip using Image J. A one way anova with Tukey's multiple comparisons tests was used to analyse data (mean ± SD, n=3 independent experiments). No significant difference was detected between sample conditions.

7.3.8. Primary Schwann cell viability modified aminosilane coverslips

Figure 7.9 shows confocal micrographs of primary Schwann cells cultured on different aminosilane modified coverslips, as well as the plain glass and tissue culture plastic controls. Visually, there are slightly lower numbers of Schwann cells on the plain glass control compared to the aminosilane modified coverslips, and that the highest cell numbers can be seen on the tissue culture plastic. These images were quantified, to determine the average live and dead cell number, per field of view, and then determined for percentage cell viability. Figure 7.10A shows that highest live cell number was on tissue plastic control, followed by the long chain aminosilane modified coverslip, 348.67 ± 55.31 and 396 ± 101.68 cells. The average number of live cells detected on the plain glass control and the short chain aminosilane modified coverslips were 299.92 ± 55.51 and 306.18 ± 68.96 cells. No significant differences were detected between samples. When the numbers of live and dead cells were expressed as a percentage of cell viability (figure 7.10B) the percentage of live cells on the short and long chain aminosilane modified coverslips was 97.15 ± 0.66 and $98.57 \pm 0.56\%$. The percentage of live cells on the plain glass and tissue culture plastic controls were $98.3 \pm 0.77\%$ and $95.67 \pm 0.76\%$. No significant differences were detected between samples. This confirmed that addition of aminosilanes to plain glass improved primary Schwann cell attachment and proliferation, and that the coatings were biocompatible. Small numbers of dead cells were detected on all samples, which indicated that the aminosilane coatings were causing detrimental effects during the time in cell culture.
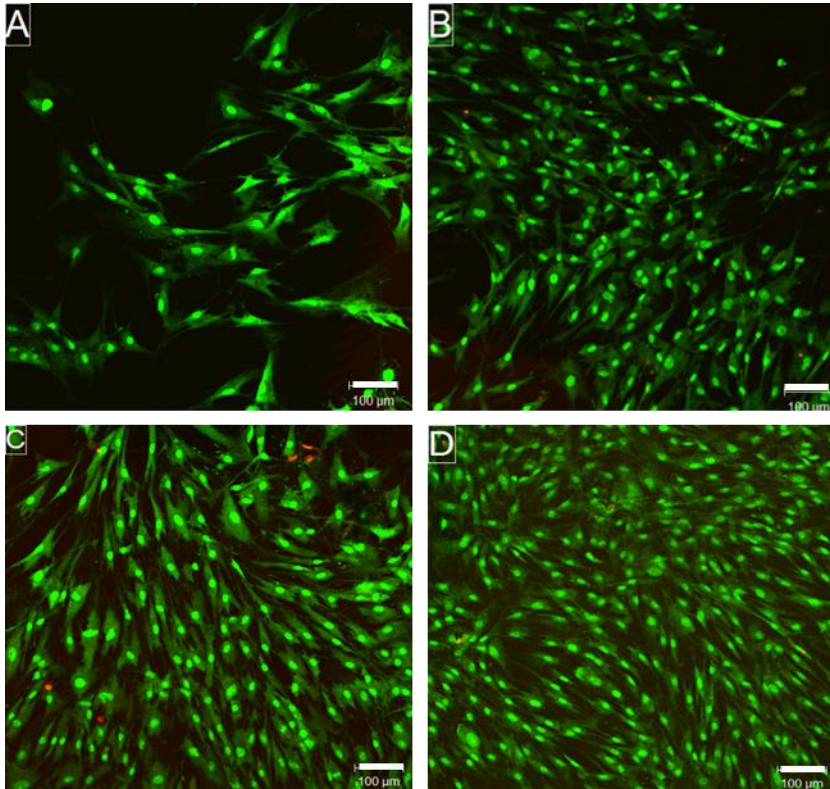
Figure 7.9. Confocal micrographs of live/dead analysis of rat primary Schwann cells. Green cells represent live cells, and red cells represent dead cells. A) Plain glass coverslips, B) short chain aminosilane modified coverslips, C) long chain aminosilane modified coverslips and D) tissue culture plastic control. Scale bar = 100µm.
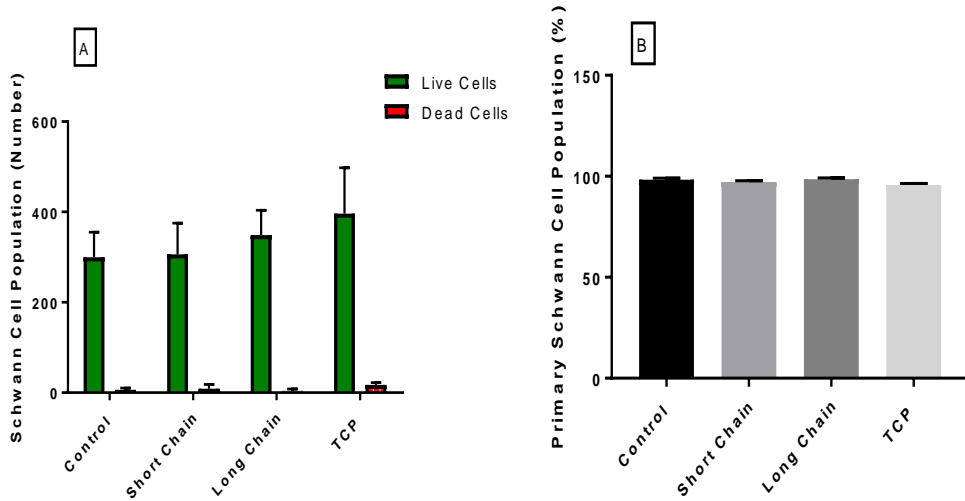
Figure 7.10. Live/dead analysis of rat primary Schwann cells cultured on different aminosilane modified glass coverslips and controls. A) Number of live cells versus dead cells per sample and B) live/dead analysis expressed as a percentage. A one way anova with Tukey's multiple comparisons tests was used to analyse data (Mean ± SD, n=3 independent experiments $P < 0.05$).

7.3.9 Primary neuron and Schwann cell co-cultures derived from dissociated dorsal root ganglion bodies

Figure 7.11 shows confocal micrographs of primary neurons (red) and Schwann cells (green) cultured on different modified aminosilane surfaces. Visually, there were higher numbers of primary Schwann cells, which were more spread out on aminosilane modified surfaces, versus tissue culture plastic control or plain glass coverslips.

There was a higher number of primary neurons on long chain aminosilane modified surfaces, and higher numbers of neurites per neuron. Figure 7.12A shows a statistically higher number of neurites present per neuron by primary neurons cultured on short and long chain aminosilanes, compared to plain glass control (*p<0.05 against plain glass control). An average of 4.66 ± 0.52 neurites and 4.51 ± 0.40 neurites per neuron cultured on the long chain and the short chain aminosilanes. 3.28 ± 0.38 neurites and 4.23 ± 0.52 neurites were extended per neuron cultured on plain glass and tissue culture plastic control surfaces. Interestingly, the average number of neurites per NG108-15 neuronal cell body was significantly higher on long chain aminosilanes, compared to those cultured on short chain aminosilane surfaces, or tissue culture plastic control (figure 7.4B).

Figure 7.12B also shows that the average length of neurites cultured on the long chain aminosilanes was significantly higher (246.68 ± 9.97μm) than average neurite lengths of neurites on plain glass control, the tissue culture plastic control or short chain aminosilane surfaces (207.15 ± 8.61μm, 199.33 ± 8.61μm and 220.30 ± 10.88μm respectively; *p<0.05 against long chain aminosilane). This suggests that the addition of aminosilanes to plain glass coverslips, significantly improves the attachment of primary neurons and Schwann cells to surfaces, and that the long chain aminosilanes supports primary neuron differentiation, resulting in an increased neurite length. The increase in Schwann cell number was associated with an increase the number of neurites expressed per neuron, and average neurite length.

The number of primary neurons and Schwann cells per field of view (841μm x 841μm) was assessed to determine the effect of aminosilanes on primary cell attachment, proliferation and differentiation. Although higher numbers of neurons and Schwann cells were detected on long chain aminosilane modified coverslips (549.72 ± 89.78 Schwann cells and 32.11 ± 6.97 neurons), no significant differences were detected between data sets. An average number of 452.33 ± 95.83, 461.05 ± 93.45 and 584.33 ± 64.68 Schwann cells per field of view were detected on plain glass, short chain aminosilane modified coverslips and the tissue culture plastic, and an average of 20.88 ± 6.41, 26.78 ± 7.35 and 28.05 ± 6.07

neurons per field of view, were detected on the plain glass, short chain aminosilane modified coverslips and the tissue culture plastic. This confirms that aminosilane modified surfaces enhance primary neuron and Schwann cell attachment, maintained Schwann cell proliferation and neuron differentiation on glass coverslips *in vitro*. Overall, figures 7.11 and 7.12 show that although the addition of aminosilanes to substrates enhanced primary neuron and Schwann cell attachment and maintained proliferation and can be applied to nerve guide conduits to encourage nerve regeneration.
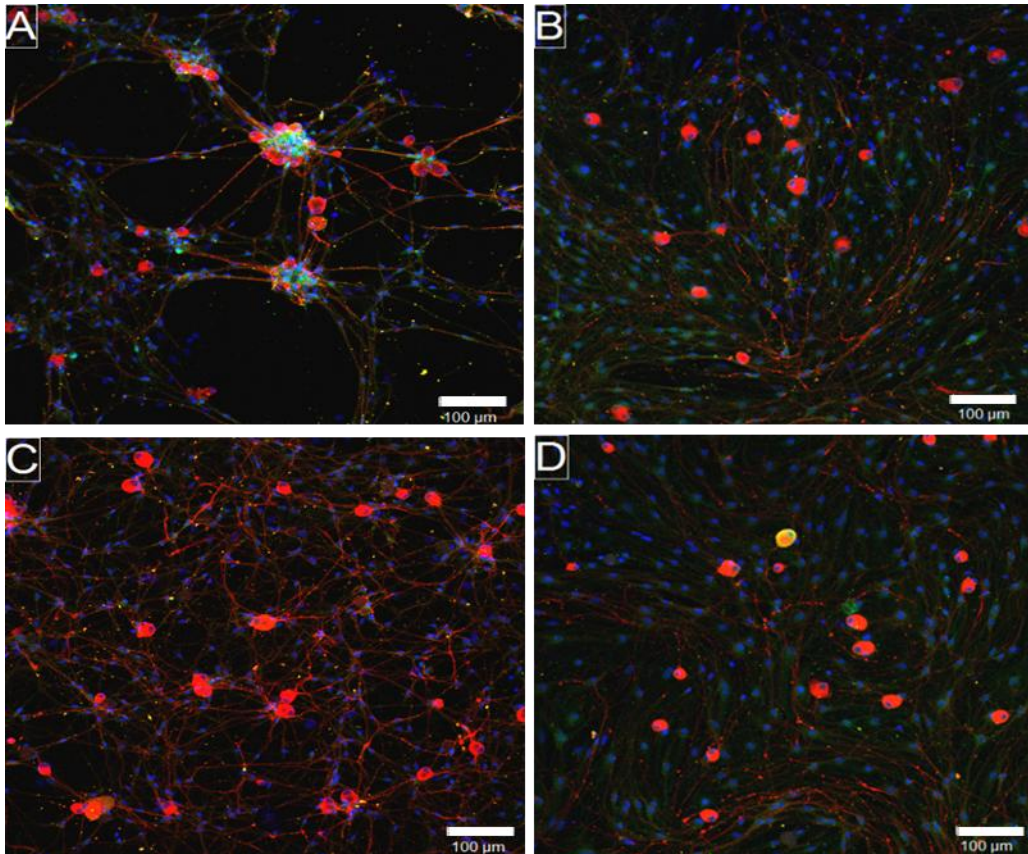
Figure 7.11. Confocal micrographs of primary neurons and primary Schwann cells, dissociated from dorsal root ganglion bodies, and immunolabelled against β-III tubulin (red-neurite marker) cell nuclei (blue) and S100β (green-Schwann cell maker). Cells were stained after 6 days in culture on A) plain glass coverslips, B) short chain aminosilane modified glass coverslips, C) long chain aminosilane modified glass coverslips, and D) tissue culture plastic control. From confocal images, average neurite length, average number of neurites per neuron, total number of primary neurons, and total number of Schwann cells was determined. Scale bar = 100μm.
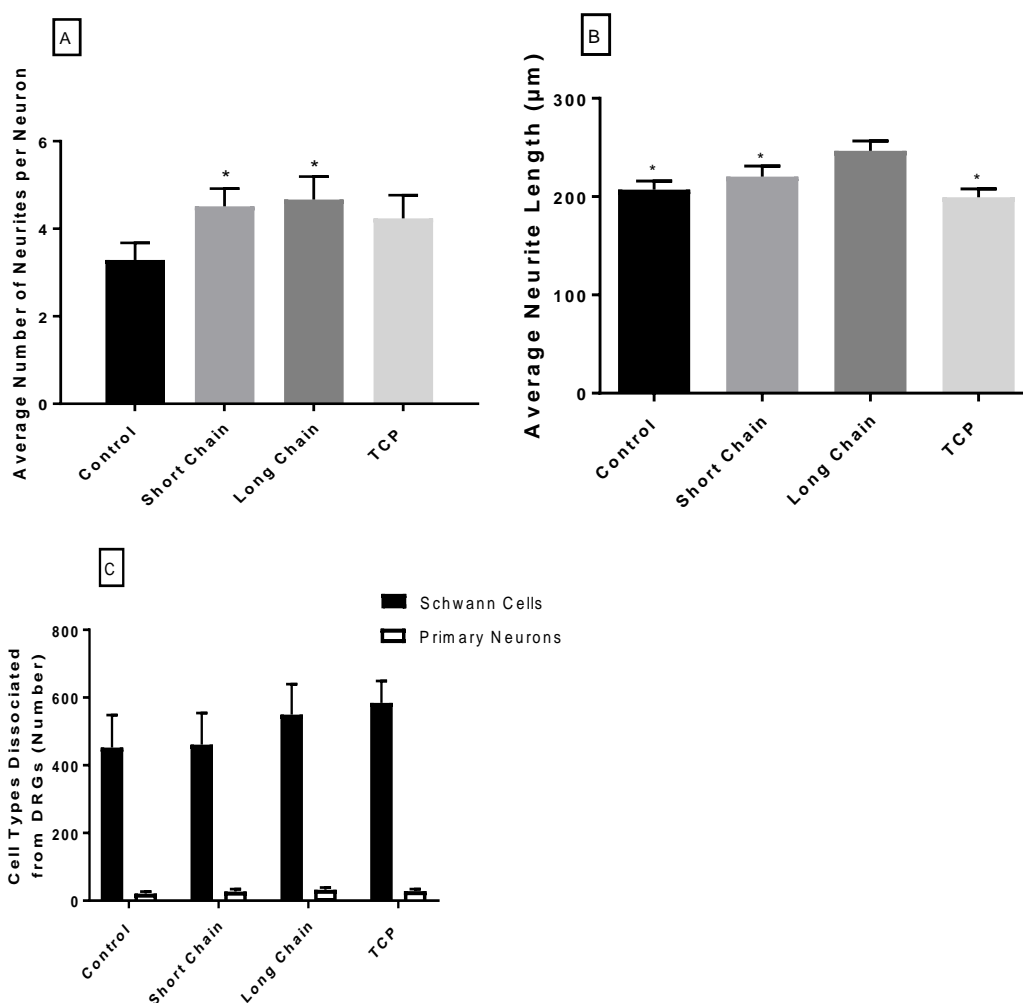
Figure 7.12. Analysis of primary neurons and Schwann cells, dissociated from dorsal root ganglion bodies, cultured on different chain length aminosilane modified glass coverslips, plain glass and tissue culture plastic controls. A) The average neurite length per condition after 7 days in culture. A one way anova with Tukey's multiple comparisons tests was used to analyse data (mean ± SD, n=3 *p<0.05 against plain glass control). 100 neurites per condition were measured, using Image J, to determine the average neurite length. B) The average number of neurites expressed per neuron. A one way anova with Tukey's multiple comparisons tests was used to analyse dat a (Mean ± SD, n=3 *p<0.05 against long chain. No statistical differences were detected between different conditions. C) The percentage of neurite bearing NG108-15 neuronal cells after 6 days in culture. For C), each cell type per field of view was counted. A one way anova with Tukey's multiple comparisons tests was used to analyse data (Mean ± SD, n=3 independent experiments p<0.05). No statistical differences were detected between data.

7.4 Discussion

Previous work has demonstrated that silane modification is a useful tool to apply a reactive group, such as an amine group, to a substrate, to enhance the biological properties of the substrate. The addition of silane chains and reactive groups, can mimic the extracellular matrix, by changing the surface nano-topography, energy and chemistry of the substrate, providing a biological surface to enhance initial cell attachment and maintain cell proliferation (Fawcett *et al.*, 2017). The use of silane modification, to coat glass substrates and biodegradable polymers is well documented and has many advantages over conventional techniques such as plasma polymerisation (Fawcett *et al.*, 2017). Overall, using NG108-15 neuronal cells, primary neuron and Schwann cells show that potential use of aminosilanes

as a coating for nerve guide conduits may enhance biocompatibility and neuro-regenerative properties.

Following data from NG108-15 neuronal cells and primary Schwann, the response of a neuronal primary co-culture to aminosilane surfaces was investigated. Dorsal root ganglion bodies were dissociated to give a co-culture of primary neurons and primary Schwann cells. Neurite outgrowth from NG108-15 neuronal cells, and primary neurons, significantly increases, when cultured on the long chain aminosilane. It was also noted that primary Schwann cells were in close proximity to neurite outgrowth, from primary neurons, corresponding to the reported literature on nerve regeneration, as neurite outgrowth is guided by the bands of Bünger (Zilic *et al.*, 2015). This shows that the dissociation DRG model is a useful pre-*in vivo* assessment tool for nerve injuries and highlights the importance of using a primary cell types rather than immortal cell lines for the investigation of materials to be considered for use in peripheral nerve repair.

Long chain aminosilanes have been shown to promote the differentiation of neuronal cells to extend a higher number of neurites per neuron, and cause neurites to grow longer (figure 7.12). This could be due to the more hydrophilic properties of the long chain aminosilanes, compared to the short chain aminosilanes, as seen in figure 7.1. Figure 7.2 also confirms that the topography of long chain aminosilanes is much rougher than the plain glass substrates and the short chain aminosilane modified coverslips, and that the coating has been applied in a homogenous consistent manner. Short chain aminosilanes displayed a patchy/heterogeneous topographical profile which may explain why the coating was not as efficient in supporting neuronal cell differentiation compared to the long chain samples. XPS and AFM were chosen as surface characterisation techniques due to looking at the aminosilanes at the sub-micron level, observing the surfaces at the level of initial cellular interactions (Curran *et al.*, 2006). An increase in protein adsorption has also been shown to be controlled by rougher surface topography due to a larger surface area, and this has an effect of initial cell adhesion, but also NG108-15 and primary neuronal cell differentiation (Anselme *et al.*, 2010). It has also be reported that surface chemistry and rougher surface topographies adsorb albumin, the main protein in foetal calf serum, more effectively than smoother surfaces (Lukasiewicz *et al.*, 2018)

It has been documented that silane chain length can be used as a method to control the deposition of the reactive chemical group and differences in chain length can have an effect on the nanotopographical profile of the additive coating, which has been seen in this study (Fawcett *et al.*, 2017). This study has also confirmed that the addition of aminosilanes to substrates does not have any adverse effects on primary Schwann cells, and that amine

groups enhance Schwann cell attachment and proliferation. Primary Schwann cells maintained their phenotype on all of the substrates, confirmed by the positive staining of Schwann cell markers S100β, GFAP and P75. Schwann cells maintained elongated phenotypes as seen in figure 7.8. Although there wasn't a significant effect on primary Schwann cells response, the addition of aminosilanes did have a neuro-regenerative effect on the neuronal cell types and both aminosilanes were deemed biocompatible from cell viability assays. Overall, the addition of the long chain aminosilane to substrates has been shown to have a neuro-regenerative affect, encouraging primary neuron differentiation and maturation. The addition of the long chain aminosilane to the glass coverslips, enhances the attachment of primary Schwann cells, and neurons, and facilitates Schwann cell proliferation, maintaining phenotype. It has been demonstrated that aminosilanes can be grafted onto glass coverslips in a reproducible, simple and cost effective way, and previous research suggests that silane modification can be used to graft amine groups to the surfaces of nerve guide conduits, or onto polymer internal fillers, to encourage nerve regeneration.

Chapter 8: Gyration, a scalable method of Polyhydroxyalkanoate processing for rapid production of scaffolds for Peripheral Nerve Repair

8.1 Introduction

Electrospinning is a popular and versatile technique to fabricate random and aligned microfibers, or nanofibres, for many different applications in tissue engineering (Bye *et al.*, 2012). It is an established technique to fabricate tissue engineered scaffolds, as a temporary device, to aid regeneration by mimicking the extra cellular matrix and increasing cell attachment, proliferation and differentiation. The concept is that nanofibres of certain diameters mimicking fibrils found in the ECM (Bhardwaj and Kundu, 2010). Electrospun tissue engineered scaffolds can be fabricated using many different natural or synthetic polymers, with different growth factors, proteins or drugs added to the polymer solution before spinning, to create carrier scaffolds (Pham *et al.*, 2006). Electrospun scaffolds have been researched for use in peripheral nerve repair, to fabricate polymer microfibers and nanofibres to aid nerve regeneration. Electrospun fibres have been used in peripheral nerve repair as use as porous nerve guide conduits (nanofibers) or as guidance cues for the regenerating axon, using microfibers (Huang *et al.*, 2015). As reported in chapters 4, 5 and 6, fibre diameter and alignment are crucial parameter in peripheral nerve repair, as both parameters effect the efficiency of nerve regeneration and Schwann cell attachment (Daud *et al.*, 2012).

Although electrospinning is a widely used technique in research applications, there are still disadvantages associated with the technique, as well as difficulties in upscaling for industrial applications. Due to the production of a single fiber from the end of the syringe/nozzle, only small quantities of fibres can be fabricated, and upscaling this would not be cost effective (Bhardwaj and Kundu, 2010). Electrospinning also requires a high voltage throughout scaffold fabrication, which can increase manufacture costs. Therefore other fibre fabrication methods, such as centrifugal spinning and pressurized gyration, offer advantages over electrospinning due to avoiding the use of high voltages, the ease of scale up, as well as the fabrication of large quantities of fibres (Shanfeng Wang and Cai, 2010). Centrifugal spinning relies on a centrifugal force to fabricate fibres in a rotary mold, as the rotational forces causes the polymer solution to form fibres. Fibres can be formed from different polymers and there are less parameters to consider compared to electrospinning (Loordhuswamy *et al.*, 2014). The principles of centrifugal spinning have been applied to a novel pressurized

gyration set up which has been developed by Professor Mohan Edirisinghe and Dr Suntharavathanan Mahalingam, at The Department of Mechanical Engineering, University College London (Mahalingam and Edirisinghe, 2013). Nanofibres, microfibres, microbeads and microspheres can be fabricated, using pressurized gyration, from various different polymers, in the process uses a combination of centrifugal spinning and solution blowing (Mahalingam and Edirisinghe, 2013). The set up consists of a rotary cylindrical drum containing holes around the middle of the axis, which is connected to a motor at one end and a gas valve at the other (see figure 7.1 for diagram). By rotating the drum at different speeds, and applying nitrogen gas under different pressures polymer fibres can be fabricated by adding polymer solutions of different concentrations into the drum and extruding the fibres out of the holes (Raimi-Abraham *et al.*, 2014). Under ambient temperatures, the solvent usually evaporates and the fibres collected on a plate. Compared to electrospinning, there are less parameters involved in the process, including polymer concentration, speed of the rotating drum, pressure of the gas applied and the distance of the collector from the holes in the drum (Mahalingam and Edirisinghe, 2013).

Pressurized gyration rigs are being used to fabricate a range of different polymer nanofibres for use in many applications in tissue engineering. Raimi-Abraham *et al.* (2015) has used pressurized gyration to fabricate poly(N-vinylpyrrolidone) (PVP) containing different concentrations of ibuprofen for potential use in controlled rate oral administration (Raimi-Abraham *et al.*, 2015). It has also been used to fabricate nanofibre blends of carboxymethylcellulose, sodium alginate and polyacrylic acid with polyethyleneoxide for use in topical/mucosa drug delivery (Brako *et al.*, 2015). More recently, pressurized gyration has been used to fabricate fibres of polycaprolactone (PCL), a polymer used in peripheral nerve repair. Hong *et al.* (2016) dissolved different concentrations of PCL into acetone, varying the speed of the rotating drum and the pressure of the gas applied in order to determine which parameters resulted in fibres versus beads (Hong *et al.*, 2016). Pressurized gyration has also been used to fabricate PCL scaffolds containing silver nanoparticles for use in antimicrobial applications (Xu *et al.*, 2016). However, the technique has not been used to fabricate scaffolds from polyhydroxyalkanoates. Centrifugal spinning has been used to fabricate nano and microfibres from PHBV and P(4HB) (Upson *et al.*, 2017). There has been success fabricating PHA fibres, though diameters above 3µm have not been produced, nor have aligned fibres been produced, required for use in peripheral nerve repair.

In this chapter, the use of gyrated PHA fibres for nerve tissue engineering has been investigated. 6µm fibres of P(3HB) and 19µm fibres of P(3HB):P(3HO-co-3HD) (80:20) were fabricated by a pressurized gyration technique developed by Professor Mohan Edirisinghe

and Dr Suntharavathanan Mahalingam, at The Department of Mechanical Engineering, University College London. Polyhydroxyalkanoates, manufactured at the University of Westminster were supplied to UCL, and fabricated into fibres by pressurized gyration. Both diameters of gyrated PHA fibres were compared to 6μm electrospun P(3HB) fibres fabricated at The University of Sheffield. It is hypothesized that pressurized gyration will not be as effective at producing aligned fibres as electrospinning is, as conditions for the gyration process are still being optimized. This chapter compared both techniques, for fabricating internal guidance cues, as potential nerve guide scaffolds.

Materials and Methods

8.2.1   Production of P(3HB) and P(3HO-co-3HD) by bacterial fermentation.

P(3HB) and P(3HO-co-3HD) was manufactured by Dr Pooja Basnett, from the Applied Biotechnology Research Group at The University of Westminster. The methods used to produce P(3HB) are described in the publication by Valappil *et al.* (2007). Briefly, *Bacillus subtilis* was cultured in Kannan and Rehacek medium under nitrogen limiting conditions, in which glucose was the carbon source, in order to cause the bacteria to produce P(3HB) (Valappil *et al.*, 2007b). P(3HO-co-3HD) was extracted from *Pseudomonas mendocina*, cultured in mineral salt medium under nitrogen limiting conditions, using octanoate and decanoate as the carbon source (Rai *et al.*, 2011). P(3HB) and P(3HO-co-3HD) were extracted and isolated from the microorganisms and purified for their use in fibre fabrication. PHAs were characterized separately by NMR, GPC and FTIR (Lorena R. Lizarraga-Valderrama *et al.*, 2015).

8.2.2   Production of P(3HB) fibres and P(3HB):P(3HO-co-3HD) (80:20) by pressurized gyration

P(3HB) and P(3HO-co-3HD) polymers were provided from the University of Westminster and fabricated into fibres using pressurized gyration at University of College London. Briefly, solutions of P(3HB) and P(3HB):P(3HO-co-3HD) (80:20) were added to the pressurized gyration set up. The speed of the rotary drum and pressure of the nitrogen gas applied were both optimized to fabricate aligned fibres of both PHA blends. Figure 8.1 shows a diagram of the pressurized gyration set up used and formation of fibres.
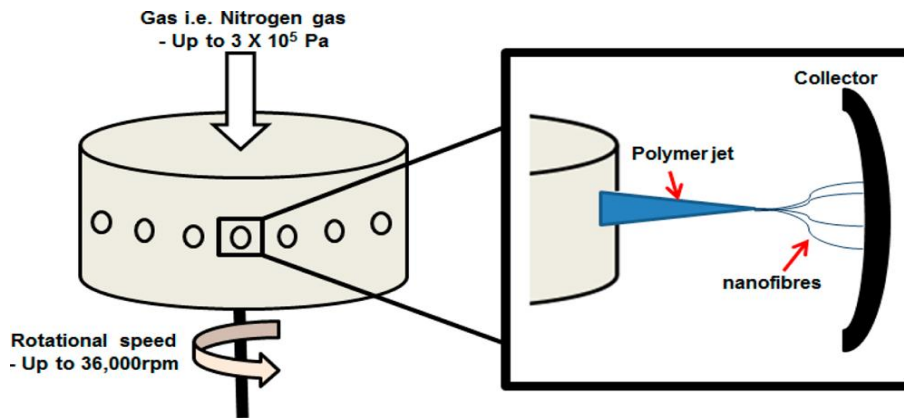
Figure 8.1. Diagram used from Raimi-Abraham et al (2015) to show the pressurized gyration set up used at UCL.

8.2.3   Preparation of P(3HB) electrospun fibres and flat polymer films for in vitro analysis

10wt% solutions of P(3HB) and P(3HB):P(3HO-co-3HD) (80:20) were produced by dissolving polymers in chloroform at room temperature overnight. 100μL of polymer solution was pipetted, using a syringe, onto a 13mm^2 glass coverslip. The solution was spun at 100xg for 30 seconds under a vacuum of 25.5C. Samples were left to dry overnight in a fume cupboard before cell culture work. Electrospun P(3HB) fibres, with an average diameter of 6μm, were fabricated using a high-power voltage supply (Genvolt UK), a single syringe pump (WPI-Europe) and a rotating cylindrical collector attached to a motor (IKA Works). A 1mL plastic syringe (Terumo) was attached to the syringe pump and a 20G needle attached to the end of the syringe. The needle was connected to the high voltage power supply. A 12 wt% solution of P(3HB) was electrospun, using a voltage of 18kV, at a flow rate of 4mL/hr. Electrospun fibres were formed on a sheet of aluminum foil on the collector, at a speed of 134xg. Three independently spun batches of electrospun fibres were imaged using a FEI Sirion field emission gun scanning electron microscope and average fibre length determined by measuring 100 fibres for each batch of fibres. Scanning electron micrographs were also taken of gyrated P(3HB) and P(3HB):P(3HO-co-3HD) (80:20) fibres to determine average fibre diameter. Samples were 'glued' down to 6 well plates using a 10% polymer solution of their respective blend and left to dry for 24 hours to ensure solvent evaporation. A medical grade stainless steel cell culture ring (inner diameter is 13 mm, outer diameter is 24 mm) was placed onto samples, which were sterilised with 70% ethanol for 3 hours. Samples were then washed three times in PBS before a final wash of PBS overnight to ensure all contamination was removed. Samples were washed once more with PBS before cell culture.

8.2.4   NG108-15 neuronal cell culture

See chapter 2, 2.2.4 *Methods* section for details.

8.2.5 Isolation of rat primary Schwann cells

See chapter 4, 4.2.7 *Methods* section for details.

8.2.6 Dorsal root ganglion isolation

See chapter 6, 6.2.6 *Methods* section for details.

8.2.7 Immunolabelling of NG108-15 neuronal cells, dorsal root ganglion bodies and rat primary Schwann cells

See chapter 4, 4.2.6 and 4.2.9 *Methods* sections for details.

8.2.7 Live/Dead measurement of NG108-15 neuronal cells and rat primary Schwann cells

See chapter 2, 2.2.6 *Methods* section for details.

8.2.8 Neurite outgrowth from NG108-15 neuronal cells and dorsal root ganglion bodies

See chapter 4, 4.2.11 *Methods* section for details.

8.2.9 Assessment of primary Schwann cell morphology and Schwann cell migration length

See chapter 4, 4.2.10 *Methods* section for details.

8.2.10 Statistical analysis

GraphPad Instat (GraphPad Software, USA) was used to perform statistical tests on data collected. One-way analysis of variance ($p < 0.05$) was conducted to analyse the differences between the data, incorporating Tukey's multiple comparisons test if $p < 0.05$. Data was reported as mean ± SD, $p<0.05$. Each experiment was performed three independent times with each sample repeated three times as n=3.

8.3 Results

8.3.1 Fabrication and characterization of gyrated and electrospun polyhydroxyalkanoate fibres

Gyrated P(3HB) and P(3HB):P(3HO-co-3HD) (80:20) fibres were fabricated at The University of Westminster using a pressurized gyration process. Samples were characterized by scanning electron microscopy to determine fibre diameter, and angular variance (an assessment of fibre alignment). Once the diameter of gyrated P(3HB) fibres was known, electrospun P(3HB) fibres of the same diameter were fabricated for a direct comparison. This was to determine if the pressurized gyration process could fabricate fibres of a known diameter, as well as fibres with good alignment. Angular variance of the P(3HB) electrospun fibres was also calculated. Figure 8.2 shows scanning electron micrographs of both gyrated and electrospun PHA fibres, as well as a flat film comparison. Visually, the most aligned fibres were fabricated by electrospinning (figure 8.2A) compared to the gyrated fibres (figure 8.2B and C). Gyrated P(3HB) fibres appeared smaller than gyrated P(3HB):P(3HO-co-3HD) (80:20), and more aligned. This was confirmed by data shown in figure 8.3 (A and B). Scanning electron micrographs of the P(3HB) and P(3HB):P(3HO-co-3HD) (80:20) spin coated films (Figure 2D and E) shows that the P(3HB) film has a smooth, pore-less and homogenous surface, compared to the P(3HB):P(3HO-co-3HD) (80:20) spin coated films, which appears rougher. Due to the presence of the P(3HO-co-3HD), the P(3HB):P(3HO-co-3HD) (80:20) was also stickier, and attracted some contaminants, which were removed before cell culture.
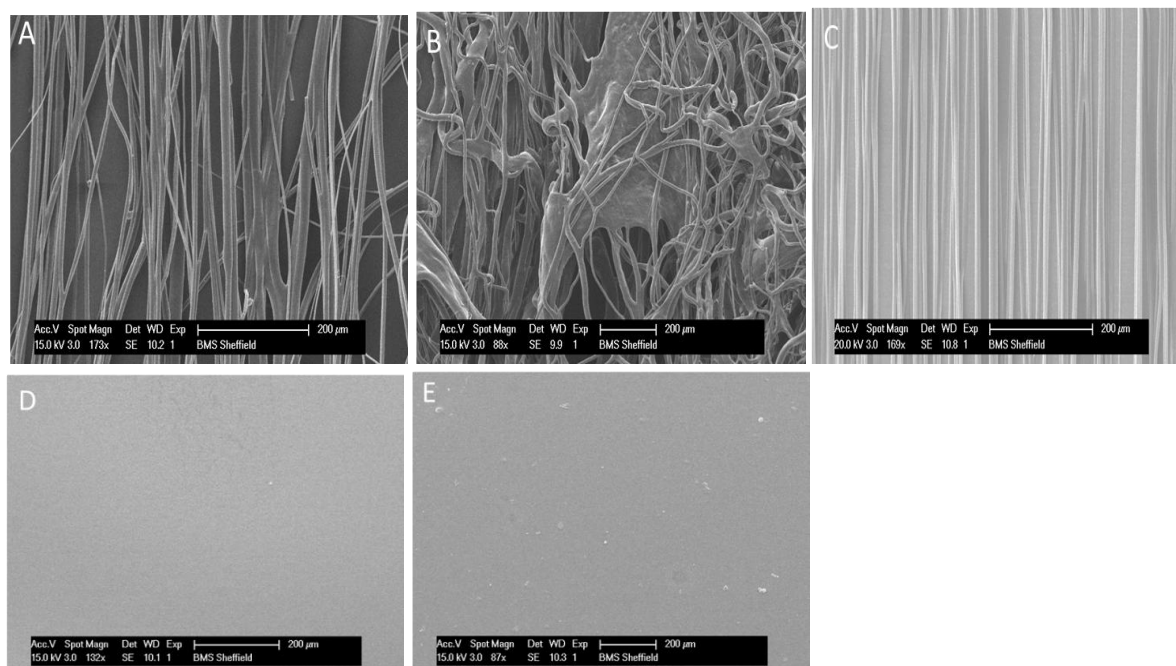
Figure 8.2. Scanning electron micrographs of (A) gyrated P(3HB) fibres, (B) gyrated P(3HB):P(3HO-co-3HD) (80:20) fibres, (C) P(3HB) electrospun fibres, (D) P(3HB) films and (E) P(3HB):P(3HO-co-3HD) (80:20) films.

Analysis of scanning electron micrographs in figure 8.2 confirmed the average fibre diameters of the gyrated fibres as 6.05 ± 1.99μm and 19.02 ± 3.69μm for the P(3HB) and P(3HB):P(3HO-co-3HD) fibres respectively. The average fibre diameter of electrospun P(3HB) fibres was 6.08 ± 0.69μm. This demonstrated that pressurized gyration can fabricate P(3HB) microfibers of similar fibre diameters to those fabricated by electrospinning. However, when calculating diameters of all fibres the standard deviation (variance) of the electrospun P(3HB) fibres was much smaller. Fibre alignment data (figure 8.3B) for electrospun P(3HB) revealed the most fibres were in a 0-2˚categorgy, compared to the gyrated PHA fibres. Gyrated P(3HB) fibres were deemed more aligned than the gyrated P(3HB):P(3HO-co-3HD) (80:20) fibres, but still had fibres present in 6-8, 8-10 and 10-12˚ categories. Fibres were also found in the 12-14 and 14-16 ˚categories in the gyrated P(3HB):P(3HO-co-3HD) (80:20) fibres confirming that these fibres were not aligned. Although different diameters of PHAs can be fabricated by gyration, fibres were not as aligned as those fabricated by electrospinning.
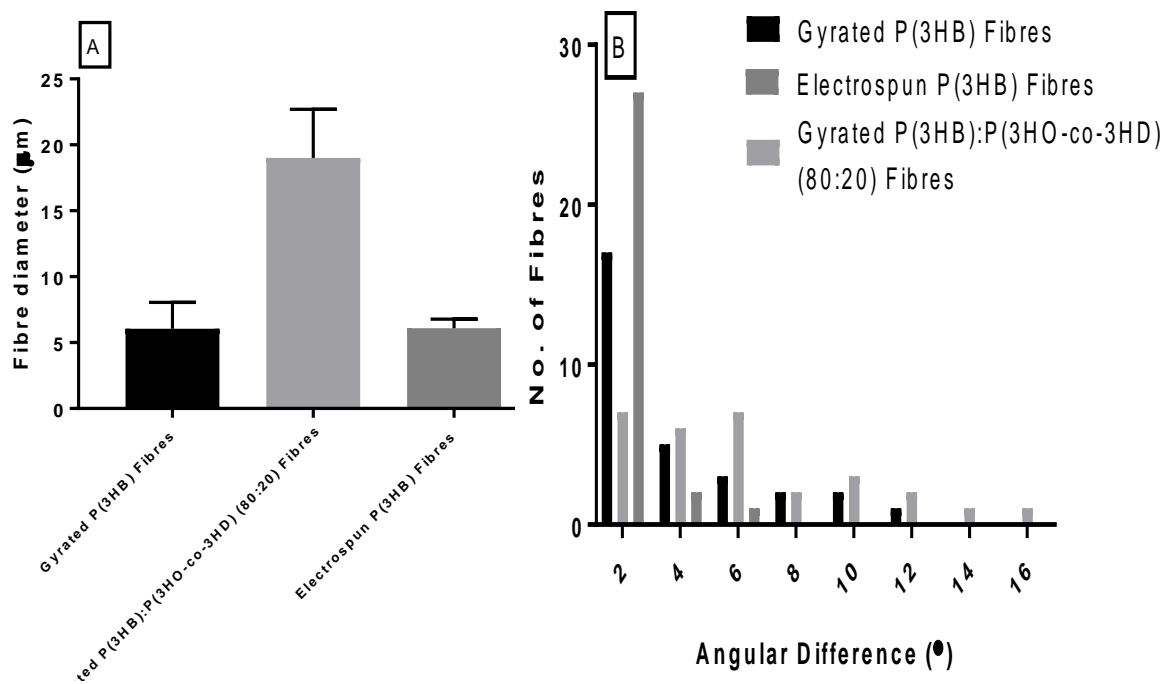
Figure 8. 3. (A) Average fibre diameter of gyrated and electrospun fibres. An average of 100 fibres was assessed for each fibre size and mean of the diameter presented. A one way anova with Tukey's multiple comparisons tests was used to analyse data (mean ± SD, n= 3 independently fabricated samples P < 0.05). (B) Angular variance between individual fibres for each condition. A central aligned fibre, at 180˚, was used as a reference point to measure the angular variance of adjacent fibres. 30 fibres were measured for independently electrospun / gyrated fibre batches. (n=3)

8.3.2 NG108-15 neuronal cell differentiation studies on spin coated PHA films, gyrated PHA fibres and electrospun fibres

Figure 8.4 shows confocal micrographs of NG108-15 neuronal cells cultured on flat

polymer films, gyrated PHA fibres and electrospun P(3HB) fibres, stained for βIII tubulin, to show neurite extension, length and direction of growth. NG108-15 neuronal cells cultured on gyrated and electrospun fibres presented neurites that extended in the same direction as fibres. NG108-15 neuronal cells cultured on flat polymer films and tissue culture plastic control showed neurites that were randomly orientated. Visually, neurites extended from cells cultured on flat surfaces appeared longer. Images were quantified to determine the percentage of NG108-15 neuronal cells bearing neurites, and the average neurite length (figure 8.5A and B).
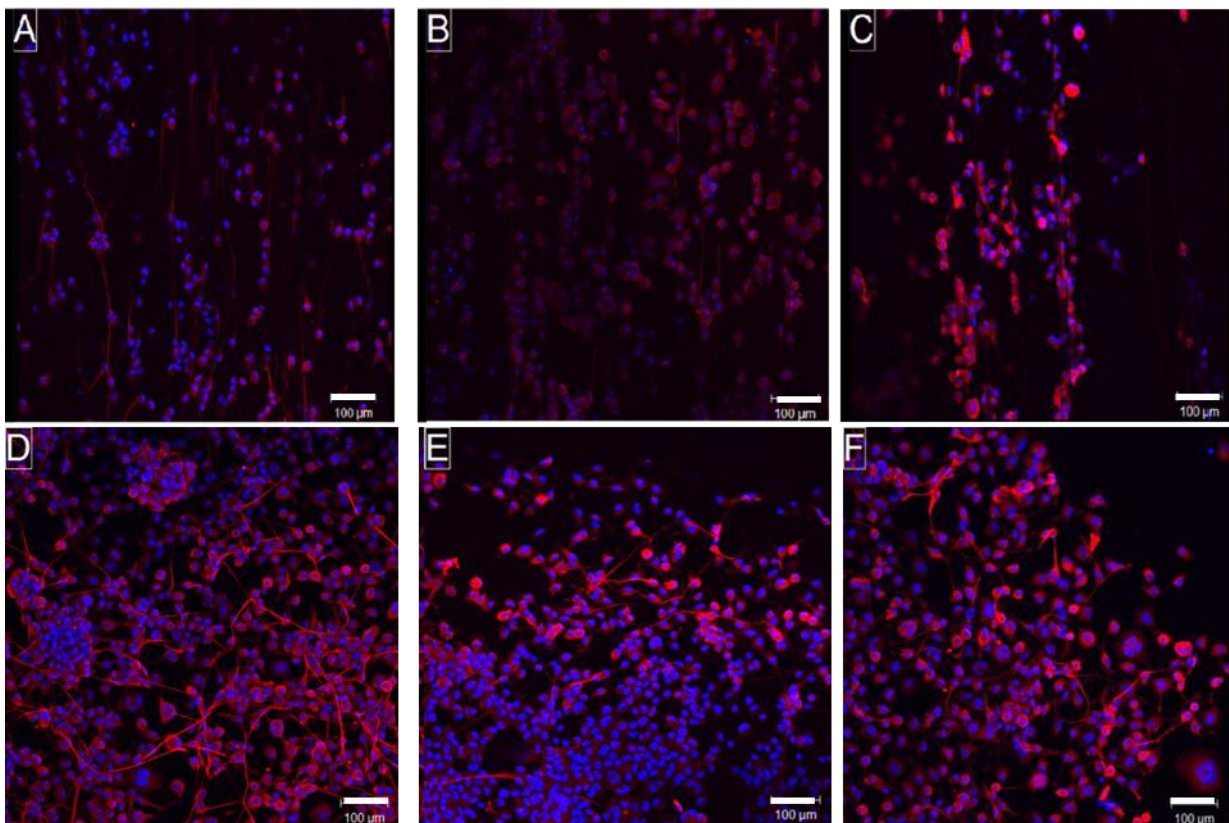
Figure 8.4. Confocal micrographs of NG108-15 neuronal cells cultured on (A) gyrated P(3HB) fibres, (B) gyrated P(3HB):P(3HO-co-3HD) (80:20) fibres, (C) electrospun P(3HB) Fibres, (D) P(3HB) films, (E) P(3HB):P(3HO-co-3HD) (80:20) films and (F) tissue cultured plastic. Neuronal cell nuclei were labelled with DAPI (blue) and neurites labelled for β III tubulin (red) to conduct NG108-15 neuronal cell differentiation studies. Scale bar = 100µm.
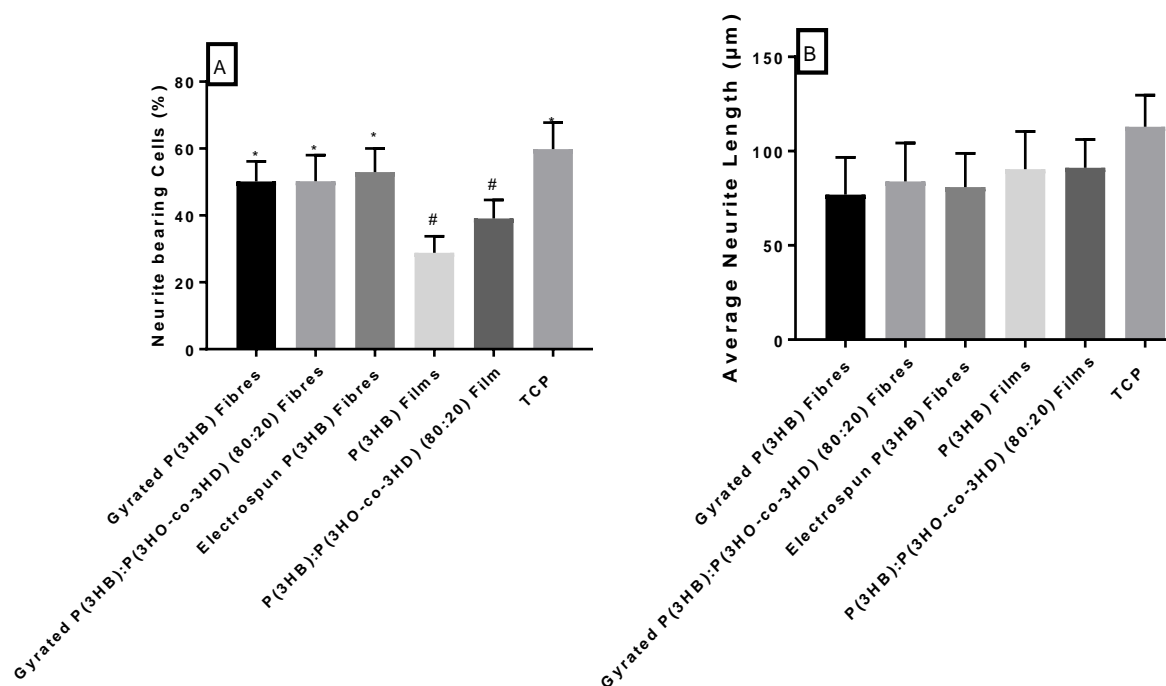
Figure 8.5. Analysis of NG108-15 neuronal cell differentiation examining (A) the percentage of neuronal cells expressing neurites and (B) the average neurite length of NG108-15 neuronal cells cultured on different fibres and polymer films. Percentage of neuronal cells expressing neurites was determined by dividing the number of cells expressing neurites by the total number of cells, per field of view. A one way anova with Tukey's multiple comparisons tests was used to analyse data (mean ± SD, n=3 independent experiments *P<0.05 in comparison to P(3HB) polymer films, #P<0.05 in comparison to TCP) 100 neurites per condition, per independent experiment, was measured to determine the average neurite length of neuronal cells cultured on gyrated and electrospun fibres, and polymer flat films.

Overall, more than 40% of NG108-15 neuronal cells presented neurites when cultured on fibres and flat surfaces (figure8. 5A). However, only 28.82 ± 4.95% of NG108-15 neuronal cells cultured on P(3HB) films appear neurites. Apart from tissue culture plastic, higher percentages of neuronal cells bearing neurites were cultured on PHA gyrated and electrospun fibres, compared to flat film counterparts, 52.98 ± 7.07%, 50.25 ± 7.75%, 50.18 ± 6.01% for electrospun P(3HB) fibres, gyrated P(3HB):P(3HO-co-3HD) (80:20) fibres and gyrated P(3HB) fibres respectively. This suggests a relationship between surface roughness and topography for the percentage of cells bearing neurites. However, no statistical differences were detected between different fibre conditions, all samples were statistically different compared to P(3HB) films.

Analysis confirmed that there were no statistical differences between average neurite lengths showed by cells on all samples. Out of the fibre samples, the longest average neurite lengths were detected on cells cultured on the gyrated P(3HB):P(3HO-co-3HD) (80:20) fibres (83.90 ± 20.35μm) followed by those cultured on electrospun P(3HB) fibres and gyrated P(3HB) fibres (80.99 ± 17.87μm and 76.89 ± 19.80μm). Cells with the longest average neurite length were cultured on the tissue culture plastic (112.94 ± 16.75μm) followed by

those cultured on P(3HB):P(3HO-co-3HD) (80:20) films and P(3HB) films (91.24 ± 14.89µm and 90.4975 ± 19.98µm).

8.3.3 NG108-15 neuronal cell viability studies on spin coated PHA films, gyrated PHA fibres and electrospun fibres.
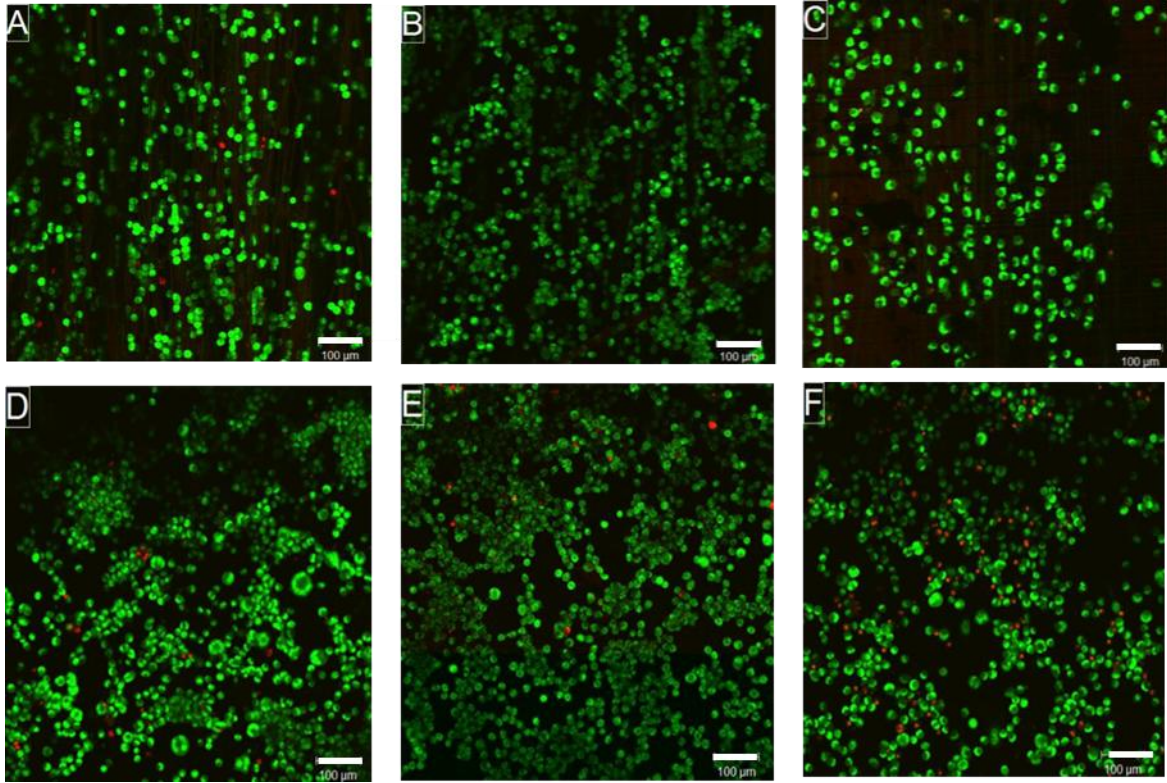
Figure 8.6. Confocal micrographs of NG108-15 neuronal cells, stained with Syto-9 and propidium iodide, cultured on (A) gyrated P(3HB) fibres, (B) gyrated P(3HB):P(3HO-co-3HD) (80:20) fibres, (C) electrospun P(3HB) Fibres, (D) P(3HB) films, (E) P(3HB):P(3HO-co-3HD) (80:20) films and (F) tissue cultured plastic. Scale bar =100µm.

Figure 8.6 shows results of live/dead analysis of NG108-15 neuronal cells cultured on gyrated fibres, electrospun fibres and polymer flat films. Cells cultured on fibres adhered in an aligned manner, whereas neuronal cells cultured on flat surfaces formed random orientations and covered the available surface. All conditions had large numbers of live cells, and relatively few numbers of dead cells. The images were quantified to determine the average number of live and dead cells, per field of view, per conditions, and expressing this as percentage of cell viability per condition.
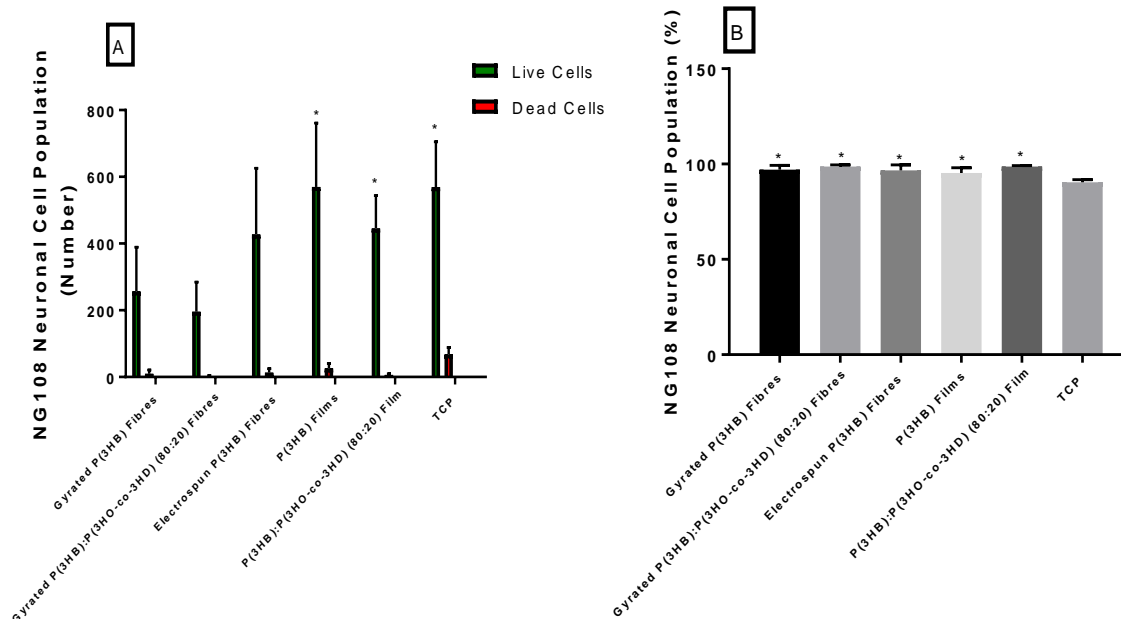
Figure 8.7. Live/dead analysis of NG108-15 neuronal cells cultured on polymer fibres and polymer films. Cell numbers of live cells versus dead cells are expressed as numbers, per field of view, (A) and as live cell percentage viability (B). A) Highest number of live cells seen on P(3HB) films. A one way anova with Tukey's multiple comparisons tests was used to analyse data (Mean ± SD, n=3 independent experiments *P<0.05 in comparison to gyrated P(3HB):P(3HO-co-3HD) (80:20) fibres). B) All samples had a cell viability of above 90% except tissue culture plastic control. A one way anova with Tukey's multiple comparisons tests was used to analyse data (Mean ± SD, n=3 independent experiments *p<0.05 in comparison to TCP)

Higher numbers of live cell numbers were seen on flat surfaces (figure 8.6) compared to fibre samples, quantified in figure 8.7A. Statistical differences were detected between the flat surfaces and gyrated P(3HB):P(3HO-co-3HD) (80:20) fibres, but no statistical differences were detected between the gyrated and electrospun P(3HB) samples compared to the flat surfaces, suggesting that larger cell numbers grew on P(3HB) compared to P(3HB):P(3HO-co-3HD) (80:20) fibre composition. The highest number of live cells were detected on P(3HB) films, and tissue culture plastic compared to P(3HB):P(3HO-co-3HD) (80:20) films, 569.88 ± 191.26 cells, 569.22 ± 135.60 cells and 444.66 ± 99.12 cells respectively. The highest number of live cells cultured on fibre samples were detected on P(3HB) fibres, followed by gyrated P(3HB) fibres and gyrated P(3HB):P(3HO-co-3HD) (80:20) fibres, 427.33 ± 198.31 cells, 256.44 ± 132.65 cells and 195.55 ± 88.66 cells. Cell viability of all conditions was above 90% indicating that all samples were biocompatible. Cell viability was significantly higher for all the materials, fibres and films, when compared to the tissue culture plastic control. This concludes that all the materials are suitable candidates for nerve cell regeneration studies when studying NG108-15 neuronal cells.

21

8.3.4 Primary Schwann cell morphology studies on spin coated PHA films, gyrated PHA fibres and electrospun fibres.

Figure 8.8 shows that Schwann cells maintained their morphology and phenotype, when cultured on the fibres and flat films, as Schwann cells stained positively for S100β (Schwann cell marker). Schwann cells adhered to fibres, and elongated in an aligned manner, whereas when cultured on flat surfaces they were randomly organized. Schwann cell length was used as marker for morphology, to determine that they had a maintained morphology when cultured on fibres and flat material surfaces. 100 Schwann cells per condition were measured using NIH Image J, and the average cell length calculated (Schneider *et al.*, 2012). No significant differences were detected between average Schwann cells lengths and Overall, Schwann cells cultured on material fibres and flat films maintained their phenotype and morphology. The average Schwann cell lengths were 79.50 ± 16.49µm and 76.16 ± 14.94µm on P(3HB):P(3HO-co-3HD) (80:20) flat films and gyrated fibres and 71.31 ± 16.14µm, 74.24 ± 13.82µm and 74.41 ± 15.73µm for the P(3HB) flat films and the electrospun and gyrated fibres.

Figure 8.8. Confocal micrographs of rat primary Schwann cells cultured on (A) gyrated P(3HB) fibres, (B) P(3HB):P(3HO-co-3HD) (80:20) fibres, (C) electrospun P(3HB) Fibres, (D) P(3HB) films, (E) P(3HB):P(3HO-co-3HD) (80:20) films and (F) tissue culture plastic. Neuronal cell nuclei were labelled with DAPI (blue) and Schwann cell bodies labelled against S100β (green-Schwann cell marker). Scale bar = 100µm.
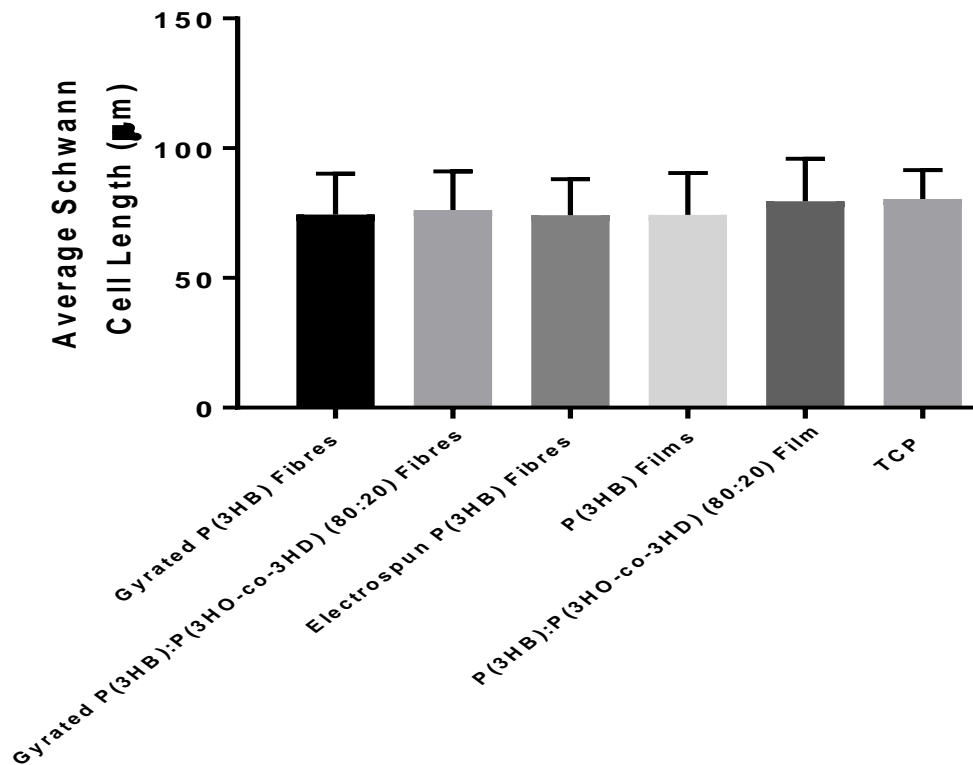
Figure 8.9. Schwann cell morphology was examined by calculating the average cell length. 100 Schwann cells, per condition were measured to determine the average Schwann cell length. A one way anova with Tukey's multiple comparisons tests was used to analyse data (mean ± SD). All Schwann cells retained phenotypical Schwann cell morphology, and no significant differences were detected between samples.

8.3.5   Primary Schwann cell viability studies on spin coated PHA films, gyrated PHA fibres and electrospun fibres

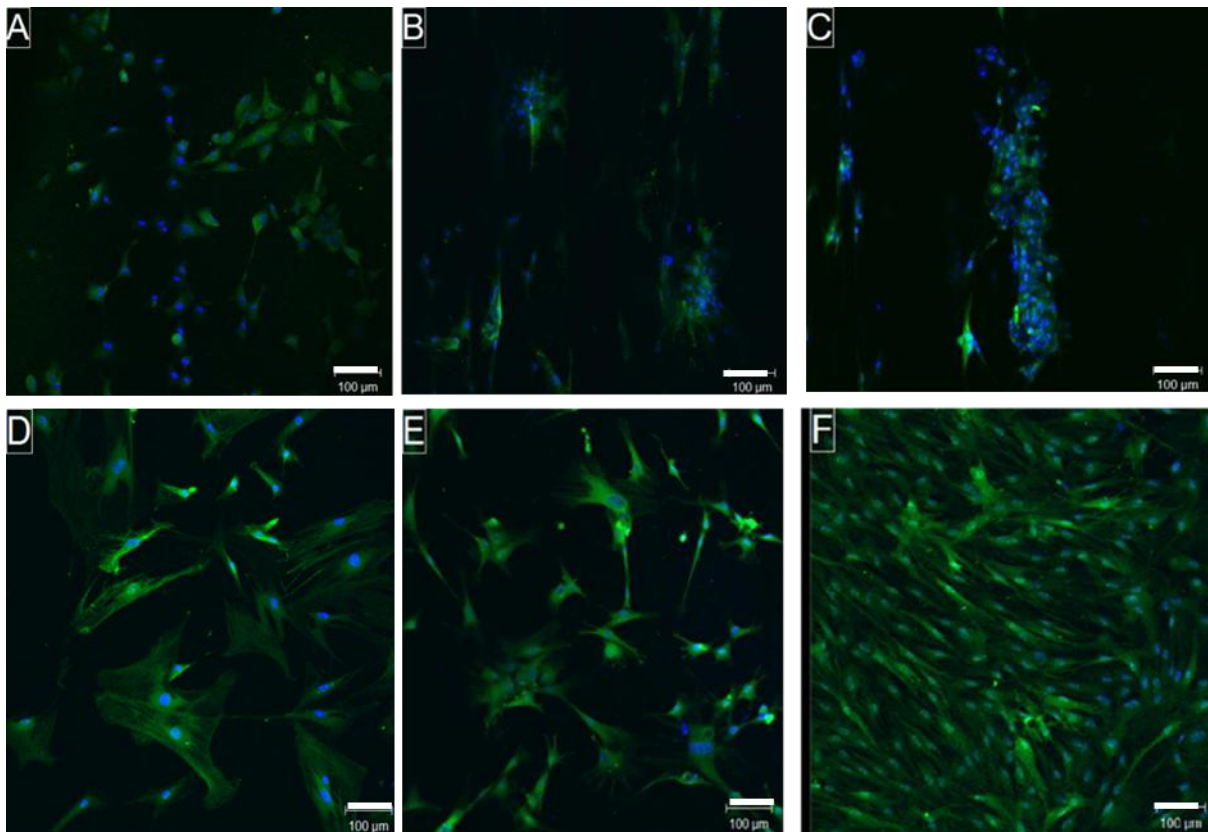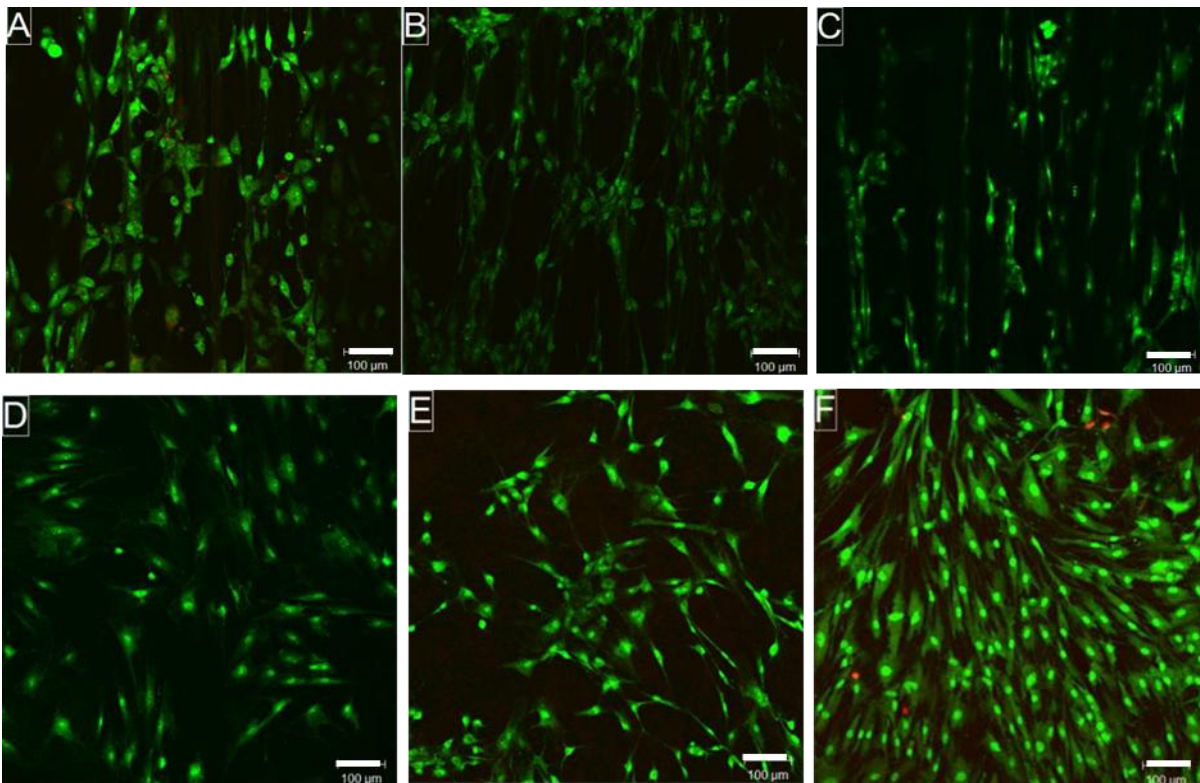Figure 8.10: Confocal micrographs of rat primary Schwann cells cultured on (A) gyrated P(3HB) fibres, (B) gyrated P(3HB):P(3HO-co-3HD) (80:20) fibres, (C) electrospun P(3HB) fibres, (D) P(3HB) films, (E) P(3HB):P(3HO-co-3HD) (80:20) PHA films and (F) tissue cultured plastic. Schwann cells were labelled with Syto-9 (live cells-green) and propidium iodide (dead cells-red). Scale bar = 100µm.

21

Figure 8.10 shows the morphological properties of rat primary Schwann cells cultured on flat films and fibres. Figure 8.10A, B and C show that Schwann cells grow and align on fibres, compared to random orientation on flat surfaces. Schwann cells appear to elongate under all conditions, and the highest number of live cells was seen on tissue culture plastic. Images were quantified to determine live cell and dead cell numbers per field of view (841µm x 841µm) for each condition (figure 8.11). The number of live cells adhered on the P(3HB):P(3HO-co-3HD) (80:20) films and the tissue culture plastic control was significantly higher than the number of live viable Schwann cells adhered to the gyrated P(3HB) and P(3HB):P(3HO-co-3HD) (80:20) fibres. The highest live Schwann cell number was detected on tissue culture plastic and P(3HB):P(3HO-co-3HD) (80:20) PHA films, 158.00 ± 24.51 cells and 150.77 ± 30.93 cells respectively. Highest live Schwann cell numbers on the fibres were detected on the electrospun P(3HB) fibres compared to gyrated P(3HB):P(3HO-co-3HD) (80:20) fibres or gyrated P(3HB) fibres, 103.8 ± 19.33 cells, 87.11 ± 22.69 cells, and 84.22 ± 23.83 cells respectively. This suggests that more cells adhered to P(3HB) fibres compared to the gyrated fibres and were more biocompatible. All conditions expressed a cell viability of above 90% suggesting that all the materials are biocompatible, and suitable for primary Schwann cell proliferation and growth.
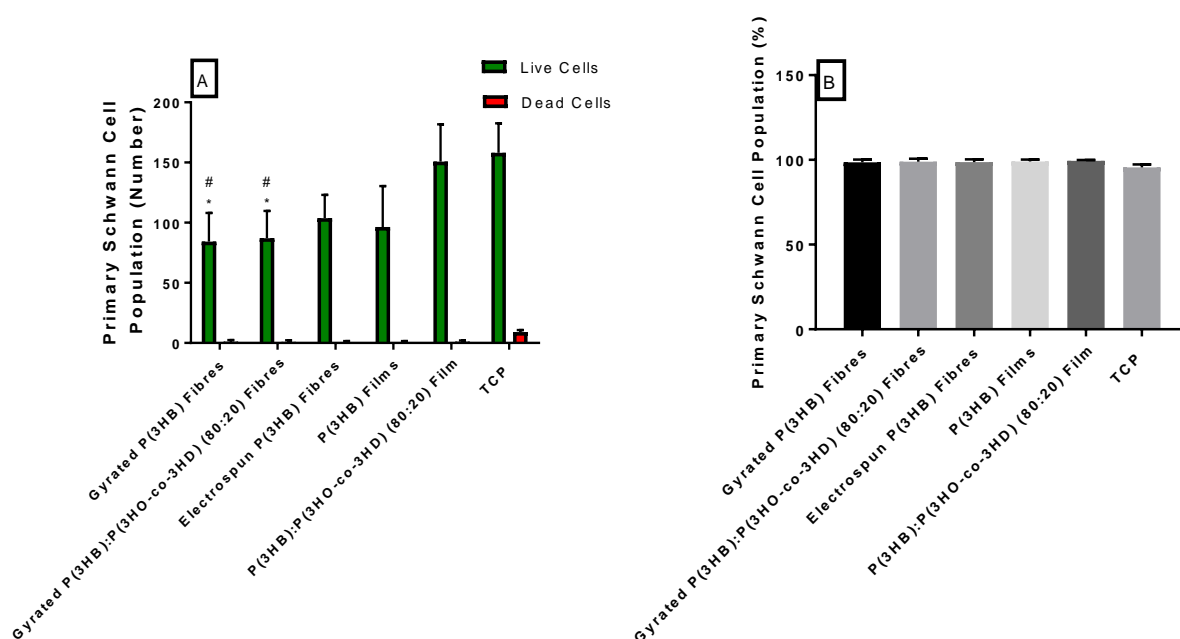
Figure 8.11. Live/dead analysis of rat primary Schwann cells cultured on polymer fibres and polymer films. Cell numbers of live cells versus dead cells are expressed as numbers per field of view, (A) and as live cell percentage viability (B). A one way anova with Tukey's multiple comparisons tests was used to analyse data (Mean ± SD, n=3 independent experiments *P<0.05 in comparison to P(3HB):P(3HO-co-3HD) (80:20) PHA films, #p<0.05 in comparison to TCP. All samples had a live cell viability of >95% and no significant difference was detected between samples.

8.3.6 Dorsal root ganglion axon outgrowth and Schwann cell migration on gyrated and electrospun PHA fibres and films
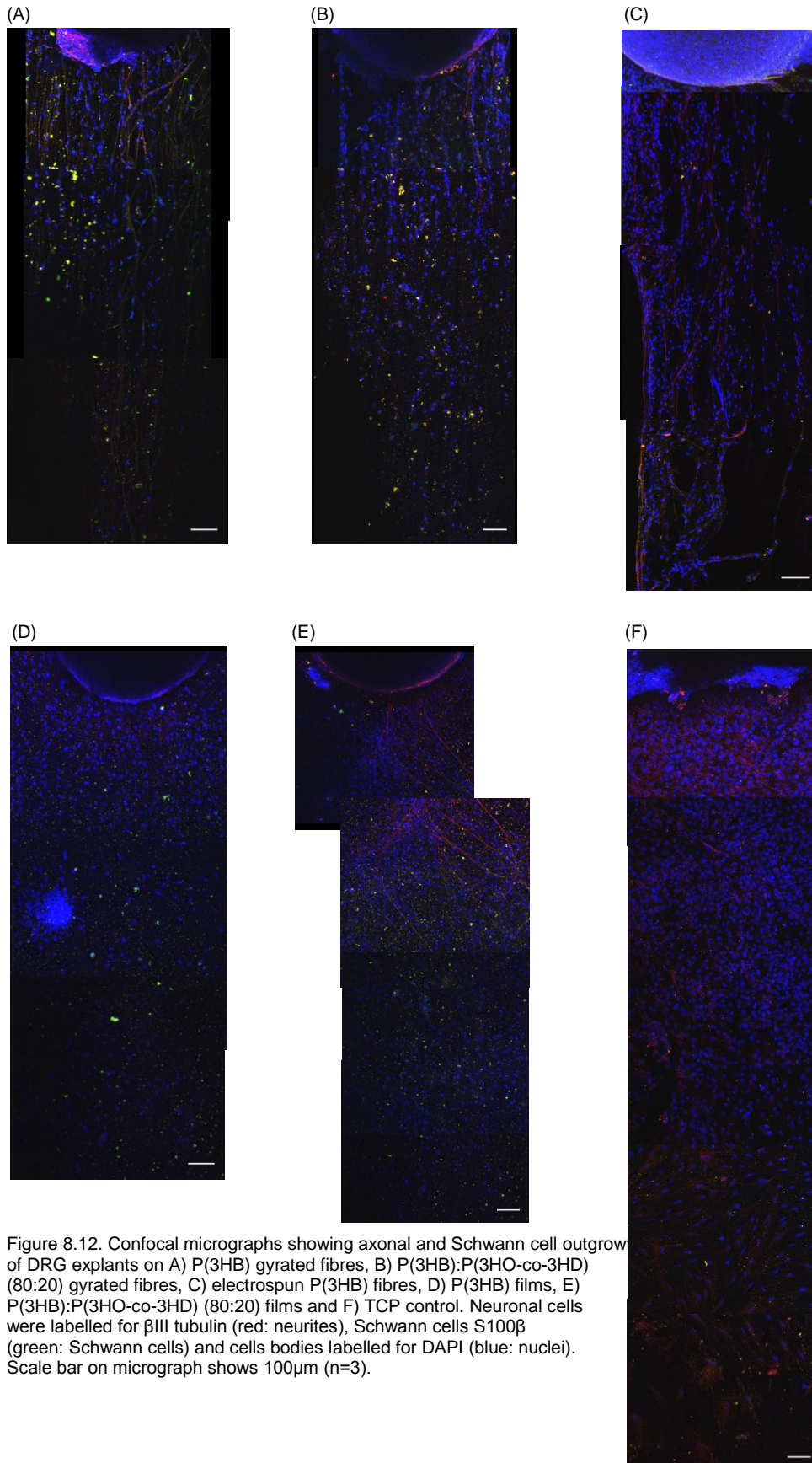
Figure 8.12. Confocal micrographs showing axonal and Schwann cell outgrowth of DRG explants on A) P(3HB) gyrated fibres, B) P(3HB):P(3HO-co-3HD) (80:20) gyrated fibres, C) electrospun P(3HB) fibres, D) P(3HB) films, E) P(3HB):P(3HO-co-3HD) (80:20) films and F) TCP control. Neuronal cells were labelled for βIII tubulin (red: neurites), Schwann cells S100β (green: Schwann cells) and cells bodies labelled for DAPI (blue: nuclei). Scale bar on micrograph shows 100μm (n=3).

Figure 8.12 shows micrographs taken of DRGs explanted onto gyrated and electrospun PHA fibres, as well as the relevant polymer flat film and tissue culture plastic control. Primary Schwann cells migrated the furthest distance on tissue culture plastic, compared to PHA flat films. When comparing gyrated and electrospun PHA fibres, primary Schwann cell migration was furthest on the P(3HB) electrospun fibres, compared to gyrated PHA fibres. This was also the same with regards to axon outgrowth. Axon outgrowth was seen to align with fibres, whereas on the films, it was random. Axon outgrowth was parallel with the attachment, and migration, of the Schwann cells.

Micrographs were quantified and figure 8.13 shows that average axon growth was observed when DRGs were cultured on tissue culture plastic, which was 3087.02 ± 225.56µm. When comparing fibres, axon outgrowth was highest on the P(3HB) fibres, compared to the gyrated P(3HB) and P(3HB):P(3HO-co-3HD) (80:20) fibres, which were 1287.02 ± 225.56µm, 417.66 ± 110.22µm and 615.18 ± 192.76µm respectively. Interestingly, axonal outgrowth was higher on P(3HB) and P(3HB):P(3HO-co-3HD) (80:20) films compared to their fibre counterpart, which was 479.12 ± 128.62µm and 830.70 ± 293.89µm. This could be due to gyrated fibres losing alignment during DRG culture, decreasing Schwann cell migration and therefore axonal outgrowth. Axon and Schwann cell outgrowth was present on material flat films, confirming that the materials were effective at supporting neuronal outgrowth and Schwann cell migration. Primary Schwann cell migration distance was in parallel with axon growth, in which the farthest cell migration distance was observed on tissue culture plastic control, up to 3960.48 ± 208.70µm.

The highest Schwann cell migration distance on PHA fibres was observed on the electrospun P(3HB) fibres, at 2452.87 ± 99.11µm, followed by the gyrated P(3HB):P(3HO-co-3HD) (80:20) fibres and P(3HB) fibres, which were 1890.08 ± 194.05µm and 1846.34 ± 182.09µm. When comparing Schwann cell migration distance on gyrated PHA fibres with PHA polymer films, highest values were observed for the relevant polymer film (2121.25 ± 229.33µm on the P(3HB) film and 2024.17 ± 82.41µm on the P(3HB):P(3HO-co-3HD) (80:20) film). Schwann cells also appeared more elongated on the electrospun P(3HB) fibres and tissue culture plastic control, compared to the other conditions, in which they appeared shorter. This indicated that electrospun P(3HB) fibres were more effective at supporting Schwann cell attachment and proliferation and providing migration guidance cues.
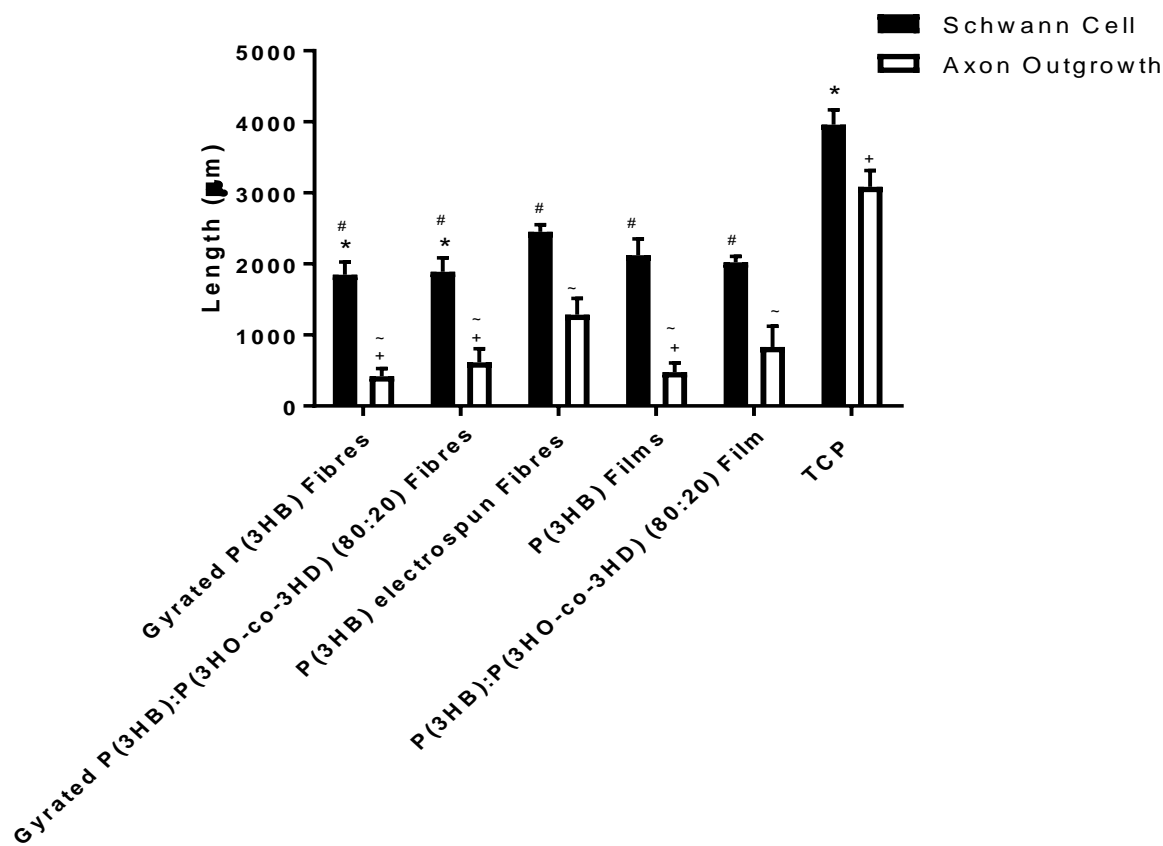
Figure 8.13. Quantification of average neurite outgrowth length, and average Schwann cell migration length, from dorsal root ganglion explants cultured onto gyrated and electrospun PHA fibres, films and TCP controls. 100 Schwann cell lengths and neurite lengths, per condition, were measured using the ruler tool on Image J. A two way anova with Tukey's multiple comparisons tests was used to analyse data(n=3 independent experiments, *$P<0.05$ in comparison to P(3HB) Electrospun Fibres Schwann Cell Migrations, #$P<0.05$ in comparison to TCP Schwann cell migration, +$P<0.05$ in comparison to P(3HB) Electrospun Fibres Axon Lengths, ~$P<0.05$ in comparison to TCP axon lengths).

8.4 Discussion

PHA fibres were fabricated by two techniques - electrospinning and pressurized gyration. As pressurized gyration is still a relatively new technique, PHAs have not been used by this method to our knowledge to fabricate nanofibres and microfibres.

Pressurized gyration is a useful manufacturing method to fabricate PHA micrometer fibres. However, there are issues regarding fibre alignment due to the collecting plate (Mahalingam and Edirisinghe, 2013). Electrospinning is a versatile and scalable technique to produce polymer fibres with excellent alignment due to the working distance between the syringe needle and rotating collector (Bhardwaj and Kundu, 2010). It has been reported that fibre diameter influences cell attachment, growth, and proliferation, and that certain diameters are preferable for different tissue engineering applications. Nanofibres are commonly used in tissue engineering applications, in which a scaffold is intended to mimic the extracellular matrix, such as skin tissue (S. MacNeil, 2007), whereas microfibres are thought more

effective in nerve tissue engineering (Daud *et al.*, 2012). Figure 8.3 also shows that pressurized gyration can be used to fabricate PHA fibres up to 20μm, a much larger diameter compared to electrospinning. It has been reported recently that pressurized gyration can fabricate polymer fibres in the nanometer range (Mahalingam and Edirisinghe, 2013).

Fibre alignment has also been reported to play a vital role on cell attachment, proliferation and differentiation, as providing a guidance cue to cells causes different cell types to elongate and align on fibres, changing their morphology (Qazi *et al.*, 2015). This has been reported in the literature using neuronal cells, smooth and skeletal muscle cell types, fibroblasts and endothelial cells. Fibre alignment has been shown to change the shape of human dermal fibroblasts, in which fibroblasts elongate on aligned fibres (Delaine-Smith *et al.*, 2014). The report by Delaine-Smith *et al.* (2014) confirmed that fibre alignment supported the deposition of collagen, secreted from human dermal fibroblasts. Fibre alignment is an important parameter in peripheral nerve repair for promoting Schwann cell elongation, direction and providing a guidance cue for the regenerating axon, as well as fibre diameter (Delaine-Smith *et al.*, 2014).

In this study, NG108-15 neuronal cells were cultured onto electrospun and gyrated PHA fibres, as well as a flat film control for a direct comparison. While all the fibres and films promoted NG108-15 neuronal cell proliferation and maturation. No fibre technique was significantly better in promoting increased neurite outgrowth. However, culturing cells on gyrated fibres and electrospun fibres significantly increased the number of NG105-15 neuronal cells expressing neurites, compared to flat film controls. This confirmed that a change in structure to a rougher, 3D surface influenced neuronal cell differentiation as well as observing that neuronal cells were more spread out on fibres. It was seen that, although there were lower numbers of attached cells on fibrous scaffolds, NG108-15 neuronal cells had attached to the scaffolds and aligned along the fibres. P(3HB) fibres supported a higher number of NG108-15 neuronal and primary Schwann cell attachment, compared to the gyrated fibres. Similarly, it could be seen that primary Schwann cells also aligned themselves to the fibres and were more evenly spread out.

Reports document that primary Schwann cells attach to fibres and elongate more so on fibres, compared to random orientated fibres or flat surface controls (Chew *et al.*, 2008). No significant differences were detected between in the average cell length of Schwann cells

cultured on the P(3HB) electrospun and gyrated fibres, the P(3HB):P(3HO-co-3HD) (80:20) fibres and flat films. With regards to Schwann cell morphology, Schwann cell aggregates were observed on gyrated P(3HB):P(3HO-co-3HD) (80:20) more prominently, than the gyrated and electrospun P(3HB) fibres, due to a higher proportion of random orientated fibres, and larger fibre diameter. Interestingly, when considering Schwann cell viability, higher numbers of Schwann cells attached on the P(3HB) electrospun fibres, compared to gyrated PHA fibres. Schwann cell attachment was also significantly higher on P(3HB):P(3HO-co-3HD) (80:20) films, compared to P(3HB) films, which indicates that addition of P(3HO-co-3HD) may support primary Schwann cell attachment. A similar observation was seen for gyrated P(3HB) and P(3HB):P(3HO-co-3HD) (80:20) fibres. Electrospun and gyrated PHA fibres maintained a Schwann cell phenotype, due to the positive staining of Schwann cell marker S100, confirming that all samples promoted Schwann cell growth and proliferation.

Due to the lack of *in vitro* 3D models for the study of peripheral nerve regeneration, it has been demonstrated in the literature, and previous chapters, that the *ex vivo* culture of dorsal root ganglion bodies on 2D and 3D structures is a useful tool for the assessment of peripheral nerve related structures and devices (Pateman *et al.*, 2015). The dorsal root ganglion body is extracted from the spine, and the nerve roots are trimmed off to promote axon re-growth. DRG bodies were explanted onto the top of the gyrated and electrospun fibres to record the maximum Schwann cell migration and neurite outgrowth length (Behbehani *et al.*, 2018). DRG bodies were placed onto the middle of flat films to assess neurite outgrowth and Schwann cell migration length, as well as direction. Overall, it was concluded that Schwann cell migration length and neurite outgrowth lengths were significantly higher on the P(3HB) electrospun fibres compared to the gyrated P(3HB) and P(3HB):P(3HO-co-3HD) (80:20) fibres, due to the fibre alignment. Schwann cell migration lengths were significantly higher than the axon outgrowth lengths for all samples, and it could also be seen that axon growth followed Schwann cell migration. This corresponded to Schwann cell behavior, and regenerating axon growth reported in the literature for nerve regeneration.

The organotypic DRG explant model is therefore a useful pre-*in vivo* assessment tool for nerve studies and highlights the importance of using a primary cell type rather than immortal cells for investigation of materials of interest for peripheral nerve repair.

Overall, it was concluded that electrospun P(3HB) fibres were the most effective materials internal guidance for use in nerve conduits, compared to gyrated fibres. This was due to

optimal alignment, as more than 80% of measured fibres were of a 0-2˚angular variance. When using NG108-15 neuronal cells, both the gyrated fibres, and electrospun fibres, supported cell attachment, maturation and differentiation. Neurite outgrowth was seen on all samples, and neurite outgrowth aligned with the fibres. Both gyrated fibres promoted cell growth, attachment and maintained Schwann cell phenotype. However, when using an *ex vivo* DRG model, P(3HB) electrospun fibres were significantly better in promoting Schwann cell migration, and neurite outgrowth. This would indicate that the electrospun P(3HB) fibres are potentially more effective in providing guidance for primary Schwann cells and regenerating axons compared to the gyrated fibres. However, this work has also confirmed that there is much promise using pressurized gyration to fabricate PHA fibres. Pressurized gyration has a fewer parameters to consider, compared to electrospinning, and that optimizing conditions fabricating better aligned fibres is possible. This work has shown that pressurized gyration can fabricate fibres in the micrometer range, as well as manufacture relatively aligned fibres of required diameters needed for peripheral nerve repair. Gyrated PHA fibres fabricated were biocompatible, promoted cell attachment, promoted neurite outgrowth from NG108-15 neuronal cells and dorsal root ganglion explants, as well as maintain Schwann cell phenotype. Future work must include optimizing gyration conditions to fabricate more aligned fibres more use in peripheral nerve repair.

Chapter 9: Discussion and future work

9.1 Discussion

The main aim of this study was to investigate a range of different synthetic materials currently investigated for applications in nerve repair, and to develop and fabricate an intraluminal scaffold for use with a nerve guide conduit. Current FDA approved nerve guide conduits are hollow tubes, and so research focuses on improving the designs of the conduit to increase nerve re-intervention (Kehoe *et al.*, 2012). One technique, to improve hollow conduit design, and increase nerve regeneration distances, is the addition of intraluminal aligned fibrous scaffolds, to provide guidance for the regenerating axon, and to increase Schwann cell attachment and proliferation, to speed up the rate of formation of the fibrin cable (W. Daly *et al.*, 2012).

5 and 8μm fibres of P(3HO):P(3HB) (50:50), P(3HO-co-3HD):PLLA (50:50), PHBV and PCL were fabricated by electrospinning. Fibres supported NG108-15 neuronal cell and primary Schwann cell attachment, proliferation and differentiation, and supported DRG neurite outgrowth and Schwann cell migration. Overall, the work demonstrates the potential use of electrospun fibres as an internal guidance scaffold, for use with a nerve guide conduit, to improve nerve regeneration length by providing guidance. Separate aims of this work were to determine the potential use of aminosilanes in peripheral nerve repair, and to investigate if pressurised gyration could replace electrospinning as the fibre manufacturing method.

FDA approved polymers, PLLA, PLGA and PCL, were investigated in this work, to determine if they could be used to fabricate an internal guidance scaffold for peripheral nerve repair. PLLA, PLGA and PCL can be formed into fibres by electrospinning, and current research focuses on improving synthetic polymers by blending with much softer elastomeric polymers, to improve mechanical properties (Arslantunali *et al.*, 2014b). The use of polyhydroxyalkanoates, for their potential role in peripheral nerve tissue engineering, was also investigated. Polyhydroxyalkanoates are an attractive family of polymers for tissue engineering applications, due to their range of mechanical and physical properties, and excellent biocompatibility and biodegradability (L. R. Lizarraga-Valderrama *et al.*, 2016). Material characterisation and evaluation resulted in the fabrication of 6 blends to be electrospun, due to mechanical and physical properties, and results of initial cell viability studies. These blends were:

- P(3HO):P(3HB) (25:75)
- P(3HO):P(3HB) (50:50)

- P(3HO):P(3HB) (75:25)
- P(3HO-co-3HD):P(3HB) (95:5)
- P(3HO-co-3HD):PLLA (95:5)
- P(3HO-co-3HD):PCL (95:5)

Well known brittle polymers, PLLA, P(3HB), and PCL were blended with higher amounts of elastomeric polymers P(3HO) and P(3HO-co-3HD) to decrease the Youngs moduli to that closer of rat sciatic nerve, 0.5MPa (Borschel *et al.*, 2003; Ulery *et al.*, 2011). However, the addition of P(3HO) and P(3HO-co-3HD) to P(3HB), PCL and PLLA in the blends caused an increase in water contact angle, due to the presence of long aliphatic chains, and increased number of carbon atoms in P(3HO) and P(3HO-co-3HD) (Basnett *et al.*, 2013). Therefore, by improving the mechanical properties of the polymer blend by using an elastomeric polymer, this caused the blend to overall become more hydrophobic. In contrast, increasing the amount of P(3HB) in the blends with P(3HO) decreased water contact angle and caused the blend to become more hydrophilic due to the lower amount of carbon atoms in the P(3HB) monomer (Basnett *et al.*, 2013). However, Young's modulus increased with the increased amount of P(3HB) in each blend. Lizarraga *et al.* (2015) reported that the higher the content of P(3HB) in blends with P(3HO), water contact angle decreased significantly (Lorena R. Lizarraga-Valderrama *et al.*, 2015). Although water contact angle did decrease by increasing the amount of P(3HB), this result was not significant. This work concludes the use of 50:50 blends, using an elastomeric and brittle polymer, such as P(3HO) and P(3HB), to compromise between mechanical and physical properties, and hydrophilicity.

Further work for the material characterisation would include SEM images and AFM analysis to determine the surface topography and roughness of the polymer films investigated. Protein adsorption studies would also be performed, to understand which proteins in the cell culture medium had an affinity to the surface, to understand why there were increases/decreases in cellular adhesion.

Electrospinning is a commonly used versatile technique, to manufacture fibres from various different polymers and polymer blends (Bye *et al.*, 2012). Electrospinning can produce fibres of varying diameters, and orientation, by changing the parameters associated with the technique (Bhardwaj and Kundu, 2010). PCL, PHBV, PLGA, PLLA and P(3HB) could all be electrospun individually and aligned fibres with a range of different diameters were produced. P(3HO) and P(3HO-co-3HD) could not be electrospun by themselves, due to elastomeric nature of the polymers, which resulted in fibre formation by incomplete solvent evaporation. Fibres could not be removed from their foil collector, and alignment could not be maintained. However, by blending P(3HO) and P(3HO-co-3HD) with more brittle

polymers, electrospinning was achieved. Electrospinning of blends was performed and both P(3HO):P(3HB) (25:75) and P(3HO):P(3HB) (50:50) could be manufactured into aligned fibres, with a range of different diameters. The P(3HO-co-3HD):PLLA blend was investigated further and aligned fibres, with varying diameters could be produced when electrospinning P(3HO-co-3HD):PLLA (50:50). Further work with regards to electrospinning would investigate the viscosity of all the polymer solutions which fabricated successful aligned fibres from their relevant material. Knowing the viscosity of the solution would aid in the reproducibility of the fibres fabricated, which would aid any future work such as commercialisation.

Fibre diameter was confirmed in chapter 4, and 5µm and 8µm fibres of P(3HO-co-3HD):PLLA (50:50), P(3HO):P(3HB) (50:50), PHBV and PCL were fabricated for *in vitro* analysis in chapter 5. Neurite outgrowth length, from NG108-15 neuronal cells was significantly larger on the 8µm PHBV fibres, and NG108-15 neuronal cells adhered and proliferated on all fibre samples. This work is comparable to the study by Daud *et al* (2012) in which it was reported that statistically larger neurites outgrew from NG108-15 neuronal cells cultured on 8µm PCL fibres, compared to 1 and 5µm fibres (Daud *et al.*, 2012). However, with regards to *in vitro* analysis using primary Schwann cells, increased numbers of Schwann cells attached to 1µm PCL fibres, compared to 5 and 8µm PCL fibres (Daud *et al.*, 2012). This was also observed in this work, in which larger numbers of Schwann cells were attached to 5µm fibres, compared to the 8µm fibres of each material type. Overall, primary Schwann cell adherence was significantly lower on the P(3HO-co-3HD):PLLA (50:50) fibres compared to all the other material types. The co-culture of rat primary Schwann cells and NG108-15 neuronal cells was supported on all fibre diameters and material type. Further work with regards to cellular adhesion on the fibres would include investigating the differentiation of the cell types. PCR would be performed to investigate any genetic changes in the cells, when orientating to the fibres. Chew *et al.* (2008) investigated the expression of 'MAG, P0, MBP, PMP22 and NCAM-1' when culturing human primary Schwann cells on aligned and random fibre scaffolds (Chew *et al.*, 2008). Focal adhesion protein expression, such as fibronectin and vitronectin, would also be investigated to understand the mechanism of how the cells adhere to the fibres. Further characterisation in chapter 2, investigating surface topography and protein adsorption, would also aid further characterisation work for chapters 3 and 4 with regards to the mechanisms behind cellular adhesion and differentiation on the fibres. Understanding which proteins adsorb to the surfaces could explain why the PHAs supported more neuronal differentiation than the other materials investigated. Further would also include looking further into the mechanisms of

degradation when the polymer blends are in their fibrous form. This was attempted originally but with little success and the fibres was too light to weigh. However, if modified, fibres could be secured in place with stainless steel cell culture rings, and at each degradation time point, SEM analysis could be performed to measure fibre diameter, pores etc. An enzymatic degradation study would also add more value to this work, as PHAs and polymers do not just degrade by hydrolytic mechanisms (E Díaz *et al.*, 2014).

 A bespoke *ex vivo* DRG model, to assess the potential of electrospun fibre diameters, and material type, was developed by Behbehani *et al* (2018) (Behbehani *et al.*, 2018). 5mm PEG tubes were fabricated by microstereolithography and fibres were threaded into conduits. Before cell culture, conduits containing fibres were analysed by microCT, to confirm the correct density of fibres in the conduit, and to confirm alignment of fibres throughout the conduit. MicroCT analysis confirmed the maintained alignment of PHBV, PCL and P(3HO):P(3HB) (50:50) fibres after the threading technique. However, P(3HO-co-3HD):PLLA (50:50) fibres did not maintain alignment after threading, and fibres fused together. This was due to elastomeric nature of the P(3HO-co-3HD). Therefore, this blend was not taken forward for *ex vivo* analysis using the DRG model. DRGs were explanted onto the top of the conduit and cultured for 21 days. DRG neurite outgrowth and Schwann cell migration lengths were then assessed for each material type, and fibre diameter, to determine the most efficient fibre blend/diameter for use as an intraluminal guidance scaffold (Behbehani *et al.*, 2018). Neurite outgrowth length from DRGs was significantly larger on the 5µm PHBV and 5µm P(3HO):P(3HB) (50:50) fibres compared to the 8µm PCL fibres. Although not significant, DRG neurite outgrowth length was larger on 5µm fibres, compared to the 8µm fibre counterparts. However, this result confirms that material type can have a significant effect on DRG neurite outgrowth. This result also highlights the importance of using a primary neuronal cell compared to using an immortal neuronal cell line, such as the NG108-15 neuronal cell line. Primary DRG neurite outgrowth length was larger on 5µm fibres, whereas NG108-15 neuronal cell neurite outgrowth length was larger on 8µm fibres. This work is comparable to that published by Daud *et al* (2012), which reported significantly larger neurite outgrowth of NG108-15 neuronal cells cultured on 8µm PCL fibres, compared to 1µm and 5µm PCL fibres (Daud *et al.*, 2012). When DRG explants were cultured on PCL fibres, no statistical differences were detected between the neurite outgrowth length of DRGs cultured on 1, 5 and 8µm fibres (Daud *et al.*, 2012). The *ex vivo* is a useful method to pre-screen fibre materials and diameter before *in vivo* analysis (Behbehani *et al.*, 2018). It also applies to the 3Rs principle, to reduce the amount of animal models used to assess fibre potential (Tannenbaum and Bennett, 2015). However, DRG neurite outgrowth rate is not still

not comparable to axon regeneration rate *in vivo,* which highlights still, the need of animal models, to assess nerve guide conduits and intraluminal guidance scaffolds, after vigorous *in vitro* and *ex vivo* analysis (Kaplan *et al.*, 2015). Schwann cell migration length, from dorsal root ganglion explants, was significantly larger when cultured on the 5µm PHBV fibres, compared to 8µm PHBV, PCL and P(3HO):P(3HB) (50:50) fibres, indicating that fibre diameter does have a significant impact on Schwann cell migration.

Further work in chapter 6 would include fabricating NGC tubes with pores. The lack of porosity in the PEG tubes would explain why DRG neurite outgrowth and Schwann cell migrations lengths are furthest on the TCP controls, compared to on the fibre scaffolds. It is clear the Schwann cells in the PEG tubes are not receiving the required nutrients and oxygen, which could inhibit any growth factors secreted to aid neurite growth from the DRG explant (Armstrong *et al.*, 2007). Pores can be incorporated into structures, using a known size porogen, but most recently creating high internal phase emulsion, using water and oil, and mixing with the photocurable polymer and photoinitiator before using the microsterealithography system (Owen *et al.*, 2016). Johnson *et al.* (2013) were able to print PCL tubes containing pores, using microstereolithography, without the use of any porogen (D. W. Johnson *et al.*, 2013). The other alternative to ensure cells in a non-porous environment receive the required nutrients is the use of a perfusion bioreactor and using dynamic culture methods throughout the tube. The use of dynamic culture and flow has been shown to improve cell viability in many different cell types (Wu *et al.*, 2010). Sun *et al.* (2008) developed a novel bioreactor system, to test the effect of RN22s in nerve guide conduits under static and dynamic conditions. RN22 cell viability increased under dynamic conditions compared to static conditions, and further work for the study included investigating the effect of dynamic and static culture on primary neurons and Schwann cells (T. Sun *et al.*, 2008).

Finally, *in vivo* testing in rat sciatic injury model would be the next investigative step after all the additional further studies explained previously. Both 5 and 8µm fibres of PHBV and P(3HO):P(3HB) (50:50) fibres would be incorporated into NGC tubes to be assessed in short, medium and long sized gap injurys (6, 10 and 15mm respectfully). *In vivo* analysis will further investigate how the fibres align in a wet environment, the degradation of the fibres, and degradation products, how fluids and immune cells penetrate the injury site and any effect they have on the material, and finally confirm whether the presence of aligned fibres do improve nerve reinnnervation rate and overall improve muscle and nerve function (Beigi *et al.*, 2014). Another method to improve nerve guide conduits is to modify polymer surfaces

with reactive chemical groups, to improve surface topography (J. H. Bell and Haycock, 2012). Aminosilanisation is surface modification technique, to graft amine groups onto polymer surfaces, to improve polymer biocompatibility (Mäkilä *et al.*, 2012). By grafting reactive groups onto the surface, surface chemistry and can be changed, without changing the bulk material properties (J. H. Bell and Haycock, 2012). Differences in chemistry and topography have been shown to control initial cell adhesion events (Curran *et al.*, 2011). The aim of this work was to investigate the potential of aminosilanes in nerve tissue engineering. Preliminary investigations have shown that changing the length of the silane can be used as a method to control deposition of NH_2, and so two different silane chain lengths were investigated, to determine whether this influenced neuronal and Schwann cell types (Curran *et al.*, 2005). Water contact and XPS analysis confirmed that amine groups had been grafted onto glass coverslips and had improved the hydrophilicity of glass. AFM demonstrated that long chain aminosilane modified surfaces were rougher, and that roughness was consistent over the whole coverslips, whereas short chain aminosilane modified surfaces demonstrated a patchy, more heterogeneous nanotopographical profile. Average neurite length of neurites expressed from NG108-15 neuronal cells cultured on long chain aminosilane modified surfaces were significantly larger, when compared to short chain surfaces. The average number of neurites expressed per neuron was also significantly higher when NG108-15 neuronal cells were cultured on long chain aminosilane modified surfaces, compared to short chain surfaces. Both modified aminosilane chain lengths supported NG108-15 neuronal cell and primary Schwann cell attachment and proliferation. DRGs were dissociated to produce a co-culture of primary neurons and Schwann cells, to assess the effect of silane chain length. Primary neuron neurite outgrowth was significantly higher when neurons were cultured on the long chain aminosilane modified surfaces, compared to the short chain aminosilane modified surfaces. This work is comparable to the study by Buttiglione *et al.* (2007) which reported increased SY5Y cell attachment and proliferation of amine grafted PET surfaces (Buttiglione *et al.*, 2007). However, the addition of aminosilanes to glass coverslips did not increase NG108-15 neuronal cell adherence but did increase primary Schwann cell adherence. This was observed when co-culturing primary Schwann cells with primary neurons, as increased Schwann cell attachment, increased neuron neurite lengths. Further work to study the effect of aminosilanes on neuronal and Schwann cells would include performing a protein adsorption study, to investigate which proteins in the culture medium have a higher affinity to the surface. Topography of the amines is already known, and the rougher surface of the long chain aminosilanes clearly has an effect of protein adsorption, resulting in NG108-15 neuronal cell and primary neuron differentiation. Another useful study

would be to investigate whether the aminosilanes can support cellular adhesion and differentiation as effectively as known ECM protein coatings, such as laminin and collagen coating (Armstrong *et al.*, 2007). Future work would also involve grafting aminosilanes on polymer surfaces, films and fibres/conduits, to determine the effect of long chain aminosilanes *in vivo*, in particular, aminosilane stability.

Polymer fibres, for use in scaffolds, can be fabricated via electrospinning (Bye *et al.*, 2012). Polymer fibres can also be fabricated using pressurized gyration (Mahalingam and Edirisinghe, 2013). Gyration involves a rotating drum containing holes in the middle of the axis, connected to a motor and a gas valve (Mahalingam and Edirisinghe, 2013). By rotating the drum at different speeds, and applying nitrogen gas at varying pressure, polymer fibres can be produced from polymer solutions, and fibres formed from the holes in the rotating drum (Mahalingam *et al.*, 2015). P(3HB) and P(3HB):P(3HO-co-3HD) (80:20) gyrated fibres were manufactured by Dr Suntharavathanan Mahalingam, at The Department of Mechanical Engineering, University College London. P(3HB) fibres were manufactured by electrospinning, to compare both techniques, using NG108-15 neuronal cells, Schwann cells, and DRG explants. No statistical differences were found between gyrated and electrospun fibres with regards to NG108-15 neuronal cell neurite outgrowth length, and fibres supported NG108-15 neuronal cell and primary Schwann cell attachment and proliferation. However, *ex vivo* analysis demonstrated that DRG neurite outgrowth length, and Schwann cell migration lengths were significantly larger when DRGs were cultured on P(3HB) electrospun fibres, compare to the P(3HB) and P(3HB):P(3HO-co-3HD) (80:20) gyrated fibres. This work demonstrates that gyration can manufacture fibrous scaffolds that support NG108-15 neuronal and primary Schwann cell attachment and proliferation. However, this work also demonstrates that fibres fabricated from pressurised gyration are not as aligned as those fabricated by electrospinning and aligned is crucial to promote DRG neurite outgrowth and Schwann cell migration. Future work would include optimising pressurised gyration parameters to fabricate more aligned fibrous scaffolds. Gyrated fibres could then be threaded into nerve guidance conduits, for use as intraluminal guidance scaffolds and assessed *in vivo* conditions.

9.2 Conclusions and key findings

Overall, the main aim of this work was to develop and fabricate an aligned fibrous intraluminal scaffold, to provide guidance for the regenerating axon and provide a scaffold for Schwann cell adherence and proliferation. Material type and diameter was assessed to

investigate the effect of cell viability, metabolic rate, and any phenotypic changes to cell shape to NG108-15 neuronal cells, primary Schwann cells and dorsal root ganglia.

The main conclusions of the study were:

- The P(3HO):P(3HB) (50:50) blend fabricated highly aligned fibres, with a range of different diameters. It also had a lower Youngs modulus compared to the P(3HO):P(3HB) (25:75) blend.

- The more well known brittle polyesters could be fabricated into aligned fibres via electrospinning. However, softer more elastomeric polymers, such as P(3HO) and P(3HO-co-3HD) could not be fabricated into fibres unless blended with more brittle polyester at a ratio of at least 50:50.

- Although 8µm fibres promoted larger neurite outgrowth lengths of NG108-15 neuronal cells, smaller fibre diameters, such as 5µm, promoted increased primary Schwann cell attachment.

- Schwann migration and DRG neurite extension lengths were larger on the 5µm fibres compared to 8µm fibres, regardless of material.

- P(3HO):P(3HB) (50:50) 5µm fibres and PHBV 5µm fibres promoted increase primary Schwann cell migration and DRG neurite outgrowth lengths compared to the 8µm PCL and PHBV fibres.

- Primary neuron neurite outgrowth length was significantly increased when neurons were cultured on long chain aminosilane modified coverslips compared to short chain aminosilane modified coverslips.

- Gyration is another fibre fabricating technique that could be applied to nerve tissue engineering. However, when culture DRGs onto fibres, electrospun fibres significantly promoted larger neurite outgrowth lengths and Schwann cell migration length. Future work is needed to improve the alignment of polymer fibres formed by pressurised gyration.

9.3 References

Akaraonye, E., Keshavarz, T. and Roy, I. (2010) 'Production of polyhydroxyalkanoates: the future green materials of choice', *Journal of Chemical Technology & Biotechnology*, 85(6), pp. 732-743.

Ali, I. and Jamil, N. (2016) 'Polyhydroxyalkanoates: Current applications in the medical field', *Frontiers in Biology*, 11(1), pp. 19-27.

Anselme, K., Ploux, L. and Ponche, A. (2010) 'Cell/Material Interfaces: Influence of Surface Chemistry and Surface Topography on Cell Adhesion', *Journal of Adhesion Science and Technology*, 24(5), pp. 831-852.

Armstrong, S. J., Wiberg, M., Terenghi, G. and Kingham, P. J. (2007) 'ECM molecules mediate both Schwann cell proliferation and activation to enhance neurite outgrowth', *Tissue Eng*, 13(12), pp. 2863-70.

Armstrong, S. J., Wiberg, M., Terenghi, G. and Kingham, P. J. (2008) 'Laminin activates NF-kappaB in Schwann cells to enhance neurite outgrowth', *Neurosci Lett*, 439(1), pp. 42-6.

Arslantunali, D., Budak, G. and Hasirci, V. (2014a) 'Multiwalled CNT-pHEMA composite conduit for peripheral nerve repair', *J Biomed Mater Res A*, 102(3), pp. 828-41.

Arslantunali, D., Dursun, T., Yucel, D., Hasirci, N. and Hasirci, V. (2014b) 'Peripheral nerve conduits: technology update', *Med Devices (Auckl)*, 7, pp. 405-24.

Assaf, K., Leal, C. V., Derami, M. S., de Rezende Duek, E. A., Ceragioli, H. J. and de Oliveira, A. L. R. (2017) 'Sciatic nerve repair using poly(ε-caprolactone) tubular prosthesis associated with nanoparticles of carbon and graphene', *Brain and Behavior*, 7(8), p. e00755.

Aviss, K. J., Gough, J. E. and Downes, S. (2010) 'Aligned electrospun polymer fibres for skeletal muscle regeneration', *Eur Cell Mater*, 19, pp. 193-204.

Bagdadi, A. V., Safari, M., Dubey, P., Basnett, P., Sofokleous, P., Humphrey, E., Locke, I., Edirisinghe, M., Terracciano, C., Boccaccini, A. R., Knowles, J. C., Harding, S. E. and Roy, I. (2016) 'Poly(3-hydroxyoctanoate), a promising new material for cardiac tissue engineering', *J Tissue Eng Regen Med*.

Basnett, P., Ching, K. Y., Stolz, M., Knowles, J. C., Boccaccini, A. R., Smith, C., Locke, I. C., Keshavarz, T. and Roy, I. (2013) 'Novel Poly(3-hydroxyoctanoate)/Poly(3-hydroxybutyrate) blends for medical applications', *Reactive and Functional Polymers*, 73(10), pp. 1340-1348.

Basnett, P., Lukasiewicz, B., Marcello, E., Gura, H. K., Knowles, J. C. and Roy, I. (2017) 'Production of a novel medium chain length poly(3-hydroxyalkanoate) using unprocessed biodiesel waste and its evaluation as a tissue engineering scaffold', *Microb Biotechnol*.

Baumann, N. and Pham-Dinh, D. (2001) 'Biology of oligodendrocyte and myelin in the mammalian central nervous system', *Physiol Rev*, 81(2), pp. 871-927.

Behbehani, M., Glen, A., Taylor, C. S., Schuhmacher, A., Claeyssens, F. and Haycock, J. W. (2018) 'Pre-clinical evaluation of advanced nerve guide conduits using a novel 3D in vitro testing model', *2018*, 4(1).

Beigi, M. H., Ghasemi-Mobarakeh, L., Prabhakaran, M. P., Karbalaie, K., Azadeh, H., Ramakrishna, S., Baharvand, H. and Nasr-Esfahani, M. H. (2014) 'In vivo integration of poly(ε-caprolactone)/gelatin nanofibrous nerve guide seeded with teeth derived stem cells for peripheral nerve regeneration', *J Biomed Mater Res A*, 102(12), pp. 4554-67.

Belkas, J. S., Shoichet, M. S. and Midha, R. (2004a) 'Axonal guidance channels in peripheral nerve regeneration', *Operative Techniques in Orthopaedics*, 14(3), pp. 190-198.

Belkas, J. S., Shoichet, M. S. and Midha, R. (2004b) 'Peripheral nerve regeneration through guidance tubes', *Neurological Research*, 26(2), pp. 151-160.

Bell, J. (2013) 'Modification of Biomaterials using Plasma Polymerisation (Doctoral Thesis)'. Available at White Rose eTheses Online: Available under License Creative Commons Attribution-Noncommercial-No Derivative Works 2.0 UK: England & Wales. Available at: http://etheses.whiterose.ac.uk/id/eprint/6579.

Bell, J. H. and Haycock, J. W. (2012) 'Next generation nerve guides: materials, fabrication, growth factors, and cell delivery', *Tissue Eng Part B Rev*, 18(2), pp. 116-28.

Bergström, J. S. and Hayman, D. (2016) 'An Overview of Mechanical Properties and Material Modeling of Polylactide (PLA) for Medical Applications', *Ann Biomed Eng*, 44(2), pp. 330-40.

Bhardwaj, N. and Kundu, S. C. (2010) 'Electrospinning: a fascinating fiber fabrication technique', *Biotechnol Adv*, 28(3), pp. 325-47.

Biazar, E. and Heidari Keshel, S. (2013) 'A nanofibrous PHBV tube with Schwann cell as artificial nerve graft contributing to Rat sciatic nerve regeneration across a 30-mm defect bridge', *Cell Communication & Adhesion*, 20(1-2), pp. 41-49.

Biazar, E. and Keshel, S. H. (2013) 'Chitosan–Cross-Linked Nanofibrous PHBV Nerve Guide for Rat Sciatic Nerve Regeneration Across a Defect Bridge', *ASAIO Journal*, 59(6), pp. 651-659.

Bini, T. B., Gao, S., Wang, S. and Ramakrishna, S. (2006) 'Poly(l-lactide-co-glycolide) biodegradable microfibers and electrospun nanofibers for nerve tissue engineering: an in vitro study', *Journal of Materials Science*, 41(19), pp. 6453-6459.

Bini, T. B., Gao, S., Xu, X., Wang, S., Ramakrishna, S. and Leong, K. W. (2004) 'Peripheral nerve regeneration by microbraided poly(L-lactide-co-glycolide) biodegradable polymer fibers', *J Biomed Mater Res A*, 68(2), pp. 286-95.

Borschel, G. H., Kia, K. F., Kuzon, W. M. and Dennis, R. G. (2003) 'Mechanical properties of acellular peripheral nerve', *J Surg Res*, 114(2), pp. 133-9.

Brako, F., Raimi-Abraham, B., , S. M., Craig, D. Q. M. and , M. E. 70 (2015) 'Making nanofibres of mucoadhesive polymer blends for vaginal   '. European Polymer Journal, pp. 186-196.

Buttiglione, M., Vitiello, F., Sardella, E., Petrone, L., Nardulli, M., Favia, P., d'Agostino, R. and Gristina, R. (2007) 'Behaviour of SH-SY5Y neuroblastoma cell line grown in different media and on different chemically modified substrates', *Biomaterials*, 28(19), pp. 2932-45.

Bye, F. J., Wang, L., Bullock, A. J., Blackwood, K. A., Ryan, A. J. and MacNeil, S. (2012) 'Postproduction processing of electrospun fibres for tissue engineering', *J Vis Exp*, (66).

Chen, G. Q. and Wu, Q. (2005) 'The application of polyhydroxyalkanoates as tissue engineering materials', *Biomaterials*, 26(33), pp. 6565-78.

Chew, S. Y., Mi, R., Hoke, A. and Leong, K. W. (2008) 'The effect of the alignment of electrospun fibrous scaffolds on Schwann cell maturation', *Biomaterials*, 29(6), pp. 653-61.

Chia, H. N. and Wu, B. M. (2015) 'Recent advances in 3D printing of biomaterials', *J Biol Eng*, 9, p. 4.

Chua, P. K., Chena, J. Y., Wanga, L. P. and Huang, N. R 36 (2002) 'Plasma-surface modification of biomaterials'. Materials Science and Engineering, pp. 143–206.

Cooperstein, I., Layani, M. and Magdassi, S. (2015) '3D printing of porous structures by UV-curable O/W emulsion for fabrication of conductive objects', *Journal of Materials Chemistry C*, 3(9), pp. 2040-2044.

Corey, J. M., Lin, D. Y., Mycek, K. B., Chen, Q., Samuel, S., Feldman, E. L. and Martin, D. C. (2007) 'Aligned electrospun nanofibers specify the direction of dorsal root ganglia neurite growth', *J Biomed Mater Res A*, 83(3), pp. 636-45.

Crowley, L. C., Scott, A. P., Marfell, B. J., Boughaba, J. A., Chojnowski, G. and Waterhouse, N. J. (2016) 'Measuring Cell Death by Propidium Iodide Uptake and Flow Cytometry', *Cold Spring Harb Protoc*, 2016(7), p. pdb.prot087163.

Curran, J. M., Chen, R. and Hunt, J. A. (2005) 'Controlling the phenotype and function of mesenchymal stem cells in vitro by adhesion to silane-modified clean glass surfaces', *Biomaterials*, 26(34), pp. 7057-67.

Curran, J. M., Chen, R. and Hunt, J. A. (2006) 'The guidance of human mesenchymal stem cell differentiation in vitro by controlled modifications to the cell substrate', *Biomaterials*, 27(27), pp. 4783-93.

Curran, J. M., Fawcett, S., Hamilton, L., Rhodes, N. P., Rahman, C. V., Alexander, M., Shakesheff, K. and Hunt, J. A. (2013) 'The osteogenic response of mesenchymal stem cells to an injectable PLGA bone regeneration system', *Biomaterials*, 34(37), pp. 9352-64.

Curran, J. M., Pu, F., Chen, R. and Hunt, J. A. (2011) 'The use of dynamic surface chemistries to control msc isolation and function', *Biomaterials*, 32(21), pp. 4753-60.

Daly, W., Yao, L., Zeugolis, D., Windebank, A. and Pandit, A. (2012) 'A biomaterials approach to peripheral nerve regeneration: bridging the peripheral nerve gap and enhancing functional recovery', *J R Soc Interface*, 9(67), pp. 202-21.

Daly, W. T., Knight, A. M., Wang, H., de Boer, R., Giusti, G., Dadsetan, M., Spinner, R. J., Yaszemski, M. J. and Windebank, A. J. (2013) 'Comparison and characterization of multiple biomaterial conduits for peripheral nerve repair', *Biomaterials*, 34(34), pp. 8630-8639.

Daud, M. F., Pawar, K. C., Claeyssens, F., Ryan, A. J. and Haycock, J. W. (2012) 'An aligned 3D neuronal-glial co-culture model for peripheral nerve studies', *Biomaterials*, 33(25), pp. 5901-13.

de Luca, A. C., Faroni, A. and Reid, A. J. (2015) 'Dorsal Root Ganglia Neurons and Differentiated Adipose-derived Stem Cells: An In Vitro Co-culture Model to Study Peripheral Nerve Regeneration', *Journal of Visualized Experiments : JoVE*, (96), p. 52543.

de Ruiter, G. C. W., Malessy, M. J. A., Yaszemski, M. J., Windebank, A. J. and Spinner, R. J. (2009) 'Designing ideal conduits for peripheral nerve repair', *Neurosurgical Focus*, 26(2), p. E5.

Delaine-Smith, R. M., Green, N. H., Matcher, S. J., MacNeil, S. and Reilly, G. C. (2014) 'Monitoring fibrous scaffold guidance of three-dimensional collagen organisation using minimally-invasive second harmonic generation', *PLoS One*, 9(2), p. e89761.

Deumens, R., Bozkurt, A., Meek, M. F., Marcus, M. A., Joosten, E. A., Weis, J. and Brook, G. A. (2010) 'Repairing injured peripheral nerves: Bridging the gap', *Prog Neurobiol*, 92(3), pp. 245-76.

E Díaz, Sandonis, I. and Valle, a. M. (2014) 'In Vitro Degradation of Poly(caprolactone)/nHA Composites', *Journal of Nanomaterials*, 2014, p. 8.

Elsawy, M. A., Kim, K.-H., Park, J.-W. and Deep, A. (2017) 'Hydrolytic degradation of polylactic acid (PLA) and its composites', *Renewable and Sustainable Energy Reviews*, 79, pp. 1346-1352.

Engelmayr, G. C., Cheng, M., Bettinger, C. J., Borenstein, J. T., Langer, R. and Freed, L. E. (2008) 'Accordion-like honeycombs for tissue engineering of cardiac anisotropy', *Nat Mater*, 7(12), pp. 1003-10.

Eshraghi, S. and Das, S. (2010) 'Mechanical and microstructural properties of polycaprolactone scaffolds with one-dimensional, two-dimensional, and three-dimensional orthogonally oriented porous architectures produced by selective laser sintering', *Acta Biomater*, 6(7), pp. 2467-76.

Evans, G. R. D., Brandt, K., Widmer, M. S., Lu, L., Meszlenyi, R. K., Gupta, P. K., Mikos, A. G., Hodges, J., Williams, J., Gürlek, A., Nabawi, A., Lohman, R. and Patrick, C. W. (1999) 'In vivo evaluation of poly(l-lactic acid) porous conduits for peripheral nerve regeneration', *Biomaterials*, 20(12), pp. 1109-1115.

Fan, Y. W., Cui, F. Z., Hou, S. P., Xu, Q. Y., Chen, L. N. and Lee, I. S. (2002) 'Culture of neural cells on silicon wafers with nano-scale surface topograph', *Journal of Neuroscience Methods*, 120(1), pp. 17-23.

Fawcett, S. A., Curran, J. M., Chen, R., Rhodes, N. P., Murphy, M. F., Wilson, P., Ranganath, L., Dillon, J. P., Gallagher, J. A. and Hunt, J. A. (2017) 'Defining the Properties of an Array of -NH2-Modified Substrates for the Induction of a Mature Osteoblast/Osteocyte Phenotype from a Primary Human Osteoblast Population Using Controlled Nanotopography and Surface Chemistry', *Calcif Tissue Int*, 100(1), pp. 95-106.

Gentile, P., Chiono, V., Carmagnola, I. and Hatton, P. V. (2014) 'An Overview of Poly(lactic-co-glycolic) Acid (PLGA)-Based Biomaterials for Bone Tissue Engineering', *International Journal of Molecular Sciences*, 15(3), pp. 3640-3659.

Gigliobianco, G., Chong, C. K. and MacNeil, S. (2015) 'Simple surface coating of electrospun poly-L-lactic acid scaffolds to induce angiogenesis', *J Biomater Appl*, 30(1), pp. 50-60.

Gnavi, S., Fornasari, B. E., Tonda-Turo, C., Ciardelli, G., Zanetti, M., Geuna, S. and Perroteau, I. (2015a) 'The influence of electrospun fibre size on Schwann cell behaviour and axonal outgrowth', *Mater Sci Eng C Mater Biol Appl*, 48, pp. 620-31.

Gnavi, S., Fornasari, B. E., Tonda-Turo, C., Laurano, R., Zanetti, M., Ciardelli, G. and Geuna, S. (2015b) 'The Effect of Electrospun Gelatin Fibers Alignment on Schwann Cell and Axon Behavior and Organization in the Perspective of Artificial Nerve Design', *Int J Mol Sci*, 16(6), pp. 12925-42.

Gu, Z.-J. and Shen, Q. (2016) 'Synthesis, characterization and comparison of polyaniline 1D-structure controlled by poly(l-lactide) and poly(d-lactide)', *Superlattices and Microstructures*, 89, pp. 53-58.

Gupta, D., Venugopal, J., Prabhakaran, M. P., Dev, V. R., Low, S., Choon, A. T. and Ramakrishna, S. (2009) 'Aligned and random nanofibrous substrate for the in vitro culture of Schwann cells for neural tissue engineering', *Acta Biomater*, 5(7), pp. 2560-9.

Hearnden, V., Sankar, V., Hull, K., Juras, D. V., Greenberg, M., Kerr, A. R., Lockhart, P. B., Patton, L. L., Porter, S. and Thornhill, M. H. (2012) 'New developments and opportunities in oral mucosal drug delivery for local and systemic disease', *Adv Drug Deliv Rev*, 64(1), pp. 16-28.

Hong, X., Edirisinghe, M. and Mahalingam, S. (2016) 'Beads, beaded-fibres and fibres: Tailoring the morphology of poly(caprolactone) using pressurised gyration', *Mater Sci Eng C Mater Biol Appl*, 69, pp. 1373-82.

Hu, F., Zhang, X., Liu, H., Xu, P., Doulathunnisa, Teng, G. and Xiao, Z. (2017) 'Neuronally differentiated adipose-derived stem cells and aligned PHBV nanofiber nerve scaffolds promote sciatic nerve regeneration', *Biochem Biophys Res Commun*, 489(2), pp. 171-178.

Hu, Y., Wu, Y., Gou, Z., Tao, J., Zhang, J., Liu, Q., Kang, T., Jiang, S., Huang, S., He, J., Chen, S., Du, Y. and Gou, M. (2016) '3D-engineering of Cellularized Conduits for Peripheral Nerve Regeneration', *Scientific Reports*, 6.

Huang, C., Ouyang, Y., Niu, H., He, N., Ke, Q., Jin, X., Li, D., Fang, J., Liu, W., Fan, C. and Lin, T. (2015) 'Nerve guidance conduits from aligned nanofibers: improvement of nerve regeneration through longitudinal nanogrooves on a fiber surface', *ACS Appl Mater Interfaces*, 7(13), pp. 7189-96.

Iijima, Y., Ajiki, T., Murayama, A. and Takeshita, K. (2016) 'Effect of Artificial Nerve Conduit Vascularization on Peripheral Nerve in a Necrotic Bed', *Plastic and reconstructive surgery. Global open*, 4(3), pp. e665-e665.

James, R., Toti, U. S., Laurencin, C. T. and Kumbar, S. G. (2011) 'Electrospun nanofibrous scaffolds for engineering soft connective tissues', *Methods Mol Biol*, 726, pp. 243-58.

Jessen, K. R., Mirsky, R. and Lloyd, A. C. (2015) 'Schwann Cells: Development and Role in Nerve Repair', *Cold Spring Harb Perspect Biol*, 7(7), p. a020487.

Jia, L., Prabhakaran, M. P., Qin, X. and Ramakrishna, S. (2014) 'Guiding the orientation of smooth muscle cells on random and aligned polyurethane/collagen nanofibers', *J Biomater Appl*, 29(3), pp. 364-77.

Jiang, X., Lim, S. H., Mao, H.-Q. and Chew, S. Y. (2010) 'Current applications and future perspectives of artificial nerve conduits', *Experimental Neurology*, 223(1), pp. 86-101.

Johnson, B. N. and Jia, X. (2016) '3D printed nerve guidance channels: computer-aided control of geometry, physical cues, biological supplements and gradients', *Neural Regen Res*, 11(10), pp. 1568-1569.

Johnson, B. N., Lancaster, K. Z., Zhen, G., He, J., Gupta, M. K., Kong, Y. L., Engel, E. A., Krick, K. D., Ju, A., Meng, F., Enquist, L. W., Jia, X. and McAlpine, M. C. (2015) '3D Printed Anatomical Nerve Regeneration Pathways', *Adv Funct Mater*, 25(39), pp. 6205-6217.

Johnson, D. W., Sherborne, C., Didsbury, M. P., Pateman, C., Cameron, N. R. and Claeyssens, F. (2013) 'Macrostructuring of emulsion-templated porous polymers by 3D laser patterning', *Adv Mater*, 25(23), pp. 3178-81.

Kaewkhaw, R., Scutt, A. M. and Haycock, J. W. (2012) 'Integrated culture and purification of rat Schwann cells from freshly isolated adult tissue', *Nat Protoc*, 7(11), pp. 1996-2004.

Kaplan, H. M., Mishra, P. and Kohn, J. (2015) 'The overwhelming use of rat models in nerve regeneration research may compromise designs of nerve guidance conduits for humans', *J Mater Sci Mater Med*, 26(8), p. 226.

Karimi, M., Biazar, E., Keshel, S. H., Ronaghi, A., Doostmohamadpour, J., Janfada, A. and Montazeri, A. (2014) 'Rat Sciatic Nerve Reconstruction Across a 30 mm Defect Bridged by an Oriented Porous PHBV Tube With Schwann Cell as Artificial Nerve Graft', *Asaio Journal*, 60(2), pp. 224-233.

Kehoe, S., Zhang, X. F. and Boyd, D. (2011) 'Composition-property relationships for an experimental composite nerve guidance conduit: evaluating cytotoxicity and initial tensile strength', *J Mater Sci Mater Med*, 22(4), pp. 945-59.

Kehoe, S., Zhang, X. F. and Boyd, D. (2012) 'FDA approved guidance conduits and wraps for peripheral nerve injury: A review of materials and efficacy', *Injury*, 43(5), pp. 553-572.

Kim, Y. T., Haftel, V. K., Kumar, S. and Bellamkonda, R. V. (2008) 'The role of aligned polymer fiber-based constructs in the bridging of long peripheral nerve gaps', *Biomaterials*, 29(21), pp. 3117-27.

Lee, D.-Y., Choi, B.-H., Park, J.-H., Zhu, S.-J., Kim, B.-Y., Huh, J.-Y., Lee, S.-H., Jung, J.-H. and Kim, S.-H. (2006) 'Nerve regeneration with the use of a poly(l-lactide-co-glycolic acid)-coated collagen tube filled with collagen gel', *Journal of Cranio-Maxillofacial Surgery*, 34(1), pp. 50-56.

Lee, J. W., Kang, K. S., Lee, S. H., Kim, J.-Y., Lee, B.-K. and Cho, D.-W. (2011) 'Bone regeneration using a microstereolithography-produced customized poly(propylene fumarate)/diethyl fumarate photopolymer 3D scaffold incorporating BMP-2 loaded PLGA microspheres', *Biomaterials*, 32(3), pp. 744-752.

Lee, S. Y., Choi, J.-i. and Wong, H. H. (1999) 'Recent advances in polyhydroxyalkanoate production by bacterial fermentation: mini-review', *International Journal of Biological Macromolecules*, 25(1), pp. 31-36.

Lee, Y. S. and Arinzeh, T. L. (2011) 'Electrospun Nanofibrous Materials for Neural Tissue Engineering', *Polymers*, 3(1), pp. 413-426.

Leung, L., Chan, C., Baek, S. and Naguib, H. (2008) 'Comparison of morphology and mechanical properties of PLGA bioscaffolds', *Biomed Mater*, 3(2), p. 025006.

Li, H. and Chang, J. (2005) 'In vitro degradation of porous degradable and bioactive PHBV/wollastonite composite scaffolds', *Polymer Degradation and Stability*, 87(2), pp. 301-307.

Li, H., Xia, Y., Wu, J., He, Q., Zhou, X., Lu, G., Shang, L., Boey, F., Venkatraman, S. S. and Zhang, H. (2012) 'Surface Modification of Smooth Poly(l-lactic acid) Films for Gelatin Immobilization', *ACS Applied Materials & Interfaces*, 4(2), pp. 687-693.

Lizarraga-Valderrama, L. R., Nigmatullin, R., Taylor, C., Haycock, J. W., Claeyssens, F., Knowles, J. C. and Roy, I. (2015) 'Nerve tissue engineering using blends of poly(3-hydroxyalkanoates) for peripheral nerve regeneration', *Engineering in Life Sciences*, 15(6), pp. 612-621.

Lizarraga-Valderrama, L. R., Panchal, B., Thomas, C., Boccaccini, A. R. and Roy, I. (2016) 'Biomedical Applications of Polyhydroxyalkanoates', in *Biomaterials from Nature for Advanced Devices and Therapies*. John Wiley & Sons, Inc., pp. 337-383.

Loordhuswamy, A. M., Krishnaswamy, V. R., Korrapati, P. S., Thinakaran, S. and Rengaswami, G. D. (2014) 'Fabrication of highly aligned fibrous scaffolds for tissue regeneration by centrifugal spinning technology', *Mater Sci Eng C Mater Biol Appl*, 42, pp. 799-807.

Lowe, J. S. and Anderson, P. G. (2015) 'Chapter 6 - Nervous Tissue', in *Stevens & Lowe's Human Histology (Fourth Edition) (Fourth Edition)*. Philadelphia: Mosby, pp. 84-104.

Lukasiewicz, B., Basnett, P., Nigmatullin, R., Matharu, R., Knowles, J. C. and Roy, I. (2018) 'Binary polyhydroxyalkanoate systems for soft tissue engineering', *Acta Biomaterialia*, 71, pp. 225-234.

MacNeil, S. (2007) 'Progress and opportunities for tissue-engineered skin', *Nature*, 445(7130), pp. 874-80.

MacNeil, S. (2008) 'Biomaterials for tissue engineering of skin', *Materials Today*, 11(5), pp. 26-35.

MacNeil, S., Shepherd, J. and Smith, L. (2011) 'Production of tissue-engineered skin and oral mucosa for clinical and experimental use', *Methods Mol Biol*, 695, pp. 129-53.

Mahalingam, S. and Edirisinghe, M. (2013) 'Forming of polymer nanofibers by a pressurised gyration process', *Macromol Rapid Commun*, 34(14), pp. 1134-9.

Mahalingam, S., Raimi-Abraham, B. T., Craig, D. Q. and Edirisinghe, M. (2015) 'Formation of protein and protein-gold nanoparticle stabilized microbubbles by pressurized gyration', *Langmuir*, 31(2), pp. 659-66.

Marani, E., Lakke, E. A. J. F. and Paxinos, G. (2012) 'Chapter 4 - Peripheral Nervous System Topics A2 - Mai, Jürgen K', in *The Human Nervous System (Third Edition)*. San Diego: Academic Press, pp. 82-140.

Martinova, L. and Lubasova, D. (2012) 'Reasons for using polymer blends in the electrospinning process', *AIP Conference Proceedings*, 1502(1), pp. 115-128.

Masaeli, E., Morshed, M., Nasr-Esfahani, M. H., Sadri, S., Hilderink, J., van Apeldoorn, A., van Blitterswijk, C. A. and Moroni, L. (2013) 'Fabrication, Characterization and Cellular Compatibility of Poly(Hydroxy Alkanoate) Composite Nanofibrous Scaffolds for Nerve Tissue Engineering', *PLoS ONE*, 8(2), p. e57157.

Melissinaki, V., Gill, A. A., Ortega, I., Vamvakaki, M., Ranella, A., Haycock, J. W., Fotakis, C., Farsari, M. and Claeyssens, F. (2011) 'Direct laser writing of 3D scaffolds for neural tissue engineering applications', *Biofabrication*, 3(4), p. 045005.

Metwalli, E., Haines, D., Becker, O., Conzone, S. and Pantano, C. G. (2006) 'Surface characterizations of mono-, di-, and tri-aminosilane treated glass substrates', *J Colloid Interface Sci*, 298(2), pp. 825-31.

Minati, L., Migliaresi, C., Lunelli, L., Viero, G., Dalla Serra, M. and Speranza, G. (2017) 'Plasma assisted surface treatments of biomaterials', *Biophys Chem*.

Miranda-Azpiazu, P., Panagiotou, S., Jose, G. and Saha, S. (2018) 'A novel dynamic multicellular co-culture system for studying individual blood-brain barrier cell types in brain diseases and cytotoxicity testing', *Scientific Reports*, 8(1), p. 8784.

Misra, S. K., Ansari, T. I., Valappil, S. P., Mohn, D., Philip, S. E., Stark, W. J., Roy, I., Knowles, J. C., Salih, V. and Boccaccini, A. R. (2010) 'Poly(3-hydroxybutyrate) multifunctional composite scaffolds for tissue engineering applications', *Biomaterials*, 31(10), pp. 2806-15.

Misra, S. K., Valappil, S. P., Roy, I. and Boccaccini, A. R. (2006) 'Polyhydroxyalkanoate (PHA)/inorganic phase composites for tissue engineering applications', *Biomacromolecules*, 7(8), pp. 2249-58.

Mohamadi, F., Ebrahimi-Barough, S., Reza Nourani, M., Ali Derakhshan, M., Goodarzi, V., Sadegh Nazockdast, M., Farokhi, M., Tajerian, R., Faridi Majidi, R. and Ai, J. (2017) 'Electrospun nerve guide scaffold of poly(ε-caprolactone)/collagen/nanobioglass: an in vitro study in peripheral nerve tissue engineering', *Journal of Biomedical Materials Research Part A*, 105(7), pp. 1960-1972.

Mosahebi, A., Wiberg, M. and Terenghi, G. (2003) 'Addition of fibronectin to alginate matrix improves peripheral nerve regeneration in tissue-engineered conduits', *Tissue Eng*, 9(2), pp. 209-18.

Mäkilä, E., Bimbo, L. M., Kaasalainen, M., Herranz, B., Airaksinen, A. J., Heinonen, M., Kukk, E., Hirvonen, J., Santos, H. A. and Salonen, J. (2012) 'Amine modification of thermally carbonized porous silicon with silane coupling chemistry', *Langmuir*, 28(39), pp. 14045-54.

Nectow, A. R., Marra, K. G. and Kaplan, D. L. (2012) 'Biomaterials for the development of peripheral nerve guidance conduits', *Tissue Eng Part B Rev*, 18(1), pp. 40-50.

Ni, H. C., Lin, Z. Y., Hsu, S. H. and Chiu, I. M. (2010) 'The use of air plasma in surface modification of peripheral nerve conduits', *Acta Biomater*, 6(6), pp. 2066-76.

Oh, S. H., Kim, J. H., Song, K. S., Jeon, B. H., Yoon, J. H., Seo, T. B., Namgung, U., Lee, I. W. and Lee, J. H. (2008) 'Peripheral nerve regeneration within an asymmetrically porous PLGA/Pluronic F127 nerve guide conduit', *Biomaterials*, 29(11), pp. 1601-1609.

Owen, R., Sherborne, C., Paterson, T., Green, N. H., Reilly, G. C. and Claeyssens, F. (2016) 'Emulsion templated scaffolds with tunable mechanical properties for bone tissue engineering', *J Mech Behav Biomed Mater*, 54, pp. 159-72.

Pateman, C. J., Harding, A. J., Glen, A., Taylor, C. S., Christmas, C. R., Robinson, P. P., Rimmer, S., Boissonade, F. M., Claeyssens, F. and Haycock, J. W. (2015) 'Nerve guides manufactured from photocurable polymers to aid peripheral nerve repair', *Biomaterials*, 49, pp. 77-89.

Paxinos, G., Xu-Feng, H., Sengul, G. and Watson, C. (2012) 'Chapter 8 - Organization of Brainstem Nuclei', in *The Human Nervous System (Third Edition).* San Diego: Academic Press, pp. 260-327.

Perry, V. H., Brown, M. C. and Gordon, S. (1987) 'The macrophage response to central and peripheral nerve injury. A possible role for macrophages in regeneration', *J Exp Med*, 165(4), pp. 1218-23.

Pfister, B. J., Gordon, T., Loverde, J. R., Kochar, A. S., Mackinnon, S. E. and Cullen, D. K. (2011) 'Biomedical engineering strategies for peripheral nerve repair: surgical applications, state of the art, and future challenges', *Crit Rev Biomed Eng*, 39(2), pp. 81-124.

Pham, Q. P., Sharma, U. and Mikos, A. G. (2006) 'Electrospinning of polymeric nanofibers for tissue engineering applications: a review', *Tissue Eng*, 12(5), pp. 1197-211.

Philip, S., Keshavarz, T. and Roy, I. (2007) 'Polyhydroxyalkanoates: biodegradable polymers with a range of applications', *Journal of Chemical Technology & Biotechnology*, 82(3), pp. 233-247.

Poncin-Epaillard, F. and Legeay, G. (2003) 'Surface engineering of biomaterials with plasma techniques', *J Biomater Sci Polym Ed*, 14(10), pp. 1005-28.

Popko, J., Fernandes, A. and Lanier, L. M. (2009) 'Automated Analysis of NeuronJ Tracing Data', *Cytometry. Part A : the journal of the International Society for Analytical Cytology*, 75(4), pp. 371-376.

Prabhakaran, M. P., Nair, A. S., Kai, D. and Ramakrishna, S. (2012) 'Electrospun composite scaffolds containing poly(octanediol-co-citrate) for cardiac tissue engineering', *Biopolymers*, 97(7), pp. 529-38.

Prabhakaran, M. P., Vatankhah, E. and Ramakrishna, S. (2013) 'Electrospun aligned PHBV/collagen nanofibers as substrates for nerve tissue engineering', *Biotechnol Bioeng*, 110(10), pp. 2775-84.

Prabhakaran, M. P., Venugopal, J., Chan, C. K. and Ramakrishna, S. (2008) 'Surface modified electrospun nanofibrous scaffolds for nerve tissue engineering', *Nanotechnology*, 19(45), p. 455102.

Qazi, T. H., Mooney, D. J., Pumberger, M., Geissler, S. and Duda, G. N. (2015) 'Biomaterials based strategies for skeletal muscle tissue engineering: existing technologies and future trends', *Biomaterials*, 53, pp. 502-21.

Rai, R., Yunos, D. M., Boccaccini, A. R., Knowles, J. C., Barker, I. A., Howdle, S. M., Tredwell, G. D., Keshavarz, T. and Roy, I. (2011) 'Poly-3-hydroxyoctanoate P(3HO), a medium chain length polyhydroxyalkanoate homopolymer from Pseudomonas mendocina', *Biomacromolecules*, 12(6), pp. 2126-36.

Raimi-Abraham, B. T., Mahalingam, S., Davies, P. J., Edirisinghe, M. and Craig, D. Q. (2015) 'Development and Characterization of Amorphous Nanofiber Drug Dispersions Prepared Using Pressurized Gyration', *Mol Pharm*, 12(11), pp. 3851-61.

Raimi-Abraham, B. T., Mahalingam, S., Edirisinghe, M. and Craig, D. Q. (2014) 'Generation of poly(N-vinylpyrrolidone) nanofibres using pressurised gyration', *Mater Sci Eng C Mater Biol Appl*, 39, pp. 168-76.

Ratner, B. D. (1992) 'Plasma deposition for biomedical applications: a brief review', *J Biomater Sci Polym Ed*, 4(1), pp. 3-11.

Renard, E., Walls, M., Guérin, P. and Langlois, V. (2004) 'Hydrolytic degradation of blends of polyhydroxyalkanoates and functionalized polyhydroxyalkanoates', *Polymer Degradation and Stability*, 85(2), pp. 779-787.

Repić, T., Madirazza, K., Bektur, E. and Sapunar, D. (2016) 'Characterization of dorsal root ganglion neurons cultured on silicon micro-pillar substrates', *Sci Rep*, 6, p. 39560.

Richardson, S. M., Curran, J. M., Chen, R., Vaughan-Thomas, A., Hunt, J. A., Freemont, A. J. and Hoyland, J. A. (2006) 'The differentiation of bone marrow mesenchymal stem cells

into chondrocyte-like cells on poly-L-lactic acid (PLLA) scaffolds', *Biomaterials*, 27(22), pp. 4069-78.

Rodríguez, F. J., Valero-Cabré, A. and Navarro, X. (2004) 'Regeneration and functional recovery following peripheral nerve injury', *Drug Discovery Today: Disease Models*, 1(2), pp. 177-185.

Roman, S., Mangir, N., Bissoli, J., Chapple, C. R. and MacNeil, S. (2016) 'Biodegradable scaffolds designed to mimic fascia-like properties for the treatment of pelvic organ prolapse and stress urinary incontinence', *J Biomater Appl*, 30(10), pp. 1578-88.

Romero-Ortega, M. (2013) 'Peripheral Nerves, Anatomy and Physiology of'. Encyclopedia of Computational Neuroscience, pp. 1-5.

Sabongi, R., Fernandes, M. and dos Santos, J. B. (2015) 'Peripheral nerve regeneration with conduits: use of vein tubes', *Neural Regeneration Research*, 10(4), pp. 529-533.

Sanchez, J. G., Tsuchii, A. and Tokiwa, Y. (2000) 'Degradation of polycaprolactone at 50 °C by a thermotolerant Aspergillus sp', *Biotechnology Letters*, 22(10), pp. 849-853.

Sangsanoh, P., Waleetorncheepsawat, S., Suwantong, O., Wutticharoenmongkol, P., Weeranantanapan, O., Chuenjitbuntaworn, B., Cheepsunthorn, P., Pavasant, P. and Supaphol, P. (2007) 'In vitro biocompatibility of schwann cells on surfaces of biocompatible polymeric electrospun fibrous and solution-cast film scaffolds', *Biomacromolecules*, 8(5), pp. 1587-94.

Scandola, M., Focarete, M. L., Adamus, G., Sikorska, W., Baranowska, I., Świerczek, S., Gnatowski, M., Kowalczuk, M. and Jedliński, Z. (1997) 'Polymer Blends of Natural Poly(3-hydroxybutyrate-co-3-hydroxyvalerate) and a Synthetic Atactic Poly(3-hydroxybutyrate). Characterization and Biodegradation Studies', *Macromolecules*, 30(9), pp. 2568-2574.

Schaub, N. J., Johnson, C. D., Cooper, B. and Gilbert, R. J. (2016) 'Electrospun Fibers for Spinal Cord Injury Research and Regeneration', *J Neurotrauma*, 33(15), pp. 1405-15.

Schaub, N. J., Le Beux, C., Miao, J., Linhardt, R. J., Alauzun, J. G., Laurencin, D. and Gilbert, R. J. (2015) 'The Effect of Surface Modification of Aligned Poly-L-Lactic Acid Electrospun Fibers on Fiber Degradation and Neurite Extension', *PLoS One*, 10(9), p. e0136780.

Schmidt, D. R., Waldeck, H. and Kao, W. J. (2009) 'Protein Adsorption to Biomaterials', in *Biological Interactions on Materials Surfaces: Understanding and Controlling Protein, Cell, and Tissue Responses.* New York, NY: Springer US, pp. 1-18.

Schneider, C. A., Rasband, W. S. and Eliceiri, K. W. (2012) 'NIH Image to ImageJ: 25 years of image analysis', *Nature Methods*, 9, p. 671.

Shabir, A., Alhusban, F., Perrie, Y. and Mohammed, A. R. (2011) 'Effects of ball-milling on PLGA polymer and its implication on lansoprazole-loaded nanoparticles', *Journal of Basic and Clinical Pharmacy*, 2(2), pp. 71-82.

Shen, H., Shen, Z. L., Zhang, P. H., Chen, N. L., Wang, Y. C., Zhang, Z. F. and Jin, Y. Q. (2010) 'Ciliary neurotrophic factor-coated polylactic-polyglycolic acid chitosan nerve conduit promotes peripheral nerve regeneration in canine tibial nerve defect repair', *Journal of Biomedical Materials Research Part B: Applied Biomaterials*, 95B(1), pp. 161-170.

Sill, T. J. and von Recum, H. A. (2008) 'Electrospinning: applications in drug delivery and tissue engineering', *Biomaterials*, 29(13), pp. 1989-2006.

Sleigh, J. N., Weir, G. A. and Schiavo, G. (2016) 'A simple, step-by-step dissection protocol for the rapid isolation of mouse dorsal root ganglia', *BMC Res Notes*, 9, p. 82.

Sombatmankhong, K., Suwantong, O. and S. Waleetorncheepsawat, P. S. 44 (2006) 'Electrospun Fiber Mats of Poly(3-Hydroxybutyrate), Poly(3-Hydroxybutyrate-co-3-Hydroxyvalerate), and Their Blends'. Journal

of Polymer Science: Part B: Polymer Physics, pp. 2923–2933.

Stiefel, P., Schmidt-Emrich, S., Maniura-Weber, K. and Ren, Q. (2015) 'Critical aspects of using bacterial cell viability assays with the fluorophores SYTO9 and propidium iodide', *BMC Microbiol*, 15, p. 36.

Subramanian, A., Krishnan, U. M. and Sethuraman, S. (2009) 'Development of biomaterial scaffold for nerve tissue engineering: Biomaterial mediated neural regeneration', *J Biomed Sci*, 16, p. 108.

Sun, M., Kingham, P. J., Reid, A. J., Armstrong, S. J., Terenghi, G. and Downes, S. (2009) 'In vitro and in vivo testing of novel ultrathin PCL and PCL/PLA blend films as peripheral nerve conduit', *Journal of Biomedical Materials Research Part A*, 93A(4), pp. 1470-1481.

Sun, T., Norton, D., Vickers, N., L McArthur, S., Neil, S. M., Ryan, A. J. and Haycock, J. W. (2008) 'Development of a bioreactor for evaluating novel nerve conduits', *Biotechnol Bioeng*, 99(5), pp. 1250-60.

Suwantong, O., Waleetorncheepsawat, S., Sanchavanakit, N., Pavasant, P., Cheepsunthorn, P., Bunaprasert, T. and Supaphol, P. (2007) 'In vitro biocompatibility of electrospun poly(3-hydroxybutyrate) and poly(3-hydroxybutyrate-co-3-hydroxyvalerate) fiber mats', *Int J Biol Macromol*, 40(3), pp. 217-23.

Taglietti, A., Arciola, C. R., D'Agostino, A., Dacarro, G., Montanaro, L., Campoccia, D., Cucca, L., Vercellino, M., Poggi, A., Pallavicini, P. and Visai, L. (2014) 'Antibiofilm activity of a monolayer of silver nanoparticles anchored to an amino-silanized glass surface', *Biomaterials*, 35(6), pp. 1779-88.

Tan, A., Rajadas, J. and Seifalian, A. M. (2012) 'Biochemical engineering nerve conduits using peptide amphiphiles', *Journal of Controlled Release*, 163(3), pp. 342-352.

Tannenbaum, J. and Bennett, B. T. (2015) 'Russell and Burch's 3Rs Then and Now: The Need for Clarity in Definition and Purpose', *Journal of the American Association for Laboratory Animal Science : JAALAS*, 54(2), pp. 120-132.

Tokiwa, Y. and Calabia, B. P. (2007) 'Biodegradability and Biodegradation of Polyesters', *Journal of Polymers and the Environment*, 15(4), pp. 259-267.

Topp, K. S. and Boyd, B. S. (2006) 'Structure and biomechanics of peripheral nerves: nerve responses to physical stresses and implications for physical therapist practice', *Phys Ther*, 86(1), pp. 92-109.

Tsai, T.-Y., Wu, S. N., Liu, Y.-C., Wu, A. Z. and Tsai, Y.-C. (2005) 'Inhibitory action of L-type Ca2+ current by paeoniflorin, a major constituent of peony root, in NG108-15 neuronal cells', *European Journal of Pharmacology*, 523(1), pp. 16-24.

Ulery, B. D., Nair, L. S. and Laurencin, C. T. (2011) 'Biomedical Applications of Biodegradable Polymers', *Journal of polymer science. Part B, Polymer physics*, 49(12), pp. 832-864.

Upson, S. J., O'Haire, T., Russell, S. J., Dalgarno, K. and Ferreira, A. M. (2017) 'Centrifugally spun PHBV micro and nanofibres', *Mater Sci Eng C Mater Biol Appl*, 76, pp. 190-195.

Usaj, M., Torkar, D., Kanduser, M. and Miklavcic, D. (2010) 'Cell counting tool parameters optimization approach for electroporation efficiency determination of attached cells in phase contrast images', *Journal of Microscopy*, 241(3), pp. 303-314.

Valappil, S. P., Misra, S. K., Boccaccini, A. R., Keshavarz, T., Bucke, C. and Roy, I. (2007a) 'Large-scale production and efficient recovery of PHB with desirable material properties, from the newly characterised Bacillus cereus SPV', *J Biotechnol*, 132(3), pp. 251-8.

Valappil, S. P., Misra, S. K., Boccaccini, A. R. and Roy, I. (2006) 'Biomedical applications of polyhydroxyalkanoates: an overview of animal testing and in vivo responses', *Expert Rev Med Devices*, 3(6), pp. 853-68.

Valappil, S. P., Peiris, D., Langley, G. J., Herniman, J. M., Boccaccini, A. R., Bucke, C. and Roy, I. (2007b) 'Polyhydroxyalkanoate (PHA) biosynthesis from structurally unrelated carbon sources by a newly characterized Bacillus spp', *J Biotechnol*, 127(3), pp. 475-87.

Verlinden, R. A., Hill, D. J., Kenward, M. A., Williams, C. D. and Radecka, I. (2007) 'Bacterial synthesis of biodegradable polyhydroxyalkanoates', *J Appl Microbiol*, 102(6), pp. 1437-49.

Verrier, S., Pallu, S., Bareille, R., Jonczyk, A., Meyer, J., Dard, M. and Amédée, J. (2002) 'Function of linear and cyclic RGD-containing peptides in osteoprogenitor cells adhesion process', *Biomaterials*, 23(2), pp. 585-96.

Vroman, I. and Tighzert, L. (2009) 'Biodegradable Polymers', *Materials*, 2(2).

Vroman, L. E. O. (1987) 'Methods of Investigating Protein Interactions on Artificial and Natural Surfaces', *Annals of the New York Academy of Sciences*, 516(1), pp. 300-305.

Wang, H. B., Mullins, M. E., Cregg, J. M., Hurtado, A., Oudega, M., Trombley, M. T. and Gilbert, R. J. (2009) 'Creation of highly aligned electrospun poly-L-lactic acid fibers for nerve regeneration applications', *J Neural Eng*, 6(1), p. 016001.

Wang, H. B., Mullins, M. E., Cregg, J. M., McCarthy, C. W. and Gilbert, R. J. (2010) 'Varying the diameter of aligned electrospun fibers alters neurite outgrowth and Schwann cell migration', *Acta Biomater*, 6(8), pp. 2970-8.

Wang, S. and Cai, L. (2010) 'Polymers for Fabricating Nerve Conduits', *International Journal of Polymer Science*, 2010.

Wang, X., Ding, B. and Li, B. (2013) 'Biomimetic electrospun nanofibrous structures for tissue engineering', *Mater Today (Kidlington)*, 16(6), pp. 229-241.

Wen, X. and Tresco, P. A. (2006) 'Effect of filament diameter and extracellular matrix molecule precoating on neurite outgrowth and Schwann cell behavior on multifilament entubulation bridging device in vitro', *J Biomed Mater Res A*, 76(3), pp. 626-37.

Wu, M. H., Huang, S. B. and Lee, G. B. (2010) 'Microfluidic cell culture systems for drug research', *Lab Chip*, 10(8), pp. 939-56.

Xiao L, Wang B, Yang G and Gauthier M (2012) 'Poly(Lactic

Acid)-Based Biomaterials: Synthesis, Modification and Applications'. https://www.intechopen.com/books/biomedical-science-engineering-and-technology/poly-lactic-acid-based-biomaterials-synthesis-modification-and-applications: Biomedical Science, Engineering and Technology.

Xu, Z., Mahalingam, S., Basnett, P., Raimi-Abraham, B., Roy, I., Craig, D. and Edirisinghe, M. 301 (2016) 'Making Nonwoven

Fibrous Poly(ε-caprolactone) Constructs for Antimicrobial and Tissue

Engineering Applications by Pressurized Melt Gyration'. Macromol. Mater.

Eng., p. 922−934.

Yang, F., Murugan, R., Wang, S. and Ramakrishna, S. (2005a) 'Electrospinning of nano/micro scale poly(L-lactic acid) aligned fibers and their potential in neural tissue engineering', *Biomaterials*, 26(15), pp. 2603-10.

Yang, Y., De Laporte, L., Rives, C. B., Jang, J.-H., Lin, W.-C., Shull, K. R. and Shea, L. D. (2005b) 'Neurotrophin releasing single and multiple lumen nerve conduits', *Journal of Controlled Release*, 104(3), pp. 433-446.

Yao, L., Billiar, K. L., Windebank, A. J. and Pandit, A. (2010) 'Multichanneled Collagen Conduits for Peripheral Nerve Regeneration: Design, Fabrication, and Characterization', *Tissue Engineering Part C: Methods*, 16(6), pp. 1585-1596.

Yao, L., O'Brien, N., Windebank, A. and Pandit, A. (2009) 'Orienting neurite growth in electrospun fibrous neural conduits', *J Biomed Mater Res B Appl Biomater*, 90(2), pp. 483-91.

Yasuda, H., Iriyama, Y., Allen, G. and Bevington, J. C. (1989) '21 - Plasma Polymerization', in *Comprehensive Polymer Science and Supplements*. Amsterdam: Pergamon, pp. 357-375.

Yoon, S.-D., Kwon, Y.-S. and Lee, K.-S. (2017) 'Biodegradation and Biocompatibility of Poly L-lactic Acid Implantable Mesh', *International Neurourology Journal*, 21(Suppl 1), pp. S48-54.

Young, R. C., Wiberg, M. and Terenghi, G. (2002) 'Poly-3-hydroxybutyrate (PHB): a resorbable conduit for long-gap repair in peripheral nerves', *Br J Plast Surg*, 55(3), pp. 235-40.

Yu, J., Lee, A. R., Lin, W. H., Lin, C. W., Wu, Y. K. and Tsai, W. B. (2014) 'Electrospun PLGA fibers incorporated with functionalized biomolecules for cardiac tissue engineering', *Tissue Eng Part A*, 20(13-14), pp. 1896-907.

Yu, W., Zhao, W., Zhu, C., Zhang, X., Ye, D., Zhang, W., Zhou, Y., Jiang, X. and Zhang, Z. (2011) 'Sciatic nerve regeneration in rats by a promising electrospun collagen/poly(ε-caprolactone) nerve conduit with tailored degradation rate', *BMC Neuroscience*, 12, pp. 68-68.

Zhao, K., Deng, Y., Chun Chen, J. and Chen, G.-Q. (2003) 'Polyhydroxyalkanoate (PHA) scaffolds with good mechanical properties and biocompatibility', *Biomaterials*, 24(6), pp. 1041-1045.

Ziats, N. P., Miller, K. M. and Anderson, J. M. (1988) 'In vitro and in vivo interactions of cells with biomaterials', *Biomaterials*, 9(1), pp. 5-13.

Zilic, L., Garner, P. E., Yu, T., Roman, S., Haycock, J. W. and Wilshaw, S. P. (2015) 'An anatomical study of porcine peripheral nerve and its potential use in nerve tissue engineering', *J Anat*, 227(3), pp. 302-14.